University of Southampton

FACULTY OF ENGINEERING AND THE ENVIRONMENT

COMPUTATIONAL ENGINEERING AND DESIGN GROUP

Analysis of human knee flexion-extension during gait, in a laboratory and a non-laboratory based environment

By

Lavinia-Alexandra Otescu, BEng MRes

Supervisors:

Dr. Martin Warner

Prof. Markus OW Heller

Prof. Maria J Stokes

Dr. Alexander IJ Forrester

A thesis submitted in partial fulfilment of the requirement of the degree of:

Master of Philosophy

September 2017

University of Southampton

Abstract

FACULTY OF ENGINEERING AND THE ENVIRONMENT
COMPUTATIONAL ENGINEERING AND DESIGN GROUP

MASTER OF PHILOSOPHY

Analysis of human knee flexion-extension during gait, in a laboratory and a non-laboratory based environment

By Lavinia-Alexandra Otescu, BEng MRes

The two major aspects with which the current thesis was concerned were firstly, validating a wireless inertial measuring unit (IMU) based motion capture system against an optical motion capture system and secondly, testing the IMU motion capture system in a non-laboratory based environment. While there are a number of protocols for IMU motion capture available in the literature to our knowledge, hitherto, the vast majority of studies merely compared this technique to optical motion capture without actually completely validating the proposed techniques against the reference system.

For the purpose of this study, the flexion-extension angle of the knee during gait was measured during two sessions, using IMU and optical motion capture in a laboratory and only IMUs in an outdoor environment, for 10 healthy non-athlete male participants, aged 22-30 years, with a weight of 69-93kg and a height of 169-193cm.

When comparing data from the two motion capture systems, variability of ΔROM = 0.2° to 16.3°, RMS = 2.9° to 6.1°, σ = 2.5° to 7.9°, CV = 3.3% to 10.3% and correlation of CMC = 0.977 to 0.994, r = 0.958 to 0.995, were discovered. Furthermore, a two sample t-test revealed that despite such high correlation statistically significant differences ($p < 0.04^{(*)}$ to $p < 0.0008^{(***)}$) were present between percentages 17 and 56, and 69 and 94 of the average knee flexion-extension angles recorded during a gait cycle with the two systems. Therefore, in order to validate the IMU motion capture protocol against the reference system, calculations were made and a vector, comprising a correction factor for the knee flexion-extension angle computed from the IMU data at every percentage of the gait cycle, was generated. Once the correction vector was applied to the IMU data, no statistically significant differences were found between the average knee flexion-extension angles of the gait cycle recorded with the two systems. When comparing laboratory to outdoor IMU motion capture variability of ΔROM = 0.1° to 14.3°, RMS = 1.8° to 6.1°, σ = 1.5° to 5.1°, CV = 2.3% to 7.8% and correlation of CMC = 0.974 to 0.998, r = 0.966 to 0.996, were discovered. Despite such large variability measures, two-sample t-tests showed no statistically significant differences between the average knee flexion-extension angles recorded during a gait cycle in the two venues.

The findings of the current study show that the IMU system and data processing protocol presented in the thesis can be used for the purpose of indoor as well as outdoor motion studies. However, for studies involving human knee flexion-extension during gait, the proposed correction factor should be applied in order for the data to be comparable to the currently accepted gold standard. For studies involving other motions further testing needs to be carried out.

Table of Contents

List of Figures

List of Tables

UNIVERSITY OF Southampton

DECLARATION OF AUTHORSHIP

I, Lavinia-Alexandra Otescu, declare that the thesis titled 'Analysis of human knee flexion-extension during gait, in a laboratory and a non-laboratory based environment' and the work presented in it are my own and have been generated by me as the result of my own original research.

I confirm that:

- This work was done wholly or mainly while in candidature for a research degree at this University;
- Where any part of this thesis has previously been submitted for a degree or any other qualification at this University or any other institution, this has been clearly stated;
- Where I have consulted the published work of others, this is always clearly attributed;
- Where I have quoted from the work of others, the source is always given. With the exception of such quotations, this thesis is entirely my own work;
- I have acknowledged all main sources of help;
- Where the thesis is based on work done by myself jointly with others, I have made clear exactly what was done by others and what I have contributed myself;
- Either none of this work has been published before submission, or parts of this work have been published as application for ethical approval.

Signed:

Date:

Acknowledgements

The past 3 and a half years have brought me both, ups and downs. My greatest struggles were not necessarily with my research, but with my health, and there were times when I did not think that I would be able to finish this degree. However, the love and support of my family and friends, the help and guidance, and not to mention understanding of my supervisors, peers, and other members of the university, have enabled me to arrive at this point, and for that I am very grateful.

Firstly, I would like to thank my family and friends for always picking me up when I felt at my lowest. I would like to thank my parents for always making sure that I am cared for properly, even though I a grown up now, and for bending over backwards to make sure that I receive the best healthcare possible whenever it was necessary, but not least, I would like to thank them for the great efforts they have made to support me financially when my funding was finished and for covering my medical costs when necessary.

I would like to thank my supervisors for always understanding my situation and focusing on how we can progress with our research and encouraging me, rather than dwelling on our draw backs.

I would like to thank my peers and friends, Konstantinos Papadopoulos and Michele Stramacchia for providing crucial help with designing the LabView interface which enabled equipment synchronisation and data logging for my sensor accuracy test, and for helping me in developing my Matlab skills, respectively.

I would like to thank Dr. Alexander Dickinson for helping me with the data acquisition for my sensor accuracy test. I would also like to thank Dr. Dickinson and Dr. Peter Worsley for the very comprehensive and constructive feedback and for the very good advice and guidance they have given me as my internal examiners.

I would like to thank my participants for agreeing to take part in this study and for all their patience. Additionally, I would like to thank David Wilson for being a great collaborator, for managing the Vicon data acquisition and processing and our joint ethical approval application.

Last but not least, I would like to express my gratitude to the Arthritis Research UK Centre and to the Engineering and Physical Sciences Research Council for funding my research for 3 years.

This would not have been possible without you all and for that I will be forever grateful.

Abbreviations

OA – osteoarthritis

FAI – femuroacetabular impingement

$H_{1, 2, 3}$ – hypothesis 1, 2 and 3

ASIS – anterior superior iliac spine

PSIS – posterior superior iliac spine

LASI – left side of anterior superior iliac spine

RASI – right side of anterior superior iliac spine

LPSI – left side of posterior superior iliac spine

RPSI – right side of posterior superior iliac spine

LTHI – left thigh

RTHI – right thigh

LMTHI – left medial thigh

RMTHI – right medial thigh

LKNE – left knee

RKNE – right knee

LMKNE – left medial knee

RMKNE – right medial knee

LTUB – left upper tibia

RTUB – right upper tibia

LTIB – left lateral tibia

RTIB – right lateral tibia

LANK – left ankle

RANK – right ankle

LMANK – left medial ankle

RMANK – right medial ankle

LHEE – left heel

RHEE – right heel

LTOE – left toe

RTOE – right toe

L5thMET – left 5th metatarsal

R5thMET – right 5th metatarsal

Q – angle – an angle formed between the quadriceps muscle and the patellar tendon

SAFLo – 'Servizio di Analisi della Funzione Locomotoria' protocol

LAMB – 'Laboratorio per l'Analisi di Movimento nel Bambino' protocol

CAST – 'Calibration Anatomical System Technique'

T3Dg – 'Total 3D Gait' protocol

SARA – Symmetrical Axis of Rotation Approach

SCoRE – Symmetrical Centre of Rotation Estimation

STA – soft tissue artefacts

OCST – Optimal Common Shape Technique

OSSCA – an approach which combines the use of the OCST, SCoRE, and SARA techniques

LVDT – Linear Variable Differential Transformer

RVDT – Rotary Variable Differential Transformer

BNC – Bayonet Neill-Concelman connector

EMG - electromyography

MTws – inertial and magnetic wireless motion tracking units

XKF-3w – Xsens on board Kalman filter

ROM – range of motion

RMS – root mean squared error

CV – coefficient of variation

σ – standard deviation

ΔROM – difference in ranges of motion

r - Pearson product-moment correlation coefficient

CMC - coefficient of multiple correlations

IR – infrared

N – number of observations

Chapter 1

1. Introduction

> "An object in motion tends to stay in motion unless an external force acts upon it. Similarly, if the object is at rest, it will remain at rest unless an unbalanced force acts upon it."
>
> "When a force acts on an object, it will cause the object to accelerate. The larger the mass of the object, the greater the force will need to be to cause it to accelerate."
>
> - Sir Isaac Newton.

Throughout centuries, people were fascinated with the study of motion. In fact, several disciplines were created, in which laws of physics and mechanics were applied to objects or biological systems in order to study the effect of the forces acting upon them. One of those disciplines is biomechanics, which involves, among others, the study of the kinetics and kinematics of the human body.

Locomotion is one of the primary functions of the human body (Moore et al. 2010) and studying its characteristics and its effects on the musculoskeletal system is of great importance, especially in our times, when musculoskeletal disorders are ranking very high amongst the top debilitating diseases worldwide, according to the World Health Organisation (Brooks 2006; Cross et al. 2014; St. John 2015).

Degenerative musculoskeletal diseases, such as osteoarthritis (OA) are most prevalent in the elderly population, of 55 years and older (Reginster 2002). Over the past decades, the United Nations reported a steady increase in the life expectancy of the world population (Oeppen and Vaupel 2008), which marked a concomitant increase in the number of years in which sufferers need to manage the disease (Cross et al. 2014), thereby not only lowering the quality of life of the patient but also putting extra strain on the health care system.

Although OA is an autoimmune disease and its origins are not yet fully understood, the literature suggests that in some patients OA can be caused by other degenerative processes such as femuroacetabular impingement (FAI) (Benedetti et al. 1998; Brennan et al. 2011a), genu varum or genu valgum (Moore et al. 2010), which have a much earlier onset than OA. Early diagnosis in such cases could help prevent or postpone the onset of OA in the patient's joints. Motion analysis has been widely tested as a means of diagnosing skeletal misalignment processes, such as the ones mentioned above.

The knee joint is not only the largest joint in the human body, but due to its position and weight bearing properties, also one of the most injurie and disease prone skeletal feature (Moore et al. 2010). After all, knee OA is one of the most prevalent types of arthritis affecting the world population (Cross et al. 2014). Moreover, the knee joint is often used in proof of concept studies, as a simplified biomechanical hinge joint (Seel et al. 2014), which only allows rotation about its main axis – the flexion – extension axis, making it ideal for the purpose of the current study. The motion to be analysed in the following chapters will be knee flexion-extension during dynamic walking conditions.

Amongst the most popular motion analysis tools are the marker based optical motion capture systems and their associated protocols. Optical motion capture is often performed in the laboratory with expensive equipment and using this type of equipment in a non-laboratory based environment presents significant limitations which can compromise the accuracy of the acquired data. However, the differences between the laboratory setting and a natural environment in which a movement is carried out could affect the manner in which the patient conducts himself.

It is therefore of great importance to find and validate an appropriate motion analysis tool which can be used accurately in a non-laboratory based environment, is user friendly, requires a short set up time and is cost effective.

The scope of the current thesis is to combine the use of state of the art equipment and a motion capture and computational data processing protocol which allows biomechanical analysis of human motion in a non-laboratory based environment. The purpose of the study

is to test the applicability, feasibility and reliability of using a network of wireless inertial sensors and a designated data acquisition and processing protocol to assess human knee flexion-extension during gait in a non-laboratory based environment.

Successfully validating such a technique and demonstrating that using it in a non-laboratory based environment is applicable and reliable, could not only offer an ambulatory, and more rapid, user friendly, and cost effective alternative to the optical motion capture – "silver standard", used currently in the laboratory, the applications of such a technique would be spread across numerous fields, e.g. diagnostics and prevention of disease, physical repair, ergonometry, engineering of prosthetic limbs.

1.1. Aims

The aim of the current study was to successfully validate an inertial motion capture technique against an optical motion capture technique and to test the applicability of the inertial motion capture technique in an outdoor environment.

1.2. Objectives

The objectives of the current study were to perform a series of experiments using a network of miniature wireless inertial and magnetic sensors, in conjunction with a data processing protocol, proposed by Seel et. al (2014) and described in detail in the following chapters, in order to validate the system for use in a non-laboratory based environment.

The experiments had the following purposes:

1. Ruling out any gyroscope bias.
2. Testing the accuracy of the gyroscope sensors and the methodology proposed by Seel et. al (2014) for deriving a rotation angle from gyroscope data, against a robotic setup - gold standard.
3. Testing the accuracy with which the cameras of the optical motion capture system track the markers in the measurement volume.

4. Testing the methodology proposed by Seel et. al (2014) for calculating a rotation angle by combining gyroscope and accelerometer data, against the Vicon calibration wand.
5. Validating the above mentioned method for calculating knee flexion-extension angles during gait, against the Vicon camera system – current "silver standard" for human motion capture.
6. Comparing knee flexion-extension angles from gait recorded in a laboratory- and a non-laboratory based environment, with the sensor system and processed with the protocol proposed by Seel et. al (2014).

1.3. Hypotheses

By following these objectives, the current study tested the following set of hypotheses:

H_1 – The sensor system and proposed protocol function together with high accuracy.

H_2 – There are no statistically significant differences between knee flexion-extension angles recorded during gait with the sensor system, and the ones recorded with the optical motion capture system.

H_3 – There are no statistically significant differences between knee flexion-extension angles recorded with the sensors system in the laboratory, and the ones recorded outdoors.

Chapter 2

2. Literature review

2.1. Anatomy and pathology of the human knee joint

The lower limbs of the human body (Fig 2.1), are part of the appendicular skeleton (Gerhardt et al. 2012). The leg is formed of three long bones, the femur constituting the thigh bone and the tibia and fibula constituting the bones of the lower leg (Rabuffetti and Crenna 2004).

FIG 2.1. BASIC ANATOMICAL REPRESENTATION OF THE LOWER LIMBS.
At a skeletal level, the human thigh, comprises the pelvic bones and femur, connected by the hip joint; The shank consists of the tibia and fibula, which are connected with the femur at the knee joint, and with the foot at the ankle joint. All these bones are part of the appendicular skeleton, which plays an important role in support and locomotion.

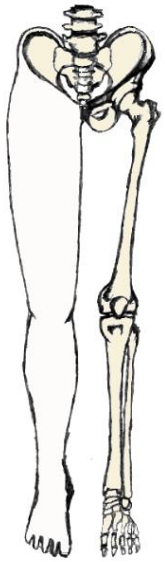

The femur (Fig 2.2A) is the largest bone in the human body. Proximally, the femur articulates with the pelvis, to form the hip joint. Distally, the femur articulates with the tibia (Fig 2.2A) to form the knee joint (Fig 2.2B)(Joseph 2014).

The femur is positioned diagonally within the thigh, forming an alignment axis along the line of force of the quadriceps femoris muscle surrounding it, which can be represented by drawing a line from the anterior superior iliac spine (ASIS) to the centre of the patella (Fig 2.2C)(Moore et al. 2010).

The tibia is almost vertically positioned within the shank, forming an alignment axis virtually parallel to the vertical gravitational axis, traversing the centre of the patella. The

alignment of the knee joint is greatly influenced by the angle between the quadriceps muscle and the patellar tendon, called the Q – angle (Fig 2.2C)(Moore et al. 2010).

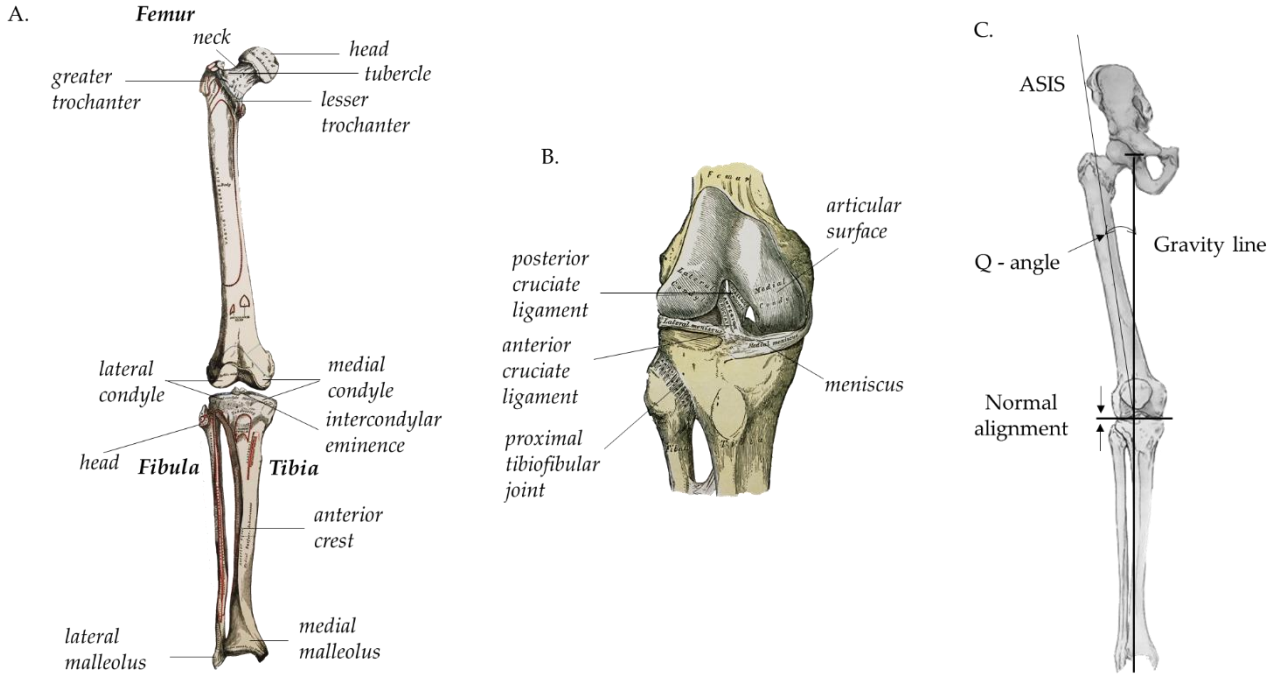

FIG 2.2. ANATOMY OF A HUMAN LEG: A. GROSS ANATOMY OF THE FEMUR, TIBIA AND FIBULA (JOSEPH 2014); B. THE KNEE JOINT (JOSEPH 2014); C. NORMAL ALIGNMENT OF A KNEE JOINT.

Distally, the femur articulates with the tibia through the cartilaginous surfaces of the lateral and medial condyles of the two bones and the surrounding soft tissue, i.e. ligaments, tendons and muscles.

The knee joint is represented by large articular surfaces, with a joint capsule consisting of a fibrous external layer and an internal synovial membrane, lining all surfaces of the articular cavity which are not covered by hyaline cartilage (Drake et al. 2012; Moore et al. 2010) .

The hyaline cartilage, covering the bony extremities of the synovial joint, lowers friction between the elements and additional structures, such as articular discs, fat pads and tendons may be present in this type of joint (Ellis 2006). The knee joint is the largest synovial joint in the human body, but it is also very vulnerable due to its complex shape, low position and weight bearing properties. However, in a healthy knee, a normal alignment of femoral

condyles and the condyles of the tibia, ensures a correct distribution of pressure and forces (Moore et al. 2010).

Mechanically, the knee is a relatively weak structure, its stability being highly dependent on the strength of the soft tissue surrounding it. The most stable position of the knee joint is when a person is standing up right and the knee is fully extended. In this position, the medial rotation of the femoral condyles on the articular surface of the tibia, creates a passive lock, which is inactivated when the femur rotates laterally to allow flexion (Moore et al. 2010).

The primary functions of the human lower limbs are support and locomotion (Drake et al. 2012; Ellis 2006; Moore et al. 2010). Functions in which the knee joints, along with the other joints of the lower limbs, play a crucial role.

Human gait, for instance, is a complex motion which, when occurring on a planar surface, can be divided in two phases, containing 7 total events. One gait cycle (Fig 2.3) consists of a stance phase (60% of the total action) and a swing phase (40% of the total action), corresponding to a single step made by one leg. It is generally accepted that the frequency of normal human gait lies within the band of 4 to 6 Hz (Antonsson and Mann 1985).

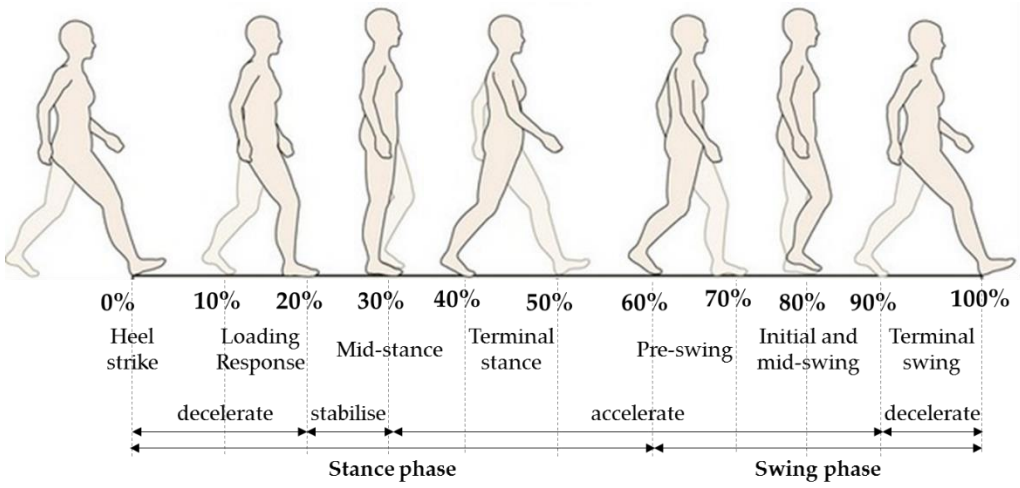

FIG 2.3. A HUMAN GAIT CYCLE.

The stance phase of a gait cycle begins when the heel of a foot strikes the floor and ends when the toes push off the ground. The immediate following swing phase starts after the foot has left the floor and ends when the heel strikes the ground again. Human walking consists of a series of gait cycles, each containing periods of acceleration, deceleration and stabilisation.

From a biomechanical point of view, joints are often classified according to their ability to move across a defined number of axes using mechanical models. The knee joint for example is often considered to be a hinge (Fig 2.4), acting like a fulcrum between two levers, represented by the femur and tibia (Moore et al. 2010; Zatsiorsky 1998).

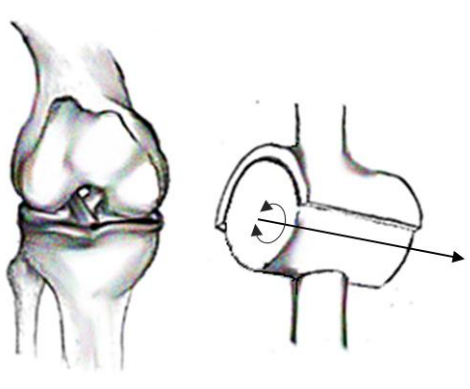

FIG 2.4. SCHEMATIC ILLUSTRATION OF A HINGE JOINT – THE KNEE.
Hinge joints are planar and allow revolution about a single axis of movement. In the case of the knee joint - the flexion-extension axis. However, when the axis of movement of a certain joint is not perpendicular to the anatomical plane, motion can occur in all three planes (Zatsiorsky 1998).

However, the movements of the knee joint are a widely discussed subject and there are at least four points of view in the literature concerning the correct identification of the flexion-extension axis of the knee joint (Zatsiorsky 1998).

The flexion-extension axis is recognized as being the main axis of rotation of the tibiofemoral joint, however, it was reported that when the knee is fully extended an endo-exo rotation of the tibia with respect to the femoral condyles occurs (Ellis 2006; Fick 1911a; Hollister et al. 1993; Moore et al. 2010). Furthermore, Hollister et al. (1993) reported that full extension of the knee is accompanied by an additional abduction-adduction of the tibia.

Firstly, based on the Reuleaux method, researchers claimed that the knee flexion-extension axis is instantaneous and displaces during motion (Blacharski and Somerset 1975; Frankel et al. 1971; Schmidt 1973; Soudan and Auderkercke 1979; Zuppinger 1904). However, this view was highly criticised by Panjabi et al. (1982), who claimed that the flawed experimental designs of the previously mentioned researchers led to inaccuracies in their results.

Secondly, a helical rather than simple rotation occurring about a flexion-extension axis, which changes its orientation during motion, and about an independent tibial endo-exo rotation axis, was suggested (Braune and Fischer 1891; Bugnion 1892; Zuppinger 1904) and later reviewed by Fick (1911b), Steindler (1955), and Strasser (1917).

However, Fick later suggested that the knee flexion-extension axis was a fixed axis located in the distal femur, traversing the lateral and medial condyle posteriorly (Fick 1911a). A hypothesis which was supported by Elias et al. (1990) findings, which further suggested an involvement of the surrounding ligaments in the motion.

Finally, Hollister et al. (1993) claimed that knee flexion-extension is indeed dependent on the movement of the collateral and cruciate ligaments and that therefore, mechanically, knee motion occurs about an infinite number of axes.

Nevertheless, most biomechanical models used in the literature for assessing motion capture data, assume a fixed flexion-extension axis for the knee (Cutti et al. 2010; Ehrig et al. 2007; Seel et al. 2014).

The physical aspects of the musculoskeletal system are, however, not the only factors concerning skeletal kinematics. On a physiological level, although often considered invariable, bones undergo constant remodelling under the influence of mechanical stimuli. Bone remodelling is, in fact, a constant balance between osteogenesis (the process of bone formation) and osteoclastogenesis (the process of bone resorption), processes which regulate bone mass and are highly dependent on mechanical stress and strain (Marieb 2009).

The effects of mechanical stimuli on the skeletal environment have been extensively studied in the past and mathematical models, such as Frost's "mechanostat", based on the theory that the human skeleton evolves for and serves mechanical needs primarily (Frost 1987), have been developed for a better understanding of this mechanism.

In Frost's view, the skeleton has an in-built mechanical feedback system which responds to increase or decrease in mechanical loading or hormonal changes by adjusting the bone mass so that it is specially distributed for optimal mechanical function (Frost 1987).

Although Frost's mathematical model took into account very important parameters, such as Young's modulus for bone, peak strain, peak stress and changes in density, it did not take into account the ability of bone cells to adapt to the environment (Brakspear and Mason 2012).

However, Turner's mathematical theory for bone biology, called " the principle of cellular accommodation" (Brakspear and Mason 2012), based on Wolff's "law of bone transformation" (Wolff 1982) and Frost's "mechanostat" (Frost 1987), offered an alternative version, which corrected for flaws discovered in the initial models (Brakspear and Mason 2012).

In 1982, Julius Wolff proposed a theory which stated that high stress-generated potentials can act as electrical stimuli for the activation of osteocyte cells within bone tissue, which in response could trigger an anabolic event following activation of bone forming cells (Wolff 1982).

Turner's "principle of cellular accommodation" corrected for the assumption in Frost's "mechanostat" that suggested that cellular sensitization is a continuous and endless process, that can eventually lead to complete loss of bone mass or ossification of bone tissue (Brakspear and Mason 2012).

In contrast to that, the "principle of cellular accommodation" stated that mechanical loading and unloading indeed stimulates bone formation and, respectively bone resorption, but that, over time the bone cells become immune to loading cycles (provided the load has an equal value over time) and their metabolic rate decreases.

Nevertheless, mechanical stress and strain are not exclusively affecting the bones within the skeletal system, but also the cartilage and surrounding tissue. Changes in the mechanical environment or properties of cartilage within a joint, can generate stimuli, which initiate degenerative processes (Boyd and Ronsky 1997; Churchill et al. 1998b; Davis and DeLuca 1996), e.g. osteoarthritis.

OA is a progressive disorder, which causes the loss of articular cartilage, exposing the joint extremities, where the direct contact between bones results in ulceration and calcification of the tissue.

OA is one of the world's leading debilitating diseases, which lowers the quality of life and can lead to immobility of the patient. The exact mechanism of OA is not clear yet,

however, there are a series of factors which researchers found to play a role in the onset, incidence and epidemiology of the disease.

For knee OA, these factors include amongst genetic background, age, gender, obesity (Felson 2004a), and occupational (Cooper et al. 1994; Maetzel et al. 1997; McMillan and Nichols 2005) or sports injuries (Roos et al. 1994), local mechanical factors affecting the integrity of the joint, such as muscle weakness, damage to the ligaments and meniscus, joint incongruity and misalignment of femoral condyles on the tibial plateau (Felson 2004b).

It has been reported that knee injury in men and obesity in women are amongst the leading and most modifiable causes of onset or progression of knee OA (Felson et al. 2000). Moreover, (Felson 2013) claimed that knee OA is almost always caused by increased forces acting on a joint and that such forces could be a result of knee malalignment (Felson and Hodgson 2014) or a combination of malalignment and obesity (Felson et al. 2004). Causes which can be addressed and treated in order to prevent progression or onset of OA, if identified in timely manner (Felson and Hodgson 2014; Teichtahl et al. 2009).

Genu varum (bowed-legs) and genu valgum (knocked-knees) are both conditions in which the alignment of the knee is affected. Genu varum is defined by a decreased Q-angle (Moore et al. 2010), and is reported to increase mechanical loading in the medial knee compartment by 70-79% (Tetsworth and Paley 1994) even in cases where the varum is as little as 5°, which can lead to substantial cartilage loss (Sharma et al. 2008; Teichtahl et al. 2009) and the onset of OA (Brouwer et al. 2007).

In contrast, genu valgum is defined by an increased Q-angle (Moore et al. 2010), which is reported to in increases loading in the lateral knee compartment, thereby, increasing the risk of progressive OA 5 fold (Sharma et al. 2001; Teichtahl et al. 2006).

Furthermore, Hsu et al. (1990) and Kettelkamp et al.(1976) report a correlation between medial lateral forces and knee alignment during standing which, however, is only present in genu varum sufferers during gait (Harrington 1983).

Motion analysis has proved to be a useful tool in the study of lower limbs kinematics and disorders of knee (Andriacchi et al. 1983; Berchuck et al. 1990; Draganich et al. 1991;

Kettelkamp et al. 1976; Noyes et al. 1992; Wang et al. 1990) and increasingly more researchers use motion capture systems and biomechanical computational models for the purpose of quantifiable and numerical motion analysis (Alexander and Andriacchi 2001; Bonci et al. 2015; Cappozzo et al. 2005; Cereatti and Della Croce 2006; Cutti et al. 2010; Davis et al. 1991; Ehrig et al. 2007; Ferrari et al. 2010a; Garofalo et al. 2009; Haid and Breitenbach 2004; Kratzenstein et al. 2010b; Leardini et al. 2005; Luinge et al. 2012; Pasciuto et al. 2015; Roetenberg et al. 2003; Schepers et al. 2010; Seel et al. 2014; Taylor et al. 2005).

2.2. Motion capture systems and protocols

During the past decades, quantifiable motion analysis has been widely studied and the need for developing a low cost and user friendly technique, which enables motion capture in a non-laboratory based environment, has been emphasised time and time again (Calliess et al. 2014; Gaffney et al. 2011; Liu et al. 2011; Pfau et al. 2005; Soangra and Lockhart 2012; Vlasic et al. 2007; Wixted et al. 2010; Yang et al. 2011; Zhou and Hu 2004, 2008).

Quite a few motion capture systems were developed in order to aid motion studies. These systems were reviewed extensively (Frey et al. 1996; Hightower and Borriello 2001; Meyer et al. 1992; Welch and Foxlin 2002) and can be largely classified in the following categories: robot aided, visual and non-visual (Vlasic et al. 2007; Zhou and Hu 2004, 2008).

Robot aided motion capture

This technique employs the use of electromechanical systems, such as Gypsy™ (Meta Motion) and ShapeWrap™ (Measurand), called exoskeletons, which the subjects are required to wear, in order to compute joint angles from electric resistance. These systems are not restricted to laboratory use, however, they are uncomfortable and motion restricting even in the most updated versions of the hardware (Vlasic et al. 2007).

Visual motion capture

Visual tracking is a camera based technique, which can be carried out with marker free systems, marker based systems or a method combining the two.

Marker free optical motion capture is based on using high speed, high accuracy camera systems to detect object movement (Bregler and Malik 1998; Chen et al. 2005; Davison et al. 2001).

The Microsoft Kinect (versions 1 and 2) for instance, combines the use of infrared cameras and infrared light emitters to visually track the movement of joints to which the emitters are attached.

Another marker free visual tracking method is the video pixel change motion extraction, which tracks the movement of a subject by quantifying the amount by which pixels change between adjacent frames of a video capture (Kupper et al. 2010; Paxton and Dale 2013; Schmidt et al. 2012).

These methods are non-constricting and cost effective, however, require extensive post processing of data and are subject to data latency (Romero et al. 2014; Stone and Skubic 2011). Furthermore, research shows that these motion capture methods are less accurate and robust than their magnetic (Romero et al. 2014) and marker based counterparts (Stone and Skubic 2011).

Biomechanical studies are often performed by means of optical marker based motion tracking systems (Bishop 1984; Davis et al. 1991; Woltring 1973), which determine the position and orientation of reflective markers within a local laboratory based coordinate system (Schepers et al. 2010). This reflective marker method has proven to be very effective (Alexander and Andriacchi 2001; Ehrig et al. 2006, 2007; Gastaldi et al. 2015; Leardini et al. 2005; Taylor et al. 2005), when used for 3D motion capture with infrared cameras, which is the most commonly used method to minimize light artefacts.

However, in order to associate the recorded marker trajectories to human motion, not only extensive data processing is required, but also the use of predefined marker position protocols, in order to facilitate the virtual reconstruction of a human biomechanical model.

For this purpose, a variety of marker position protocols have been developed, in order to associate the motion of the recorded marker set to skeletal motion, such as the 'Newington model' (Davis et al. 1991; Kadaba and Ramakrishnan 1990), from which the Plug-in Gait software package derived (Vicon Motion Systems, Oxford Metrics), the 'Servizio di Analisi della Funzione Locomotoria' (SAFLo) protocol (Frigo et al. 1998), the 'Calibration Anatomical System Technique' (CAST) (Benedetti et al. 1998; Cappozzo 1984; Cappozzo et al. 1995), the 'Laboratorio per l'Analisi di Movimento nel Bambino' (LAMB) protocol (Rabuffetti and Crenna 2004), and the 'Istituti Ortopedici Rizzoli Gait' protocol, on which the 'Total 3D Gait' (T3Dg) (Aurion) software package was based.

These protocols were, however, all derived from the 'Newington' model (Fig 2.5), and are based on identifying specific bone structures or landmarks and then positioning the markers in their vicinity. Geometric regression relationships are then used to estimate the joint centre location with respect to the position of specific markers placed on the adjacent anatomical segments (Davis et al. 1991; Kadaba and Ramakrishnan 1990).

However, such regression models are subject to substantial errors (Bell et al. 1990), due to bony deformities, skeletal differences between genders (Dandachli et al. 2009; Shultz et al. 2008) and differences in marker placement, which cannot be accounted for in data post processing protocols.

Additionally, Ferrari et al. (2008) have reviewed and compared the above mentioned protocols and concluded that, although the correlation between the protocols is very good, despite differences in marker positioning and data reduction and processing, these methods are susceptible to a phenomenon called the "cross-talk effect", in which segment axis misalignments lead to severe overestimation of the varus-valgus and endo-exo rotation of the knee and, thereby, affect the accuracy of the flexion extension estimates (Chao 1980; Ramsey and Wretenberg 1999).

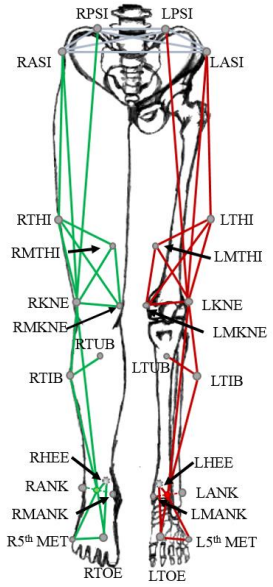

FIG 2.5. REFLECTIVE MARKER SET-UP FOR OPTICAL MOTION CAPTURE – AN EXTENSION OF THE NEWINGTON MODEL.

Where additional markers were used in order to reduce cross-talk effect. In this model markers were placed on the left (L) and right (R) side of the anterior superior iliac spine (ASI), posterior superior iliac spine (PSI), the lateral (THI) and medial (MTHI) thigh, the lateral (KNE) and medial (MKNE) femoral condyle, the anterior superior tibia (TUB), the lateral superior tibia (TIB), the medial (MANK) and lateral (ANK) malleolus, the heel (HEE), and the 1st (TOE) and 5th metatarsals (5th MET).

These findings concurred with other studies (Baker et al. 1999; Blankevoort et al. 1988; Della Croce et al. 1999; Hollister et al. 1993; Piazza and Cavanagh 2000; Ramakrishnan and

Kadaba 1991; Woltring 1994) and different protocols had to be implemented to correct for this cross-talk effect (Baker et al. 1999; Besier et al. 2003; Ehrig et al. 2007; Marin et al. 2003).

For example the flexion-extension axis of the knee is often used to characterise the function of the knee joint (Asano et al. 2005; Churchill et al. 1998a; Li et al. 2002; Piazza et al. 2004). The axis of rotation can provide a time dependant anatomical reference to rotational motion and there are currently a few approaches commonly used when estimating the knee flexion-extension axis from marker data.

These approaches involved the identification of the knee flexion-extension axis, by employing different methods, such as defining the axis as being a finite helical axis (Marin et al. 2003), an instantaneous helical axis (Boyd and Ronsky 1997) or an optimal helical axis (Churchill et al. 1998a). Reproduced in methods such as the knee alignment device (Davis and DeLuca 1996), the transepicondylar axis method (Cappozzo et al. 1995) and the dynamic optimisation procedure (Schache et al. 2006). The latter one being by far superior in accuracy compared to the other methods (Schache et al. 2006).

Woltring's instantaneous helical axis mathematical algorithm is based on the assumption that the total amount of translations and rotations along a path of motion can be represented by time integrals of instantaneous translation and rotation velocities from a given reference in time (Woltring et al. 1985).

Further, the finite helical axis approach (Kelkar et al. 2001), based on the theory of (Woltring et al. 1985) on the instantaneous helical axis, estimates the movement of the joint axis between two time increments. This approach is often used in research for time dependent joint parametrisation.

Some optimisation based approaches function on the assumption that one of the anatomical segments forming the joint is at rest and that the other segment is moving with respect to the first one. Cylindrical arcs are fitted to the orbits of the moving segment markers to track the motion of each marker in a time dependent manner and to estimate the axis of rotation from that information (Gamage and Lasenby 2002; Halvorsen et al. 1999).

However, current approaches often require that the local coordinate system of one segment has to be transformed in the local coordinate system of the other segment forming the joint, in order to use a global reference frame. Therefore, any artefacts and errors are transferred and propagated, producing inaccuracies in the estimation of the axis of rotation.

Recently, more robust, accurate and rapid methods to determine functional joint centres and axes have been developed, such as the Symmetrical Centre of Rotation Estimation (SCoRE)(Ehrig et al. 2006) and the Symmetrical Axis of Rotation Approach (SARA)(Ehrig et al. 2007).

The SCoRE technique is based on the assumption that the joint centre must only remain constant with respect to the segments forming the joint, and therefore does not require that one of the segments remains fixed when calculating the centre of rotation from kinematic marker data.

This is a symmetrical mathematical approach, in which the joint centre is represented in the local coordinate systems of both adjacent anatomical segments. This method has proven to be the most rapid, robust and accurate technique available yet for estimating joint centres from marker data (Ehrig et al. 2006; Rozumalski and Schwartz 2008).

However, when transforming the biomechanical model from local to global reference frame, any small imperfection in the manner in which the movement was executed can result in substantial misalignments of the two centres of rotation expressed in the adjacent anatomical segments.

In order to deal with this issue, a solution has been proposed in which a quality index has been provided for the estimation of the centres of rotation from marker data, by using computer simulation to find a relationship between the mean error of the globally estimated joint position and the residual of underlying linear least squared problem (Kratzenstein et al. 2010a).

Further, an estimation of the axis of rotation technique is used when analysing joints which have a more complex pattern of movement and which require a more detailed definition of movement than what the joint centres can offer by themselves.

The SARA technique is capable of determining a unique axis of rotation, by considering the rotational movement of the marker sets on two dynamic anatomical segments independently, and by including a rotation and transformation term for the second segment. This approach has the benefit that no prior coordinate system transformation is needed (Ehrig et al. 2007).

Although, these techniques perform more accurately than most of the previously mentioned ones (Ehrig et al. 2007), there remains an important issue which needs to be addressed when using any marker based motion capture technique: the soft tissue artefacts (STA) (Cereatti and Della Croce 2006; Kratzenstein et al. 2010b; Taylor et al. 2005), produced by the displacement of an individual marker with respect to the marker cluster, or by the movement of the marker cluster with respect to the underlying bones, which can result in poor reliability of the method in clinical gait analysis (Schwartz and Rozumalski 2005).

Furthermore, the skin movement displaces the position of the markers with respect to joints, causing errors when estimating the functional centres of rotation (Cappozzo et al. 1996; Cereatti and Della Croce 2006; Leardini et al. 2005) and the higher the soft tissue coverage in a subject, the higher the error.

Due to the significant issue that STA pose, a few techniques have been developed to help reduce their effect on the final output data, e.g. Point Cluster Technique (Alexander and Andriacchi 2001) and Optimal Common Shape Technique (OCST) (Taylor et al. 2005).

The OCST, for example, is based on using a Procrustes Analysis (Dryden and Mardia 1998) to minimise the motion of the markers with respect to one another, by generating a rigid configuration of the segment marker set formed from all time frames of one motion trial. The original marker set from the motion trial is then replaced with the OCST configuration.

Furthermore, in a study which meant to determine a correlation between centre of rotation estimation errors and SCoRE residuals in spherical joint, Ehrig et al. (2011) demonstrated that using the OCST in conjunction with the SCoRE method significantly improves the centre of rotation output.

Additionally, Taylor et al. (2010) demonstrated that the OSSCA method, which employs a combined use of OCST, SCoRE, and SARA techniques to process marker data and allows the estimation of joint parameters from kinematic data alone, without the necessity to use generic anatomical relationship assumptions, returns more reliable, repeatable and reproducible results than a standard generic regression approach.

Although the accuracy of the data acquired by means of optical motion capture systems is very high in the controlled environment of the lab, the ambulatory use of this type of equipment is cumbersome and presents significant limitations which can not only compromise the precision of the acquired data, e.g. dependency on line-of-sight, limited range and latency of data (Schepers et al. 2010), but also the practicability of the acquisition itself, e.g. necessity of power source, set-up time, outdoor calibration of the system.

Non-visual motion tracking

Non-visual motion tracking is a sensor based technique, which can be carried out, amongst others, with acoustic, magnetic, or inertial sensors, or with a combination of these methods.

Ultrasound based acoustic systems, e.g. 'the Bat system' (Ward et al. 1997), 'Vallidis' (Hazas and Ward 2002), 'the Cricket location system' (Priyantha et al. 2000) and 'WearTrack' (Foxlin and Harrington 2000), are capable of tracking the locations of pulse emitting beckons by using the time-of-flight information of audio signals.

This type of motion tracking system is wireless, however, as with visual motion tracking, occlusion of the signal emitter poses a significant limitation.

In contrast, magnetic systems, e.g. MotionStar® (Ascension Technology), are capable of estimating their position and orientation within the global coordinate system, by using information from the local magnetic environment, and are, therefore, not constricted by line-of-sight. However, these systems are very sensitive to ferromagnetic interferences.

Inertial motion capture systems, e.g. Moven (Xsens Technologies) and Alert (Verhaert), employ the use of accelerometer and gyroscopes to measure inclination angles.

These systems are highly accurate, however, sensitive to vibration and subject to integration drift over time.

In fact, throughout the past decade, the use of inertial sensors has gained increased popularity within researchers (Foxlin 1996; Roetenberg et al. 2007a; Roetenberg et al. 2005; Roetenberg et al. 2009; Roetenberg et al. 2003; Roetenberg et al. 2007b; Roetenberg and Veltink 2005), as well as general population.

Many people schedule their daily activity based on the data presented by certain applications on their smartphones (e.g. Health app, Argus, MyFitnessPal), their smartwatches (e.g. Sony, LG, AppleWatch, Fitbit Surge) or pedometers and wristbands (e.g. Fitbit Flex, Garmin vivofit, Polar Loop, Jawbone).

However, in the field of research, there is a need for more complex systems, which can provide more comprehensive information, of a larger variety.

For this purpose, hybrid systems, combine the use of different techniques to compensate for the shortcomings of individual systems. Such hybrid systems are represented by acoustic-inertial systems (Vlasic et al. 2007; Ward et al. 2005), e.g. Constellation™ (Foxlin et al. 1998), optical-inertial systems, e.g. Hy-Bird™ (Ascension Technology) and inertial-magnetic systems, e.g. MERG sensors (Bachmann 2000), MTw development kit (Xsens Technologies), MVN Biomech and MVN Awinda (Xsens Technologies).

Combined inertial and magnetic sensing is currently one of the more popular choices in this area of study and will be discussed at length in the following paragraphs.

The light weight, wireless and cheap, inertial sensors equipped with accelerometers, gyroscopes and magnetometers enable, when positioned on the human body, the computation of angular orientation of the anatomical segments to which they are attached to (Guergueltcheva et al. 2012; Roetenberg et al. 2003).

The on-board gyroscopes measure angular velocity, based on the principle of angular momentum, according to the following fundamental equation:

$$\tau = \frac{dL}{dt} = \frac{dI\omega}{dt} = I\alpha \quad (1)$$

Where: τ – torque on the gyroscope; L – angular momentum; I – moment of inertia; ω – angular velocity; α – angular acceleration.

The most commonly used gyroscopes for human motion studies are piezo-electric, capable of detecting vibration of mass.

When an object vibrates while rotating, it is subject to the Coriolis Effect. This causes a second vibration to occur orthogonally to the initial vibration direction. The rate of turn can be calculated from this latter vibration. According to the following equations:

$$F_c = -2m\,(\omega * v) \quad (2)$$

Where: m – mass; v – momentary speed of the mass with reference to the moving object to which it is attached.

The resulting gyroscope signals are then defined as being the sum of angular velocity ω_t, offset due to temperature of gyroscope b_t, and white noise $v_{G,t}$ (Eq. 3).

$$y_{G,t} = \omega_t + b_t + v_{G,t} \quad (3)$$

The gyroscope output is very accurate, however, it is subject to errors and drift caused by integration of the signal over time, and the gyroscope temperature which can produce small offset errors, leading to large integration errors when calculating orientation. The use of compensatory estimation algorithms, such as Kalman filters can reduce the inherent errors in the gyroscope output signal (Roetenberg et al. 2003).

Kalman filters are mathematical algorithms used to efficiently minimize the mean of the squared error of a system output (Welch and Bishop 1995). Kalman filters are particularly useful for combining parameters of different measurement systems so that the advantages of one compensates for the weakness of the other, e.g. accelerometers are often used in conjunction with gyroscopes, in order to compensate for inclination drifts in the gyroscope signal.

The accelerometers measure the gravitational acceleration g and the vector sum of acceleration a. The output accelerometer signals are defined as the sum of acceleration a_t, gravity g_t and white noise $v_{A,t.}$

$$y_{A,t} = a_t + g_t + v_{A,t} \quad (4)$$

The inclination information provided by g_t can be used to correct the orientation drifts of the gyroscope (Roetenberg et al. 2003). A further common example of Kalman filtering, is using magnetometer readings to correct for the gyroscope's vertical axis drifts (Roetenberg et al. 2003).

Magnetometers have the ability to detect local magnetic north and adjust heading direction. The principles by which the magnetometers work are described by following equation:

$$y_{M,t} = m_t + d_t + v_{m,t} \quad (5)$$

Where: $y_{m,t}$ – magnetic signals;

m_t – earth magnetic field vector;

d_t – disturbance vector;

$v_{m,t}$ –white noise.

In real life measuring conditions the distribution of the magnetic field is often more complex and other parameters, such as changes in magnetic flux and the magnetic inclination angle, which can affect the magnitude of the magnetic disturbance, should be taken in consideration.

The major limitations of using inertial and magnetic sensing for motion tracking are represented by the following factors:

- Ferromagnetic interferences can distort the local magnetic field and affect the measurements for the orientation about the vertical axis (Roetenberg et al. 2003).
- The velocity and type of movement performed and the geometry of the body segment to which the sensor is applied can affect the accuracy of the measurements

(Roetenberg et al. 2005). This is true especially for very low or very high frequency movements;

- Distances between body segments cannot be assessed by means of numerical integration (Roetenberg and Veltink 2005);

Previous studies in which this type of equipment was used report a high accuracy of the output data when compared to the optical motion capture (current silver standard) counterparts (Brennan et al. 2011b; Cooper et al. 2009; Cutti et al. 2010; Favre et al. 2008; Ferrari et al. 2010a; Liu et al. 2009; Seel et al. 2014; Takeda et al. 2009; Van den Noort et al. 2013a; Zhang et al. 2013). However, the limitations of using this motion capture system are far from being overcome, as the majority of the studies mentioned above either had an insufficient number of participants, or lacked sufficient statistical analysis to validate a sensor system against optical motion capture. Additionally, there were some important aspects of sensor based human motion capture which were ignored or not treated appropriately in the majority of the studies in the literature. These issues will be discussed further in the following paragraphs.

The most important and challenging aspect of human motion capture is to use the acquired information in a biomechanically meaningful manner, e.g. the parameters declared as joint angles, need to be as anatomically accurate as possible, for this purpose assuming the joint angles can be calculated as the angles of movement between two anatomical segments is not enough, a more complex mathematical model needs to be developed in order to address the biomechanical characteristics of the studied joint.

There are a variety of protocols and algorithms available for post processing of sensor data stemming from human motion studies. A common approach for solving a human kinematics problem is to compare the human body to a robot manipulator.

Similarly, to a robot manipulator, which forms a kinematic chain from links interconnected by joints, the human body can be considered a kinematic chain formed of anatomical segments connected by articulations. In theory, this is a very efficient manner to solve a biomechanical problem.

Cutti et al., for example, use the Denavit-Hartenberg convention of robotics in their "Outwalk" protocol, which states that a kinematic chain with n joints will have n+1 links (Fig 2.6). To solve the kinematics, a coordinate system is rigidly attached to each link. In this case, when joint $\boldsymbol{j_i}$ is actuated, the adjacent $\boldsymbol{link_i}$ and its attached coordinate frame $\boldsymbol{o_i x_i y_i z_i}$ perform a motion. Whichever motion is performed by the kinematic chain, the coordinates of each point on $\boldsymbol{link_i}$ are constant when expressed in the $\boldsymbol{i^{th}}$ coordinate frame (Zatsiorsky 1998).

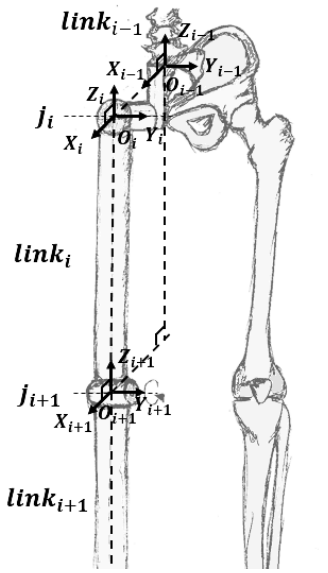

FIG 2.6. THE DENAVIT-HARTENBERG CONVENTION FOR ROBOTICS APPLIED TO A HUMAN MODEL.
In a kinematic chain with n joints and n+1 links, each joint connects two links. The joints are numbered from i to n and the links are numbered from i-1 to n, starting from the root, which is fixed. The Denavit-Hartenberg conditions, which are necessary for solving the kinematic model are: (1) $x_i \perp z_{i-1}$ and (2) $x_i \cap z_{i-1}$.

The Denavit-Hartenberg convention has two conditions which need to be satisfied in order for the kinematic solution to be effective. The variables of a joint (e.g. rotation angles) are defined by the two coordinate systems of the links adjacent to the joint. So, for example, the coordinates of the $\boldsymbol{i^{th}}$ frame are expressed in the $\boldsymbol{i-1^{th}}$ frame. Firstly, the orthonormality of the frames needs to be established, meaning $\boldsymbol{x_i}$ needs to be perpendicular to $\boldsymbol{z_{i-1}}$. Secondly, the projection of $\boldsymbol{x_i}$ in the $\boldsymbol{i-1^{th}}$ frame ought to intersect $\boldsymbol{z_{i-1}}$.

Comparing the human body to a robotics model is a good starting point. However, using the, frequently associated, strap-down integration method when measuring human kinematics with sensing units poses a very important limitation (Seel et al. 2014).

The strap-down-integration method is based on using sensing units securely fixed to the even surfaces of robotic elements. However, there is a significant difference between a robotic setup and an anatomical system.

Firstly, aligning the sensor to an anatomical location, such that one axes of the sensor coordinate system coincides exactly with an axis of the anatomical joint, is nearly impossible (Seel et al. 2014). This issue has been addressed in different manners by researchers so far.

In the "Outwalk" protocol, Cutti and Ferrari et al. define as many coordinate frames for each link as the joints they form. Each anatomical segment has, therefore, a distal and a proximal coordinate frame. The joint variables are defined by the distal coordinate frame of one segment and the proximal coordinate frame of its adjacent segment.

Another issue that needs to be addressed, when discussing a human biomechanical model, is an almost certain misalignment of the thigh axis with the segments' coordinate system. Some studies completely ignore the misalignment between the anatomical and the sensor axes (Seel et al. 2014).

In the "Outwalk" protocol this problem is solved by expressing the flexion-extension axis of the knee in the coordinate system of the distal femur and defining the other revolution axes of the coordinate frame as being orthogonal with respect to the new axis.

This is another promising approach, however, in order for this method to be effective, the knee flexion-extension axis needs to be accurately identified.

In the case of hinge joints, such as the simplified model of a knee joint, it is possible to calculate data from inertial sensors attached to both ends of the joint. However, this resulting data still needs to be translated into joint related coordinate systems and although, it is impossible to determine the initial position of the sensors on the anatomical segment, there is a possibility to determine the direction of the joint axes, by using different approaches to identify a functional movement axis from a set of dynamic motion data (Cutti et al. 2010; Ferrari et al. 2010a; Seel et al. 2014).

In their protocol Cutti and Ferrari et al. use Woltring's mathematical solution for determining the finite helical axis (reviewed in (Zatsiorsky 1998)) to identify the knee flexion-extension axis. Woltring's solution appears to be fitting at least for most motion capture systems (Seel et al. 2014). However, the sensing units used in the current study cannot

measure translation, and in order to apply Woltring's mathematical solution appropriately, the use of both rotation and translation data is needed.

Seel et al. offer a solution based on rotational angle estimates alone, which is not only more simple from a data acquisition and processing point of view, but also functions on principles similar to the SARA and SCoRE techniques, which the current study will employ for processing the optical motion capture data.

In the protocol proposed by Seel et al. the knee is assumed to be a simple hinge, with one sensor attached to each segment forming the joint. In order to compensate for the lack of information concerning the initial position of the sensors on the anatomical segments, the unit length direction vectors and the orientations of the two segments attached to the hinge joint (Fig 2.7) are estimated as described below.

The Seel et al. solution only employs the use of what is considered to be "raw" accelerometer and gyroscope output data from the two sensors, the thigh sensor and the shank sensor. In reality, any output data produced by the Xsens sensors, used in Seel et al.'s study and the current study, is pre-processed in real-time by the on-board Kalman filter.

For the purpose of the summary of the following protocol, all data indexed with 1 refers to thigh sensor data and data derived there from, and all data indexed with 2 refers to shank data and data derived there from.

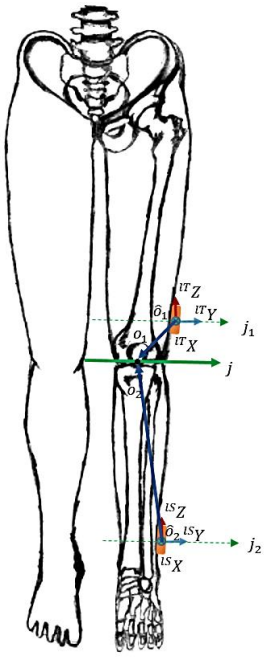

FIG 2.7. REPRESENTATION OF UNIT LENGTH DIRECTION VECTORS AND JOINT CENTER ESTIMATIONS, FROM SENSING UNITS.

The direction of the knee flexion extension axis (j) is measured by looking at the unit length direction vectors (j_1 ; j_2) of the transverse (Y) axis of the left thigh, and shank sensing units with the coordinate frames $\hat{\boldsymbol{o}}_{\boldsymbol{1}}{}^{\boldsymbol{lT}}\boldsymbol{X}^{\boldsymbol{lT}}\boldsymbol{Y}^{\boldsymbol{lT}}\boldsymbol{Z}$ and $\hat{\boldsymbol{o}}_{\boldsymbol{2}}{}^{\boldsymbol{lS}}\boldsymbol{X}^{\boldsymbol{lS}}\boldsymbol{Y}^{\boldsymbol{lS}}\boldsymbol{Z}$, respectively. The vectors from the knee joint center to the origins of the two sensing units are represented by the points $\boldsymbol{o_1}$ and $\boldsymbol{o_2}$, respectively.

Firstly, the unit length direction vectors of the flexion-extension axis of the knee $\boldsymbol{j_1}, \boldsymbol{j_2} \in \mathbb{R}^{\boldsymbol{2}}$, are identified in the local coordinates of the sensors, by using an optimisation algorithm to compute the values of $\boldsymbol{j_1}$ and $\boldsymbol{j_2}$. Where the spherical coordinates for $\boldsymbol{j_1}, \boldsymbol{j_2}$ are:

$$\mathrm{j}_1 = (\cos(\phi_1)\cos(\theta_1),\ \cos(\phi_1)\sin(\theta_1),\ \sin(\phi_1))^{\mathrm{T}} \tag{6}$$

$$\mathrm{j}_2 = (\cos(\phi_2)\cos(\theta_2),\ \cos(\phi_2)\sin(\theta_2),\ \sin(\phi_2))^{\mathrm{T}} \tag{7}$$

With the following sum of squared errors:

$$\Psi(\phi_1, \theta_1, \phi_2, \theta_2) \coloneqq \sum_{\mathrm{i}=1}^{\mathrm{N}} \mathrm{e}_\mathrm{i}^2;\ \mathrm{e}_\mathrm{i} = \left\|\mathrm{g}_{1(\mathrm{t_i})} \times \mathrm{j}_1\right\|_2 - \left\|\mathrm{g}_{2(\mathrm{t_i})} \times \mathrm{j}_2\right\|_2 \tag{8}$$

A search function is then used to find $\boldsymbol{j_1}$ and $\boldsymbol{j_2}$ which satisfy the following condition:

$$\left\|\mathrm{g}_{1(\mathrm{t})} \times \mathrm{j}_1\right\|_2 - \left\|\mathrm{g}_{2(\mathrm{t})} \times \mathrm{j}_2\right\|_2 = 0\ \forall\ \mathrm{t} \tag{9}$$

Where: $\boldsymbol{g_{1(t)}}, \boldsymbol{g_{2(t)}} \in \mathbb{R}^{\boldsymbol{2}}$ angular rates recorded by the thigh and shank sensor, respectively, with the sample period: $\Delta\boldsymbol{t}$, $(\Delta\boldsymbol{t}|\boldsymbol{t_{i+1}} - \boldsymbol{t_i})\ \forall\ \boldsymbol{i}$; $\boldsymbol{j_1}, \boldsymbol{j_2}$ – constant; $\|\cdot\|_2$ – Euclidean norm.

The acceleration measured by each sensor $\boldsymbol{a_1}, \boldsymbol{a_2} \in \mathbb{R}^{\boldsymbol{2}}$ is the sum of the acceleration due to movement around the joint centre and the acceleration due to the rotation of the sensor around the joint centre.

In order to estimate the knee joint position $\boldsymbol{o_1, o_2} \in \mathbb{R}^2$ expressed in the local coordinate systems of the sensors, the amounts by which $\boldsymbol{a_1, a_2}$ are shifted in order to obtain the acceleration of the joint centre, are estimated first.

Two arbitrary points along the $\boldsymbol{j}$ axes $\boldsymbol{\hat{o}_1, \hat{o}_2}$ are estimated using a Gauss-Newton optimization algorithm. These points are shifted as close as possible to the sensor origin by applying:

$$o_1 = \hat{o}_1 - j_1 \cdot \frac{\hat{o}_1 \cdot j_1 + \hat{o}_2 \cdot j_2}{2} \tag{10}$$

$$o_2 = \hat{o}_2 - j_2 \cdot \frac{\hat{o}_1 \cdot j_1 + \hat{o}_2 \cdot j_2}{2} \tag{11}$$

The radial and tangential acceleration due to the rotation of the sensor around the joint centre is computed:

$$\Gamma_{g_{i(t)(o_i)}} \coloneqq \quad g_{i(t)} \times \left(g_{i(t)} \times o_i\right) + \dot{g}_{i(t)} \times o_i \; ; \; i=1,2 \tag{12}$$

Where: $\boldsymbol{\dot{g}_{1(t)}, \dot{g}_{2(t)}} \in \mathbb{R}^2$ are time derivatives for angular rate and

$$\dot{g}_{(t)} = \frac{g(t-\Delta 2t) - 8g(t-\Delta t) + 8g(t+\Delta t) - g(t+2\Delta t)}{12\Delta t} \tag{13}$$

The following sum of squared errors is calculated:

$$\Psi\,(o_1, o_2) \coloneqq \sum_{i=1}^{N} e_i^2; \; e_i = \left\| a_{1(t)} \times \Gamma\, g_{1_{(t)(o_1)}} \right\|_2 - \left\| a_{2(t)} \times \Gamma\, g_{2_{(t)(o_2)}} \right\|_2 \tag{14}$$

A search function is used to find $\boldsymbol{o_1}$ and $\boldsymbol{o_2}$ which satisfy the following constrain:

$$\left\| a_{1(t)} \times \Gamma\, g_{1_{(t)(o_1)}} \right\|_2 - \left\| a_{2(t)} \times \Gamma_{g_{i(t)(o_i)}} \right\|_2 = 0 \; \forall \; t \tag{15}$$

The knee flexion/extension angle based on the gyroscope information is calculated with the following equation:

$$\alpha_{gyro(t)} = \int_0^t (g_1(\tau) \cdot j_1 - g_2(\tau) \cdot j_2) d\tau \quad (16)$$

The measured accelerations are shifted onto the joint axes by applying the following:

$$\tilde{a}_{1\,(t)} = a_{1(t)} - \Gamma\, g_{1_{(t)(o_1)}} \quad (17)$$

$$\tilde{a}_{2\,(t)} = a_{2(t)} - \Gamma\, g_{2_{(t)(o_2)}} \quad (18)$$

Where, $\tilde{a}_{1/2\,(t)}$ represent the same quantity in the local coordinate systems of the two sensors, which rotate with respect to each other around the flexion-extension axis.

The flexion/extension angle calculated according to acceleration data $\alpha_{accel\,(t)}$ can be defined as the angle between the projections of $\tilde{a}_{1\,/2(t)}$.

$$\alpha_{accel\,(t)} = \measuredangle 2d \left(\begin{bmatrix} \tilde{a}_{1\,(t)} \cdot x_1 \\ \tilde{a}_{1\,(t)} \cdot y_1 \end{bmatrix}, \begin{bmatrix} \tilde{a}_{2\,(t)} \cdot x_2 \\ \tilde{a}_{2\,(t)} \cdot y_2 \end{bmatrix} \right) \quad (19)$$

Where, $x_{1/2}$ and $y_{1/2} \in \mathbb{R}^3$ are pairs of joint plane axes, defined by:

$$x_1 = j_1 \times c;\; y_1 = j_1 \times x_1;\; c_1 \nparallel j_1; \quad (20)$$

$$x_2 = j_2 \times c;\; y_2 = j_2 \times x_2;\; c_2 \nparallel j_2; \quad (21)$$

The knee flexion/extension angle defined by fusing the accelerometer and gyro data is defined by:

$$\alpha_{accel+gyro\,(t)} = \lambda \cdot \alpha_{accel\,(t)} + (1-\lambda)\left(\alpha_{accel+gyro\,(t-\Delta t)} + \alpha_{gyro\,(t)} - \alpha_{gyro\,(t-\Delta t)}\right),\; \lambda \in [0,1] \quad (22)$$

Where: $\alpha_{accel\,(t)}$ - knee flexion extension angle calculated according to accelerometer data at time t; $\alpha_{gyro\,(t)}$ - knee flexion extension angle calculated according to gyroscope data at time t; λ – the weight of the accelerometer data.

While the data processing protocol proposed by Seel et al. presents a sound theoretical background and promising results, the study only had one participant. In order to appropriately test reliability, repeatability and reproducibility of the protocol, and in order

to perform statistical comparative studies between the protocol and optical motion capture systems, a far larger sample size and multiple testing sessions are required.

Furthermore, while this protocol provides a suitable alternative for joint axes and joint centre estimation, the issue regarding soft tissue artefacts remains unaddressed. The data stemming from the skin mounted sensors is, however, at least as much affected by STA as marker data, as the muscle movement, below the skin, produces vibrations to which the inertial sensors are susceptible.

Unfortunately, the literature, regarding management of STA in inertial sensing is very sparse and the only recommendations regarding this subject are to employ the use of light weight sensors and to attach the sensors to the anatomical segments as tight as possible, while still allowing un-constricted movement for the participant (Forner-Cordero et al. 2008; Nokes et al. 1984; Saha and Lakes 1977; Trujillo and Busby 1990; Ziegert and Lewis 1979).

By using the most effective methods presented in the literature review, the current study managed to validate the inertial sensor protocol proposed by Seel et. al (2014) against a OSSCA method and compared laboratory and non-laboratory based inertial motion capture, as well as tested reliability, repeatability and reproducibility of the Seel et al. protocol.

Chapter 3

3. Experiment 1: gyroscope accuracy

The first experiment of this study involved testing the accuracy of the gyroscopes within the sensors against a calibrated robotic arm. Although, the manufacturers guaranteed a high accuracy of their equipment, errors and inconsistencies in the data could stem from various sources and sometimes faulty equipment could be a source of error itself.

Fortunately, since inertial sensor units' measurements errors are widely studied, there are several methods to address issues and correct for them. The nature of these errors can vary from deterministic, to persistent non-zero inertial gyroscope integration.

In a recent study, Pasciuto et al. (2015) have made a review of how deterministic (systematic) errors can be addressed. For example, a constant bias of gyroscope data can be accounted for by placing the sensor on a flat surface and averaging the gyroscope signal obtained during a 20 second data capture.

Another deterministic gyroscope error worth measuring is the scale factor. The scale factor is defined as the ratio between the angular velocity given by the gyroscope data and a predefined angular velocity. A large scale factor can be caused by errors affecting the calibration of the sensor during manufacturing. Pasciuto et al. (2015) have found in their study that during gait analysis, the shank sensor data was particularly sensitive to scale factor errors. It is, therefore, very important to test the equipment against a pre-calibrated system, with a fixed axis of revolution.

3.1. Equipment

The sensing equipment chosen for the current study was an Xsens MTw Development Kit (Xsens Technologies, Netherlands), which comprised:

- 7 small wireless motion tracker systems (MTws) (34,5mm x 57,8mm x 14,5mm, 27g) equipped with 3D axis accelerometers, 3D axis gyroscopes and 3D axis magnetometers.
- One wireless Awinda ® station (148mm x 104mm x 61,9mm) equipped with 2 sync in and 2 sync out ports.

The Awinda station interfaces the sensors with the MT Manager software. It receives data from the MTws, keeps global synchronization between the MTws and allows live streaming of the acquired data. The Awinda station can also be used to synch the sensors with a third party system.

The MTw's are pre-calibrated and have an on-board Kalman filter (XKF-3w) - a sensor fusion algorithm in which the information from the accelerometer compensate for the inclination errors of the gyroscope and the magnetometers correct for the drift about the vertical axis (Guergueltcheva et al. 2012).

The XKF-3w has an integrated "34.3 human filter profile", which follows a strap-down integration system based on the assumption that the sensors are strapped to a human anatomical segment. The Xsens Kalman filter is based on Daniel Roetenberg's (2003) fusion algorithm and has the following structure (Fig 3.1):

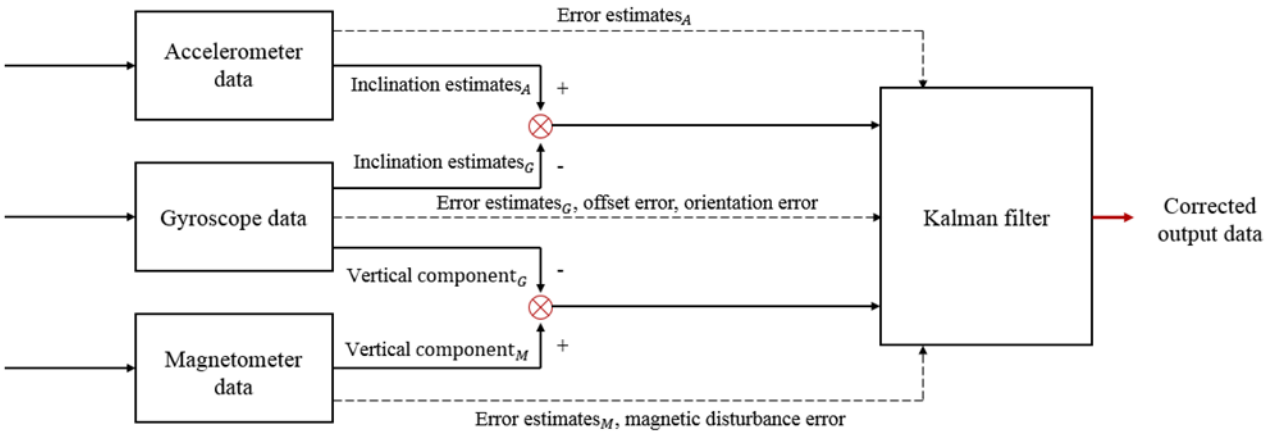

Fig 3.1. KALMAN FILTER FUSION ALGORITHM (Roetenberg et al. 2003), where (-) represents a weaker component and (+) the component by which it is corrected.

The sensor error estimates are modelled as follows:

- For the variation of the gyroscope offset, a first order Markov process, driven by a white Gaussian noise vector, is used.
  - $b_t = b_{t-1} + w_{b,t}$ (24)
- The acceleration is a first order low-pass filtered white noise with a cut-off frequency of c_a.
  - $a_t = c_a * a_{t-1} + w_{a,t}$ (25)
- The magnetic disturbance is modelled by the same principle as the acceleration with c_d constant between 0 and 1.

$$d_t = c_d * d_{t-1} + w_{d,t} \quad (26)$$

Where: w_t – driving Gaussian noise.

The physical wireless connection between the Awinda station and the MTws is based on IEEE 802.15.4 PHY standard with an Industrial, Scientific and Medical (ISM) radio band of approximately 2.4 GHz and a 50m range (Guergueltcheva et al. 2012).

The reference system for the proposed experiment was the Instron D8874 (Fig 5.2). Although, the Instron is a fatigue testing system, our interest in the machine was purely based on its kinematic setup. The Instron is a three-link cylindrical manipulator, which has the ability to accurately measure rotation (±1-2°) and translation about the vertical axis (yaw) of its local coordinate system. The status monitoring enables the user to see a live stream of the rotation, in a form of a sine wave.

Fig 3.2. INSTRON D8874 – AXIAL – TORSION FATIGUE TESTING SYSTEM. The Instron D 8874 is a bi-axial servo hydraulic testing system, often used in Biomedical and component testing applications. The Instron is equipped with a Linear Variable Differential Transformer and a Rotational Variable Differential Transformer, which guarantee translational and rotational measurements to an accuracy of up to ± 1-2°.

The console interface provides full control over the system from a PC: including waveform generation, calibration, limit set up, and status monitoring.

By performing the testing against the pre-calibrated robotic setup, the accuracy of using the gyroscope readings in conjunction with the Seel et. al (2015) method, to estimate a gyroscope rotational angle was determined.

Although, the Instron system is manufactured of heavy metal and the expectancy of ferromagnetic interference was high, it was expected that the gyroscope data remained unaffected by the magnetic conditions. However, due to the nature of the on-board Kalman filter of the Xsens sensors, it was necessary to determine whether a distorted magnetic field could have affected the gyroscope output or not. This was done by repeating the gyroscope bias test when the sensors were in very close proximity to a metal bar and when the bar moved with respect to the sensors.

Although, the Instron system is highly accurate, performing the proposed experiment presented a few limitations. Firstly, the axis of revolution of the robotic arm is placed vertically, along the gravitational line, analysing data derived from the accelerometer signals would have likely returned erroneous data.

Furthermore, the design of the robotic arm only allowed attachment of the sensor casing in a vertical or a horizontal position, thus allowing only analysis of rotation about the local X and Y axes of the sensor coordinates system. The accuracy of the gyroscope angle estimates about the Z axis could, therefore, not have been

determined, and an assumption had to be made that, based on the orthogonality of the sensor axes, the accuracy of the readings about X and Y local coordinates axes, could have also reflected the accuracy of the readings about the Z axis.

Additionally, there were limitations involved when using the Instron equipment itself, e.g. the console interface does not provide the possibility to log the data generated by the LVDT and RVDT sensors. Furthermore, synching the sensor system with the Instron is very difficult, as the Instron is incapable of receiving analogue input and the only output it can generate is a continuous infinite variable voltage signal, which starts the instance a BNC probe is connected to the system and stops only when it is disconnected. Therefore, it was impossible to create a successful direct link between the Instron and the Awinda station. In order to address the equipment related limitations, a myDAQ (National Instruments) was used as a third party portable measurement and instrumentation device, which acted as a data logger for the Instron and a synch enabler between the two systems. A detailed diagram of the system synchronisation is presented in Fig 3.3.

3.2. Data acquisition

Firstly, it was important to determine whether the Xsens sensors presented a gyroscope bias and whether the accuracy of the gyroscope output data was affected by ferromagnetic interferences.

For this purpose, the sensors were connected to the MT Manager interface, as explained in the paragraphs which follow, and the sensors were placed flat on a table where an approximately 30 second resting time was recorded. The test was repeated with a metal bar placed in close proximity to the sensors and with the metal bar moving with respect to the sensors.

The sensor accuracy (scale factor) test was carried out in the Bioengineering laboratory of the Lanchester Building, at University of Southampton, Highfield Campus, were the Instron D8874 is kept.

Prior to commencing the data acquisition, the myDAQ® (National Instruments) was connected to the Instron® (Dynacell™) via a BNC cable, so that the myDAQ received the voltage output signal from the Instron. Additionally, the myDAQ was connected to the Awinda® station (Xsens Technologies), so that the Awinda could receive an input signal from the myDAQ, under the form of a rising or a falling edge voltage pulse, and, following that, to execute a command.

The synchronisation configuration for the Awinda was set up in the MT Manager, so that when the 'record' button was pushed, the Awinda station was waiting for an infinite rising edge voltage pulse to start recording and an infinite falling edge voltage pulse to stop recording. The wireless connection between the Awinda station and the sensors was then established.

The myDAQ interfaced with Labview (National Instruments) through a customized software built in-house, in collaboration with Mr. Konstantinos Papadopoulos. Once the three systems were connected the Instron sent a continuous

voltage signal to the myDAQ. This signal was approximately 0 V when the Instron was not executing any motion.

Once the Instron started rotating and the signal became positive from 0 V, the myDAQ started logging the Instron data and sent a rising edge pulse of 3.3V to the Awinda station, so the Awinda station started recording. When the Instron stopped moving, the myDAQ stored the logged data into a .txt file and sent a falling edge pulse to the Awinda station, and the Awinda station stopped recording. A block chart describing the synchronisation between the three systems is presented in Fig. 3.3.

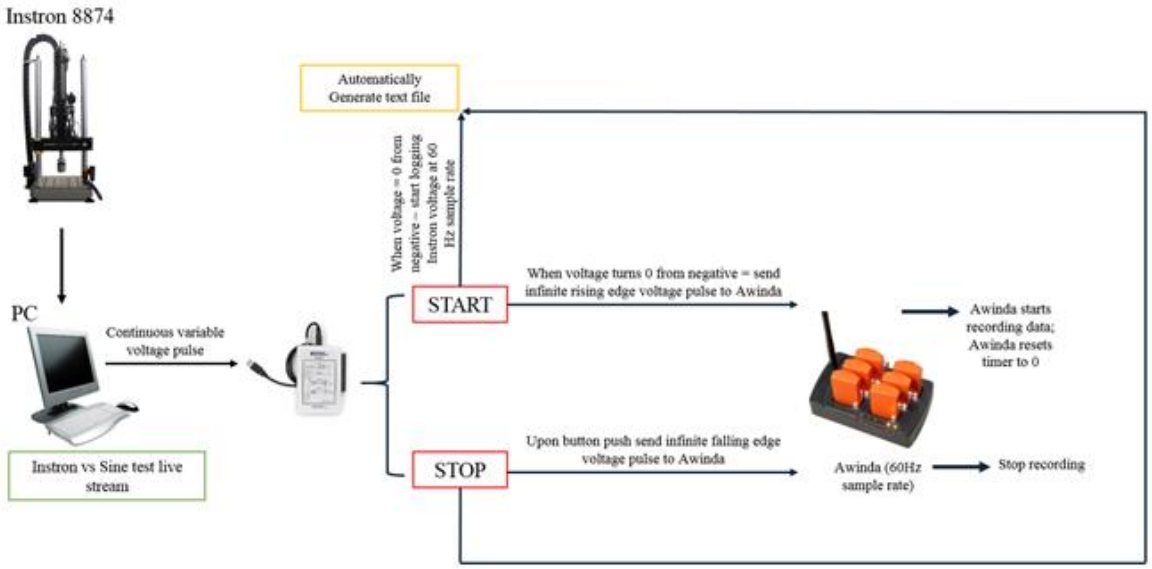

FIG 3.3. BLOCK CHART DESCRIBING SYNCHRONISATION BETWEEN THE INSTRON D8874, THE MYDAQ AND THE XSENS SENSOR SYSTEM.

Once the synchronisation between the systems was established, the sensors with the following serial numbers were tested against the Instron:

- 00341957 (1);
- 00341958 (2);
- 00341959 (3);
- 00341960 (4);
- 00341961 (5);
- 00341962 (6);

- 00341963 (7).

The sensors were attached directly to the Instron beam with double-sided tape and fastened with cohesive tape, as seen in Fig 3.4 The test was performed at 1Hz for both, vertical (rotation about X) and horizontal (rotation about Y) positions of the sensors.

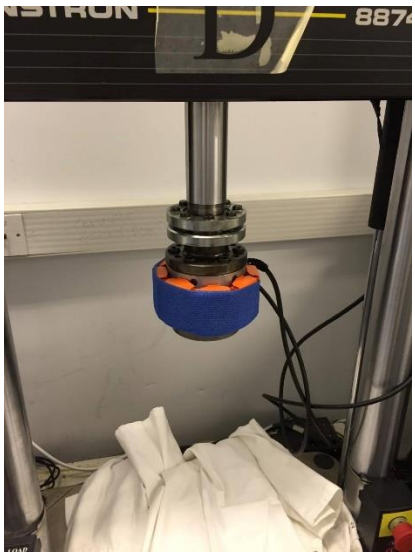

Fig 3.4. LABORATORY SETUP FOR SENSOR ACCURACY TEST.

Sensors 1 to 7 were mounted on the Instron D8874 in a vertical position, in preparation for the rotation about the X axis test.

The rotation of the beam was set up to a range of 90° starting from 0 and reaching -45° and +45°. The status monitor showed a live stream from the Instron data, which would have allowed us to act immediately in case of an error. The myDAQ sampled the Instron data at 1000Hz. The data for sensor 3 was sampled at 120Hz, and the data for the other sensors was sampled at 60Hz.

The Instron output data was presented in voltage. In order to transform the data into degrees, a multiplication by a 15°/V factor, as stated by the Instron interface, had to be performed. The Xsens data was presented in radians/degree and needed to be multiplied by a 180°/π factor.

The variability between the data recorded by the two systems was assessed using the statistical analysis methods described in chapter 3.4. Due to the difference in local coordinate systems of the two systems, an offset between the resulting data sets was

expected. This offset was removed before the statistical analysis and the figures were produced.

3.3. *Data processing*

Instron data

The Instron data was processed in Matlab using the method described in the following pseudocode:

```
Instron data processing sequence:

Input: Instron data

For direction number = 1 to 2 (where 1 = horizontal and 2 = vertical)

       Set passband = 0.1

       Set stopband = 0.4

       Set sample frequency = 1000

Initiate filtering sequence:

       Call Filter design (arguments: direction number, Instron data, sample
       frequency, passband, stopband)

       Filter design (input parameters: direction number, Instron data, sample
       frequency, passband, stopband)

              X = Instron data – average of Instron data           \\remove DC
       offset

              Niquist number = sample frequency/2

              Call Welch power spectral density (arguments: X, Hamming windowing
              (sample frequency), Niquist number, default frequency vector,
              sample frequency)

              Return (power spectral density estimate, frequency vector)

              Call Butterworth filter order (arguments: passband, stopband,
              passband ripple = 5dB, stopband ripple = 40dB)

              Return (filter order, cut-off frequency)

              Call Butterworth filter (arguments: filter order, cut-off
              frequency, filter type = low)

              Return (bandpass design, bandstop design)

              Call Filter data (arguments: bandpass design, bandstop design,
              Instron data)

       Return (filtered Instron data)                 \\use filtfilt Matlab
                                                      function to avoid phase
                                                      shift
```

```
Initiate rotation cycle interpolation sequence:

       Call Find local minima (arguments: filtered Instron data, minimum distance
       between peaks = 70)

       Return (peak number, peak location)

       Set rotation cycle count = 1

       For peak number = 1 to length of peak number

              Rotation cycle = filtered Instron data from peak number to peak
              number + 1

              Add 1 to cycle count

       End for

       For cycle frame = 1 to length of rotational cycle

              Rotational cycle time variable = 0 to 1, with the increment 1/
              (length of rotational cycle - 1)

              Call Fit data to curve (arguments: rotational cycle time variable,
              rotational cycle, curve type = smoothing spline)

              Return (fitted rotational cycle)

              Call Evaluate function (arguments; fitted rotational cycle,
              0:0.01:1)

              Return (interpolated rotation)

       End for

       Set degrees per Volt = 15

       For rotation frames = 1 to length of interpolated rotation

              Instron rotation = interpolated rotation * degrees per Volt

       End for

End for
```

Xsens data

In order to assess the gyroscope bias in a resting condition and to observe differences between the resting undisturbed sensor signals and the sensor signals under the two described ferromagnetic disrupted conditions, the unprocessed, unfiltered gyroscope, accelerometer and magnetometer output data were plotted against each other in the X, Y, and Z planes (Fig 3.5).

For the scale factor experiment, the gyroscope data for each sensor was processed in Matlab and stored in an individual folder. Starting from sensor number 00341957, in an ascending and consecutive order, the sensors were re-assigned a number from 1 to 7.

In order for the gyroscope angle to be calculated according to Seel et al.'s $\alpha_{gyroscope}$, a virtual joint was created. The rotation of the sensors was calculated with respect to a fixed 'dummy' sensor.

The data was then processed using the method described in the following source code:

```
Xsens data processing sequence:

Input: sensor data

For sensor number = 1 to 7

     For direction number = 1 to 2 (where 1 = horizontal and 2 = vertical)

             Read gyroscope data for every sensor number

             Read sampling frequency for every sensor number

             Time variable = (frame count – value of first frame)/sample
      frequency

             Set dummy sensor matrix = zeros matrix the size of sensor number
             gyroscope data matrix

             Set passband = 0.1

             Set stopband = 0.4

Initiate filtering sequence:

             Call Filter design (arguments: sensor number, direction number,
             gyroscope data, sample frequency (sensor number), passband,
             stopband)
```

```
            Return (filtered gyroscope data)              //see filter
                                                          description for
                                                          Instron data

Initiate gyroscope angle calculation sequence:

            Gyroscope concatenated = concatenate filtered gyroscope data and
            dummy sensor data over 3 dimensions

            Call Compute rotation axes (arguments: gyroscope concatenated)

                  Call Sum of squared errors rotation axes (arguments:
                  gyroscope concatenated)

                  Compute sum of squared errors for rotational axes from

                  equation 8

                  Return (sum squared errors axes)

                  Compute best angle estimates and minimum sum squared errors
                  using an optimisation algorithm

                        //e.g. use a genetic algorithm to find global minimum
                  values for sum squared errors and phi and theta angle
                  estimates, which satisfy the constrains from equation 8;
                        //then find the local minimum values for sum squared
                  errors and phi and theta angle estimates, which satisfy the
                  linear and non-linear constrains and bounds of the quadratic
                  objective function
                  Return (best angle estimates and minimum sum squared errors)

                  Compute axes coordinates from equation 6 and 7 (input: phi
                  estimate, theta estimate)

      Return (axes coordinates)

      Call Compute gyroscope angles (arguments: axes coordinates, gyroscope
      concatenated)

            Δt = 1/sample frequency

            Compute gyroscope angles from equation 16

      Return (gyroscope angles)

Initiate gyroscope rotation cycles interpolation sequence:

//see solution for Instron data

            Return (interpolated gyroscope rotation cycles)

            Convert interpolated gyroscope rotation cycles from radian to
            degrees

            Return (gyroscope rotations in degrees)

      End for

End for
```

3.4. Statistical analysis

In order to perform a correct and comprehensive data analysis, first the range of motion (ROM) and variability, by means of the root mean squared error (RMS) and average standard deviation (σ), within a certain motion trial had to be measured.

The ROM describing the difference between the minimum and maximum points of the average rotation within a recorded trial is calculated using the following formula:

$$ROM = max(P_{(t)}) - min\,(P_{(t)}) \tag{27}$$

Where, $max(P_{(t)})$ – maximum value recorded with system P at time t;
$min(P_{(t)})$ – minimum value recorded with system P at time t.

The RMS is the amount by which each rotation cycle differs from the average within a trial.

$$RMS = \sqrt{\frac{1}{n}\sum_{i=1}^{n}(P_i - \mu)^2} \tag{28}$$

Where, $\mu = \frac{1}{n-1}\sum_{i=1}^{N} P_i$ and:

n – the total number of rotations within a trial;
P_i – rotation data corresponding to system P for cycle number I;
μ - average rotation cycle.

Similar to the RMS, the standard error is a measure of variability between each rotational cycle and the average rotation within a certain trial.

$$\boldsymbol{\sigma} = mean\left(\sqrt{\frac{1}{n-1}\sum_{i=1}^{N}|P_i - \mu|^2}\right) \tag{29}$$

Further, the variability between motion trials recorded with different systems can be measured by means of difference in range of motion (ΔROM), Pearson product-moment correlation coefficient (r), coefficient of variability (CV), and coefficient of multiple correlations (CMC).

The difference in range of motion can be used as an indicative of how accurate a tested measuring system is functioning against a reference system.

$$\Delta ROM = ROM(Xsens_{(t)}) - ROM\ (Instron_{(t)}) \tag{30}$$

The CV, r and CMC are used to measure variability between data recorded synchronously with multiple systems and are defined by following equations:

$$r = \frac{\sum_{t=1}^{n}(Xsens_{(t)} - \mu_{Xsens})(Instron_{(t)} - \mu_{Instron})}{\sqrt{\sum_{t=1}^{n}(Xsens_{(t)} - \mu_{Xsens})^2}\sqrt{\sum_{t=1}^{n}(Instron_{(t)} - \mu_{Instron})^2}} \tag{31}$$

Where, $\mu_{Xsens}, \mu_{Instron}$ – means of Xsens and Instron data.

Pearson's r is used to measure linear dependence between two data sets. The values r returns can range between +1 and -1, where +1 is a complete positive linear correlation, -1 is a complete negative linear correlation and 0 is no correlation at all.

The CV expresses the deviation of the tested system relative to the entire range of motion performed by the reference system.

$$CV = \frac{\sigma_{Xsens}}{ROM_{Instron}} \tag{32}$$

The CMC is used to measure similarities between waveforms which stem from different motion trials, waveforms which have been processed using different protocols, or waveforms which have been recorded with different data acquisition systems.

Similarly, to r the CMC usually returns a value between 0 and 1, where 1 is a total correlation of the two data sets and 0 is no correlation at all. However, in some cases using the CMC to compute variability of two data sets can return complex numbers or non-assigned values (Ferrari et al. 2010b; Røislien et al. 2012).

This issue seems to be strongly connected to the ROM and some researchers (McGinley et al. 2009) advise against using this method to assess waveform variability by itself, which is the reason for using merrier measures of variability in the current study.

$$CMC = \sqrt{1 - \frac{\sum_{w=1}^{W} [\sum_{s=1}^{S} \sum_{f=1}^{F} (y_{wsf} - \overline{y_{wf}})^2 / (WF(S-1))]}{\sum_{w=1}^{W} [\sum_{s=1}^{S} \sum_{f=1}^{F} (y_{wsf} - \overline{y_{w}})^2 / (W(SF-1))]}} \quad (31)$$

Where: w – waveform; s – system; f – frame; W – total number of waveforms; S – total number of systems; F – total number of frames; y_{wsf} - ordinate at frame (f) of the waveform provided by the system (s) and the rotation cycle (w); $\overline{y_{wf}}$ - ordinate at frame (f) of the average waveform among (w) rotation cycles provided by the system (s); $\overline{y_{w}}$ – grand mean of the $\overline{y_{wf}}$ recorded with the system (s).

Another debated issue regarding the CMC is posed by the removal of the offset between the analysed data sets prior to the CMC calculation (Kadaba et al. 1989; Yu et al. 1997). When analysing motion data stemming from two different systems, due to the different manners in which the data is processed and in which the local coordinate frames for each motion capture system are declared, an almost certain offset between the data sets is expected.

In some cases, especially when analysing motion data from two different participants, removing the offset can generate an overestimation of the CMC (Røislien et al. 2012), due to the removal of both systematic differences due to measurement processes and natural offset due to individual differences.

However, this situation does not apply to the current experiment, as the difference in the initial position of each sensor with respect to the other sensors and

the Instron, will introduce an offset of a systematic nature which, if removed, will not affect the ROM of the data set significantly, but rather the overall values of the angles in degrees, and therefore make the data sets easier to compare.

Furthermore, the offset removal proposed in the current study, uses a scalar offset value (Equation 32), rather than removing the difference between the two data sets at every given time point. By implementing this method, the average difference between the two data sets is removed without affecting any natural offset.

$$off = mean\,(Xsens_{(t)}) - mean\,(Instron_{(t)}) \tag{32}$$

Similar to the interpretation of CMC and r values reported previously in the literature (Cutti et al. 2010; Ferrari et al. 2010a; Garofalo et al. 2009; Kadaba et al. 1989; Yavuzer et al. 2008), the following guidelines are used for the current project:

- 0.65-0.75 – moderate agreement;
- 0.75-0.85 – good agreement;
- 0.85-0.95 – very good agreement;
- 0.95-1 – excellent agreement.

3.5. Results

The gyroscope bias experiment returned similar results for all sensors (Fig 3.5). No true gyroscope bias could be determined from the experiment. Furthermore, when the effect of ferromagnetic interferences on the gyroscope and accelerometer output was tested, the graphic results for both tests revealed the only real visible effect of the disturbed magnetic field lies within the magnetometer data (Fig 3.5.G, H and I).

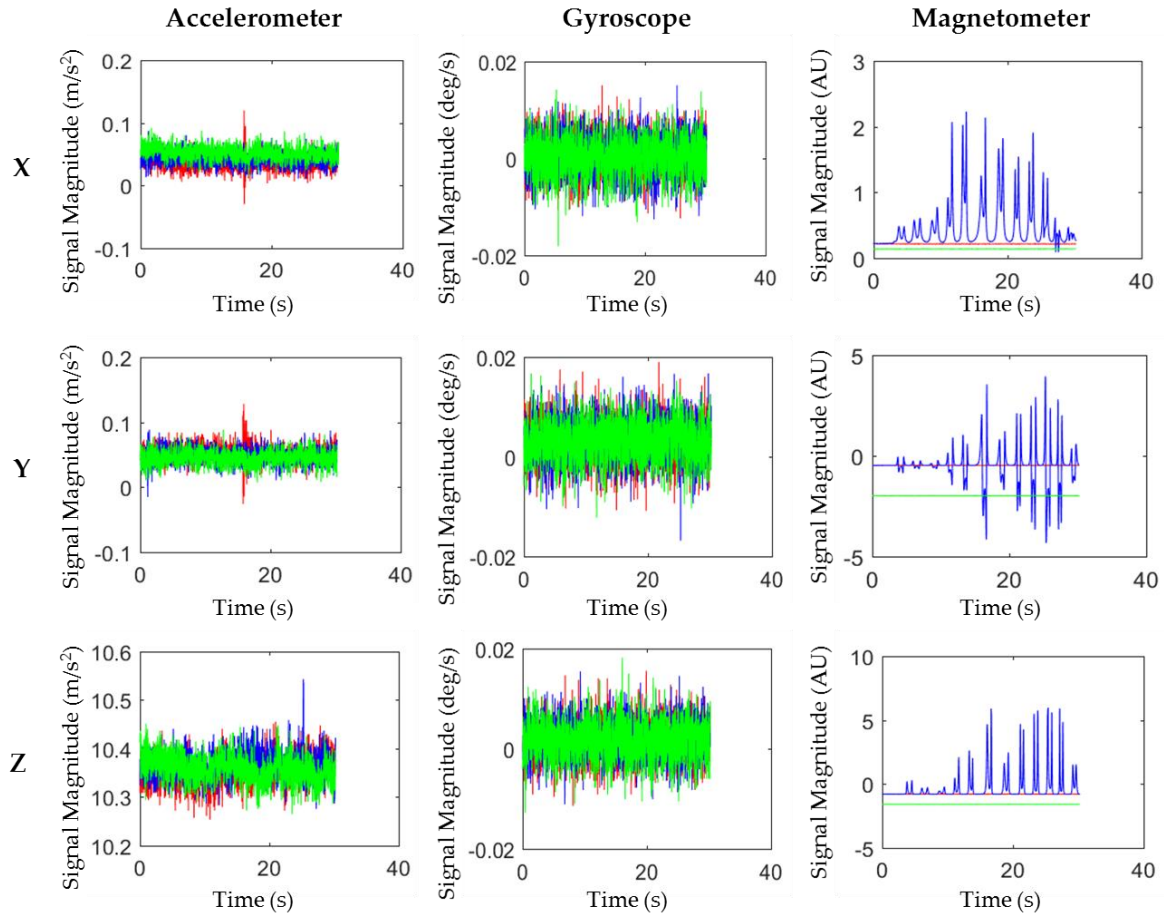

FIG 3.5. GYROSCOPE BIAS experiment results for accelerometer signal (column 1), gyroscope signal (column 2), and magnetometer signal (column 3), about the X (row 1), Y (row 2), and Z (row 3) axes of a single sensor. Where red represents the magnitude of each signal under undisturbed ferromagnetic conditions; green represents the magnitude of each signal when a metal lies in close proximity to the static sensors; and blue represents the magnitude of each signal when the metal moves with respect to the static sensors.

The results for the variability and correlation between the gyroscope output of the sensors and the Instron system, for both instances, where X represents the local vertical axis of the sensors, and where Y represents the local vertical, are presented in Table 3.1, and Fig 3.1 and Fig 3.2 below.

The ΔROM of the two systems is < 0.7° for any of the two tested positions. The RMS for the rotation about the local vertical X is ≤ 1°, whereas the RMS for the rotation about the local vertical Y is ≤ 1.5°. These results are further corroborated by the σ, which is ≤ 0.8° for vertical X and ≤ 1.2° for vertical Y.

Taking into account the total range of the rotation performed by the robotic arm ≈ 90°, this brings the coefficient of variation for vertical X to ≤ 0.8% and for vertical Y to ≤ 1.4%. Additionally, the correlation of the sensor and Instron data sets are excellent for both, X – local vertical (CMC = 1, r = 1) and Y – local vertical (CMC = 1, r = 0.999).

TABLE 3.1. VARIABILITY BETWEEN THE XSENS GYROSCOPES AND THE INSTRON SYSTEM.

Between system variability of recorded rotation	*Experimental results*	
Sensors 1 to 7 against Instron	Vertical [X] [1 Hz]	Horizontal [Y] [1 Hz]
Number of observations (N)	26 to 28	7 to 43
Difference between range of motion (ΔROM)	<0.1° to 0.6°	<0.1° to 0.7°
Root mean squared error (RMS)	0.7° to 1°	0.6° to 1.5°
Standard error (σ)	0.6° to 0.8°	0.5° to 1.2°
Coefficient of variation (CV)	0.6% to 0.8%	0.6% to 1.4%
Coefficient of Multiple correlations (CMC)	1	1
Pearson product-moment correlation coefficient (r)	1	0.999

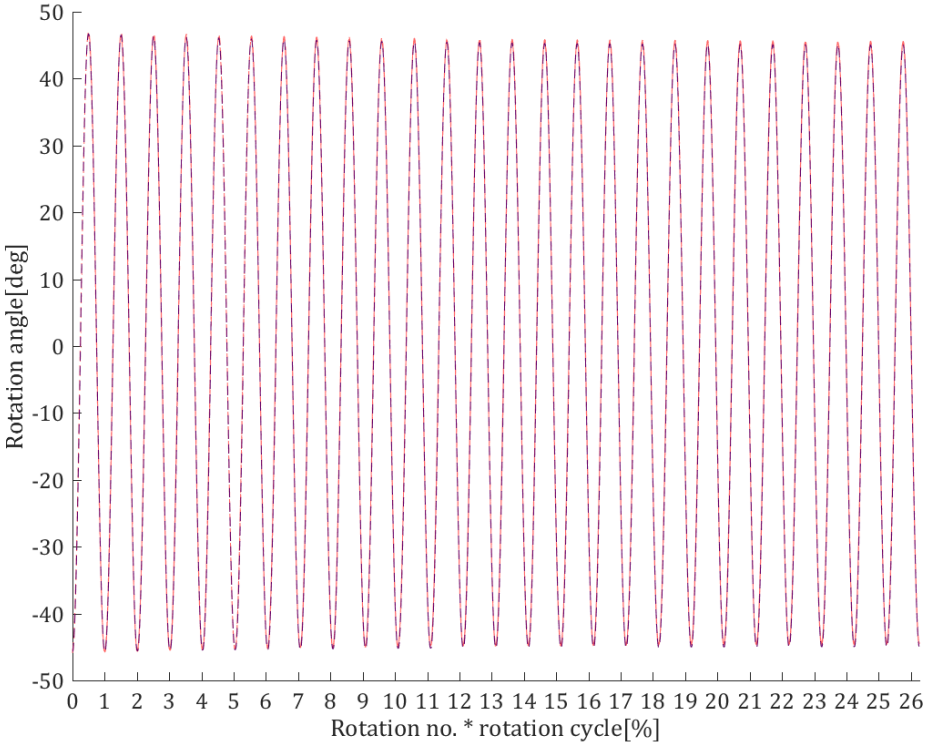

FIG 3.6. VARIABILITY BETWEEN THE XSENS SENSORS AND THE INSTRON FOR ROTATION ABOUT THE LOCAL SENSOR AXIS X at 1Hz, for the first 26 observations. The Instron data is represented in purple and the Xsens data in light pink. The correlation between the two systems is excellent with CMC = 1, r = 1.

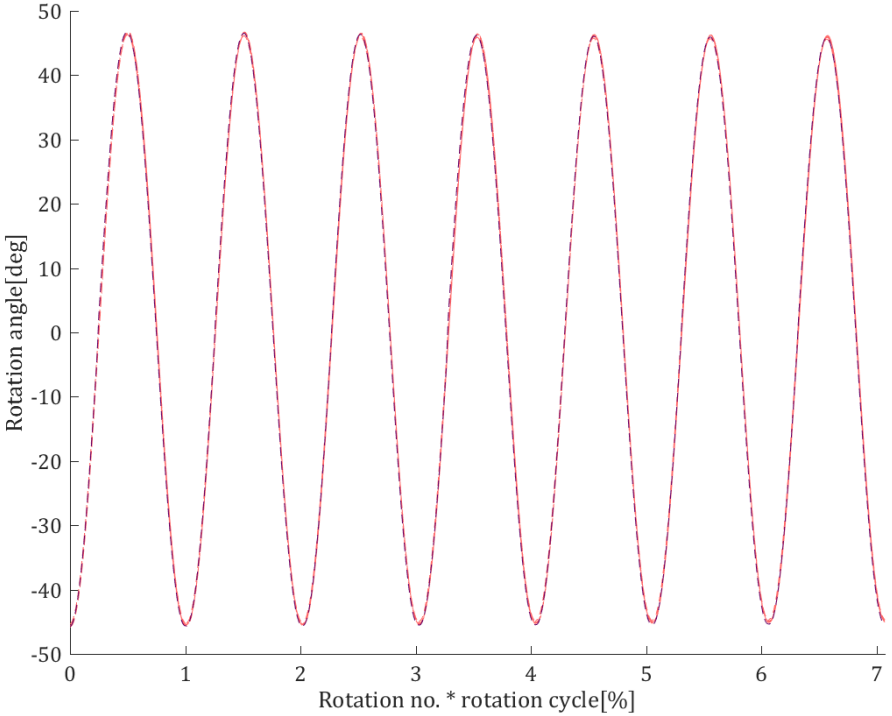

FIG 3.7. VARIABILITY BETWEEN THE XSENS SENSORS AND THE INSTRON FOR ROTATION ABOUT THE LOCAL SENSOR AXIS Y at 1Hz for the first 7 observations. Similarly, to the vertical position, the Instron data is represented in purple and the Xsens data in light pink and the correlation between the two systems is excellent with CMC = 1, r = 0.999.

3.6. Discussion

The gyroscope accuracy experiment revealed no sensor bias under normal testing conditions. Furthermore, the gyroscope and accelerometer data remain unaffected by the surrounding magnetic field, even though the raw output data from the sensors is in fact processed by the Xsens on-board Kalman filter.

The magnetometer data, however, shows a constant linear bias, across all three axes, during testing conditions in which the magnetic field is distorted homogenously. Moreover, in conditions with variable ferromagnetic interferences, the magnetometer data is very unreliable and varies as well.

The scale factor experiment shows an excellent correlation between the gyroscopes within the Xsens sensors and the Instron D8874. Furthermore, the variability between the two systems is < 1.5° in all measured parameters, for the two tested axes of rotation, which corresponds with the ±2° accuracy during dynamic motion guaranteed by Xsens manufacturers (Xsens Technologies 2013).

Seeing that the gyroscope signal is the main signal used in the protocol proposed by Seel et al. and assuming that the orthogonality of the axes within the local coordinate system of the sensors indicate the accuracy about all three axes of the sensors, it is safe to conclude that the Xsens equipment, chosen for the current study, functions accurately and is, therefore, fit for purpose.

Chapter 4

4. Experiment 2: Vicon accuracy test

The manufacturers of the optical motion capture system (Vicon Motion Systems) used as a reference in the current study state that an accuracy of the system with an up to 1mm precision is achievable with the system. However, it is important to determine if the calibration of the Vicon camera system is indeed operating at this high accuracy at the moment at which this study is conducted. As the fundamental accuracy of the sensor system was tested in the previous chapter, the fundamental accuracy of the optical motion capture reference system used in the current study was determined using an analogous experiment.

4.1. Equipment

The Vicon system within the biomechanics laboratory at University of Southampton is a state-of-the-art infrared marker tracking system that consists of a network of high accuracy cameras equipped with infra-red (IR) optical filters and an array of IR LEDs, which can detect the position of reflective markers with high precision within a known local coordinate system, called the capture volume.

The camera network consists of 12 Vicon Mx T-series cameras operating at 100Hz, of which 6 are T40, 4 megapixel cameras and the other 6 are T160, 16 megapixel cameras. Additionally, to the camera systems and the Vicon platform, the biomechanics laboratory is equipped with a 10 m long force platform which contains two Kistler piezoelectric force plates, one mobile and one fixed, which operate at 1000Hz and provide the ability to precisely calculate ground reaction forces and momentum, highly relevant to the human motion study described in chapter 6.

The software provided with the system allows labelling and calibration of the marker set in order to create a 'rigid marker set frame' defined by local coordinate systems which

allows the computation of the movement of each marker within the laboratory volume. The reference system for this experiment is a FARO® Prime arm (metrology gold standard).

4.2. *Data acquisition and processing*

The data acquisition involving the Vicon system, was carried out in the Biomechanics laboratory within the Health Science Building (45) at University of Southampton (Fig 4.1).

At the beginning of every laboratory session the Vicon system is set up in preparation for the data acquisition. This is done by performing a wand calibration, where every camera in the system in set up to correctly identify the positions of the markers attached to the T – shaped calibration wand, initially during a dynamic calibration and then in a static position, in which the wand is waved in a circular motion across the entire measuring volume. The global coordinate system employed by the Vicon system is a right handed Cartesian coordinate system.

Once the IR camera system was calibrated the software was set up for a new trial and the data acquisition commences.

FIG 4.1. BIOMECHANICS LABORATORY, HEALTH SCIENCE BUILDING, UNIVERSITY OF SOUTHAMPTON. Dr. Martin Warner performing a Vicon wand calibration.

The second experiment involved, testing the accuracy with which the cameras of the Vicon system track a set of markers, attached to a rigid plastic frame, in a specific pattern (Fig

4.2), within the measurement volume during one static and two dynamic conditions. For the first dynamic trial, David Wilson (DW) walked up and down within the measurement volume holding the marker plate steady. For the second trial, the marker plate was arbitrarily waved around the measurement volume.

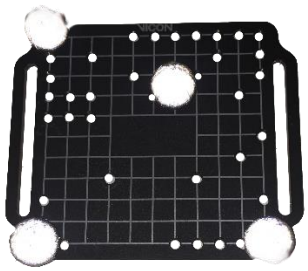

FIG 4.2. VICON MARKER PLATE
The spherical markers attached to the rigid plastic frame have a diameter of 14mm.

Following data acquisition, the Vicon data required a pre-processing step, which was carried out using the Nexus module. The data pre-processing involved labelling the markers, and estimating and filling in lost marker trajectory data by using a 'rigid body algorithm' available in Nexus. The aforementioned algorithm takes the marker set into account as being a rigid entity, each marker having a fixed position relative to the other surrounding markers. In order to recreate lost marker trajectory data for one marker, 3 proximal markers from different planes, visible at all times during data acquisition, were selected and missing data was computed and filled in. This pre-processing step has been carried out by David Wilson for all Vicon data presented in the current study.

The Vicon software generated an output file containing the trajectories for each marker. In order to assess the accuracy of the Vicon the position of each marker with respect to the other markers is estimated in a time dependent manner by calculating the distance between the centres of the markers from the trajectories information using Equation 33 (Fig 4.3).

FIG 4.2. VICON MODEL OF THE MARKER PLATE, where the markers are numbered and represented as follows: 1 – orange; 2 – green; 3 – purple; 4 – blue. The distances between marker centres will be labelled as follows: D1 –between marker 1 and 2; D2 – between marker 2 and 3; D3 – between marker 1 and 3; D4 – between marker 3 and 4; D5 – between marker 1 and 4; D6 – between marker 2 and 4.

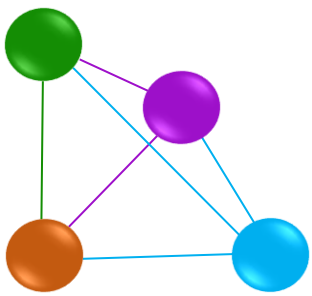

$$D = \sqrt{(x_1 - x_2)^2 + (y_1 - y_2)^2 + (z_1 - z_2)^2} \quad (33)$$

Where D – the distance between the centres of two markers; x_i – the trajectories of marker i in plane X, y_i – the trajectories of marker i in plane Y, and z_i - the trajectories of marker i in plane Z of the local coordinate system of the laboratory measurement volume.

For the purpose of this experiment, the marker plate has been reverse engineered in order to facilitate the computation of true distances between the centres of the markers. Measurements of the marker plate were taken with the FARO® Prime arm , a metrology tool which has a guaranteed accuracy of ± 0.023mm and a tested repeatability of < 0.07mm (FARO 2012), and used to generate a virtual 3 dimensional model of the marker plate, in Solidworks. The technical drawing of which is presented in Fig 4.3 alongside the distance measurements calculated using the FARO metrology tool.

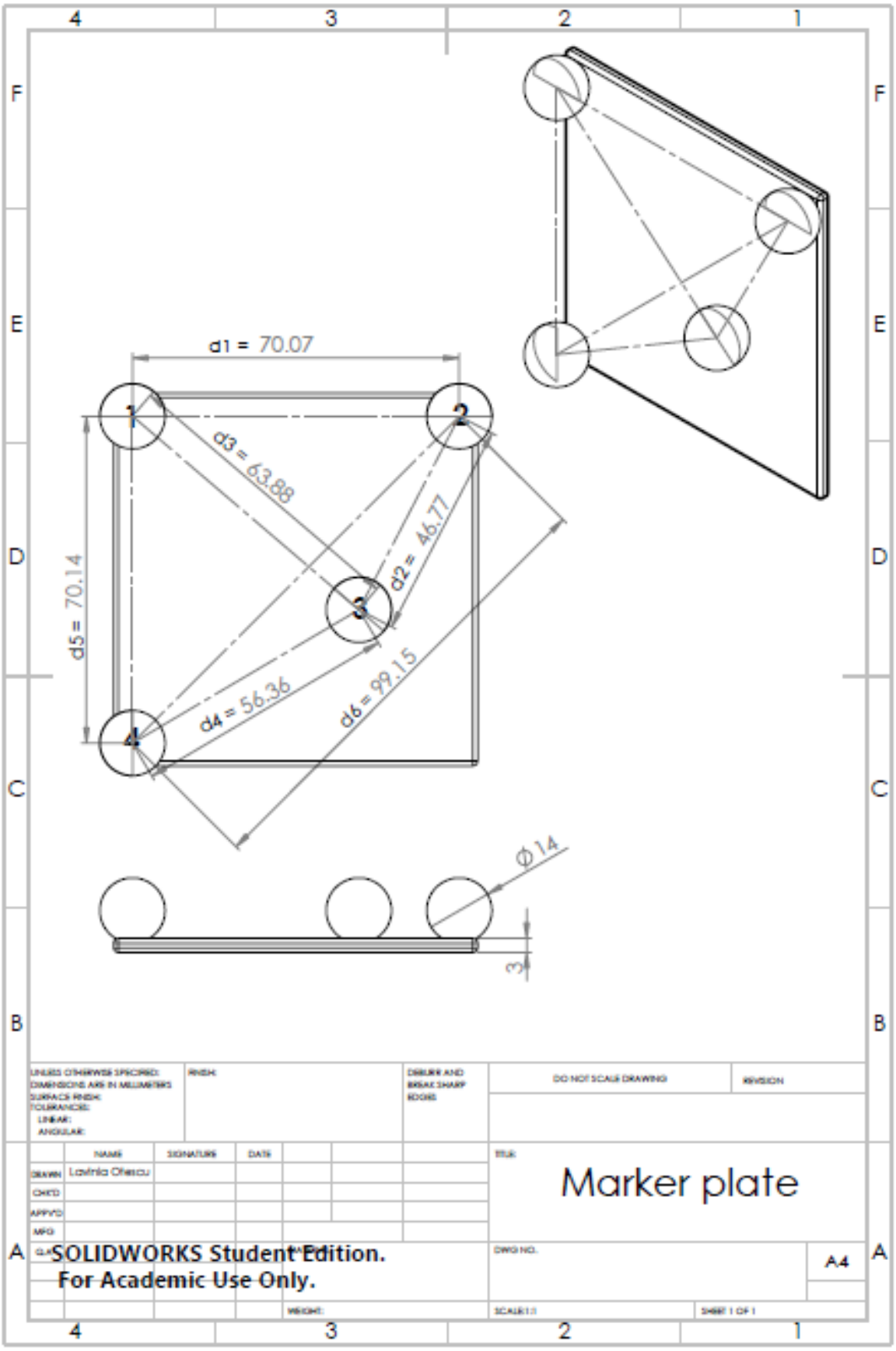

FIG 4.4. TECHNICAL DRAWING OF REVERSE ENGINEERED MARKER PLATE

4.3. Results

The distances between markers estimated by the FARO and by the Vicon system, for the static and two dynamic motions, are presented in Table 4.1 below. The differences between the distances measured by Vicon and the reference measurements were < 1.1 mm for any of the trials recorded with the Vicon system.

TABLE 4.1. RESULTS FOR THE VICON ACCURACY STUDY where D1 – distance between marker 1 and 2; D2 – distance between marker 2 and 3; D3 – distance between marker 1 and 3; D4 – distance between marker 3 and 4; D5 – distance between marker 1 and 4; and D6 – distance between marker 2 and 4. The distances are averaged over the total number of recorded frames.

Vicon accuracy Study	*Experimental results*				
Distances between markers	FARO	Vicon Static	Vicon dynamic - walk	Vicon dynamic - wave	Difference between Vicon and reference (Δd)
D1 (mm)	70.1	69.9 ± 0.01	69.9 ± 0.36	70.1 ± 0.72	<0.2
D2 (mm)	46.8	46.4 ± 0.01	46.5 ± 1.07	46.4 ± 0.68	<0.4
D3 (mm)	63.9	64.8 ± 0.01	64.9 ± 0.93	65 ± 1	<1.1
D4 (mm)	56.4	56.6 ± 0.01	56.7 ± 0.61	56.9 ± 0.82	<0.5
D5 (mm)	70.1	70.3 ± 0.01	70.1 ± 0.91	70.3 ± 0.75	<0.2
D6 (mm)	99.2	98.6 ± 0.01	98.6 ± 0.62	98.8 ± 0.70	<0.6

4.4. Discussion

The Vicon accuracy study revealed that, the accuracy of the optical motion capture system was well within the ~ 1mm stated by the manufacturers. Therefore, it can be concluded that the Vicon camera system functioned optimally at the time of the data acquisition.

However, it should be kept in mind that the current experiment takes into account the tracking of a marker set fixed to a rigid surface. In the case of human motion tracking the markers would, however, be fixed to soft tissue, in which case the markers are likely to move with respect to each other during dynamic conditions.

Chapter 5

5. Experiment 3: Agreement between Xsens and Vicon systems – Wand study

The aim of the third experiment was to test the first hypothesis (H_1) stated in Chapter 1 by determining the agreement between the optical motion capture and the sensor systems. This chapter involved the use of both, gyroscope and accelerometer data to calculate the movement of the marker calibration wand to which the sensors were attached. The scope of the experiment was to assess the agreement between data recorded with the two systems in a scenario where STA were eliminated.

5.1. Data acquisition

During this experiment all Xsens sensors were attached to the Vicon calibration wand (Fig 5.1) and by manoeuvring the wand through wrist movements, three simple rotation motions were performed across the X, Y and Z axes of the Xsens sensors.

FIG 5.1. SENSOR SETUP FOR SYSTEM AGREEMENT EXPERIMENT.
During the wand study, the sensors were attached to the wand with double sided tape and fixed in position with cohesive tape.

The two systems were initially set up as described in the previous experimental chapters (Chapter 3.2 and Chapter 4.2). However, the Vicon and the Xsens systems sampled at different frequencies. Therefore, prior to the data acquisition, the Vicon system and the Awinda station were synchronised. The Awinda ® station (Xsens Technologies) was connected to the MTw interface via USB and a synchronisation between the Awinda station and the Vicon system was set up via a BNC cable which was connected to an output port on the Awinda station and to an input on the Vicon station via an analogue to digital screw terminal panel and sampled at 1000Hz. An

"Internal Transition Recording" synchronisation option was set up from inside the MT Manager. The manner in which the synchronisation worked is explained in a flow chart in Fig 5.2.

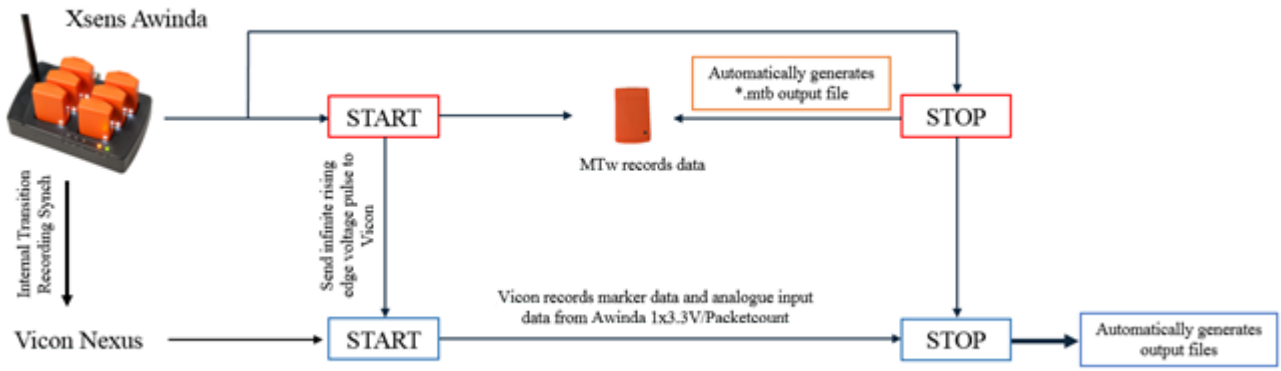

FIG 5.2. FLOW CHART FOR INTERNAL TRANSITION RECORDING SYNCH.
Upon pressing the record button in the MT Manager, the Awinda station sends an infinite rising edge 3.3 V analogue pulse to the Vicon at every frame at which the Xsens records a data series. The Vicon system embeds the analogue data in the output file. When the "Stop" button is pressed, the MT Manager automatically generates an output file for the sensor data.

5.2. *Data processing*

Vicon data

The Vicon wand model presented in Fig 5.3 was produced by David Wilson and the trajectories of the markers were computed for that model.

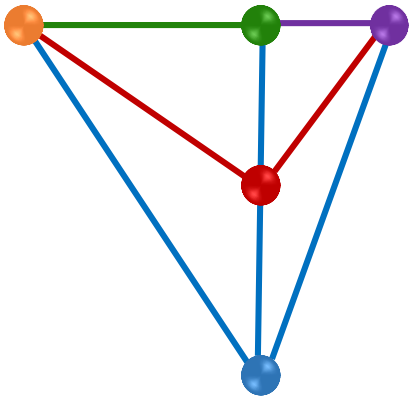

FIG 5.3. VICON WAND MODEL, where the markers are numbered and represented as follows: 1 – orange; 2 – green; 3 – purple; 4 – red; 5 - blue.

The comma delimited output files produced by the Vicon software contained the embedded analogue signals sent by the Awinda station for every sample of the Vicon system. The Vicon data matching an analogue value of 1 was identified and

declared as the data to be processed. The data was then processed using the method described in the following pseudocode:

```
Vicon data processing sequence (Vicon wand study):
Input: Marker trajectories data
For direction number = 1 to 3
       Set passband = 0.1
       Set stopband = 0.6
       Set sample frequency = 100

       Declare global X = [1 0 0]                    //Declare laboratory coordinate
                                                     system
       Declare global Y = [0 1 0]
       Declare global Z = [0 0 1]
Call Declare local coordinate system of the wand (arguments: marker trajectories)
              Declare local X = marker 3 – marker 1
              Declare local Y = marker 5 – marker 2
              For frame number = 1 to length of motion study
                     Wand X = local X/normalized local X          //data is normalized
                                                                  using Euclidean norm
                     Wand Y = local Y/normalized local Y
                     Wand Z = cross product of wand X and wand Y
               End for
       Return (wand coordinate system)
Initiate Euler angle computation sequence:
       Call Compute wand rotation in laboratory volume (arguments: wand X, wand Y, wand
       Z, global Z)
              Declare X' = cross product of wand Z and global Z
              Compute X'x = dot product of wand X and X'
              Compute X'y = dot product of wand Y and X'
              Compute α = arctangent of X'y/X'x
              Compute Zx = wand Z coordinates in plane X
              Compute Zy = wand Z coordinates in plane Y
              Compute Zxy = square root of (Zx squared + Zy squared)
              Compute Zz = wand Z coordinates in plane Z
              Compute β = arctangent of Zxy/Zz
              Compute γ = - arctangent of X'y/X'x
Return (Euler angles α, β, γ)
```

```
        If α, β or γ ≥ 180 degrees
                Multiply α, β or γ with -1                    //eliminate gimbal lock
        End if
        If α, β or γ have non assigned numerical values
                Fill in missing data points by using an interpolation process
        End if
Initiate filtering sequence:
        Call Filter design (arguments: direction number, Euler angles, sample frequency,
        passband, stopband)
        Return (filtered Euler angles)                                //see filter
                                                                      description in
                                                                      chapter 5.2
Initiate rotation angle interpolation sequence:
//see solution in chapter 5.2
        Return (interpolated rotation angles)
End for
```

Xsens data

The Xsens accelerometer and gyroscope data was processed following Seel et al.'s (2014) fusion algorithm for determining a rotation angle. Again, a virtual joint was built, by declaring a dummy sensor, assumed to be the fixed link of the kinematic chain, which builds the joint. The wand holding the sensors was assumed to be the dynamic link, which moved with respect to fixed segment defining the angles of movement.

Additionally, in order to rule out any disagreement between the two systems stemming from the use of the Seel et al. (2014) protocol, the Euler angles computed by the Xsens software were exported and compared to the Vicon data and the data was processed using the Seel et al. method.

The Xsens Euler data was filtered, divided into rotation cycles and interpolated in a similar manner to the fused accelerometer and gyroscope data, using the method described in the following pseudocode:

Xsens data processing sequence (Wand study):

Input: sensor data

```
For sensor number = 1 to 6

     For direction number = 1 to 3                    //where 1 – rotation about
            Y axis; 2 – rotation about Z axis; and 3 – rotation about X axis

            Set sample frequency = 60 Hz

            Read gyroscope data for every sensor number

            Read accelerometer data for every sensor number

            Read sampling frequency for every sensor number

            Time variable = (frame count – value of first frame number)/sample
      frequency

            Set dummy gyroscope matrix = zeros matrix the size of sensor number
            gyroscope data matrix

            Set dummy accelerometer matrix = zeros matrix the size of sensor
            number accelerometer data matrix

            Declare the 3rd column of the dummy accelerometer matrix = 9.81

            //representing the gravitational component of the vertical Z axis
            (in this experiment)

            Set passband = 0.1

            Set stopband = 0.4
```

Initiate filtering sequence:

```
            Call Filter design (arguments: sensor number, direction number,
            gyroscope data, sample frequency (sensor number), passband,
            stopband)

            Return (filtered gyroscope data)

            Call Filter design (arguments: sensor number, direction number,
            accelerometer data, sample frequency (sensor number), passband,
            stopband)

            Return (filtered accelerometer data)          //see filter
                                                          description in
                                                          chapter 5.2
```

Initiate gyroscope angle calculation sequence:

```
            Call Compute rotation axes (arguments: filtered gyroscope data from
            the two sensors concatenated about the 3 dimensions)

            Return (axes coordinates)                     //see axes
                                                          computation
                                                          algorithm in chapter
                                                          5.3

            Call Compute joint centre estimations (arguments: filtered
            gyroscope data from the two sensors, filtered accelerometer data
            from the two sensors)
```

```
                    Call Sum of squared errors joint centres (arguments:
                    filtered gyroscope and accelerometer data)

                    Compute sum of squared errors for joint centre estimates
                    from equation 14

                    Δt = sample rate

                    Compute radial and tangential acceleration from equation
                    12 and 13

                    Return (sum squared errors joint centre estimates)

                    Compute best arbitrary location estimates and minimum sum
                    squared errors using an optimisation algorithm

                          //e.g. use a genetic algorithm to find global minimum
                    values for sum squared errors and joint centre estimates,
                    which satisfy the constrains from equation 15;
                          //then find the local minimum values for sum squared
                    errors and joint centre estimates, which satisfy the linear
                    and non-linear constrains and bounds of the quadratic
                    objective function
                    Return (best joint centre estimates and minimum sum squared
                    errors)

                    Shift joint centre estimates as close as possible to sensor
                    origin using equations 10 and 11

              Return (joint centres)

              Call Compute fused accelerometer and gyroscope rotation angle
              (arguments: axes coordinates, filtered gyroscope data from the two
              sensors, filtered accelerometer data from the two sensors, joint
              centres)

                    C = [1,0,0]                       //a vector which makes none
                                                      of the vector products 0

                    Compute x1,2 and y1,2 from equations 20 and 21

                    Shift acceleration onto rotation axes using equations 17 and
                                                      18

                    Compute accelerometer rotation angles from equation 19

                    Compute gyroscope rotation angles from equation 16

                    Compute fused accelerometer and gyroscope rotation angle
                                                      from equation 22

                    //where the weight of the accelerometer data λ = 0.2

              Return (fused sensor rotation angles)

Initiate gyroscope rotation cycles interpolation sequence:

              //see solution from chapter 5.2

              Return (interpolated fused sensor rotation angle)

              Convert interpolated fused sensor rotation cycles from radian to
              degrees
```

```
            Return (sensor rotations in degrees)
        End for
End for
```

The correlation and variability between data recorded with the two systems was assessed using the statistical analysis methods described in Chapter 3.4.

5.3. Results

The correlation and variability between the Xsens gyroscope and accelerometer fused angles and the Vicon data for the wand rotation study are presented in Table 5.1 below. Additionally, correlation and variability between the Xsens gyroscope and accelerometer fused angles and the Xsens Euler angle output computed in this study are presented in Table 5.2. Fig 5.1 presents the Xsens gyroscope and accelerometer fused angle data alongside the Xsens Euler angles and the Vicon data for the wand rotations performed about the 3 axes of the local coordinate system.

For the wand rotation in the first direction – about the Y axis of the local coordinate system of the sensors, ΔROM of the Xsens fused angle and the Vicon data was < 6.6°, RMS < 3°, σ =2°, and CV = 2.7%, for all sensors involved in the experiment.

TABLE 5.1. AGREEMENT BETWEEN VICON AND XSENS – Experimental results for the wand study.

Between system variability of recorded rotation	*Experimental results – wand study*		
Xsens α fused against Vicon	Direction 1 [Y]	Direction 2 [Z]	Direction 3 [X]
Number of observations (N)	4	4	4
Difference between range of motion (ΔROM)	< 6.6°	< 47.8°	< 15°
Root mean squared error (RMS)	< 3°	10.2°	5.1°
Standard error (σ)	2°	8.2°	4.1°
Coefficient of variation (CV)	2.7%	7.2%	4.5%
Pearson product-moment correlation coefficient (r)	0.996	0.964	0.995

For the second direction – rotation about the local Z axis of the sensor coordinate system, along the gravitation axis of the Earth, ΔROM < 47.8°, RMS = 10.2°, σ = 8.2°, and CV = 7.2%.

For the third direction – rotation about the local X axis of the sensor coordinate system, ΔROM < 15°, RMS = 5.1°, σ = 4.1°, and CV = 4.5%. However, for all three directions, the correlation between the data sets is excellent, with r = 0.996 for rotation in direction 1, r = 0.964 for rotation in direction 2, and r = 0.995 for rotation in direction 3.

When comparing the Xsens fused angle against the Xsens Euler output, for the rotation about the Y axis of the sensors ΔROM < 1.2°, RMS < 0.6°, σ < 0.5°, and CV < 0.6% for all sensors involved in the experiment. For the rotation about the Z axis of the sensors, ΔROM < 2.9°, RMS < 2.6°, σ < 2.3°, and CV < 3.5% and for the rotation about the X axis of the sensors ΔROM < 0.2°, RMS < 0.9°, σ < 0.8°, and CV < 0.7%. The correlation between the Xsens fused and Xsens Euler angle data is, in this case as well, excellent with r = 1 for rotation about Y, r > 0.993 for rotation about Z and r = 1 for rotation about X. The CMC could not be computed for either of the experiments.

TABLE 5.1. AGREEMENT BETWEEN XSENS FUSED ROTATION ANGLE AND XSENS EULER ROTATION – Experimental results for the wand study.

Between system variability of recorded rotation	*Experimental results – wand study*		
Xsens α fused against Xsens Euler	Direction 1 [Y]	Direction 2 [Z]	Direction 3 [X]
Number of observations (N)	4	4	4
Difference between range of motion (ΔROM)	< 1.2°	< 2.9°	< 0.2°
Root mean squared error (RMS)	< 0.6°	< 2.6°	< 0.9°
Standard error (σ)	< 0.5°	< 2.3°	< 0.8°
Coefficient of variation (CV)	< 0.6%	< 3.5%	< 0.7%
Pearson product-moment correlation coefficient (r)	1	> 0.993	1

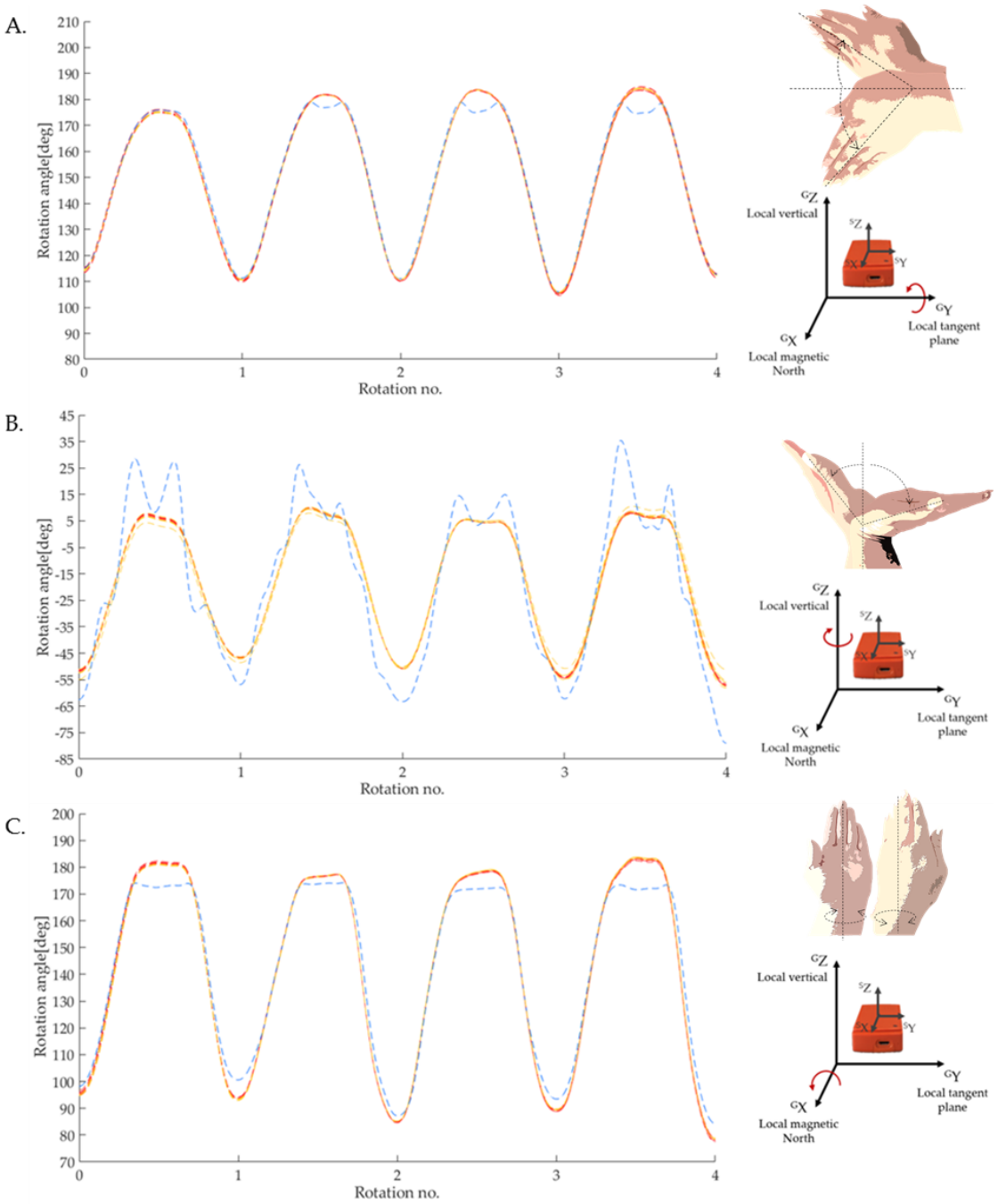

FIG 5.1. AGREEMENT BETWEEN XSENS AND VICON DATA – WAND STUDY. A. Rotation about Y axis; B. Rotation about Z axis; and C. Rotation about the X axis of the sensor local coordinate system. Where Vicon data is represented in blue, Xsens accelerometer and gyroscope fused angle represented in red, and Xsens Euler angles in yellow. In the top right corner, the wrist movement used to manoeuvre the Vicon calibrated wand, corresponding to each rotation, is presented. Below that, the local coordinate system of the sensors is presented with respect to the Earth global coordinate system. The rotation about the corresponding axis is marked with a red arrow, for each instance.

5.4. Discussion

During the experiment determining the agreement between the sensors and the optical motion capture system, the results revealed quite high differences in terms of ROM, ranging from up to 6.6°, when movement occurred about the Y axis, to up to 47.8°, when movement occurred about the Z axis, along the gravitation line.

The variability between data stemming from the two systems was further confirmed by the RMS, which ranged from 3°, for movement about the Y axis, to 10.2°, for movement about the Z axis, and the σ, ranging from 2°, for movement about Y axis, to 8.2°, for movement about Z axis.

However, when looking at the correlation of the data (Fig 5.1), it can be observed that the differences between the data sets appear to be cyclical and especially occurring at maxima and minima peaks. Furthermore, although both data sets were filtered, it appears that the sensors data is far smoother than the Vicon data, which is especially visible in the rotation about the Z axis of the sensors.

As the wand rotations in the current experiment were performed by manoeuvring the wand via wrist movements, it is impossible to guarantee that rotations occurred about a single axis at a time, and there is a possibility that composite movements, about more than one axis, or involving other joints, such as the elbow, occurred instead.

If this would be the case, the assumption made when post processing the sensor data, that the sensors placed on the wand move with respect to a fixed point, a dummy sensor, would be flawed. As the wand and the arm, manoeuvring it, move with respect to each other.

Additionally, when discussing motions recorded with an optical motion capture system, it is important to take into consideration the possibility of a kinematic cross-talk effect, produced by such a composite movement, as well.

Studies (Ferrari et al. 2008; Kok et al. 2014; Marin et al. 2003) in which human motion has been analysed, which corresponds to the rotations about the X and Z axes, presented in this experiment, such as adduction-abduction (varus-valgus) and internal-external (endo-exo) rotation of the knee, reported much higher rotation angles than physically possible in a

healthy human knee, if no method of compensating for the cross-talk effect was used in the data post processing.

For example, (Kok et al. 2014) reported an endo-exo rotation of the knee (corresponding to movement about Z axis in the current study) of approximately 40°, and a vargus-valgus rotation of the knee (corresponding to rotation about X axis in the current study) of approximately 20°. From an anatomical point of view, the endo-exo rotation of the healthy human knee should not exceed 10°, and vargus-valgus should be undetectable (Moore et al. 2010).

Furthermore, even when additional markers have been used in the literature as a means to address cross-talk effect, while results have improved significantly, in some cases errors still remain within the data. However, it should be noted that human motion is effected by other factors, e.g. soft tissue artefacts, which are not applicable when discussing the current experiment.

In fact, optical motion capture, is considered to be a gold standard when analysing flexion-extension movements, especially in the knee (corresponding to movements about Y axis in the current experiment), although, it is thought to be less accurate when addressing other movements, and therefore considered a silver standard for motion capture.

Nonetheless, the discrepancies between the inertial motion capture and the Vicon were significant and, in order to rule out mistakes in implementing the fused gyroscope and accelerometer algorithm, the fused sensor data has been compared with Euler angles, exported from the Xsens software directly.

The variability between fused sensor data and the Euler angles, was far smaller than the variability between the fused sensor data and the optical motion capture system, with the highest difference in ROM, RMS, and σ occurring about the Z axis, along the gravity line (ROM < 2.9°, RMS < 2.6°, σ < 2.3°), however with even smaller variance in rotations occurring about the other axes, (ROM < 1.2°, RMS < 0.9°, σ < 0.8°).

These small variations between the fused sensor data and the Euler angles, could be due to the implication of the magnetometers in the calculation of the Euler angles, which

could affect the heading estimates, and due to the λ value, the accelerometer weight, chosen for the current experiment, which could affect inclination estimates.

Since there were no apparent mistakes in the implementation of the protocol used to compute the fused accelerometer and gyroscope rotation angle, and RMS between the sensor data and the Vicon data, for rotation about Y axis, which corresponded with the flexion-extension axis of the knee, was RMS < 3°, similar to Seel et al. results for the healthy human leg (Seel et al. 2014), it was concluded that the protocol used in the current experiment to compute the fused sensor data could be applied further for the human gait experiments.

Chapter 6

6. Experiment 4: Laboratory based human gait study

The aim of the forth experiment was to test the second hypothesis (H_2) stated in Chapter 1, by determining whether there are any statistically significant differences between knee flexion-extension angles recorded in a laboratory during gait with a sensor system and an optical motion capture system. For this purpose, knee flexion-extension of 10 healthy participants was recorded with the Xsens sensors and processed from the gyroscope and accelerometer data using the fusion algorithm proposed by Seel et al.

The resulting output was compared to the data recorded simultaneously with the Vicon system and processed with a combination of the OCST, SARA and SCoRE techniques.

The interchangeability between using the sensor method and the optical motion capture method (current silver standard in laboratory based motion capture) was assessed by means of statistical analysis, further detailed in the following sections of this chapter.

Additionally, the repeatability of the Xsens/fused angle technique was assessed by comparing the within–day and between-day studies obtained from the sensor data against the ones obtained by processing Vicon data.

6.1. Participants

For the current study, 10 healthy male participants aged 22-30, with a weight of 69-93 kg and height of 169-193 cm, were recruited and asked to participate in a gait assessment study consisting of two sessions, two hours each. The participants taking part in this study were engaged in different levels of activities and met all the inclusion criteria specified in the ethics proposal with the number: 14083 for which approval was granted. None of the participants engaged in professional athletic activities or had suffered any injuries or pain in the joints of the lower limbs.

Prior to agreeing to take part in the study, the participants received a participant information sheet (Appendix 2). At the start of the first laboratory session the participants

were debriefed with regards to the procedure of the data acquisition and participant consent forms (Appendix 3) were handed to them for completion. Unfortunately, one participant dropped out of the study following the first session, due to health issues. However, there were no ethical concerns regarding the current study.

6.2. *Frames of reference*

When working with several different systems, the frames of reference in which the systems operate are often different from the one in which the output data needs to be translated. For example, when referring to human motion, the International Society of Biomechanics recommends a standardisation of the anatomical coordinate systems, so that flexion-extension is defined as movement occurring about the Z - axis of the human boday, along the frontal plane, abduction-adduction is the movement occurring around the X - axis, across the medial plane, and internal-external rotation is defined as movement about the Y-axis, in the horizontal plane (Wu et al. 2002).

However, the Vicon camera system follows the movement of the marker set within a known laboratory based coordinate system (global), called the capture volume. The marker set identified by the cameras is labelled and declared as a human kinematic model, with a body embedded coordinate system (local) and the locations of joint centres are defined with reference to the body embedded coordinate system's origin.

In the case of a lower limb model, the origin of the coordinate system lies within the pelvis and is declared first. Following that, the joint centres between the distal part of an anatomical segment and the proximal part of the next are defined with reference to the origins of the local coordinate systems of the anatomical segments. For example, the knee joint centre is declared relative to the thigh and shank local coordinate systems. The orientations of the distal local coordinate system and the proximal local coordinate system are defined by a transformation matrix and the joint angles are calculated from Euler equations in a right -handed Cartesian coordinate system.

The sensing equipment also uses a right-handed Cartesian coordinate system as a reference frame. In fact, there are two coordinate systems which need to be considered when working with the Xsens equipment; the local sensors fixed coordinate system (S) and the global Earth coordinate system (G).

When comparing two motion capture systems, all data must be processed within the same frame of reference, even if this requires translating data from one coordinate system to another. Not doing so, could not only substantially affect the accuracy of data, it could also prevent the data from being comparable.

6.3. Data acquisition

The first 1 hour and 30 minutes of each session was dedicated to the laboratory based motion capture. Firstly, the Vicon system was calibrated as described in Chapter 4 and the Awinda station was set up. Then, the synchronisation configuration between the two systems was set up as described in Chapter 5 and a wireless connection was established between the Xsens sensors and the Awinda station.

Upon arrival, the participants were asked to change into a non-constricting pair of short trousers. Then, the height, weight, anatomical segment lengths and widths were recorded and DW placed a total of 48 markers on specific anatomical landmarks (Fig 6.1).

Four markers were placed on the upper body, in the region of the 7th cervical vertebrae, the 8th thoracic vertebrae, the suprasternal notch and the xiphoid process.

On the lower limbs, the markers were placed on both, the left and right side on the anterior superior iliac spine (ASIS), the posterior superior iliac spine (PSIS), the iliac crest, the anterior superior and inferior thigh, the posterior superior and inferior thigh, the lateral superior and inferior thigh, lateral and medial femoral condyle, the anterior superior and inferior shank, the posterior superior and inferior shank, the lateral superior and inferior shank, the medial and lateral malleolus, the heel, and the 1st and 5th metatarsals.

The total set up of the experiment took up to 1 hour. Following that, the motion capture started and the participants were asked to carry out a set of movements, following the instructions of DW.

A part of these initial motion capture trials had the purpose of calibrating the human Vicon model (Fig 6.2) created by DW from the marker data. The other recorded motions are part of a study conducted by DW and are not included in the current thesis.

Following the conclusion of the initial motion studies, the sensors were attached to the participants' lower limbs (Fig 6.1) with double sided tape, respecting the positioning of the sensors suggested in the Outwalk and Seel et al. protocols (Cutti et al. 2010; Ferrari et al. 2010a; Seel et al. 2014). The sensors were fixed in place with cohesive tape.

FIG 6.1. MARKER AND SENSOR SETUP FOR LABORATORY BASED MOTION CAPTURE. A total of 48 fluorescent markers of varying sizes were attached to the participant's torso and legs, in order to facilitate the creation of a complex virtual human biomechanical model for the purpose of motion analysis. Additionally, 3 inertial and magnetic sensors were attached to the sacral area, the distal thigh and the distal shank for the purpose of validating a relatively new motion capture method.

The final part of the laboratory based motion capture was based on recording 5 gait trials for every participant. Each gait trial containing multiple gait cycles (steps).

6.4. Data processing

Vicon data

The Vicon data was analysed by David Wilson using a combined approach, involving compensating for soft tissue artefacts using a OCST method (Taylor et al. 2005), identification of joint centres using the SCoRE method and identification of the joint axis using the SARA method (Ehrig et al. 2011; Ehrig et al. 2006, 2007).

The above mentioned methods were used in conjunction with the calibration movement data to optimise marker positions when declaring the 'rigid frame' of the marker set, to estimate the hip joint centres and knee flexion extension axes of every participant. The Vicon model created by DW for the purpose of this motion analysis is presented in Fig 6.2 below.

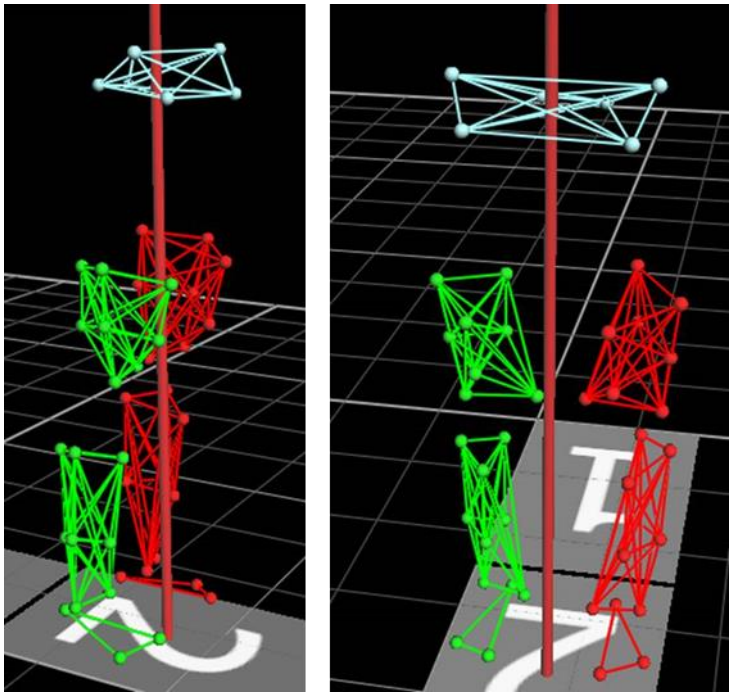

FIG 6.2. VICON VIRTUAL HUMAN LOWER LIMBS MODEL. The pelvis model is represented in grey, the right leg in green, and the left leg in red. The grey rectangles marked with 1 and 2 represent the force platforms and the thick red line emerging from force platform 2 represents the ground reaction force for the participant in the recorded static pose.

The orientation of the two resulting knee flexion extension axes was determined using the movement of the tibia with respect to the femur for the local coordinate system of the femur, and vice versa for the local coordinate system of the tibia. The knee joint centre was declared as an equidistant point between the lateral and medial extremities of the femoral condyles and projected onto the knee flexion extension axes within both local coordinate systems. The joint centre for the ankle was declared as the equidistant point between the lateral and medial extremities of the malleoli. The global coordinates of the joint centres were then declared according to their known positions within the local coordinate frames. Another set of anatomical local coordinate systems were then assigned to the analysed limbs. Finally, Euler angle decompositions were then calculated to obtain joint kinematics.

Following DW's data processing, a '.mat' file was produced, containing an array of data which contains the raw unfiltered knee flexion-extension information processed from the marker data. The raw knee flexion-extension information was then processed using the method described in the following pseudocode:

```
Vicon data processing sequence (Vicon gait):

Input: processed Vicon data

For participant number = 1 to 10

       For gait trial number = 1 to 5

              Set passband = 0.1

              Set stopband = 0.6

              Set sample frequency = 100

              Select gait data corresponding to knee flexion-extension from processed
data file

              Include only data which has a corresponding value > 1 in the analogue
              data column

Initiate filtering sequence:

              Call Filter design (arguments: participant number, gait number, knee
              flexion-extension angle, sample frequency, passband, stopband)

              Return (filtered knee flexion-extension angles)      //see filter
                                                                   description in
                                                                   chapter 5.2

Initiate knee flexion-extension angles interpolation sequence:

//see solution in chapter 5.2
```

```
            Return (interpolated knee flexion-extension angles)
        End for
End for
```

- *Xsens data*

The sensor data was calculated using a similar method as the one laid out in Chapter 5, Experiment 3 – the wand study. However, rather than calculating the rotation of a moving sensor with respect to a fixed one, in this instance, the rotation of the shank sensor was calculated with respect to the thigh sensor.

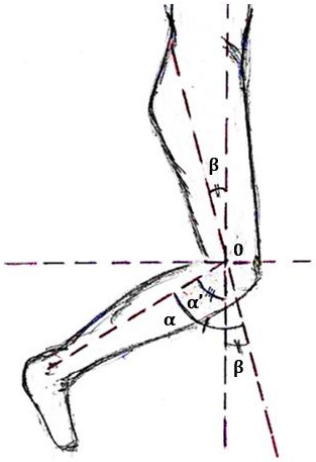

FIG 6.3. KNEE FLEXION/EXTENSION ANGLE CALCULATED WITH THE CURRENT PROTOCOL.

α - angle calculated between the thigh and the shank sensors. β – thigh flexion angle. α' – knee flexion/extension with respect to 0 flexion/extension assumed for a participant standing in a static pose.

In this case, the two sensors were moving with respect to each other, and both sensors produced gyroscope rotation angles with values different than the initial neutral position (Fig 6.3). In order to estimate the true flexion-extension angle of the knee, the estimated thigh flexion-extension angle was subtracted from the shank flexion-extension estimate.

6.5. *Statistical analysis*

Additionally, to the statistical analysis methods presented in Chapter 2, which was used to assess the variability and correlation between the sensor and the optical motion capture knee flexion-extension data, summary statistics were performed in order to assess statistically significant differences between the average step recorded with the sensor and the average step recorded with the Vicon.

For the summary statistics, the average gait cycle (determined as stated in the pseudo code above) performed by each participant during each recording session and processed with the two methods was considered. The data from the two sessions were concatenated in order to form a larger cohort.

F – statistics tests were carried out, in order to check if the distribution of gait cycle data within the participant cohort is normal. If a normal distribution of the data set was established, two sample t-test were carried out to assess the statistically significant differences between the average gait cycles of the entire participant cohort calculated for each of the two motion capture methods.

The differences between the mean output gait cycle of the two motion capture techniques were assessed at every percentage of the gait cycle. The interpretation of the p-values for this study were as follows:

- $p < 0.05$ – probability of statistically significant differences;
- $p < 0.01$ – high probability of statistically significant differences;
- $p < 0.001$ - very high probability of statistically significant differences.

6.6. Results

The distribution of all data sets used for calculating the summary statistics were normal. The summary statistics for the participant cohort revealed no statistically significant differences between the mean gait cycle (at any percentage), the standard deviation and the range of motion of the between-day laboratory sensor study and the between-day Vicon study.

However, t-tests revealed high to very high statistically significant differences between the mean gait cycle recorded with the sensors and the mean gait cycle recorded with the optical motion capture system in the laboratory, between percentages 17 (end of loading phase) to 56 (end of stance phase), and 69 to 94 (initial and mid swing phase) of a gait cycle.

Additionally, very high statistically significant differences between the ranges of gait cycles recorded with the sensors in the laboratory and the ranges of gait cycles recorded with

the optical motion capture system were discovered ($p < 0.001$). These findings will be discussed in more detail and addressed in Chapter 7.

The results for the studies assessing variability and correlation between the data recorded simultaneously with the inertial sensors and the Vicon optical motion capture system in the laboratory, can be found for each participant individually in Appendix 2. A summary of these results is written in the paragraphs below.

The within-day variability of knee flexion-extension recorded for the participants during gait in the first session was RMS between 1° and 2.2°, σ between 1.1° and 2.5° for Vicon data, and RMS between 1.2° and 2.1°, σ between 1.3° and 2.2° for sensor data recorded in the laboratory. Similarly, for the second session RMS were between 1.1° and 2.1°, and σ between 1.1° and 2.1° for Vicon data, and RMS between 0.9° and 2.9°, and σ between 1° and 2.9° for sensor data recorded in the laboratory (Appendix 1). The within day correlation of individual gait cycles (Appendix 1) for the sensor data for both sessions was represented by a CMC value comprised between 0.650 and 0.956, and for the Vicon data CMC was between 0.706 and 0.839. However, for most Vicon data CMC for within day correlation could not be computed.

Between day variability of gait knee flexion-extension for the participants (Appendix 1) was determined by ΔROM between 0.1° and 8.7°, RMS between 3.2° and 4.1°, σ between 1.6° and 3.7°, CV between 2.6% and 6% for Vicon data, and ΔROM between 0.9° and 7.5°, RMS between 2.6° and 5°, σ between 1.8° and 4.1°, CV between 2.8% and 6.3% for laboratory sensor data. The correlation between the data sets of the two sessions (Appendix 1) was excellent with CMC > 0.988, r > 0.983 for Vicon data, and CMC > 0.973, r > 0.959 for laboratory sensor data.

The variability between data recorded with the two systems (Appendix 2) was defined by ΔROM between 1° and 10.9°, RMS between 2.9° and 6.1°, σ between 2.5° and 7.9°, CV between 3.8% and 10.3% for the first session and ΔROM between 0.2° and 16.3°, RMS between 3.1° and 6.1°, σ between 2.5 and 5.1°, CV between 3.3% and 7.7% for the second session. The correlation between the data sets of the two motion capture systems (Appendix

2) was excellent with CMC > 0.977, r > 0.972 for the first session, and CMC > 0.966, r > 0.958 for the second session. An example of such correlation can be seen in Fig 6.4 Below.

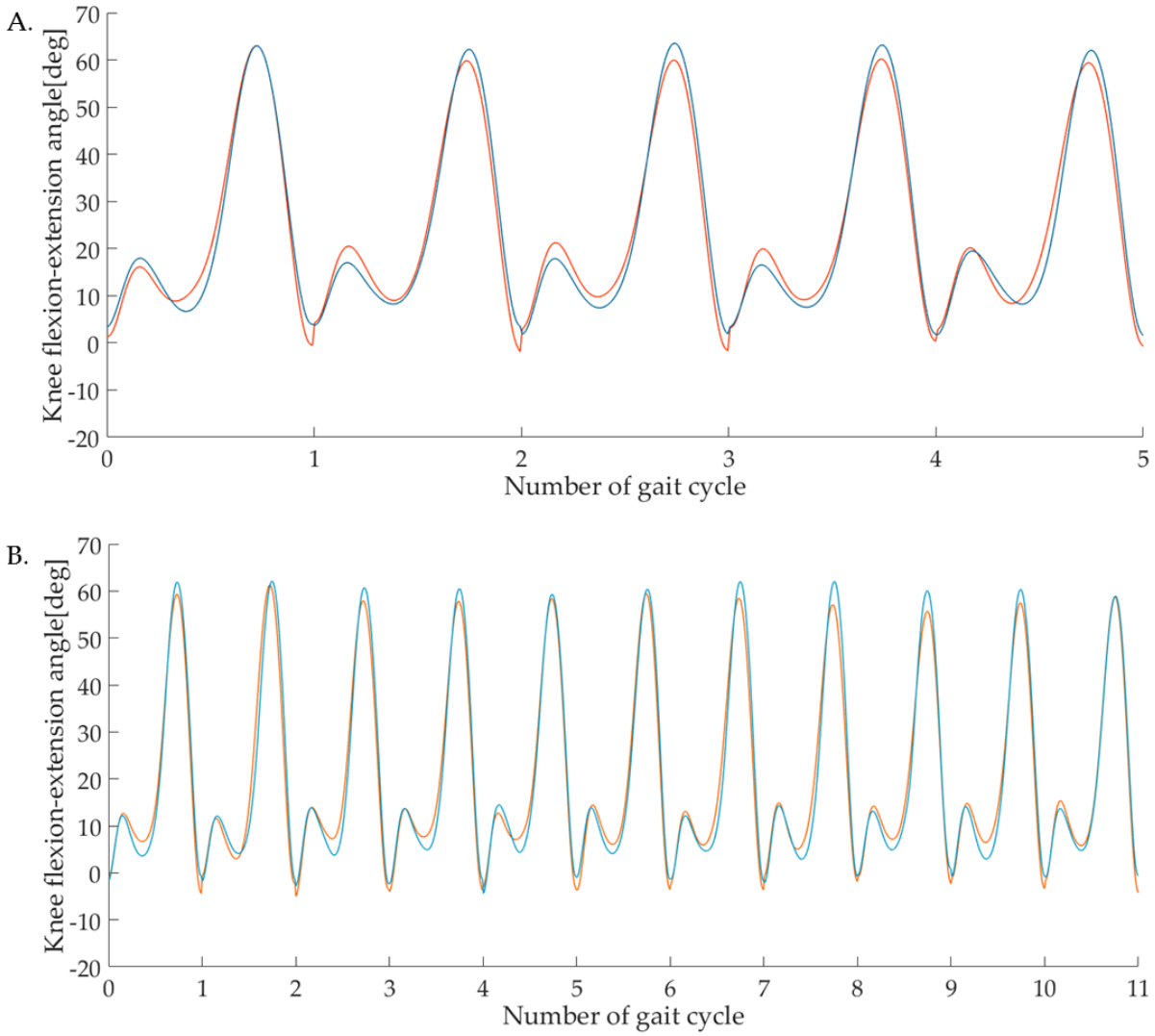

FIG 6.4. CORRELATION OF KNEE FLEXION EXTENSION RECORDED SYNCHRONOSLY WITH TWO MOTION CAPTURE SYSTEMS DURING GAIT PERFORMED IN A LABORATORY

A. Data from first session, where sensor data is represented in red and Vicon data in blue; B. Data from the second session, where sensor data is represented in orange and Vicon data in light blue.

6.7. Discussion

The laboratory based human gait study involved assessing knee-flexion extension of 10 healthy participants with an optical and an inertial motion capture technique, in order to validate the latter one against the first.

In order to do so, but also, in order to assess repeatability and reproducibility of the inertial sensing technique, within-day and between–day variability have been assessed.

Within day and between day variability are usually measured by means of ROM or correlation measures. However, researchers (Bland and Altman 1986; McGinley et al. 2009) suggested that using these methods alone, could lead to overestimation of agreement and furthermore, it was suggested that using additional measures of variability for this purpose would be highly recommended (McGinley et al. 2009).

The current study employed the use of several variability and correlation measures to assess within day and between day variability. However, although clinically acceptable correlation values for repeatability studies are known, the literature is yet unclear with regards to the clinically acceptable variability values.

For this purpose, as an additional measure, the within day and between day variability of the inertial sensing data was compared against the within day and between day variability of the optical motion capture data.

Firstly, the within day variability of the knee flexion extension recorded during gait with the inertial motion capture, considering all participants and all recording sessions was comprised between 0.9° and 2.9° for RMS, and between 1° and 2.9° for σ. These results are similar to the within day variability results for the optical motion capture, which were comprised between the bounds of 0.9 and 2.1 for RMS, and 0.9 and 2.5° for σ.

Unfortunately, the within day correlation for most of the Vicon data could not be computed. This is most likely due to the small number of observations produced by the, line of sight dependent, optical motion capture system.

In contrast, the within day correlation for the sensor data had shown, for most participants, very good to excellent results.

Furthermore, between day variability of the sensor data, considering all participants, was comparable to the between day variability of the optical motion capture data and to Ferrari et al.'s (2008) findings, which report an intra-protocol variability of 3.3°± 0.2°, deduced from mean absolute variability, i.e. the equivalent of our σ, for the T3Dg, PiG, SAFLo, CAST, and LAMB optical motion capture protocols. Additionally, between day correlation of data was excellent for both systems and two-sample t-test revealed that there is no statistically significant difference between the between day variability of the optical and the inertial motion capture systems.

The evidence from this experiment shows that the protocol proposed by Seel at el. for inertial motion capture is repeatable and reproducible to a similar extent to the OSSCA technique used for optical motion capture.

Proceeding to the validation of the inertial sensing technique against the OSSCA technique, inter-system variability measures for the knee flexion-extension recorded during gait for the 10 participants, revealed values between the following bounds: 1° to 10.9° for ΔROM, 2.9° to 6.1° for RMS, 2.5° to 7.9° for σ, and 3.8% to 10.3% for CV, for the first recording session, and 0.2° to 16.3° for ΔROM, 3.1° to 6.1° for RMS, 2.5° to 5.1° for σ, and 3.3% to 7.7% for CV, for the second recording session. Compared to the study conducted by Takeda et al. (2009), in which accelerometer and gyroscope based knee flexion-extension from gait was compared to its optical motion capture counterpart, obtaining RMS = 6.79°, absolute deviation = 4.65°, and percentage of variance = 14.60%, the current study reveals smaller RMS and percentage of variance for both recording sessions. However, the standard error is slightly higher in both recording sessions, than the absolute deviation reported by Takeda et al.

Furthermore, other studies comparing inertial sensing to optical motion capture, such as the one conducted by Jakob et al. (2013) reported a RMS of 7° ± 1.7° between the two systems, for gait knee flexion-extension, whereas the study conducted by Seel et al. (2014) reported a RMS of 3.7°, and the studies validating the Outwalk protocol reported RMS < 4° between knee flexion-extension recorded with the two systems (Van den Noort et al. 2013b).

Additionally, further studies employing the use of semi-wireless inertial sensing systems and an optical motion capture reference, reported RMS < 2° for gait knee flexion-extension (Cooper et al. 2009; Zhang et al. 2013).

It should be, however, noted that most of the aforementioned studies, with the exception of the studies conducted by Takeda et al., Jakob et al., and Seel et al, used methods in which marker clusters were either rigidly attached to plastic frames, or attached to plastic frames which were attached to the sensing units, and that the optical motion capture data was derived from these marker cluster models, rather than a biomechanical model derived from markers attached to anatomical landmarks.

Furthermore, it should be noted that each of these studies employed the use of different data processing protocols, using different anatomical constraints and that most of the studies, with the exception of the study conducted by Seel et al., were performed using semi-wireless, or wired inertial sensing units, which are more constricting and less compact than the wireless sensors, however, offer a higher sample frequency, higher update rate and a higher on board logging possibility.

This being the background, it can be observed that compared to the studies in which anatomical landmarks were used in order to produce the optical motion capture data (Jakob et al. 2013; Takeda et al. 2009), the RMS and CV values for the current study were lower. The exception in this case being the study by Seel et al. (2014), where the RMS value was within the upper and lower bounds of the RMS values of the current study.

However, it should be noted that the study by Seel et al. was a case study involving a single participant and that the probability of the RMS value differing when a larger number of participants is involved is very high.

In fact, the results in the current study were comparable to the results in most of the aforementioned studies, with the exception of the studies conducted by Cooper et al. (2009), and Zhang et al. (2013).

Moreover, Brennan et al. (2011b) have conducted a study in which inertial sensors were attached to a robotic knee joint, simulated by a rotating gimbal. In their study, the researchers

obtained a RMS of 3.2° between simulated flexion/extension and the reference, and they concluded that even under most ideal conditions, the results of motion studies could return a few degrees of error.

However, in their study, Seel et al. (2014) tested their protocol on a unilateral amputee's prosthetic leg. The results for the prosthetic limb showed a RMS of no more than 0.57° for knee flexion-extension during gait.

It is, therefore, highly probable that the minimum inter-system variability, depends not only on factors such as STA and the motion capture system used in the study, but is also highly dependent on the data processing method used and the accuracy with which this method was implemented.

When looking at correlation between knee flexion-extension recorded with the two motion capture systems, the results for the current experiment reveal excellent results with both, CMC > 0.97 and r > 0.97, for all participants considering both recording session. These correlations are comparable to the ones reported by Takeda el al. (CMC = 0.92) and Jakob et al. ($r = 0.97 \pm 0.02$).

Nonetheless, when looking at Fig 6.1 to Fig 6.10, the errors between the waveforms produced by the data from the two systems appear to be of cyclical nature, and being particularly pronounced during the mid-stance, and initial and mid-swing phase of the gait cycle.

Seel et al. reported similar findings, however, in their study, these differences were most prominent during push-off and heel-strike. The researchers dismissed those errors as being due to soft tissue artefacts. However, the current study investigated these errors further by performing two-sample t-tests to analyse the statistical differences, between the average gait cycle recorded by the two systems, at every percentage of the gait cycle.

The results from the t-test revealed high to very high statistically significant differences between percentages 17 to 56, and 69 to 94 of the average gait cycle recorded with the two systems. Furthermore, a very high statistically significant difference was found between the ROM of these average gait cycles.

This evidence indicates that, despite the similarities between the results of the current study and the other results reported in the literature, the current experiment failed to validate the inertial motion capture technique, used in the study, against the optical motion capture technique. A solution to this problem is proposed in the following chapter.

Chapter 7

7. Experiment 5: Sensor data correction

In order to address the seemingly cyclical differences between the sensor data and the reference system, discovered during Experiments 3 and 4, the generation of a standardized sensor data correction vector was proposed.

However, it should be noted, that the correction vector proposed in the current experiment only addresses one cycle of rotation at a time, produced about the Y axis of the sensors, e.g. knee flexion-extension of a single gait cycle.

The correction vector, is a 1-by-101 array of correction factors (see Appendix 2), addressing every percentage of the gait cycle, starting with 0%.

In order to increase the number of data sets within the tested cohorts, for the current experiment, all gait sessions from all participants, recorded in the laboratory, were considered and a correction vector was calculated for each session individually. In order to avoid bias, when calculating the correction factor for a specific session, the data recorded during that session is excluded from the calculation.

To further test the applicability of the proposed standardized correction vector, a pseudo population of participants was created by picking 1000 times, 100 pseudo random values between 1 and 19, which represented the numbers of specific sessions.

The standardized correction vector represents the average of all the correction factor arrays produced for every instance of the pseudo population. The method used to calculate and apply the standardized correction vector is laid out in the following pseudocode:

```
Generating standardized correction coefficient vector sequence:
Input: Sensor data - mean gait cycle of each participant for sessions 1 and 2
Input: Vicon data - mean gait cycle of each participant for sessions 1 and 2
Concatenate gait cycle cohorts from the two sessions for sensor data
Concatenate gait cycle cohorts from the two sessions for Vicon data
For session number = 1 to 19
```

```
For random picks number = 1:1000
Compute A = a 100-by-1 array of pseudorandom integers between 1 and 19
              Compute B by eliminating the value of current session number from A
              For session number = 1 to 19
                    Declare a = participant's mean gait cycle from sensor data
                    Declare b = participant's mean gait cycle from Vicon data
                    Declare c = minimum value of participant's mean gait cycle from
                    sensor data
                    Declare d = range of participant's mean gait cycle from sensor
                    data
                    Scale sensor data by subtracting c from a and dividing by d
                    Scale Vicon data by subtracting c from b and dividing by d
              End for
              For session number = 1 to 19
                    Compute correction vector by subtracting scaled sensor data from
                    scaled Vicon Data
              End for
              Return matrix containing correction coefficient vectors specific to each
              session
       End for
       Declare a = participant's mean gait cycle from sensor data
       Declare b = correction coefficient vector specific to the session
       Declare c = minimum value of participant's mean gait cycle from sensor data
       Declare d = range of participant's mean gait cycle from sensor data
       Correct sensor data by adding b to a and multiplying by d, then add c
       Return corrected sensor data
End for
```

Similarly, to the uncorrected data (Fig 7.1) in Experiment 4, summary statistics were computed in order to assess statistically significant differences between the corrected data and the reference system at every percentage of the gait cycle (Fig 7.1). The summary statistics for the corrected data were compared against the results of the uncorrected data.

7.1. Results

As previously laid out, in the Results section in Chapter 6, the two sample t-test revealed a statistically significant difference between the mean gait cycle recorded with sensors in the laboratory and the mean gait cycle recorded with the Vicon (Fig 7.1).

The statistical significance of the discovered differences is further detailed in Table 7.1 below.

TABLE 7.1. STATISTICALLY SIGNIFICANT DIFFERENCES ACROSS A GAIT CYCLE RECORDED WITH TWO DIFFERENT MOTION CAPTURE METHODS. Where * - confirmed statistically significant difference; ** - high statistically significant difference; and *** - very high statistically significant difference.

Gait cycle [%]	*Statistical significance*
	p - value
17 to 20	< 0.04 (*)
21 to 51	< 0.008 (**)
52 to 56	< 0.04 (*)
69 to 70	< 0.05 (*)
71	0.004 (**)
72 to 91	< 0.0008 (***)
92 to 93	< 0.009 (**)
94	0.03 (*)

After applying the correction vector (Fig 7.2), the statistically significant differences between the average gait cycles recorded with the two systems are eliminated. The p-values returned by the two sample t-test exceed p = 0.87 for every percentage of the gait cycle.

Additionally, after the application of the correction vector the previously reported statistically significant differences ($p < 0.001$) in range of motion for the knee flexion-extension recorded with the two systems during a gait cycle are eliminated. The two-sample t-test returning a p-value of 0.53, in this case.

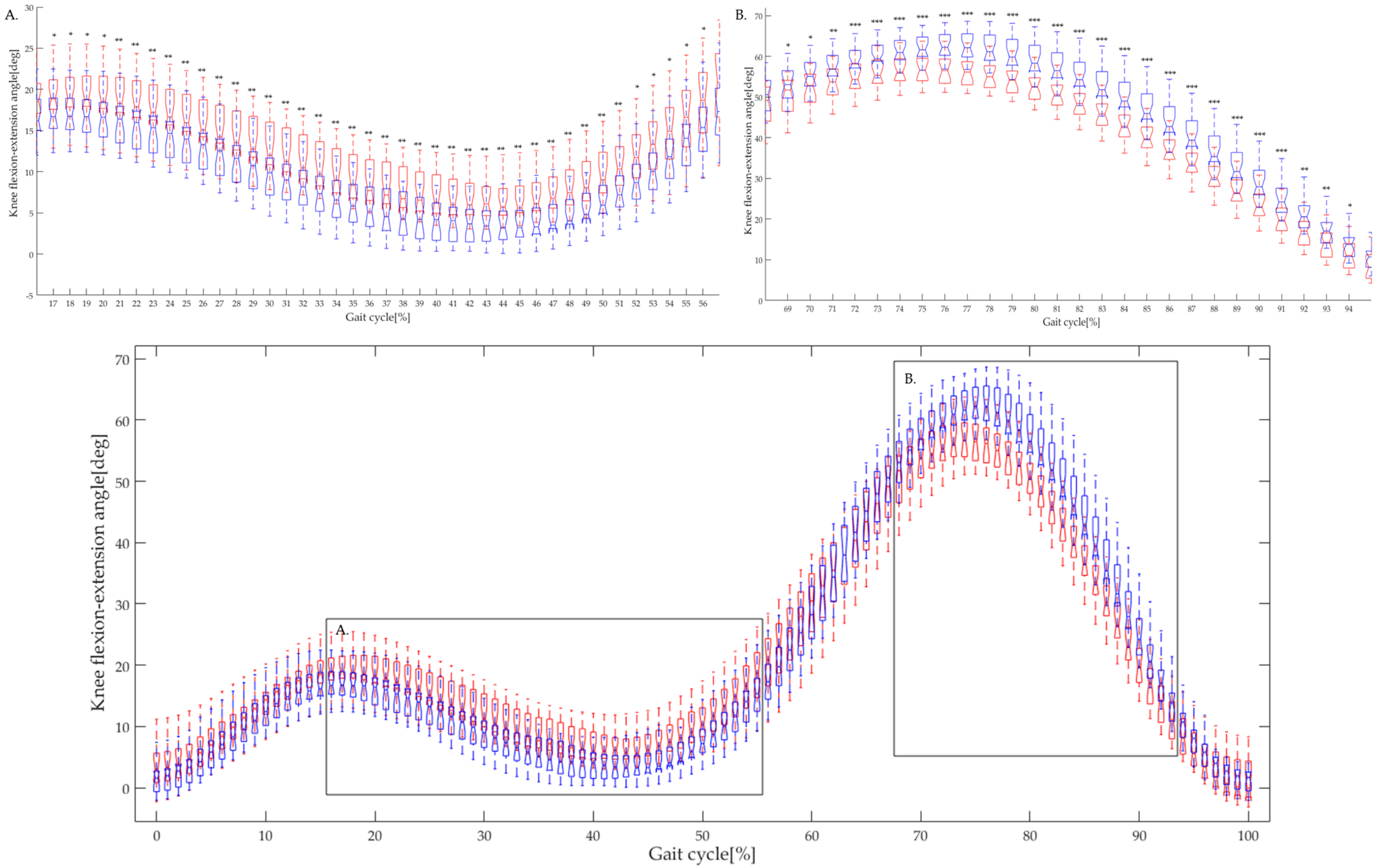

FIG 7.1. BOXPLOT REPRESENTING THE STATISTICALLY SIGNIFICANT DIFFERENCES BETWEEN KNEE FLEXION-EXTENSION RECORDED DURING AN ENTIRE GAIT CYCLE WITH TWO DIFFERENT MOTION CAPTURE SYSTEMS. Where inertial sensor data is represented in red and optical motion capture data in blue. * - confirmed statistically significant difference; ** - high statistically significant difference; and *** - very high statistically significant difference.

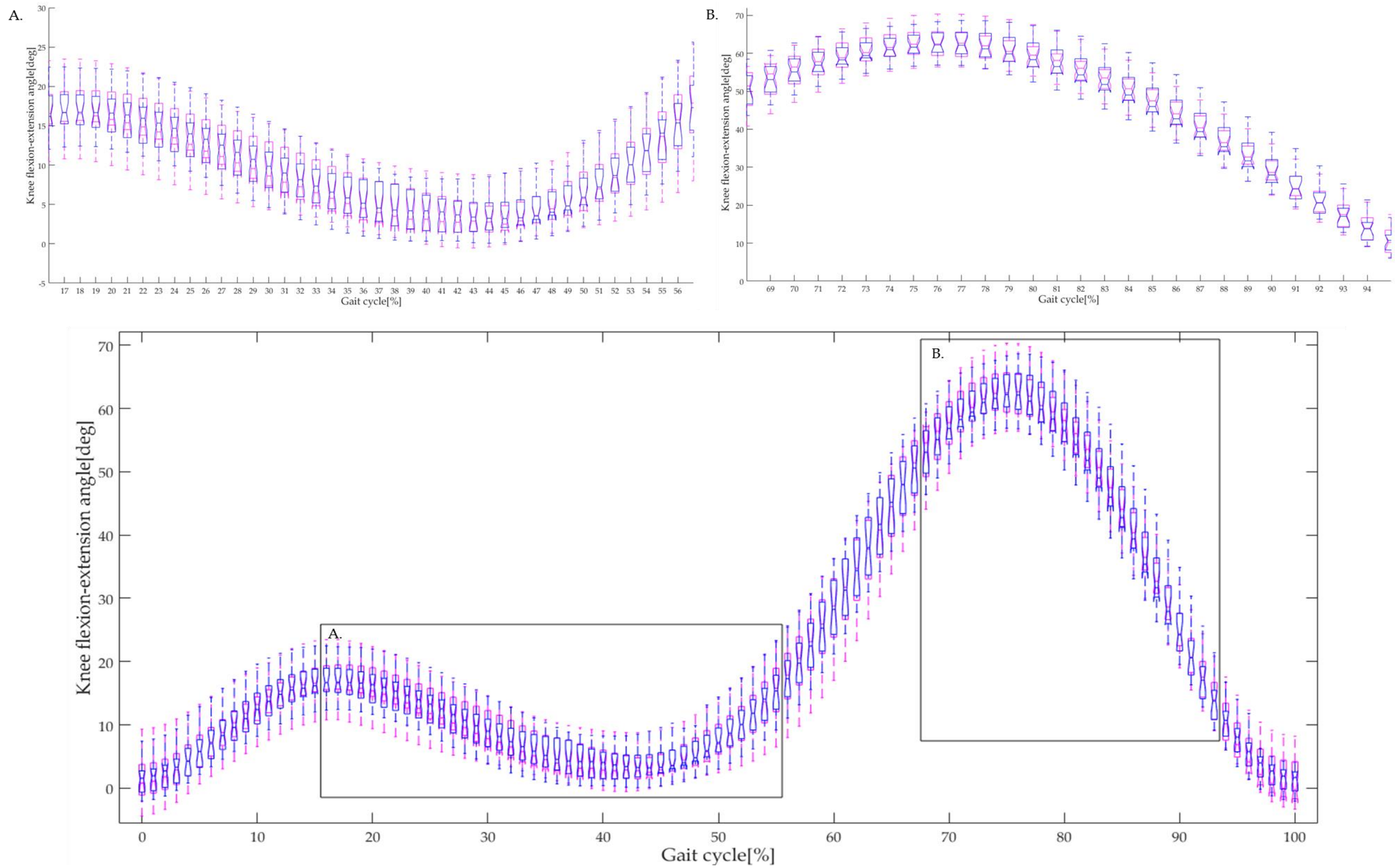

FIG 7.2. BOXPLOT REPRESENTING THE STATISTICALLY SIGNIFICANT DIFFERENCES BETWEEN KNEE FLEXION-EXTENSION RECORDED DURING AN ENTIRE GAIT CYCLE WITH TWO MOTION CAPTURE SYSTEMS, AFTER THE INERTIAL SENSOR DATA WAS CORRECTED. Where the inertial sensor data is represented in magenta and the optical motion capture data in blue.

7.2. Discussion

This chapter proposed a solution to the failure of validating the inertial motion capture technique against the optical motion capture technique.

The source of the, previously mentioned, statistically significant differences discovered between walking knee flexion-extension recorded with the two motion capture systems is yet unclear. However, while the assumption made by Seel et al., that such differences are likely caused by soft tissue artefacts, produced when the skin mounted markers and the skin mounted sensors move with respect to each other, are worth considering, there is simply not enough information or evidence in the literature to support such claims.

When it comes to soft tissue artefacts in inertial motion capture, very little research has been conducted to investigate the effects of this phenomenon on the output of the data, or to provide a method to eliminate such errors from the data altogether. However, despite the lack of evidence, researchers seem to find this STA grey area, a very popular source of error to cite.

From the very little information found in the literature on STA in inertial motion capture, it resulted that using light weight sensing units and using a strap down method, to reduce the movement of the sensing unit with respect to the limb, would ultimately reduce STA significantly (Forner-Cordero et al. 2008).

These prevention measures have been employed in the current study. Furthermore, measures have been taken to reduce STA in the optical motion capture data. It is, therefore, highly unlikely that STA alone could cause the errors, leading to such high discrepancies between data recorded by the two motion capture systems.

Thus, it would be more likely to assume, that alongside some STA, the sources of error for these statistically significant differences would relate to the systematic differences in estimating joint axes with the two techniques. This would possibly explain the cyclical nature of the errors as well.

Nonetheless, the method proposed in the current chapter, eliminates these errors, as well as the differences in ROM between the data recorded with the two systems, by applying a correction factor to each percentage of a gait cycles recorded with the inertial sensing units. Ultimately, applying this array of correction factors enables the validation of the inertial motion capture technique against the optical motion capture technique.

Chapter 8

8. Experiment 6: Non – laboratory based human motion study

The aim of the sixth and final experiment was to test the third hypothesis (H_3) stated in Chapter 1, by determining whether there are any statistically significant differences between knee flexion-extension angles recorded in a laboratory during gait with a sensor system and knee flexion-extension angles recorded outdoors during gait with a sensor system.

Once the data acquisition in the laboratory was completed the markers were removed from the participant's body and the participant was asked to get dressed and put shoes on. The connection between the sensors and the MT Manager remained uninterrupted during the entire data acquisition session.

The participant and the researcher walked outside the building to a paved area and carried on with recording the 5 non-laboratory based gait trials. The capturing of the gait trials outdoors concludes the data acquisition session.

Knee flexion-extension angles were estimated from the outdoor gait data, using the same method detailed in Chapter 6, Experiment 4. The outdoor sensor data was compared against the indoor sensor data, using the same statistical analysis procedures from Chapter 6. For the purpose of the current experiment, all sensor data presented in this chapter is uncorrected.

8.1. Results

The distribution of all data sets used for calculating the summary statistics were normal. The summary statistics for the participant cohort revealed no statistically significant differences between the mean gait cycle (at any percentage), the standard deviation and the range of motion of the between-day laboratory sensor study and the between-day outdoor sensor study. Additionally, no statistically significant differences were found between the

mean gait cycle and the ranges of gait cycles recorded with the sensors in the laboratory and the mean gait cycle and the ranges of gait cycles recorded with the sensors outdoor.

The within-day and between-day variability and correlation of knee flexion-extension recorded for the participants with the sensors in the laboratory during gait was reported in chapter 6.6. Therefore, only within-day and between-day variability and correlation data concerning knee flexion-extension recorded with the sensors outdoor during gait will be presented in the current chapter. The results for the studies assessing variability and correlation between the data recorded in the laboratory and the non-laboratory environments with the inertial sensor system, can be found for each participant individually in Appendix 3. A summary of these results is written in the paragraphs below.

The within-day variability of knee flexion-extension recorded for the participants during gait outdoors in the first session was RMS between 1° and 2°, σ between 1° and 2.2°, and RMS between 0.9° and 3.7°, σ between 0.9° and 3.8° in the second session (Appendix 1). The within day correlation of individual gait cycles for the outdoor sensor data for both sessions was represented by a CMC value comprised between 0.735 and 0.984 (Appendix 1).

Between day variability of gait knee flexion-extension recorded with the sensor system outdoors for the participants was determined by ΔROM between 0.3° and 9.1°, RMS between 2° and 6.6°, σ between 1.6° and 5.6°, and CV between 2.5% and 7.2%. The correlation between the data sets of the two sessions was excellent with CMC > 0.968, r > 0.953 (Appendix 1).

The variability between data recorded with the sensor system in the two environments (Appendix 3) was defined by ΔROM between 0.3° and 14.3°, RMS between 1.8° and 5.4°, σ between 1.5° and 4.4°, CV between 2.3% and 7.8% for the first session and ΔROM between 0.1° and 13.9°, RMS between 2.2° and 6.1°, σ between 1.6 and 5.1°, CV between 2.8% and 6.5% for the second session. The correlation between the data recorded in the two venues (Appendix 3) was excellent with CMC > 0.979, r > 0.971 for the first session, and CMC > 0.974, r > 0.966 for the second session. An example of a such correlation is presented in Fig 8.1 below.

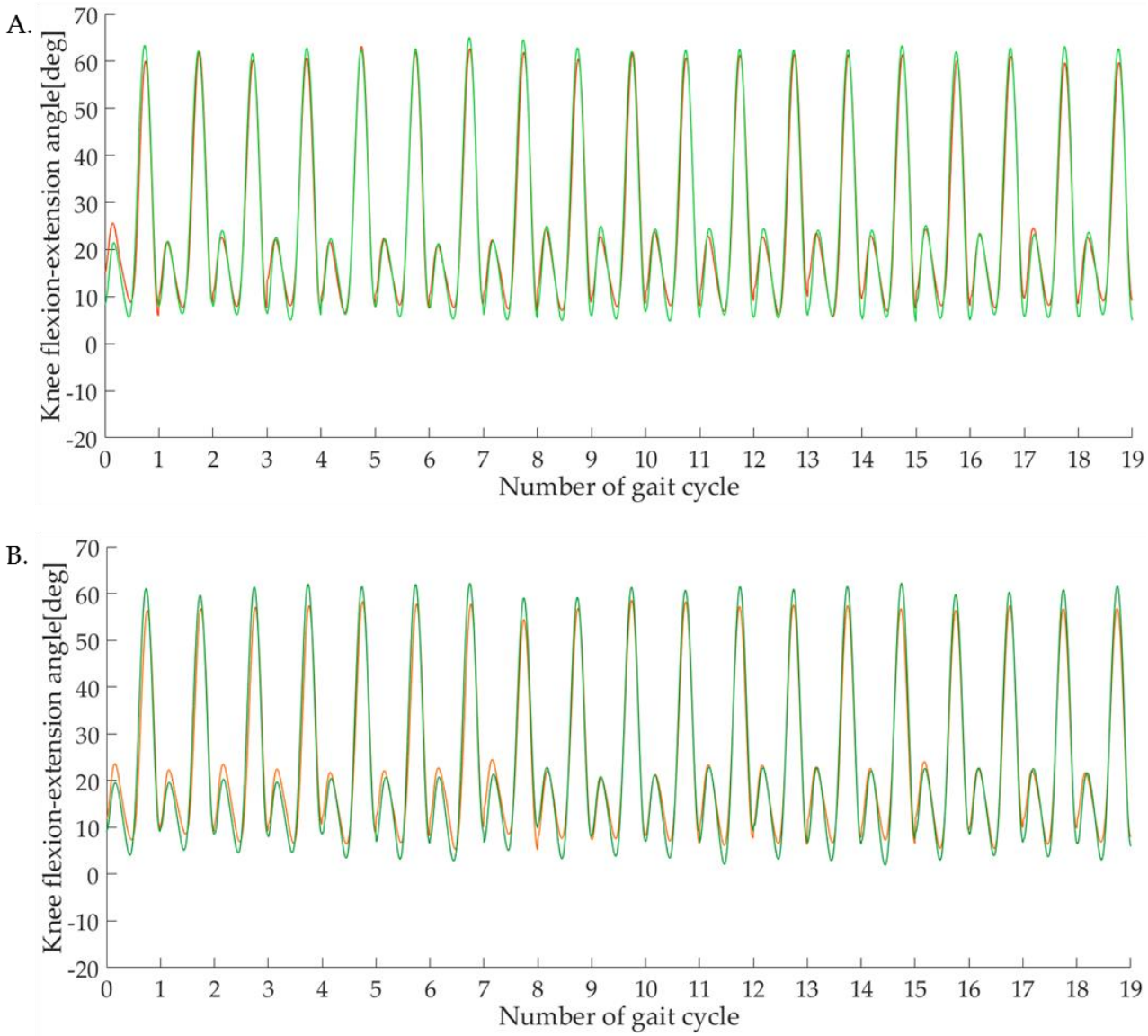

FIG 8.1. CORRELATION OF KNEE FLEXION EXTENSION RECORDED IN A LABORATORY AND A NON-LABORATORY BASED ENVIRONMENT WITH A SENSOR SYSTEM

A. Data from first session, where data recorded in the laboratory is represented in red and outdoor data in dark green; B. Data from the second session, where data recorded in the laboratory is represented in orange and outdoor data in green.

8.2. Discussion

For the non-laboratory based human motion study, the within day variability results are slightly higher than the within day variability results for the indoor inertial motion capture and the optical motion capture, presented in chapter 6. Similarly, to the indoor

inertial motion capture, the within day correlation for the outdoor data had shown, for most participants, very good to excellent results.

Between day variability of the outdoor sensor data was slightly larger than the between day variability of the indoor sensor data as well. However, between day correlation of data was excellent for both venues, with CMC > 0.97 and r > 0.95 and two-sample t-test revealed that there is no statistically significant difference between the between day variability of the outdoor and the indoor inertial motion capture data.

The within day and between day variability for the outdoor inertial motion capture were slightly higher than the indoor and the optical motion capture. However, these results could be explained by a few factors, such as a more natural and less calculated manner of executing movement in a non-laboratory based environment, wearing different garment and/or footwear during the two recording sessions, variances in weather between testing sessions, etc.

Proceeding to the comparison between indoor and outdoor inertial motion capture, inter-venue variability measures for the knee flexion-extension recorded during gait for the 10 participants, revealed values between the following bounds: 0.3° to 14.3° for ΔROM, 2.4° to 5.4° for RMS, 1.5° to 4.4° for σ, and 2.3% to 7.8% for CV, for the first recording session, and 0.1° to 13.9° for ΔROM, 2.2° to 6.1° for RMS, 1.8° to 5.1° for σ, and 2.8% to 6.5% for CV, for the second recording session. Additionally, between venue correlations are excellent, with CMC > 0.97 and r > 0.96. These results are comparable to the ones presented in chapter 6, for the laboratory based human motion capture, and to the results presented in the literature for other comparative human motion capture studies (Jakob et al. 2013; Seel et al. 2014; Takeda et al. 2009; Van den Noort et al. 2013b).

However, while there is an evident between venue variability, two-sample t-tests show no statistically significant differences between an average gait cycle recorded indoor and an average gait cycle recorded outdoor, when compared at every percentage of the gait cycle. Furthermore, there were no statistically significant differences between ROM of the average gait cycles recorded indoor and outdoor with the inertial motion capture system.

Between venue variability could, however, be explained by the fact that during laboratory based motion capture, the participants were barefoot, whereas during outdoor motion capture the participants were wearing shoes. Additionally, during laboratory based motion capture, the participants wear less garment and have markers and EMG sensors attached to their limbs. However, the markers and EMG sensors are removed prior to the outdoor motion capture and the participants are asked to dress in their usual outdoor garment. Furthermore, the measurement volume in the laboratory is covered by a layer of rubber, whereas the outdoor motion capture is carried out on pavement. The difference in ground reaction forces, may play a role in the execution of the movement.

Finally, in contrast to the measurement volume, the force platforms and the camera setup within the laboratory, the outdoor environment may seem more familiar and a less constricting environment, and the motion may therefore be carried out in a more relaxed manner.

Chapter 9

9. General discussion

The six experiments conducted in the current study addressed the aims and objectives stated in the introduction of this thesis. The first two experiments demonstrated that the equipment chosen for this study, when compared to gold standards, functioned to the high accuracy guaranteed by the manufacturers.

Furthermore, the tested data processing protocol for the inertial motion capture proved to have a similar repeatability and reproducibility in the analysis of human walking knee flexion-extension, as the OSSCA technique used for optical motion capture, the most robust visual data processing protocol hitherto.

The results for the laboratory based human gait study revealed that the inter-system variability of the two motion capture systems, with the afferent protocols which were employed, was comparable to inter-system variability and correlation previously reported in the literature (Cutti et al. 2010; Ferrari et al. 2010a; Jakob et al. 2013; Seel et al. 2014; Takeda et al. 2009; Van den Noort et al. 2013b), indicating that the inertial motion capture system and the tested data processing protocol function together to the expected accuracy. Thereby, confirming the first hypothesis (H_1).

However, this evidence does not necessarily confirm the validation of the inertial sensing method against the optical motion capture method as, despite the fact that the results from the current study are comparable to the ones in the literature, the literature does not provide any indication of what an acceptable inter-system variability is for human motion capture. Furthermore, there was an apparent cyclical pattern to the occurrence of the inter-system errors, visible in the laboratory based human motion capture, as well as the wand study.

In fact, when analysing these errors further, by performing two-sample t-test to assess the differences between knee flexion extension during the average gait cycle recorded with each motion capture system, statistically significant differences were discovered between

percentages 17 and 56, and 69 and 94 of the gait cycle, and between the overall ROM, rejecting the second hypothesis (H_2). This evidence indicates the failure to validate the tested inertial sensing data processing protocol against the optical motion capture data processing protocol.

While these errors were apparent in the aforementioned studies as well, none of the researchers performed any statistical analysis assessing the significance of these errors. Although, Seel et al. mention in their study that the errors are most obvious during the push-off and heel-strike phases of the gait cycle, and suggested that STA may be the source of these errors, based on the comparison between the healthy leg knee flexion-extension and the prosthetic leg contralateral. However, this assumption may not be so accurate after all, as knee flexion-extension during the stance phase of a gait cycles is very different for the healthy leg compared to the prosthetic. Furthermore, there is very little information in the literature on the effects of STA in inertial motion capture, and while it may seem a plausible source of error to cite in such cases, further research into this matter is necessary before being able to make such assumptions with certainty.

Additionally, the current study employed the use of a strap-down method, proposed by (Forner-Cordero et al. 2008), in order to attenuate STA in the inertial motion capture and an OCST data processing method was used to eliminate STA in the optical motion capture data. The probability of the STA alone causing these significant inter-system differences is, therefore, quite low.

Due to the cyclical pattern of the errors, the fifth experiment of the current study, proposed employing the use of an array of correction factors (Appendix 2), addressing every percentage of the gait cycle, in order to attempt to reduce the inter-system variability. After this correction vector was applied to the inertial sensor data, t-test were carried out to assess inter-system variability between the corrected sensor data and the optical motion capture data. No statistically significant differences were observed between the corrected knee flexion extension for the average gait cycle recorded with the sensors and the knee flexion extension for the average gait cycle recorded with the optical motion capture system.

Furthermore, no statistically significant differences were found for between the ROM of the corrected knee flexion extension for the average gait cycle recorded with the sensors and the ROM of the knee flexion extension for the average gait cycle recorded with the optical motion capture system. Therefore, the inertial data processing protocol proposed by Seel et al. (2014), could be validated against the OSSCA optical motion capture data processing protocol, if used in conjunction with the proposed correction vector.

This may indicate that, in fact, the aforementioned inter-system variability, could stem from the different approaches employed by the two protocols, to estimate joint axes. As a matter of fact, when comparing the proposed correction vector to the mean standard deviation of the sensor data with respect to the optical motion capture data, for rotation about the Y axis (corresponding to the axis of knee flexion extension), from the wand study (Fig 9.1), similarities between the pattern and the range of excursion (mean standard deviation range = 9.28°; correction factor range = 10.5°) of the two, can be observed.

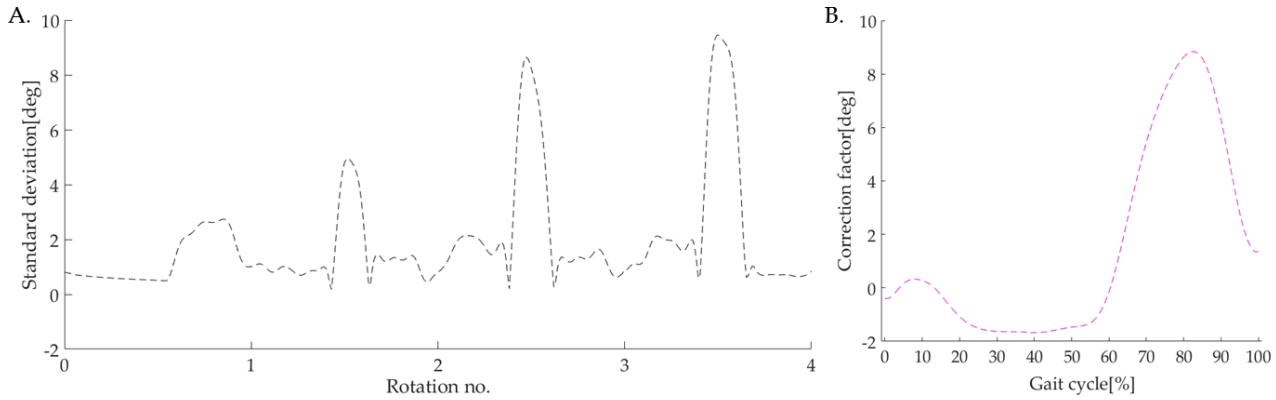

FIG 9.1. COMPARISON BETWEEN THE PROPOSED STANDARDIZED CORRECTION VECTOR (B.) AND THE MEAN STANDARD DEVIATION BETWEEN SENSOR AND OPTICAL MOTION CAPTURE DATA, FOR ROTATION ABOUT THE Y AXIS OF THE SENSOR LOCAL COORDINATE SYSTEM (A.).

This evidence further suggests that STA are not the main source of error in the discovered inter-system variability, as the sensors were attached to the rigid frame of the Vicon calibration wand, during the sensor to optical motion capture agreement study.

Moving further, the final experiment of the current study, assessing differences between laboratory and non-laboratory based human motion capture, revealed a slightly

higher variability for the non-laboratory based inertial motion capture repeatability studies, than the laboratory based inertial and optical motion capture repeatability studies. Nonetheless, even though the values for the inter-venue variability and correlation measures were similar to the ones for the inter-system variability, no statistically significant differences were discovered between the average gait cycle recorded indoor and the average gait cycle recorded outdoor. These findings confirm, therefore, the third and final hypothesis (H_3).

9.1. Conclusions

This study has confirmed that the Xsens MTw inertial sensing units and the inertial motion capture data processing protocol proposed by Seel et al. (2014) function together to the expected accuracy, when estimating knee flexion extension from gait trials. However, data obtained using the sensors in conjunction with Seel et al.'s protocol is only comparable to data obtained by using an optical protocol combined with an OSSCA data processing approach when the proposed array of data correction factors (Appendix 4) is applied.

Furthermore, the current study showed there is no statistically significant difference between knee flexion extension recorded during gait with inertial motion capture in a laboratory and a non-laboratory based environment. This evidence suggests that accurate outdoor inertial motion capture, for walking knee flexion extension, is possible if the tested data processing protocol is implemented correctly and in conjunction with the proposed correction vector.

However, the possibility of light weight ambulatory motion tracking is not the only advantage the inertial sensing technique provides. Compared to the optical motion capture the inertial sensing equipment is far cheaper, more compact and provides a much more rapid set-up. Furthermore, the data acquisition is not limited by line-of-sight, therefore, recording a larger quantity of data within the same measurement volume as the optical motion capture.

Nonetheless, even if most disadvantages relating to inertial motion capture, have been addressed in the tested data processing protocol, such as ferromagnetic interferences, inability to estimate sensor position on anatomical segment, there still remains an important

aspect which needs to be taken in consideration when using this data acquisition and processing technique. The inertial sensing method could only be validated against the optical motion capture method if the proposed correction vector was applied.

9.2. Limitations

One of the limitations of the current study was the fact that validating the inertial sensing method, employed in the experiments, against the optical motion capture was impossible without using the proposed array of correction factors to shift the sensor data closer to the optical motion capture data.

Furthermore, gaps in the research literature regarding, management of inertial motion capture related soft tissue artefacts, a standardized inter-system/inter-venue/inter-participant data offset removal, or an indication as to what an acceptable inter-system variability is, for system validation purposes, made the interpretation of the results in this study much harder. For example, obtaining similar results for RMS, CMC, r and percentage of variation as the ones reported in the literature, could have indicated the validation of the tested sensor technique against the optical motion capture, without any need for further action. In reality, the two-sample t-tests revealed the opposite.

Furthermore, without a standardized inter-system offset removal, it is hard to compare results from different studies, especially since most researchers do not report their offset removal method in their work. Different offset removal techniques can affect the accuracy of the resulting data to different degrees and in some cases offset removal can eliminate natural errors and lead to an overestimation of the accuracy (Røislien et al. 2012). Additionally, not all variability measures used in the current study had a match in other research. It was therefore difficult to interpret these results.

A final limitation was represented by the line-of-sight dependency of the optical motion capture, which resulted in a reduced number of observations compared to the number of observation available from the inertial motion capture, reducing the strength of the statistical analysis in the laboratory based motion capture experiment.

Chapter 10

10. Future perspectives

Future work in the field could, firstly, address some of the gaps in the current research, such as proposing the use of a standardized method to remove offset between data sets of comparative studies.

A few offset removal methods were described in the literature, such as calculating the average positions of local minima within the two data sets and computing the offset between these values (Jakob et al. 2013) as being the value which needs to be subtracted from one of the systems, or calculating the offset as being the average value of the difference between the waveform which needs to be shifted and the average waveform of the reference (Cutti et al. 2010).

However, most researchers do not report the method used for between system offset removal in their studies and a possibility exists that the data sets are simply shifted closed together by removing the difference between the two studied waveforms. This practice might remove some natural differences as well and cause overestimation of accuracy.

Employing the use of a standardized method for offset removal, would therefore generate more comparable results and eliminate at least one source of between study variability, in the motion capture field.

Another present short coming in inertial motion capture, which needs to be addressed is posed by the management of STA. While Forner-Cordero et al.'s (2008) research proposed the use of a strap-down method to reduce STA when working with skin mounted sensors, using e.g. cohesive tape to hold the sensors in place is by no means a real match for the OCST algorithm used in the OSSCA technique to reduce STA. For this purpose, a method may be developed to identify the frequency at which the STA occur and to extrapolate the movement of the sensors with respect to the skin and other underlying tissue, from the final joint motion output data.

Relating to the discoveries from the current study, perhaps an analysis comparing the joint axes estimates from the sensor protocol and the ones from the optical motion capture could shed more light on the statistically significant differences discovered between the two motion capture data processing protocols used in our study.

Furthermore, a popular debate in the motion capture field, posed by the degree of freedom of the joint axes (fixed axes vs. axes moving with motion), could be addressed by simply modifying the sensor data processing protocol to re-compute the joint axis at a set time interval for a given motion study. By carrying out this experiment, the joint axes can be tracked throughout the entire motion study, and any change in joint axes position can be detected.

Finally, the sensor data processing protocol can be validated against the optical motion capture data processing protocol, for other joints and other motions as well, determining, if needed, the joint and motion specific correction vectors, using the method described in chapter 7 of the current study.

Alexander, E. J. and Andriacchi, T. P. 2001. Correcting for deformation in skin-based marker systems. *Journal of biomechanics*.

Andriacchi, T. P. et al. 1983. A study of factors influencing muscle activity about the knee joint. *Journal of orthopaedic research* 1(3), pp. 266-275.

Antonsson, E. K. and Mann, R. W. 1985. The frequency content of gait. *Journal of Biomechanics* 18, pp. 39-47.

Asano, T. et al. 2005. The functional flexion-extension axis of the knee corresponds to the surgical epicondylar axis: in vivo analysis using a biplanar image-matching technique. *The Journal of arthroplasty*.

Bachmann, E. R. 2000. *Inertial and magnetic tracking of limb segment orientation for inserting humans into synthetic environments*. DTIC Document.

Baker, R. et al. 1999. A new approach to determine the hip rotation profile from clinical gait analysis data. *Human Movement Science* 18(5), pp. 655-667.

Bell, A. L. et al. 1990. A comparison of the accuracy of several hip center location prediction methods. *Journal of biomechanics* 23(6), pp. 617-621.

Benedetti, M. G. et al. 1998. Data management in gait analysis for clinical applications. *Clinical Biomechanics* 13(3), pp. 204-215.

Berchuck, M. et al. 1990. Gait adaptations by patients who have a deficient anterior cruciate ligament. *J Bone Joint Surg Am*.

Besier, T. F. et al. 2003. Repeatability of gait data using a functional hip joint centre and a mean helical knee axis. *Journal of Biomechanics* 36(8), pp. 1159-1168.

Bishop, G. 1984. Self-tracker: A smart optical sensor on silicon.

Blacharski, P. A. and Somerset, J. H. 1975. A three-dimensional study of the kinematics of the human knee. *Journal of Biomechanics* 8(375).

Bland, J. M. and Altman, D. 1986. Statistical methods for assessing agreement between two methods of clinical measurement. *The lancet* 327(8476), pp. 307-310.

Blankevoort, L. et al. 1988. The envelope of passive knee joint motion. *Journal of biomechanics* 21(9), pp. 705711-709720.

Bonci, T. et al. 2015. Rigid and non-rigid geometrical transformations of a marker-cluster and their impact on bone-pose estimation. *J Biomech* 48(15), pp. 4166-4172.

Boyd, S. K. and Ronsky, J. L. 1997. Instantaneous moment arm determination of the cat knee. *Journal of Biomechanics* 31(3), pp. 279-283.

Brakspear, K. S. and Mason, D. J. 2012. Glutamate signaling in bone. *Front Endocrinol (Lausanne)* 3, p. 97.

Braune, W. and Fischer, O. 1891. Die Bewegungen des Kniegelenkes nach einer neuen Methode am lebenden Menschen gemessen. *Abhandlungen der mathematisch-physischen Klasse der Koniglich-Sachsischen Gesellschaft der Wissenschaften No II* 17(75).

Bregler, C. and Malik, J. eds. 1998. *Tracking people with twists and exponential maps*. Computer Vision and Pattern Recognition, 1998. Proceedings. 1998. IEEE.

Brennan, A. et al. 2011a. Quantification of inertial sensor-based 3D joint angle measurement accuracy using an instrumented gimbal. *Gait & posture* 34(3), pp. 320-323.

Brennan, A. et al. 2011b. Quantification of inertial sensor-based 3D joint angle measurement accuracy using an instrumented gimbal. *Gait & posture* 34(3), pp. 320-323.

Brooks, P. M. 2006. The burden of musculoskeletal disease—a global perspective. *Clinical rheumatology* 25(6), pp. 778-781.

Brouwer, G. M. et al. 2007. Association between valgus and varus alignment and the development and progression of radiographic osteoarthritis of the knee. *Arthritis and rheumatism* 56(4), pp. 1204-1211.

Bugnion, E. 1892. Le Mechanisme du Genou. In: Lausanne, L.U. ed. *Recueil inaugural*. France.

Calliess, T. et al. 2014. Clinical evaluation of a mobile sensor-based gait analysis method for outcome measurement after knee arthroplasty. *Sensors*.

Cappozzo, A. 1984. Gait analysis methodology. *Human Movement Science* 3(1), pp. 27-50.

Cappozzo, A. et al. 1995. Position and orientation in space of bones during movement: anatomical frame definition and determination. *Clinical biomechanics* 10(4), pp. 171-178.

Cappozzo, A. et al. 1996. Position and orientation in space of bones during movement: experimental artefacts. *Clinical ….*

Cappozzo, A. et al. 2005. Human movement analysis using stereophotogrammetry: Part 1: theoretical background. *Gait & posture*.

Cereatti, A. and Della Croce, U. 2006. Reconstruction of skeletal movement using skin markers: comparative assessment of bone pose estimators. *Journal of ….*

Chao, E. Y. S. 1980. Justification of triaxial goniometer for the measurement of joint rotation. *Journal of Biomechanics* 13(12), pp. 989995-9931006.

Chen, Y. et al. eds. 2005. *Markerless monocular motion capture using image features and physical constraints*. Computer Graphics International 2005
2005. IEEE.

Churchill, D. L. et al. 1998a. The transepicondylar axis approximates the optimal flexion axis of the knee. *… and related research*.

Churchill, D. L. et al. 1998b. The transepicondylar axis approximates the optimal flexion axis of the knee. *Clinical orthopaedics and related research* 356, pp. 111-118.

Cooper, C. et al. 1994. Occupational activity and osteoarthritis of the knee. *Annals of the rheumatic diseases* 53(2), pp. 90-93.

Cooper, G. et al. 2009. Inertial sensor-based knee flexion/extension angle estimation. *Journal of biomechanics* 42(16), pp. 2678-2685.

Cross, M. et al. 2014. The global burden of hip and knee osteoarthritis: estimates from the Global Burden of Disease 2010 study. *Annals of the Rheumatic Diseases* 73(7), pp. 1323-1330.

Cutti, A. et al. 2010. 'Outwalk': a protocol for clinical gait analysis based on inertial and magnetic sensors. *Medical & Biological Engineering & Computing* 48(1), pp. 17-25.

Dandachli, W. et al. 2009. Can the acetabular position be derived from a pelvic frame of reference? *… and related research*.

Davis, R. and DeLuca, P. 1996. Clinical gait analysis: current methods and future directions. *Human motion analysis: current applications and future directions*, pp. 17-42.

Davis, R. B. et al. 1991. A gait analysis data collection and reduction technique. *Human movement science*.

Davison, A. J. et al. 2001. Markerless motion capture of complex full-body movement for character animation.*Computer Animation and Simulation 2001*. Springer, pp. 3-14.

Della Croce, U. et al. 1999. Pelvis and lower limb anatomical landmark calibration precision and its propagation to bone geometry and joint angles. *Medical and Biological Engineering and Computing* 37(2), pp. 155-161.

Draganich, L. F. et al. 1991. The effects of resection of the proximal part of the fibula on stability of the knee and on gait. *The Journal of bone and joint surgery. American volume* 73(4), pp. 575-583.

Drake, R. L. et al. 2012. *Gray's Basic Anatomy*. Philadelphia: Elsevier Churchill Livingstone.

Dryden, I. L. and Mardia, K. V. 1998. Statistical shape analysis. *Statistical shape analysis*.

Ehrig, R. M. et al. 2011. The SCoRE residual: a quality index to assess the accuracy of joint estimations. *Journal of biomechanics* 44(7), pp. 1400-1404.

Ehrig, R. M. et al. 2006. A survey of formal methods for determining the centre of rotation of ball joints. *Journal of biomechanics*.

Ehrig, R. M. et al. 2007. A survey of formal methods for determining functional joint axes. *Journal of biomechanics*.

Elias, S. G. et al. 1990. A correlative study of the geometry and anatomy of the distal femur. *Clinical Orthopaedics* 260(98).

Ellis, H. 2006. *Clinical Anatomy - a revision and applied anatomy for clinical students*. 11th ed. Oxford: Blackwell Publishing.

FARO. 2012. *FARO® Prime - FARO's best accuracy, best value measurement arm* [Online]. Available at: http://az751159.vo.msecnd.net/download-center/download-centre/04ref201-472-en---faro-prime-tech-sheet.pdf?sfvrsn=17 [Accessed: 15 December].

Favre, J. et al. 2008. Ambulatory measurement of 3D knee joint angle. *Journal of biomechanics* 41(5), pp. 1029-1035.

Felson, D. T. 2004a. An update on the pathogenesis and epidemiology of osteoarthritis. *Radiologic Clinics* 42(1), pp. 1-9.

Felson, D. T. 2004b. Risk factors for osteoarthritis: understanding joint vulnerability. *Clinical orthopaedics and related research*.

Felson, D. T. 2013. Osteoarthritis as a disease of mechanics. *Osteoarthritis and cartilage* 21(1), pp. 10-15.

Felson, D. T. et al. 2004. The effect of body weight on progression of knee osteoarthritis is dependent on alignment. *Arthritis and rheumatism* 50(12), pp. 3904-3909.

Felson, D. T. and Hodgson, R. 2014. Identifying and treating preclinical and early osteoarthritis. *Rheumatic diseases clinics of North America* 40(4), pp. 699-710.

Felson, D. T. et al. 2000. Osteoarthritis: new insights. Part 1: the disease and its risk factors. *Ann Intern Med* 133(8), pp. 635-646.

Ferrari, A. et al. 2008. Quantitative comparison of five current protocols in gait analysis. *Gait & posture* 28(2), pp. 207-216.

Ferrari, A. et al. 2010a. First in vivo assessment of "Outwalk": a novel protocol for clinical gait analysis based on inertial and magnetic sensors. *Medical & Biological Engineering & Computing* 48(1), pp. 1-15.

Ferrari, A. et al. 2010b. A new formulation of the coefficient of multiple correlation to assess the similarity of waveforms measured synchronously by different motion analysis protocols. *Gait & posture* 31(4), pp. 540-542.

Fick, R. 1911a. *Handbuch der Anatomie und Mechanik der Gelenke*. Jena: Verlag Gustav von Fischer.

Fick, R. 1911b. *Handbuch der Anatomie und Mechanik der Gelenke*. Jena: Verlag Gustav von Fischer.

Forner-Cordero, A. et al. 2008. Study of the motion artefacts of skin-mounted inertial sensors under different attachment conditions. *Physiol Meas* 29(4), pp. N21-31.

Foxlin, E. 1996. Inertial head-tracker sensor fusion by a complementary separate-bias Kalman filter. *IEEE*, p. 185.

Foxlin, E. and Harrington, M. eds. 2000. *Weartrack: A self-referenced head and hand tracker for wearable computers and portable vr*. The Fourth International Symposium on Wearable Computers. IEEE.

Foxlin, E. et al. eds. 1998. *Constellation: A wide-range wireless motion-tracking system for augmented reality and virtual set applications*. Proceedings of the 25th annual conference on Computer graphics and interactive techniques. 1998. ACM.

Frankel, V. H. et al. 1971. Biomechanics of internal derangement of the knee. *Journal of Bone Joint Surgery* 53A(945).

Frey, W. et al. 1996. Off-the-shelf, real-time, human body motion capture for synthetic environments. *Computer Science Department, Naval Postgraduate School, USA* 24.

Frigo, C. et al. 1998. Functionally oriented and clinically feasible quantitative gait analysis method. *Medical and Biological Engineering and Computing* 36(2), pp. 179-185.

Frost, H. M. 1987. Bone "mass" and the "mechanostat": a proposal. *The Anatomical Record* (219), pp. 1-9.

Gaffney, M. et al. 2011. An automated calibration tool for high performance Wireless Inertial Measurement in professional sports. *Sensors*.

Gamage, S. and Lasenby, J. 2002. New least squares solutions for estimating the average centre of rotation and the axis of rotation. *Journal of biomechanics*.

Garofalo, P. et al. 2009. Inter-operator reliability and prediction bands of a novel protocol to measure the coordinated movements of shoulder-girdle and humerus in clinical settings. *Med Biol Eng Comput* 47(5), pp. 475-486.

Gastaldi, L. et al. 2015. Evaluation of functional methods for human movement modelling. *Acta of bioengineering and ….*

Gerhardt, M. B. et al. 2012. The prevalence of radiographic hip abnormalities in elite soccer players. *Am J Sports Med* 40(3), pp. 584-588.

Guergueltcheva, V. et al. 2012. Autosomal-recessive congenital cerebellar ataxia is caused by mutations in metabotropic glutamate receptor 1. *Am J Hum Genet* 91(3), pp. 553-564.

Haid, M. and Breitenbach, J. 2004. Low cost inertial orientation tracking with Kalman filter. *Applied Mathematics and Computation* 153.

Halvorsen, K. et al. 1999. A new method for estimating the axis of rotation and the center of rotation. *Journal of biomechanics*.

Harrington, I. J. 1983. Static and dynamic loading patterns in knee joints with deformities. *The Journal of bone and joint surgery. American volume* 65(2), pp. 247-259.

Hazas, M. and Ward, A. eds. 2002. *A novel broadband ultrasonic location system*. International Conference on Ubiquitous Computing. 2002. Springer.

Hightower, J. and Borriello, G. 2001. Location systems for ubiquitous computing. *Computer* 34(8), pp. 57-66.

Hollister, A. M. et al. 1993. The Axes of Rotation of the Knee. *Clinical Orthopaedics and Related Research* (290), pp. 259-268.

Hsu, R. W. et al. 1990. Normal axial alignment of the lower extremity and load-bearing distribution at the knee. *Clin Orthop Relat Res* (255), pp. 215-227.

Jakob, C. et al. eds. 2013. *Estimation of the knee flexion-extension angle during dynamic sport motions using body-worn inertial sensors*. Proceedings of the 8th International Conference on Body Area Networks. ICST (Institute for Computer Sciences, Social-Informatics and Telecommunications Engineering).

Joseph, C. 2014. *Anatomy - a complete guide to the human body, for artists and students, illustrated with the original drawings from the classic Gray's Anatomy*. Great Britain: Ivy Press.

Kadaba, M. P. and Ramakrishnan, H. K. 1990. Measurement of lower extremity kinematics during level walking. *Journal of orthopaedic ….*

Kadaba, M. P. et al. 1989. Repeatability of kinematic, kinetic, and electromyographic data in normal adult gait. *Journal of Orthopaedic Research* 7(6), pp. 849-860.

Kelkar, R. et al. 2001. Glenohumeral mechanics: a study of articular geometry, contact, and kinematics. *Journal of Shoulder and*.

Kettelkamp, D. B. et al. 1976. Results of proximal tibial osteotomy. The effects of tibiofemoral angle, stance-phase flexion-extension, and medial-plateau force. *J Bone Joint Surg Am* 58(7), pp. 952-960.

Kok, M. et al. 2014. An optimization-based approach to human body motion capture using inertial sensors. *IFAC Proceedings Volumes* 47(3), pp. 79-85.

Kratzenstein, S. et al. 2010a. The Residual: A Reliable Measure of Accuracy in the Determination of Joint Centers. *The Residual: A Reliable Measure of Accuracy in the Determination of Joint Centers*.

Kratzenstein, S. et al. 2010b. A new approach for optimally reducing skin marker artifact allows determination of the hip joint center within 3mm. *A new approach for optimally reducing skin marker artifact allows determination of the hip joint center within 3mm*.

Kupper, Z. et al. 2010. Video-based quantification of body movement during social interaction indicates the severity of negative symptoms in patients with schizophrenia. *Schizophrenia research* 121(1), pp. 90-100.

Leardini, A. et al. 2005. Human movement analysis using stereophotogrammetry: Part 3. Soft tissue artifact assessment and compensation. *Gait & posture*.

Li, G. et al. 2002. Biomechanics of posterior-substituting total knee arthroplasty: an in vitro study. *… and related research*.

Liu, K. et al. eds. 2009. *Ambulatory measurement and analysis of the lower limb 3D posture using wearable sensor system*. International Conference on Mechatronics and Automation, 2009. ICMA 2009. IEEE.

Liu, T. et al. 2011. Three-dimensional lower limb kinematic and kinetic analysis based on a wireless sensor system. *Robotics and Automation (….*

Luinge, H. et al. 2012. Motion tracking system. *Google Patents*.

Maetzel, A. et al. 1997. Osteoarthritis of the hip and knee and mechanical occupational exposure--a systematic overview of the evidence. *J Rheumatol* 24(8), pp. 1599-1607.

Marieb, E. N. 2009. *Essentials of Human Anatomy and Phisiology*. London: Pearson Benjamin Cummings.

Marin, F. et al. 2003. Correction of axis misalignment in the analysis of knee rotations. *Human Movement Science* 22(3), pp. 285-296.

McGinley, J. L. et al. 2009. The reliability of three-dimensional kinematic gait measurements: a systematic review. *Gait & posture* 29(3), pp. 360-369.

McMillan, G. and Nichols, L. 2005. Osteoarthritis and meniscus disorders of the knee as occupational diseases of miners. *Occupational and environmental medicine* 62(8), pp. 567-575.

Meyer, K. et al. 1992. A survey of position trackers. *Presence: Teleoperators & Virtual Environments* 1(2), pp. 173-200.

Moore, K. L. et al. 2010. *Clinically Oriented Anatomy*. 6 ed. Baltimore: Wolters Kluwer | Lippincott Williams & Wilkins, pp. 510-665.

Nokes, L. et al. 1984. Vibration analysis of human tibia: the effect of soft tissue on the output from skin-mounted accelerometers. *J Biomed Eng* 6(3), pp. 223-226.

Noyes, F. R. et al. 1992. The anterior cruciate ligament-deficient knee with varus alignment. An analysis of gait adaptations and dynamic joint loadings. *Am J Sports Med* 20(6), pp. 707-716.

Oeppen, J. and Vaupel, J. W. 2008. Broken Limits to Life Expectancy. American Association for the Advancement of Science. pp. Edited after: *Science* **296** , 1029 (2002).

Panjabi, M. M. et al. 1982. Errors in kinematic parameters of a planar joint:Guidelines for optimal experimental design. *Journal of Biomechanics* 15(537).

Pasciuto, I. et al. 2015. How Angular Velocity Features and Different Gyroscope Noise Types Interact and Determine Orientation Estimation Accuracy. *Sensors (Basel)* 15(9), pp. 23983-24001.

Paxton, A. and Dale, R. 2013. Frame-differencing methods for measuring bodily synchrony in conversation. *Behavior research methods* 45(2), pp. 329-343.

Pfau, T. et al. 2005. A method for deriving displacement data during cyclical movement using an inertial sensor. *Journal of Experimental Biology*.

Piazza, S. J. and Cavanagh, P. R. 2000. Measurement of the screw-home motion of the knee is sensitive to errors in axis alignment. *Journal of biomechanics* 33(8), pp. 1029-1034.

Piazza, S. J. et al. 2004. Assessment of the functional method of hip joint center location subject to reduced range of hip motion. *Journal of Biomechanics*.

Priyantha, N. B. et al. eds. 2000. *The cricket location-support system*. Proceedings of the 6th annual international conference on Mobile computing and networking. 2000. ACM.

Rabuffetti, M. and Crenna, P. 2004. A modular protocol for the analysis of movement in children. *Gait Posture* 20, pp. S77-S78.

Ramakrishnan, H. K. and Kadaba, M. P. 1991. On the estimation of joint kinematics during gait. *Journal of Biomechanics* 24(10), pp. 969-977.

Ramsey, D. K. and Wretenberg, P. F. 1999. Biomechanics of the knee: methodological considerations in the in vivo kinematic analysis of the tibiofemoral and patellofemoral joint. *Clinical Biomechanics* 14(9), pp. 595-611.

Reginster, J. Y. 2002. The prevalence and burden of arthritis. *Rheumatology*.

Roetenberg, D. et al. 2007a. Estimating body segment orientation by applying inertial and magnetic sensing near ferromagnetic materials. *IEEE transactions on neural systems and rehabilitation engineering : a publication of the IEEE Engineering in Medicine and Biology Society* 15(3), pp. 469-471.

Roetenberg, D. et al. 2005. Compensation of magnetic disturbances improves inertial and magnetic sensing of human body segment orientation. *IEEE transactions on neural systems and rehabilitation engineering : a publication of the IEEE Engineering in Medicine and Biology Society* 13(3), pp. 395-405.

Roetenberg, D. et al. 2009. Xsens MVN: full 6DOF human motion tracking using miniature inertial sensors. *… Motion Technologies BV*.

Roetenberg, D. et al. 2003. Inertial and magnetic sensing of human movement near ferromagnetic materials. *Proceedings of the 2nd IEEE/ACM ….*

Roetenberg, D. et al. 2007b. Ambulatory position and orientation tracking fusing magnetic and inertial sensing. *IEEE transactions on bio-medical engineering* 54(5), pp. 883-890.

Roetenberg, D. and Veltink, P. 2005. Camera-marker and inertial sensor fusion for improved motion tracking. *Gait and Posture*.

Romero, V. et al. 2014. Capturing Social Motor Coordination: A comparison of the Microsoft Kinect, Video-Motion Analysis and the Polhemus Latus Motion Tracking System. In: *International Meeting for Autism Research.*

Roos, H. et al. 1994. The prevalence of gonarthrosis and its relation to meniscectomy in former soccer players. *Am J Sports Med* 22(2), pp. 219-222.

Rozumalski, A. and Schwartz, M. H. 2008. P041 A comparison of two functional methods for calculating joint centers and axes in a clinical setting. *Gait & Posture* 28, pp. S74-S75.

Røislien, J. et al. 2012. Evaluating the properties of the coefficient of multiple correlation (CMC) for kinematic gait data. *Journal of biomechanics* 45(11), pp. 2014-2018.

Saha, S. and Lakes, R. S. 1977. The effect of soft tissue on wave-propagation and vibration tests for determining the in vivo properties of bone. *J Biomech* 10(7), pp. 393-401.

Schache, A. G. et al. 2006. Defining the knee joint flexion–extension axis for purposes of quantitative gait analysis: an evaluation of methods. *Gait & posture* 24(1), pp. 100-109.

Schepers, H. et al. 2010. Ambulatory human motion tracking by fusion of inertial and magnetic sensing with adaptive actuation. *Medical & biological engineering & computing* 48(1), pp. 27-37.

Schmidt, G. L. 1973. Biomechanical analysis of knee flexion-extension. *Journal of Biomechanics* 6(79).

Schmidt, R. C. et al. 2012. Measuring the dynamics of interactional synchrony. *Journal of Nonverbal Behavior* 36(4), pp. 263-279.

Schwartz, M. H. and Rozumalski, A. 2005. A new method for estimating joint parameters from motion data. *Journal of biomechanics*.

Seel, T. et al. 2014. IMU-based joint angle measurement for gait analysis. *Sensors (Basel, Switzerland)* 14(4), pp. 6891-6909.

Sharma, L. et al. 2008. Relationship of meniscal damage, meniscal extrusion, malalignment, and joint laxity to subsequent cartilage loss in osteoarthritic knees. *Arthritis & ….*

Sharma, L. et al. 2001. The role of knee alignment in disease progression and functional decline in knee osteoarthritis. *JAMA* 286(2), pp. 188-195.

Shultz, S. J. et al. 2008. Differences in lower extremity anatomical and postural characteristics in males and females between maturation groups. *journal of orthopaedic & sports ….*

Soangra, R. and Lockhart, T. E. 2012. A comparative study for performance evaluation of sit-to-stand task with body worn sensor and existing laboratory methods. *Biomedical sciences instrumentation*.

Soudan, K. and Auderkercke, R. V. 1979. Methods, difficulties and inaccuracies in the study of human joint mechanics and pathokinematics by the instant axis concept. Example: the knee joint. *Journal of Biomechanics* 12(27).

St. John, T. M. 2015. *List of debilitating diseases* [Online]. Available at: http://www.livestrong.com/article/161052-list-of-debilitating-diseases/ [Accessed: 12 December].

Steindler, A. 1955. *Kinesiology of the human body*. Springfield, Illinois: Charles Thomas.

Stone, E. E. and Skubic, M. 2011. Passive in-home measurement of stride-to-stride gait variability comparing vision and Kinect sensing. *… conference of the IEEE engineering in ….*

Strasser, H. 1917. *Lehrbuch der Muskeln und Gelenkmechanik*. Berlin: Springer.

Takeda, R. et al. 2009. Gait posture estimation using wearable acceleration and gyro sensors. *Journal of biomechanics* 42(15), pp. 2486-2494.

Taylor, W. R. et al. 2005. On the influence of soft tissue coverage in the determination of bone kinematics using skin markers. *Journal of ….*

Taylor, W. R. et al. 2010. Repeatability and reproducibility of OSSCA, a functional approach for assessing the kinematics of the lower limb. *Gait & posture* 32(2), pp. 231-236.

Teichtahl, A. J. et al. 2006. Static knee alignment and its association with radiographic knee osteoarthritis. *Osteoarthritis and cartilage* 14(9), pp. 958-962.

Teichtahl, A. J. et al. 2009. Change in knee angle influences the rate of medial tibial cartilage volume loss in knee osteoarthritis. *Osteoarthritis and ….*

Tetsworth, K. and Paley, D. 1994. Malalignment and degenerative arthropathy. *Orthop Clin North Am* 25(3), pp. 367-377.

Trujillo, D. M. and Busby, H. R. 1990. A mathematical method for the measurement of bone motion with skin-mounted accelerometers. *J Biomech Eng* 112(2), pp. 229-231.

Van den Noort, J. C. et al. 2013a. Gait analysis in children with cerebral palsy via inertial and magnetic sensors. *Medical & biological engineering & computing* 51(4), pp. 377-386.

Van den Noort, J. C. et al. 2013b. Gait analysis in children with cerebral palsy via inertial and magnetic sensors. *Medical & biological engineering & computing* 51(4), pp. 377-386.

Vlasic, D. et al. 2007. Practical motion capture in everyday surroundings. *ACM transactions on ….*

Wang, J. W. et al. 1990. The influence of walking mechanics and time on the results of proximal tibial osteotomy. *J Bone Joint Surg Am* 72(6), pp. 905-909.

Ward, A. et al. 1997. A new location technique for the active office. *IEEE Personal communications* 4(5), pp. 42-47.

Ward, J. A. et al. eds. 2005. *Gesture spotting using wrist worn microphone and 3-axis accelerometer*. Proceedings of the 2005 joint conference on Smart objects and ambient intelligence: innovative context-aware services: usages and technologies. ACM.

Welch, G. and Bishop, G. 1995. An introduction to the Kalman filter.

Welch, G. and Foxlin, E. 2002. Motion tracking: No silver bullet, but a respectable arsenal. *IEEE Computer graphics and Applications* 22(6), pp. 24-38.

Wixted, A. et al. eds. 2010. *Wearable sensors for on field near real time detection of illegal bowling actions*. Wearable sensors for on field near real time detection of illegal bowling actions.

Wolff, J. D. 1982. *Das Gesetz der Transformation der Knochen*. Berlin.

Woltring, H. J. 1973. New possibilities for human motion studies by real-time light spot position measurement. *Biotelemetry* 1(3), pp. 132-146.

Woltring, H. J. 1994. 3-D attitude representation of human joints: a standardization proposal. *Journal of biomechanics* 27(12), pp. 1399-1414.

Woltring, H. J. et al. 1985. Finite centroid and helical axis estimation from noisy landmark measurements in the study of human joint kinematics. *Journal of biomechanics*.

Wu, G. et al. 2002. ISB recommendation on definitions of joint coordinate system of various joints for the reporting of human joint motion—part I: ankle, hip, and spine. *Journal of Biomechanics* 35(4), pp. 543-548.

Xsens Technologies 2013. MTw User Manual.

Yang, S. et al. 2011. Ambulatory running speed estimation using an inertial sensor. *Gait & posture*.

Yavuzer, G. et al. 2008. Repeatability of lower limb three-dimensional kinematics in patients with stroke. *Gait Posture* 27(1), pp. 31-35.

Yu, B. et al. 1997. Reproducibility of the kinematics and kinetics of the lower extremity during normal stair-climbing. *Journal of orthopaedic research : official publication of the Orthopaedic Research Society* 15(3), pp. 348-352.

Zatsiorsky, V. M. 1998. *Kinematics of Human Motion*. USA: Human Kinetics.

Zhang, J.-T. et al. 2013. Concurrent validation of Xsens MVN measurement of lower limb joint angular kinematics. *Physiological measurement* 34(8), p. N63.

Zhou, H. and Hu, H. 2004. A survey-human movement tracking and stroke rehabilitation. *University of Essex*.

Zhou, H. and Hu, H. 2008. Human motion tracking for rehabilitation—A survey. *Biomedical Signal Processing and Control*.

Ziegert, J. C. and Lewis, J. L. 1979. The effect of soft tissue on measurements of vibrational bone motion by skin-mounted accelerometers. *Journal of Biomechanical Engineering* 101(3), pp. 218-220.

Zuppinger, H. 1904. *Die aktive Flexion im unbelasteten Kniegelenk*. Wiesbaden: Habilitationsschrift.

Appendix 1

Within-day and between-day variability of human knee flexion-extension during gait

Participant 1

APPENDIX TABLE 1. WITHIN DAY VARIABILITY OF KNEE FLEXION EXTENSION DURING GAIT recorded in a laboratory simultaneously with inertial sensors and an optical motion capture system, and in a non-laboratory based environment with the inertial sensors only, during two separate sessions – Participant 1.

Within day variability of human gait	*Experimental results*					
Participant 1	Vicon Session 1	Indoor Session 1	Outdoor Session 1	Vicon Session 2	Indoor Session 2	Outdoor Session 2
Number of observations (N)	5	20	20	11	20	20
Range of motion (ROM)	60.2°	60.5°	68.2°	62.5°	61.5°	66.2°
Root mean squared error (RMS)	1.1°	1.4°	1.6°	1.1°	1.3°	1.3°
Standard error (σ)	1.2°	1.5°	1.6°	1.1°	1.4°	1.4°
Coefficient of multiple correlations (CMC)	NaN	0.956	0.949	0.839	0.960	0.965

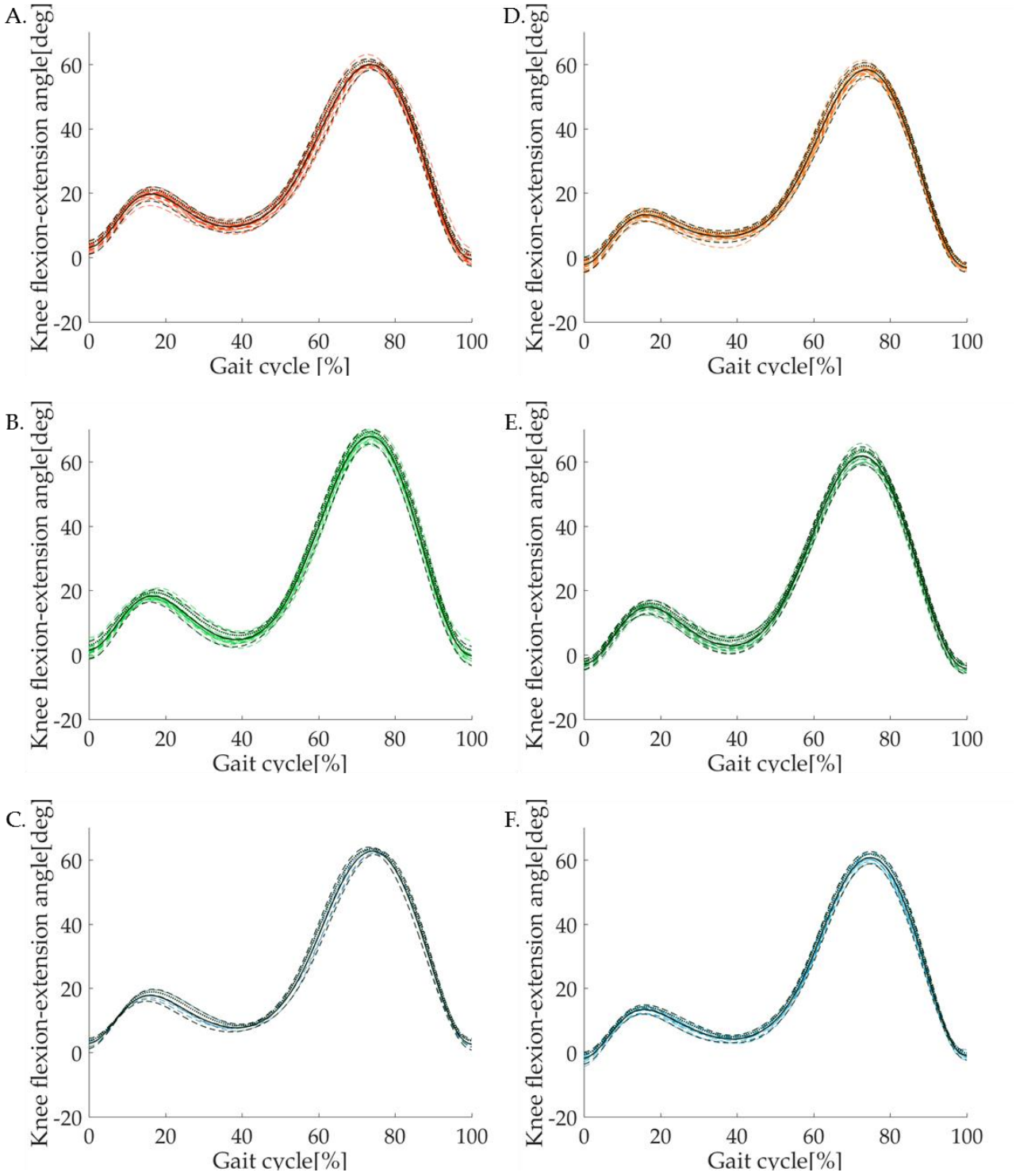

APPENDIX FIG 1. WITHIN DAY VARIABILITY OF KNEE FLEXION EXTENSION DURING GAIT PERFORMED BY PARTICIPANT 1

A. recorded with the sensors in the first laboratory session; B. recorded with the Vicon in the first laboratory session; C. recorded with the sensors in the first outdoor session; D. recorded with the sensors in the second laboratory session; E. recorded with the Vicon in the second laboratory session; F. recorded with the sensors in the second outdoor session. Where individual gait cycles are marked with coloured dotted lines, the average gait cycle of the session with full black line, and 95% confidence intervals with black dotted lines.

APPENDIX TABLE 2. BETWEEN DAY VARIABILITY OF KNEE FLEXION EXTENSION DURING GAIT recorded in a laboratory simultaneously with inertial sensors and an optical motion capture system, and in a non-laboratory based environment with the inertial sensors only, during two separate sessions – Participant 1.

Between day variability of human gait	*Experimental results*		
Participant 1	Vicon	Indoor	Outdoor
Number of observations (N)	5	20	20
Difference between range of motion (ΔROM)	4.4°	0.9°	1.7°
Root mean squared error (RMS)	4.1°	4.5°	4.5°
Standard error (σ)	3.7°	3.9°	3.8°
Coefficient of variation (CV)	6%	5.9%	5.2%
Coefficient of Multiple correlations (CMC)	0.989	0.986	0.989
Pearson product-moment correlation coefficient (r)	0.996	0.991	0.993

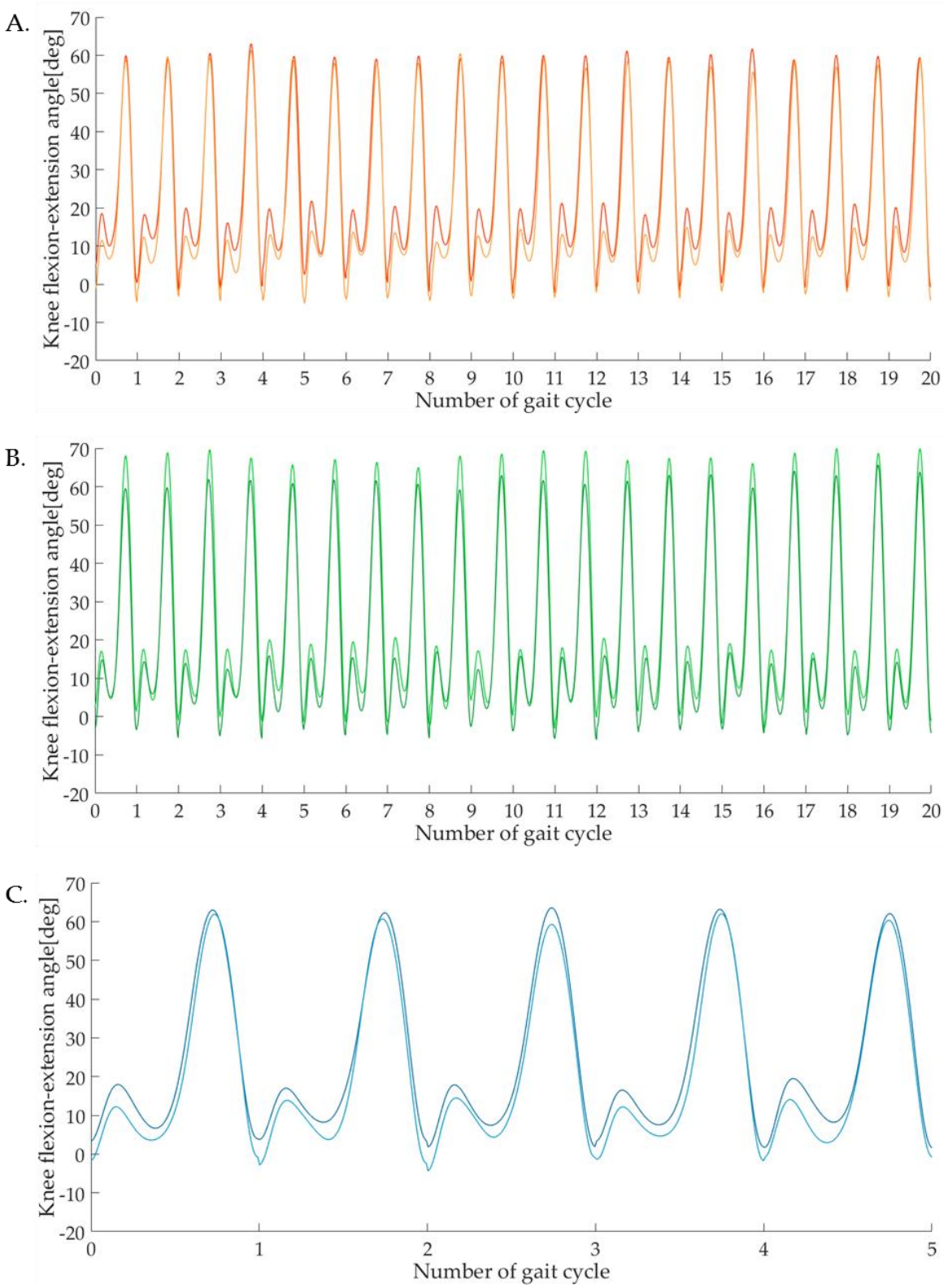

APPENDIX FIG 2. BETWEEN DAY VARIABILITY OF KNEE FLEXION EXTENSION DURING GAIT PERFORMED BY PARTICIPANT 1

A. recorded with the sensors during the first (red) and second (orange) laboratory session; B. recorded with the sensors during the first (dark green) and second (light green) outdoor session; C. recorded with the Vicon during the first (blue) and second (light blue) laboratory session outdoor.

Participant 2

APPENDIX TABLE 3. WITHIN DAY VARIABILITY OF KNEE FLEXION EXTENSION DURING GAIT recorded in a laboratory simultaneously with inertial sensors and an optical motion capture system, and in a non-laboratory based environment with the inertial sensors only, during two separate sessions – Participant 2.

Within day variability of human gait	*Experimental results*					
Participant 2	Vicon Session 1	Indoor Session 1	Outdoor Session 1	Vicon Session 2	Indoor Session 2	Outdoor Session 2
Number of observations (N)	7	17	20	7	11	20
Range of motion (ROM)	56°	54.3°	54.5°	57.1°	48.8°	56.2°
Root mean squared error (RMS)	1.2°	2°	1°	1°	1.7°	1.2°
Standard error (σ)	1.3°	2.1°	1.1°	1.1°	1.8°	1.3°
Coefficient of multiple correlations (CMC)	NaN	0.892	0.980	NaN	NaN	0.961

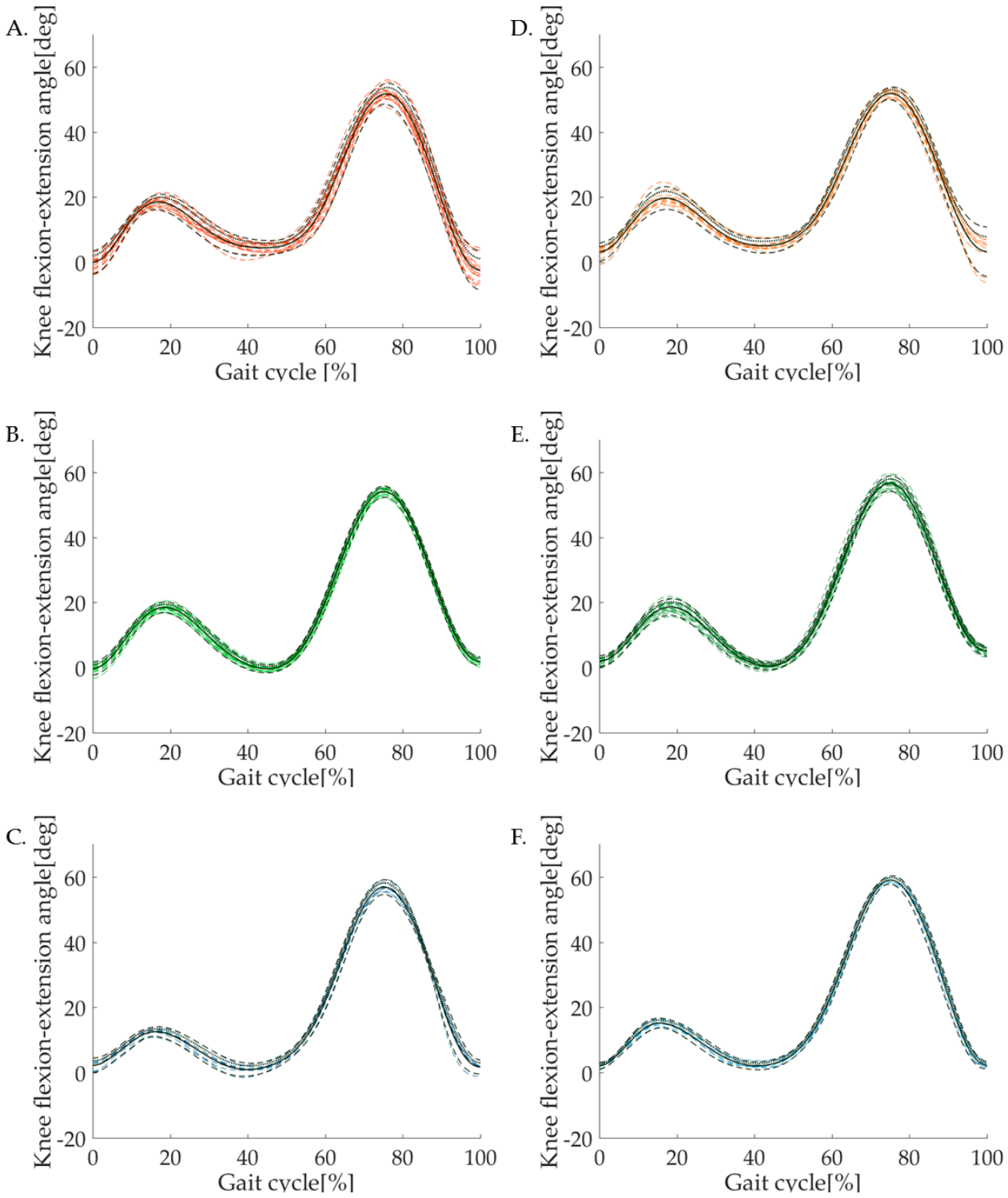

APPENDIX FIG 3. WITHIN DAY VARIABILITY OF KNEE FLEXION EXTENSION DURING GAIT PERFORMED BY PARTICIPANT 2

A. recorded with the sensors in the first laboratory session; B. recorded with the Vicon in the first laboratory session; C. recorded with the sensors in the first outdoor session; D. recorded with the sensors in the second laboratory session; E. recorded with the Vicon in the second laboratory session; F. recorded with the sensors in the second outdoor session. Where individual gait cycles are marked with coloured dotted lines, the average gait cycle of the session with full black line, and 95% confidence intervals with black dotted lines.

APPENDIX TABLE 4. BETWEEN DAY VARIABILITY OF KNEE FLEXION EXTENSION DURING GAIT recorded in a laboratory simultaneously with inertial sensors and an optical motion capture system, and in a non-laboratory based environment with the inertial sensors only, during two separate sessions – Participant 2.

Between day variability of human gait	*Experimental results*		
Participant 2	Vicon	Indoor	Outdoor
Number of observations (N)	7	11	20
Difference between range of motion (ΔROM)	1.4°	1.8°	1.5°
Root mean squared error (RMS)	2.6°	3.4°	2.8°
Standard error (σ)	2°	2.6°	2.2°
Coefficient of variation (CV)	3.3%	4.3%	3.6%
Coefficient of Multiple correlations (CMC)	0.995	0.988	0.994
Pearson product-moment correlation coefficient (r)	0.995	0.983	0.993

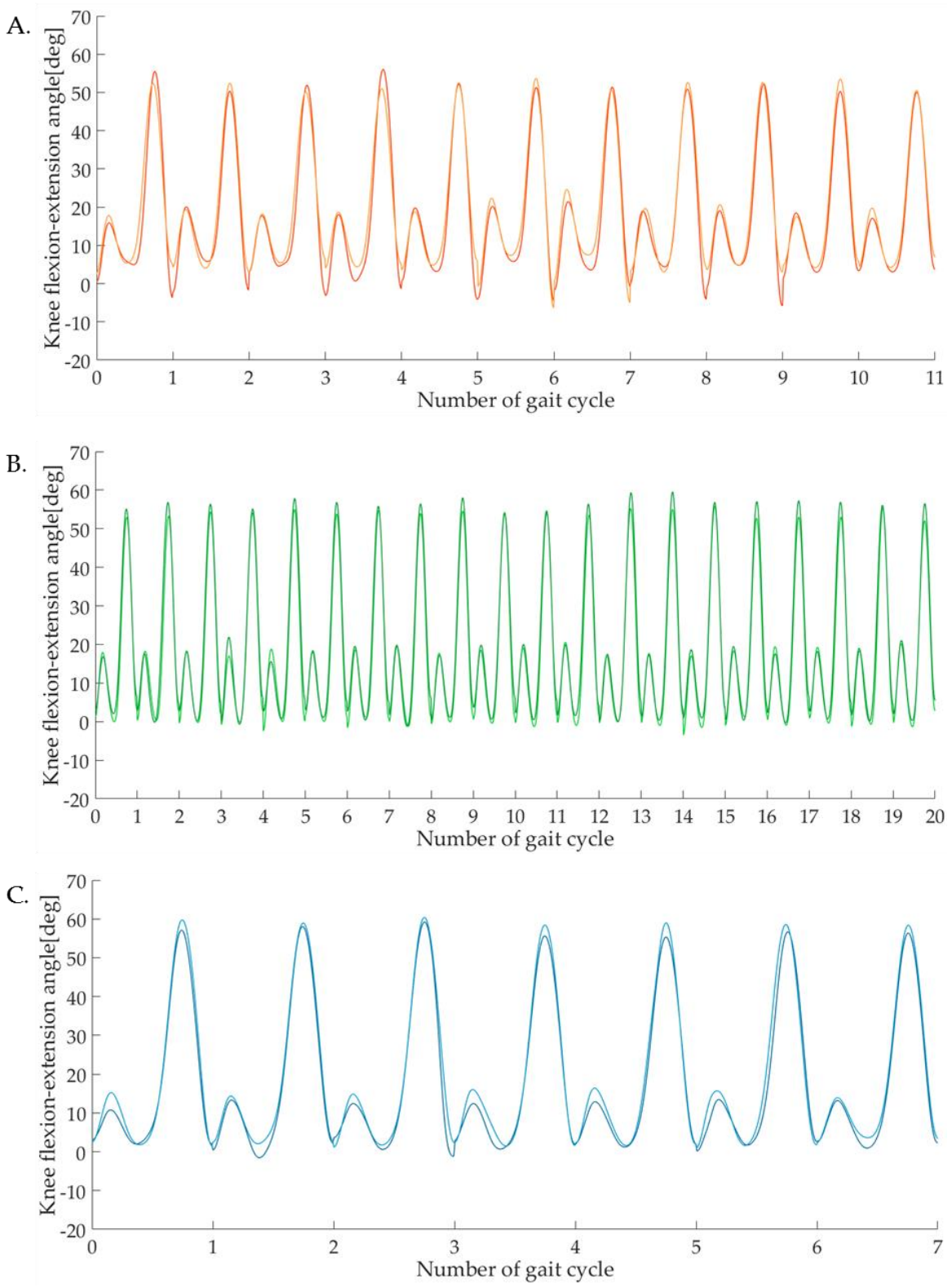

APPENDIX FIG 4. BETWEEN DAY VARIABILITY OF KNEE FLEXION EXTENSION DURING GAIT PERFORMED BY PARTICIPANT 2

A. recorded with the sensors during the first (red) and second (orange) laboratory session; B. recorded with the sensors during the first (dark green) and second (light green) outdoor session; C. recorded with the Vicon during the first (blue) and second (light blue) laboratory session outdoor.

Participant 3

APPENDIX TABLE 5. WITHIN DAY VARIABILITY OF KNEE FLEXION EXTENSION DURING GAIT recorded in a laboratory simultaneously with inertial sensors and an optical motion capture system, and in a non-laboratory based environment with the inertial sensors only, during two separate sessions – Participant 3.

Within day variability of human gait	*Experimental results*					
Participant 3	Vicon Session 1	Indoor Session 1	Outdoor Session 1	Vicon Session 2	Indoor Session 2	Outdoor Session 2
Number of observations (N)	8	19	20	10	18	20
Range of motion (ROM)	59.7°	58°	62°	58.5°	53.4°	57.8°
Root mean squared error (RMS)	1.5°	2°	1.7°	1.5°	1.9°	1.3°
Standard error (σ)	1.6°	2.1°	1.7°	1.7°	2°	1.3°
Coefficient of multiple correlations (CMC)	NaN	0.902	0.974	NaN	0.934	0.984

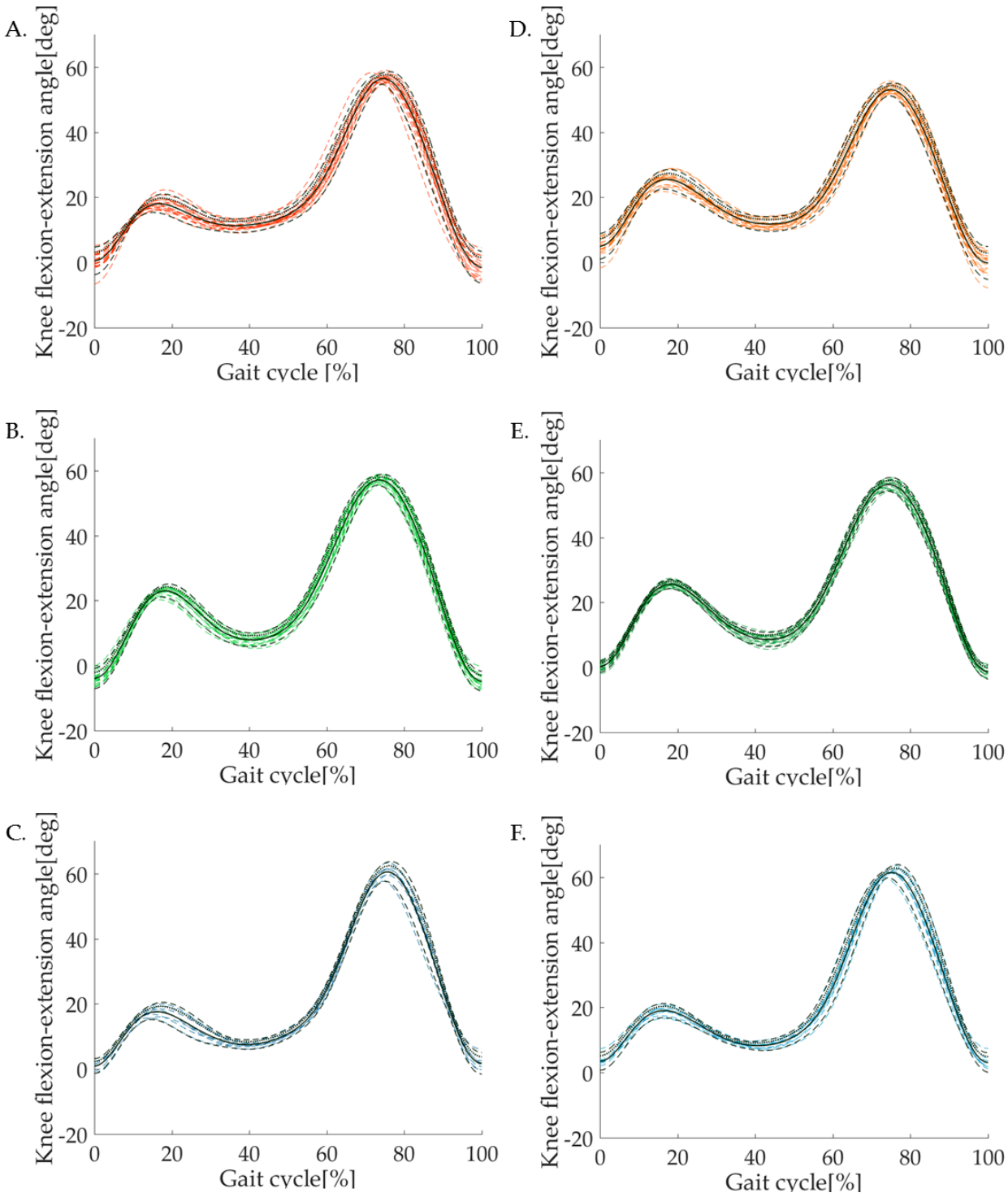

APPENDIX FIG 5. WITHIN DAY VARIABILITY OF KNEE FLEXION EXTENSION DURING GAIT PERFORMED BY PARTICIPANT 3

A. recorded with the sensors in the first laboratory session; B. recorded with the Vicon in the first laboratory session; C. recorded with the sensors in the first outdoor session; D. recorded with the sensors in the second laboratory session; E. recorded with the Vicon in the second laboratory session; F. recorded with the sensors in the second outdoor session. Where individual gait cycles are marked with coloured dotted lines, the average gait cycle of the session with full black line, and 95% confidence intervals with black dotted lines.

APPENDIX TABLE 6. BETWEEN DAY VARIABILITY OF KNEE FLEXION EXTENSION DURING GAIT recorded in a laboratory simultaneously with inertial sensors and an optical motion capture system, and in a non-laboratory based environment with the inertial sensors only, during two separate sessions – Participant 3.

Between day variability of human gait	*Experimental results*		
Participant 3	Vicon	Indoor	Outdoor
Number of observations (N)	7	18	20
Difference between range of motion (ΔROM)	0.1°	2.2°	4.1°
Root mean squared error (RMS)	2.7°	5°	3.3°
Standard error (σ)	2.1°	4.1°	2.8°
Coefficient of variation (CV)	3.4%	6.2%	4.2%
Coefficient of Multiple correlations (CMC)	0.994	0.973	0.991
Pearson product-moment correlation coefficient (r)	0.991	0.959	0.987

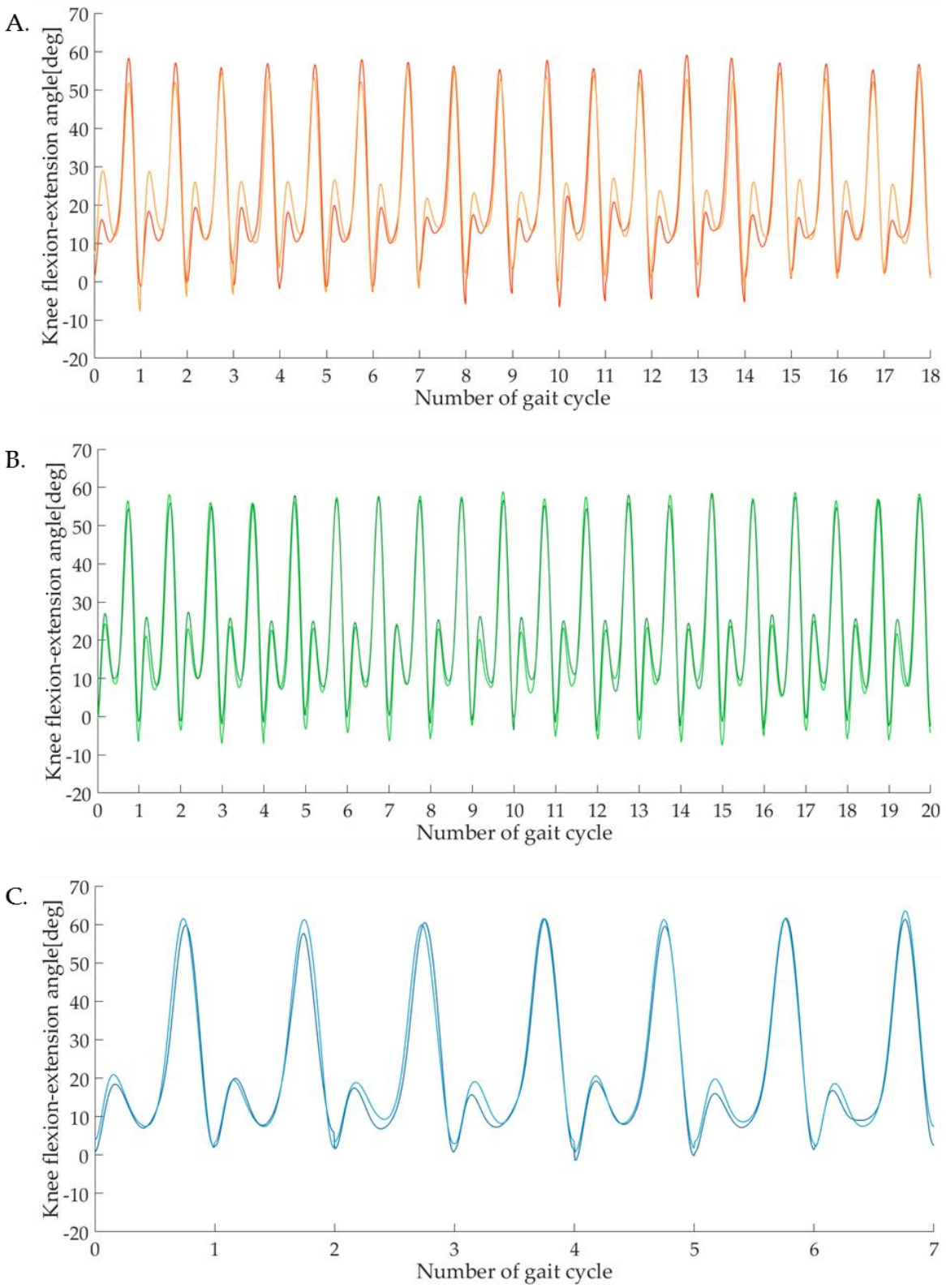

APPENDIX FIG 6. BETWEEN DAY VARIABILITY OF KNEE FLEXION EXTENSION DURING GAIT PERFORMED BY PARTICIPANT 3

A. recorded with the sensors during the first (red) and second (orange) laboratory session; B. recorded with the sensors during the first (dark green) and second (light green) outdoor session; C. recorded with the Vicon during the first (blue) and second (light blue) laboratory session outdoor.

Participant 4

APPENDIX TABLE 7. WITHIN DAY VARIABILITY OF KNEE FLEXION EXTENSION DURING GAIT recorded in a laboratory simultaneously with inertial sensors and an optical motion capture system, and in a non-laboratory based environment with the inertial sensors only, during two separate sessions – Participant 4.

Within day variability of human gait	*Experimental results*					
Participant 4	Vicon Session 1	Indoor Session 1	Outdoor Session 1	Vicon Session 2	Indoor Session 2	Outdoor Session 2
Number of observations (N)	9	20	20	4	20	20
Range of motion (ROM)	61°	58.1°	60.4°	62.2°	56°	57°
Root mean squared error (RMS)	1.5°	1.3°	1.3°	0.9°	1.6°	1.6°
Standard error (σ)	1.5°	1.3°	1.4°	0.9°	1.6°	1.6°
Coefficient of multiple correlations (CMC)	NaN	0.942	0.941	NaN	0.922	0.919

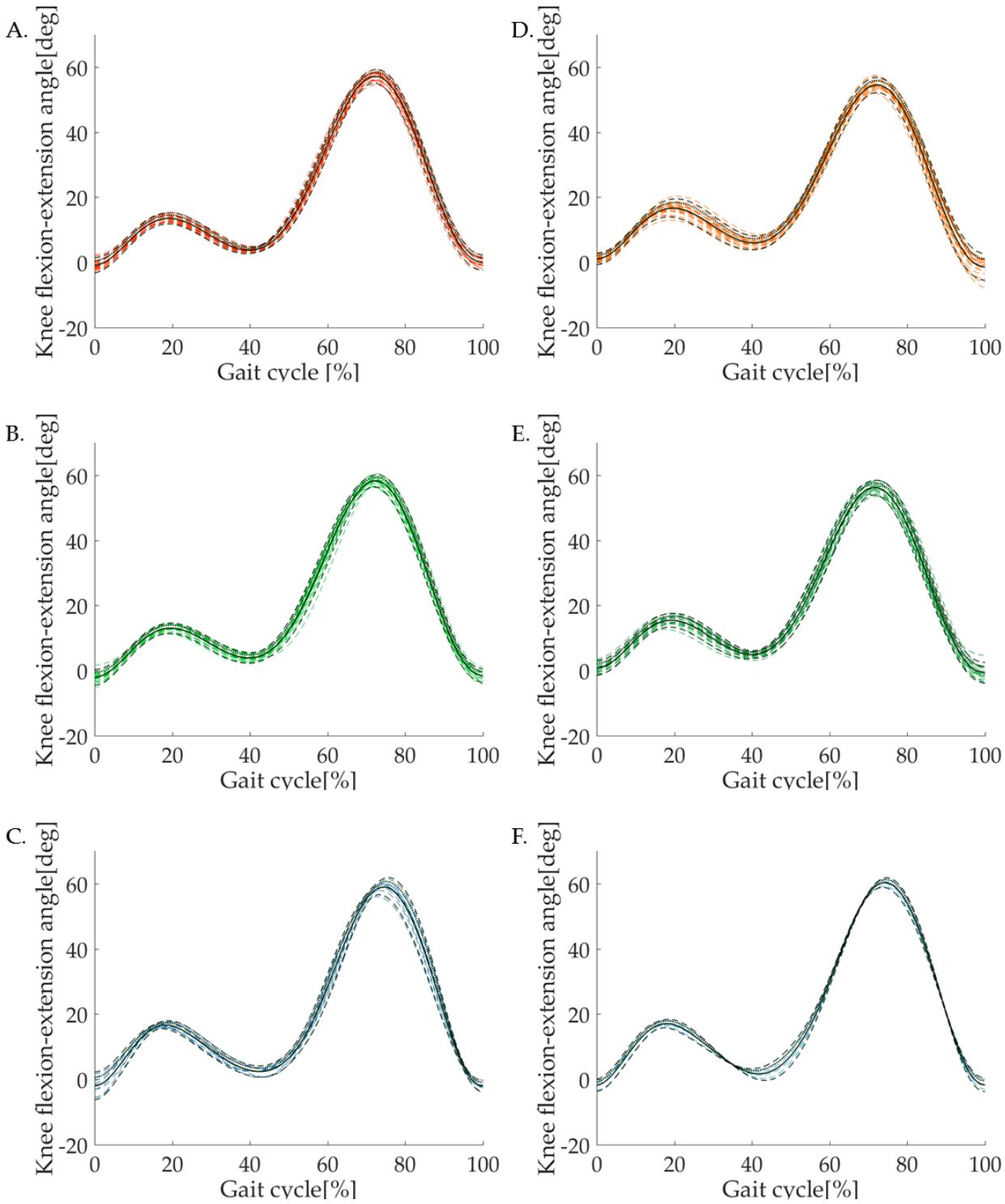

APPENDIX FIG 7. WITHIN DAY VARIABILITY OF KNEE FLEXION EXTENSION DURING GAIT PERFORMED BY PARTICIPANT 4

A. recorded with the sensors in the first laboratory session; B. recorded with the Vicon in the first laboratory session; C. recorded with the sensors in the first outdoor session; D. recorded with the sensors in the second laboratory session; E. recorded with the Vicon in the second laboratory session; F. recorded with the sensors in the second outdoor session. Where individual gait cycles are marked with coloured dotted lines, the average gait cycle of the session with full black line, and 95% confidence intervals with black dotted lines.

APPENDIX TABLE 8. BETWEEN DAY VARIABILITY OF KNEE FLEXION EXTENSION DURING GAIT recorded in a laboratory simultaneously with inertial sensors and an optical motion capture system, and in a non-laboratory based environment with the inertial sensors only, during two separate sessions – Participant 4.

Between day variability of human gait	*Experimental results*		
Participant 4	Vicon	Indoor	Outdoor
Number of observations (N)	4	20	20
Difference between range of motion (ΔROM)	2°	3.5°	3.7°
Root mean squared error (RMS)	2.2°	3.1°	2.8°
Standard error (σ)	1.6°	2.5°	2.3°
Coefficient of variation (CV)	2.6%	4.1%	3.4%
Coefficient of Multiple correlations (CMC)	0.997	0.992	0.994
Pearson product-moment correlation coefficient (r)	0.995	0.989	0.992

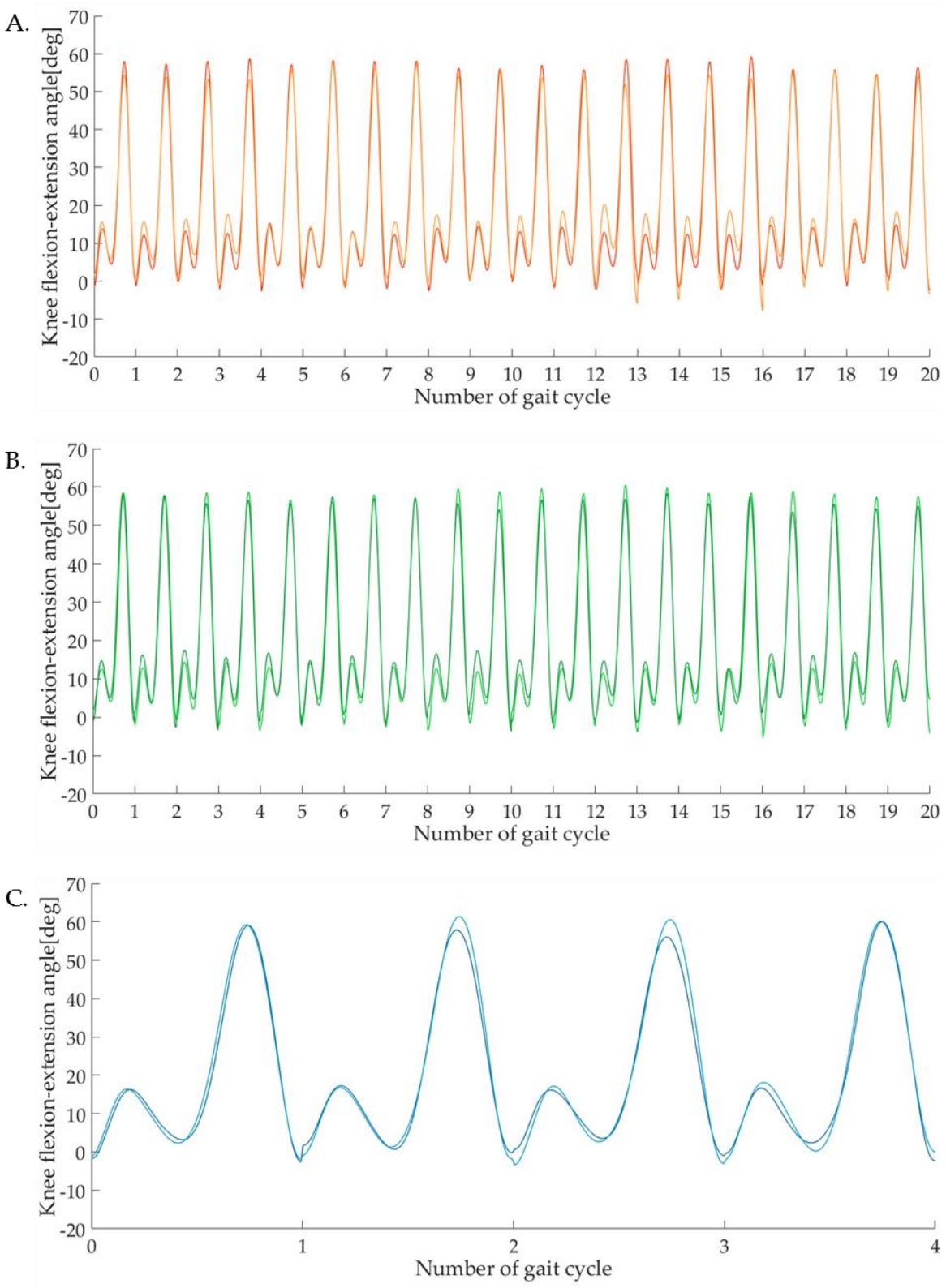

APPENDIX FIG 8. BETWEEN DAY VARIABILITY OF KNEE FLEXION EXTENSION DURING GAIT PERFORMED BY PARTICIPANT 4

A. recorded with the sensors during the first (red) and second (orange) laboratory session; B. recorded with the sensors during the first (dark green) and second (light green) outdoor session; C. recorded with the Vicon during the first (blue) and second (light blue) laboratory session outdoor.

Participant 5

APPENDIX TABLE 9. WITHIN DAY VARIABILITY OF KNEE FLEXION EXTENSION DURING GAIT recorded in a laboratory simultaneously with inertial sensors and an optical motion capture system, and in a non-laboratory based environment with the inertial sensors only, during two separate sessions – Participant 5.

Within day variability of human gait	*Experimental results*					
Participant 5	Vicon Session 1	Indoor Session 1	Outdoor Session 1	Vicon Session 2	Indoor Session 2	Outdoor Session 2
Number of observations (N)	10	20	20	8	20	20
Range of motion (ROM)	66.1°	61°	61.8°	67°	56.7°	59°
Root mean squared error (RMS)	1.1°	1.3°	1°	1.8°	0.9°	0.9°
Standard error (σ)	1.3°	1.4°	1°	2.1°	1°	0.9°
Coefficient of multiple correlations (CMC)	0.706	0.951	0.984	NaN	0.975	0.988

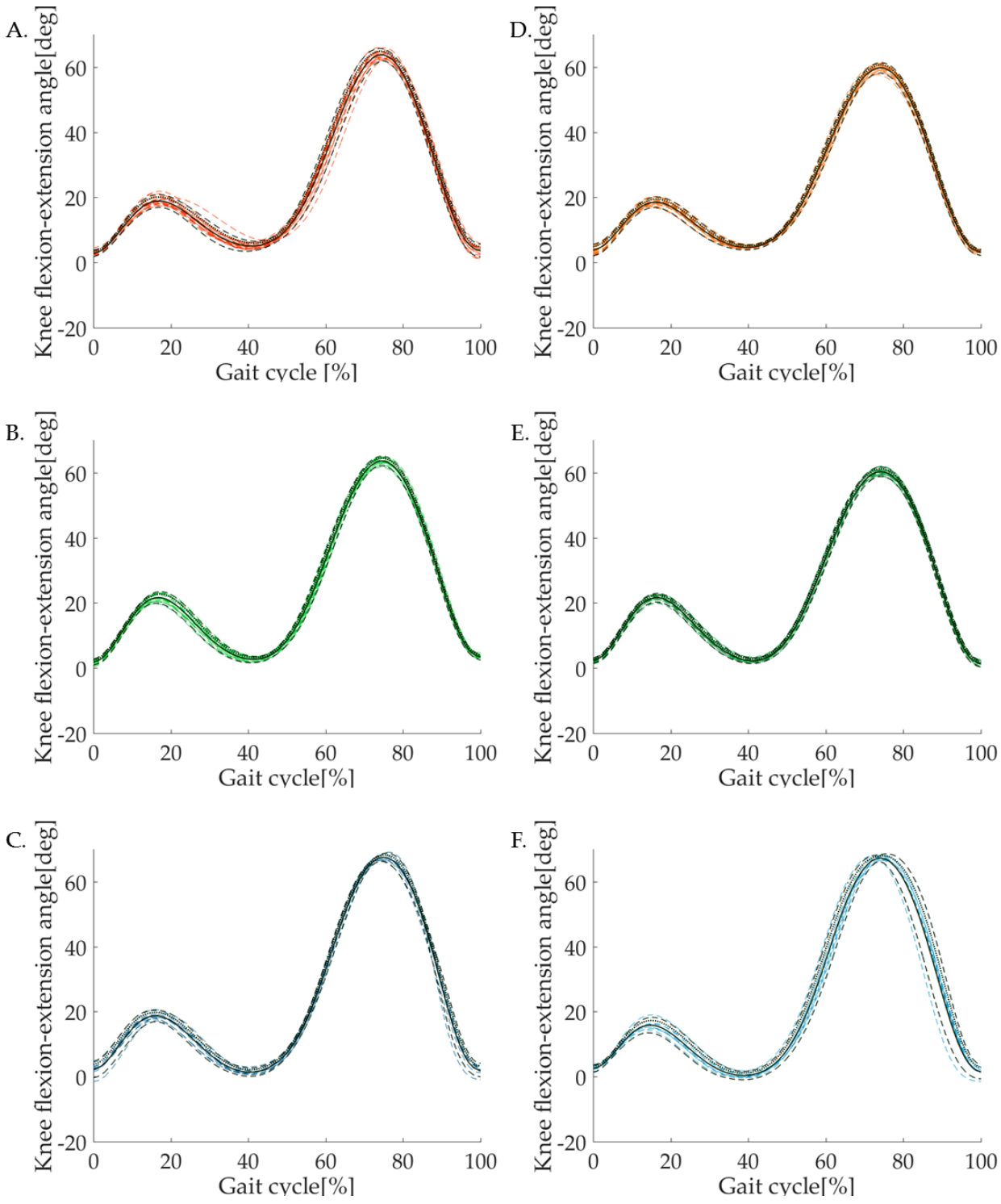

APPENDIX FIG 9. WITHIN DAY VARIABILITY OF KNEE FLEXION EXTENSION DURING GAIT PERFORMED BY PARTICIPANT 5

A. recorded with the sensors in the first laboratory session; B. recorded with the Vicon in the first laboratory session; C. recorded with the sensors in the first outdoor session; D. recorded with the sensors in the second laboratory session; E. recorded with the Vicon in the second laboratory session; F. recorded with the sensors in the second outdoor session. Where individual gait cycles are marked with coloured dotted lines, the average gait cycle of the session with full black line, and 95% confidence intervals with black dotted lines.

APPENDIX TABLE 10. BETWEEN DAY VARIABILITY OF KNEE FLEXION EXTENSION DURING GAIT recorded in a laboratory simultaneously with inertial sensors and an optical motion capture system, and in a non-laboratory based environment with the inertial sensors only, during two separate sessions – Participant 5.

Between day variability of human gait	*Experimental results*		
Participant 5	Vicon	Indoor	Outdoor
Number of observations (N)	7	20	20
Difference between range of motion (ΔROM)	0.9°	5.7°	2.9°
Root mean squared error (RMS)	3.2°	2.5°	2°
Standard error (σ)	2.4°	1.8°	1.6°
Coefficient of variation (CV)	3.4%	2.8%	2.5%
Coefficient of Multiple correlations (CMC)	0.995	0.996	0.997
Pearson product-moment correlation coefficient (r)	0.991	0.994	0.996

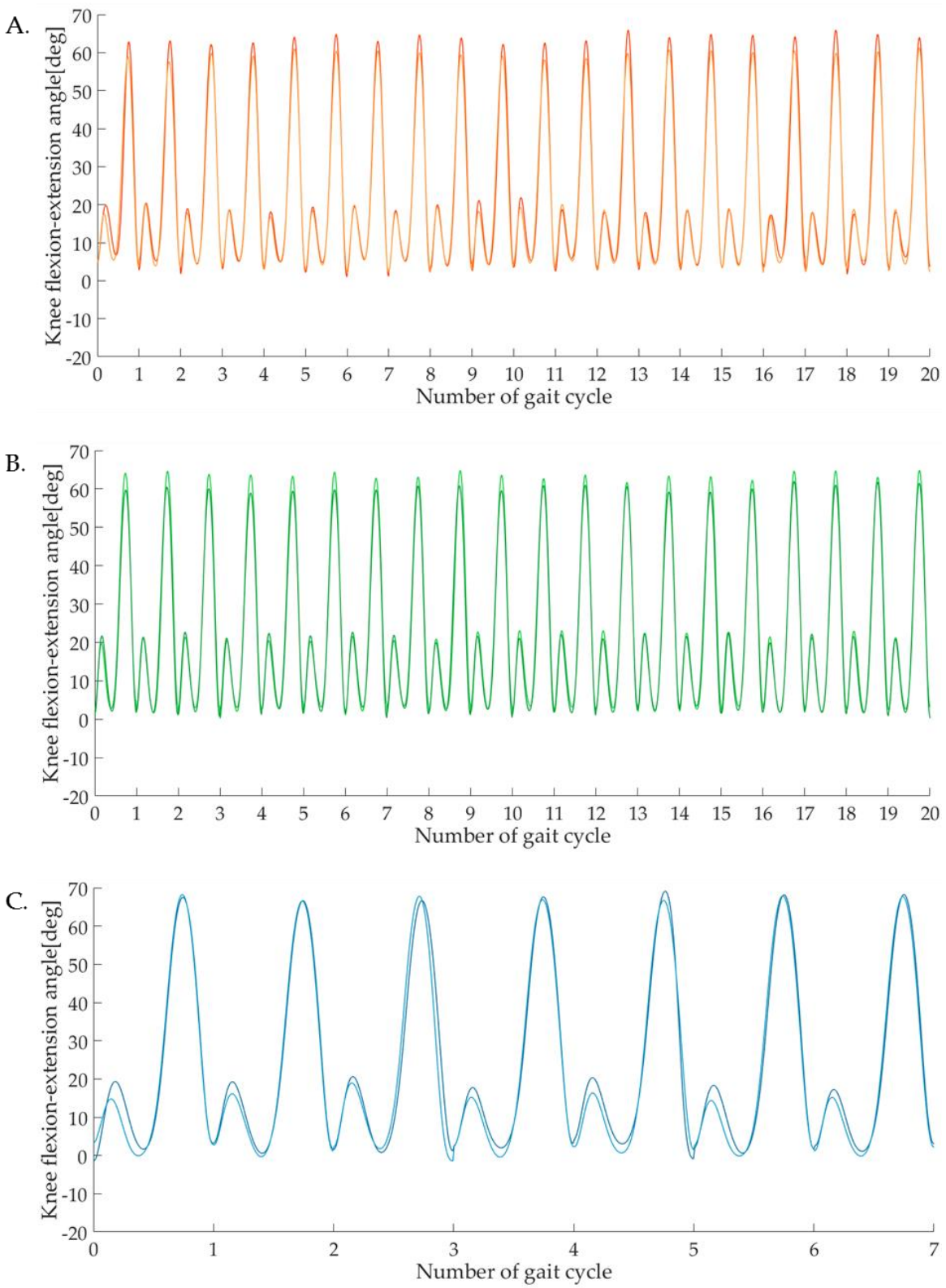

APPENDIX FIG 10. BETWEEN DAY VARIABILITY OF KNEE FLEXION EXTENSION DURING GAIT PERFORMED BY PARTICIPANT 5

A. recorded with the sensors during the first (red) and second (orange) laboratory session; B. recorded with the sensors during the first (dark green) and second (light green) outdoor session; C. recorded with the Vicon during the first (blue) and second (light blue) laboratory session outdoor.

Participant 6

APPENDIX TABLE 11. WITHIN DAY VARIABILITY OF KNEE FLEXION EXTENSION DURING GAIT recorded in a laboratory simultaneously with inertial sensors and an optical motion capture system, and in a non-laboratory based environment with the inertial sensors only, during two separate sessions – Participant 6.

Within day variability of human gait	*Experimental results*					
Participant 6	Vicon Session 1	Indoor Session 1	Outdoor Session 1	Vicon Session 2	Indoor Session 2	Outdoor Session 2
Number of observations (N)	10	13	20	7	12	8
Range of motion (ROM)	63.4°	55.8°	70.8°	69.1°	60.7°	69.1°
Root mean squared error (RMS)	1.5°	2.1°	2°	2.1°	2.9°	3.7°
Standard error (σ)	1.6°	2.2°	2.1°	2.1°	2.9°	3.8°
Coefficient of multiple correlations (CMC)	NaN	0.534	0.973	NaN	NaN	NaN

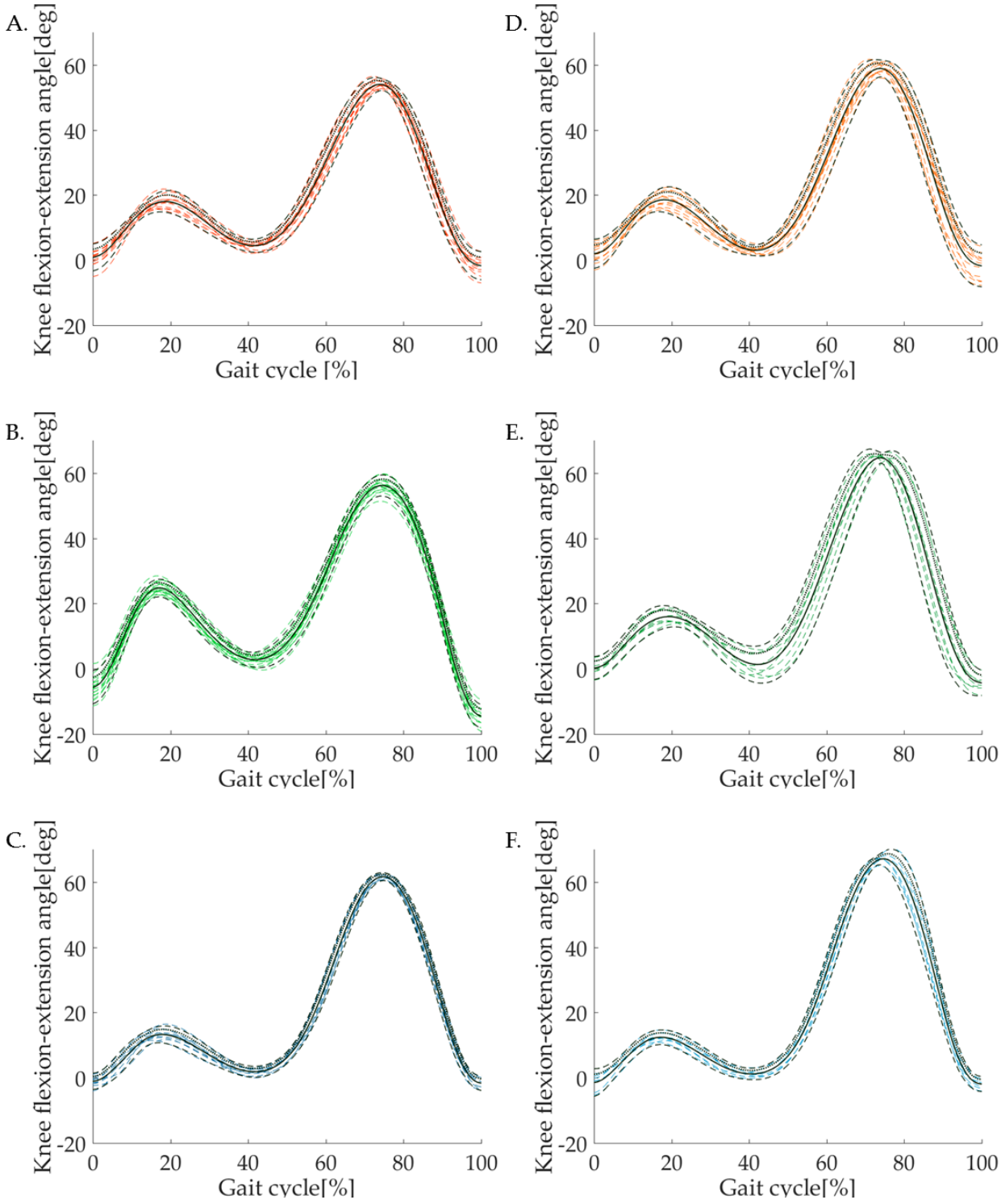

APPENDIX FIG 11. WITHIN DAY VARIABILITY OF KNEE FLEXION EXTENSION DURING GAIT PERFORMED BY PARTICIPANT 6

A. recorded with the sensors in the first laboratory session; B. recorded with the Vicon in the first laboratory session; C. recorded with the sensors in the first outdoor session; D. recorded with the sensors in the second laboratory session; E. recorded with the Vicon in the second laboratory session; F. recorded with the sensors in the second outdoor session. Where individual gait cycles are marked with coloured dotted lines, the average gait cycle of the session with full black line, and 95% confidence intervals with black dotted lines.

APPENDIX TABLE 12. BETWEEN DAY VARIABILITY OF KNEE FLEXION EXTENSION DURING GAIT recorded in a laboratory simultaneously with inertial sensors and an optical motion capture system, and in a non-laboratory based environment with the inertial sensors only, during two separate sessions – Participant 6.

Between day variability of human gait	*Experimental results*		
Participant 6	Vicon	Indoor	Outdoor
Number of observations (N)	7	8	10
Difference between range of motion (ΔROM)	8.7°	7.5°	4.4°
Root mean squared error (RMS)	3.5°	3.9°	6.6°
Standard error (σ)	2.6°	3.2°	5.6°
Coefficient of variation (CV)	3.8%	5.2%	7.1%
Coefficient of Multiple correlations (CMC)	0.994	0.988	0.974
Pearson product-moment correlation coefficient (r)	0.993	0.983	0.953

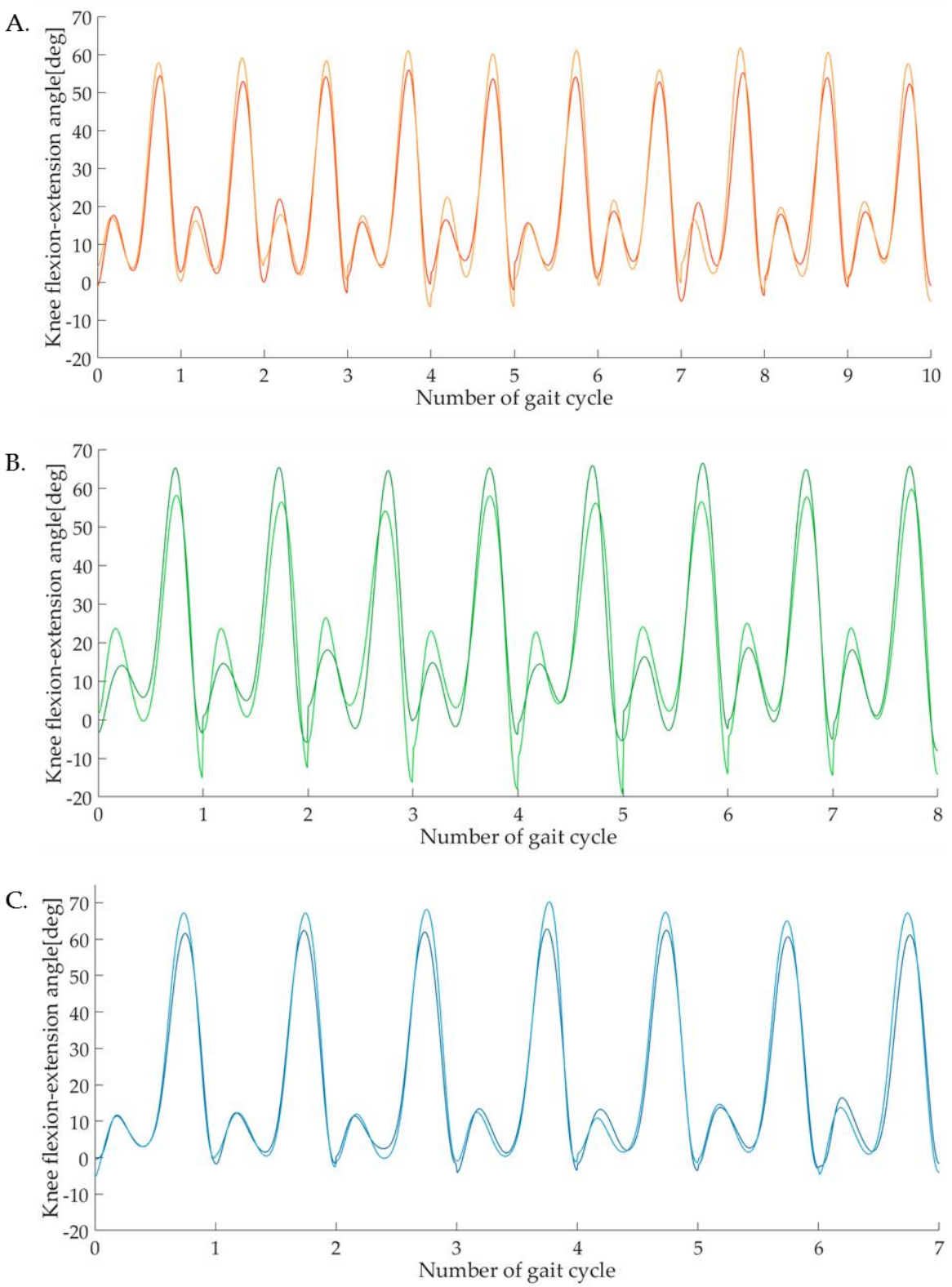

APPENDIX FIG 12. BETWEEN DAY VARIABILITY OF KNEE FLEXION EXTENSION DURING GAIT PERFORMED BY PARTICIPANT 6

A. recorded with the sensors during the first (red) and second (orange) laboratory session; B. recorded with the sensors during the first (dark green) and second (light green) outdoor session; C. recorded with the Vicon during the first (blue) and second (light blue) laboratory session outdoor.

Participant 7

APPENDIX TABLE 13. WITHIN DAY VARIABILITY OF KNEE FLEXION EXTENSION DURING GAIT recorded in a laboratory simultaneously with inertial sensors and an optical motion capture system, and in a non-laboratory based environment with the inertial sensors only, during two separate sessions – Participant 7.

Within day variability of human gait	*Experimental results*					
Participant 7	Vicon Session 1	Indoor Session 1	Outdoor Session 1	Vicon Session 2	Indoor Session 2	Outdoor Session 2
Number of observations (N)	10	19	15	7	20	15
Range of motion (ROM)	57.7°	59.3°	73.2°	61.9°	53.8°	68.8°
Root mean squared error (RMS)	2°	1.6°	1.7°	2°	1.8°	1.7°
Standard error (σ)	2.1°	1.7°	1.8°	2.1°	2°	1.8°
Coefficient of multiple correlations (CMC)	NaN	0.904	0.893	NaN	0.917	0.912

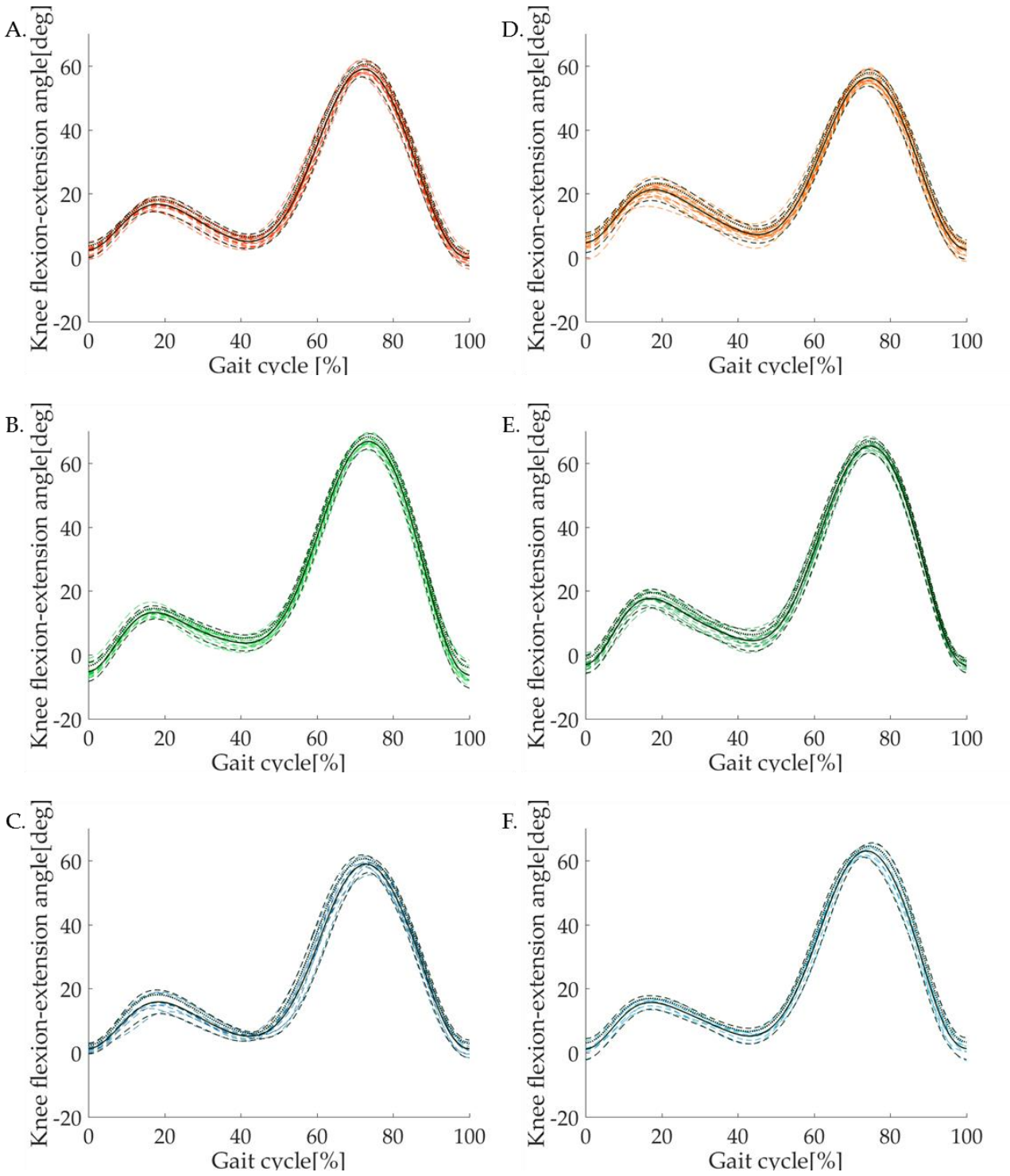

APPENDIX FIG 13. WITHIN DAY VARIABILITY OF KNEE FLEXION EXTENSION DURING GAIT PERFORMED BY PARTICIPANT 7

A. recorded with the sensors in the first laboratory session; B. recorded with the Vicon in the first laboratory session; C. recorded with the sensors in the first outdoor session; D. recorded with the sensors in the second laboratory session; E. recorded with the Vicon in the second laboratory session; F. recorded with the sensors in the second outdoor session. Where individual gait cycles are marked with coloured dotted lines, the average gait cycle of the session with full black line, and 95% confidence intervals with black dotted lines.

APPENDIX TABLE 14. BETWEEN DAY VARIABILITY OF KNEE FLEXION EXTENSION DURING GAIT recorded in a laboratory simultaneously with inertial sensors and an optical motion capture system, and in a non-laboratory based environment with the inertial sensors only, during two separate sessions – Participant 7.

Between day variability of human gait	*Experimental results*		
Participant 7	Vicon	Indoor	Outdoor
Number of observations (N)	7	19	15
Difference between range of motion (ΔROM)	4.7°	5.2°	5.2°
Root mean squared error (RMS)	3.4°	4.9°	4.2°
Standard error (σ)	2.6°	4.1°	3.4°
Coefficient of variation (CV)	4.2%	6.3%	4.3%
Coefficient of Multiple correlations (CMC)	0.992	0.980	0.991
Pearson product-moment correlation coefficient (r)	0.990	0.969	0.986

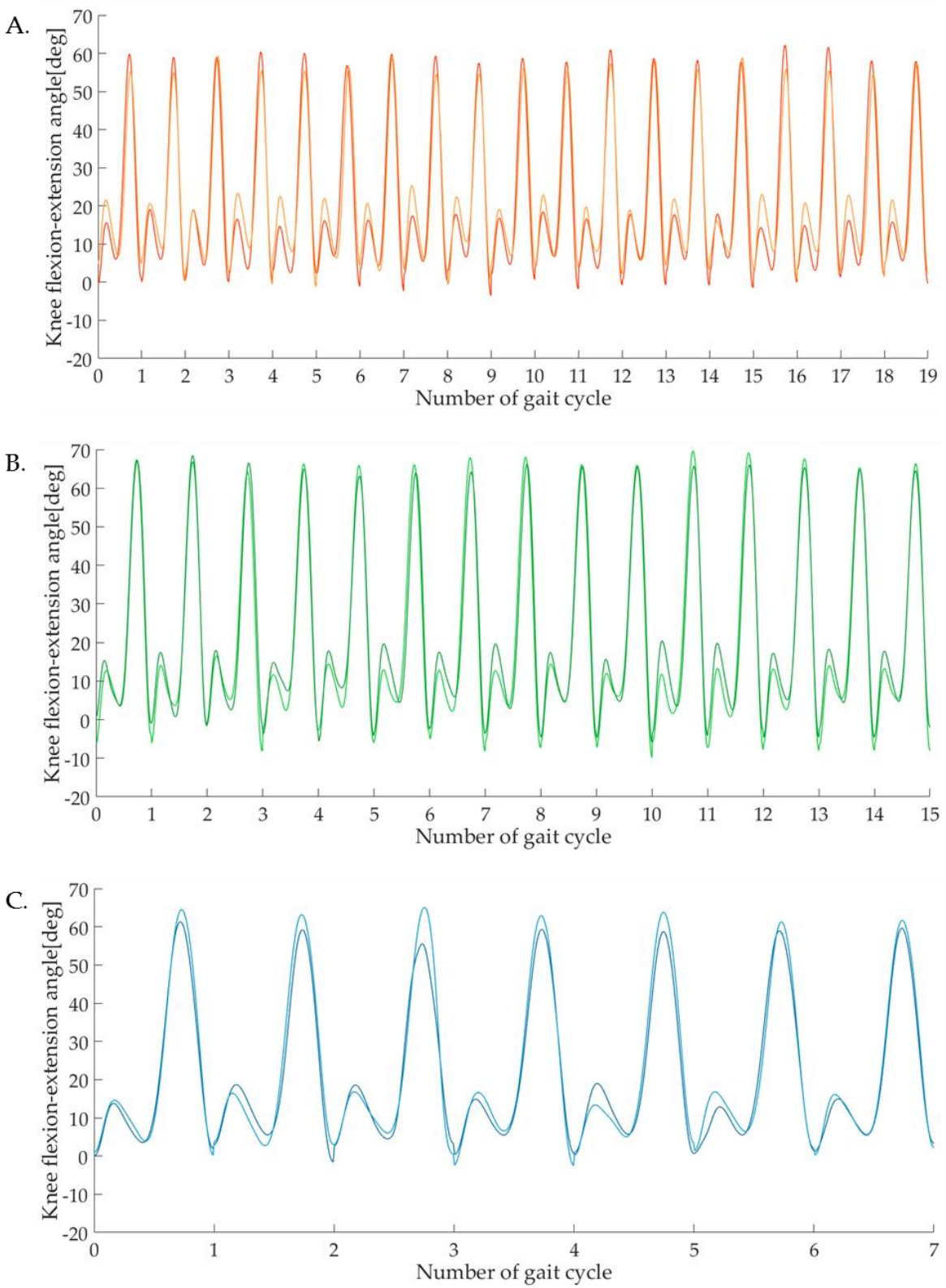

APPENDIX FIG 14. BETWEEN DAY VARIABILITY OF KNEE FLEXION EXTENSION DURING GAIT PERFORMED BY PARTICIPANT 7

A. recorded with the sensors during the first (red) and second (orange) laboratory session; B. recorded with the sensors during the first (dark green) and second (light green) outdoor session; C. recorded with the Vicon during the first (blue) and second (light blue) laboratory session outdoor.

Participant 8

APPENDIX TABLE 15. WITHIN DAY VARIABILITY OF KNEE FLEXION EXTENSION DURING GAIT recorded in a laboratory simultaneously with inertial sensors and an optical motion capture system, and in a non-laboratory based environment with the inertial sensors only, during two separate sessions – Participant 8.

Within day variability of human gait	*Experimental results*					
Participant 8	Vicon Session 1	Indoor Session 1	Outdoor Session 1	Vicon Session 2	Indoor Session 2	Outdoor Session 2
Number of observations (N)	8	19	20	5	19	20
Range of motion (ROM)	62.3°	53.5°	57.2°	60.2°	50.1°	57.5°
Root mean squared error (RMS)	1.1°	1.2°	1°	1.2°	1.5°	1.1°
Standard error (σ)	1.2°	1.3°	1.1°	1.3°	1.5°	1.2°
Coefficient of multiple correlations (CMC)	NaN	0.928	0.977	NaN	0.890	0.956

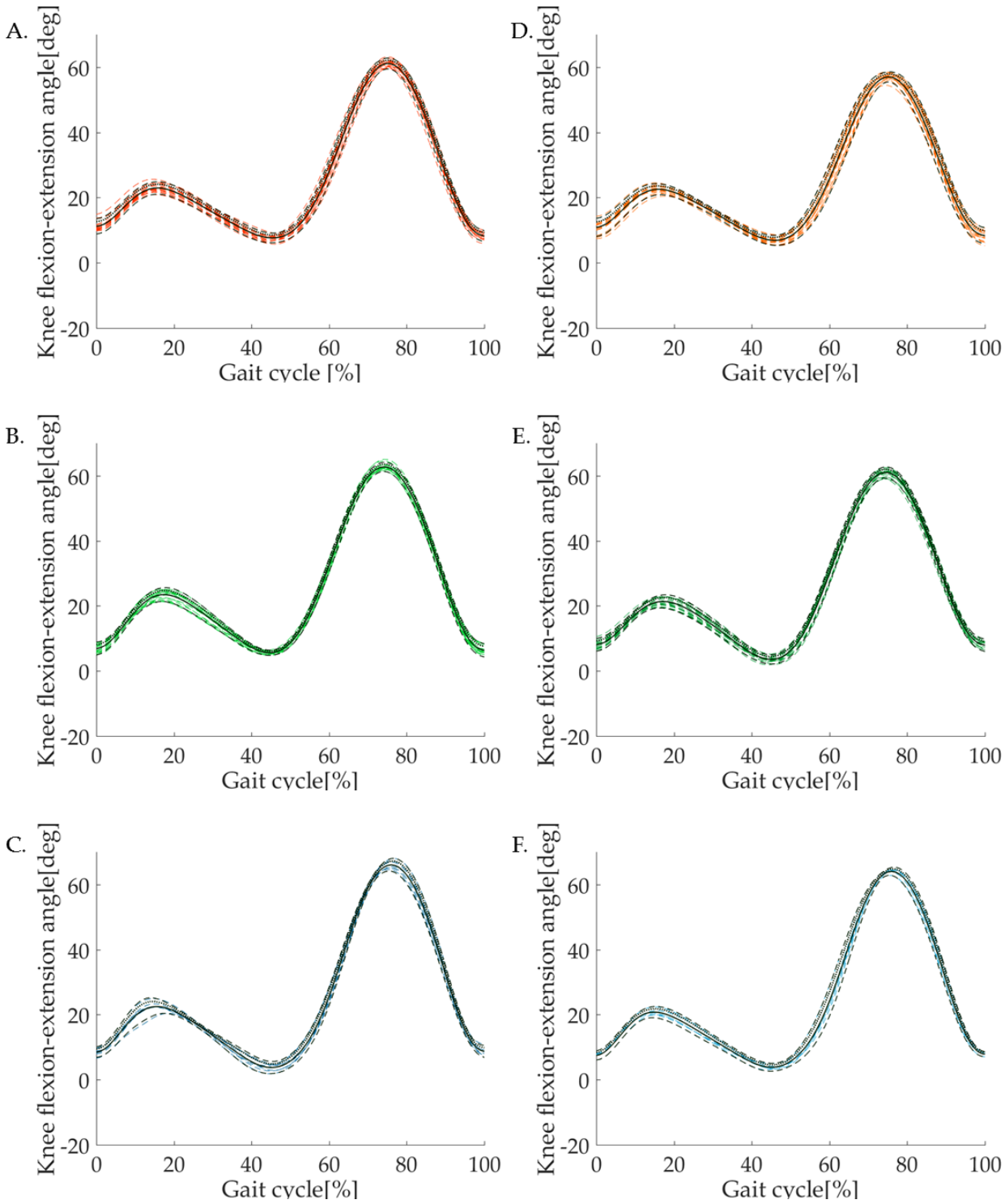

APPENDIX FIG 15. WITHIN DAY VARIABILITY OF KNEE FLEXION EXTENSION DURING GAIT PERFORMED BY PARTICIPANT 8

A. recorded with the sensors in the first laboratory session; B. recorded with the Vicon in the first laboratory session; C. recorded with the sensors in the first outdoor session; D. recorded with the sensors in the second laboratory session; E. recorded with the Vicon in the second laboratory session; F. recorded with the sensors in the second outdoor session. Where individual gait cycles are marked with coloured dotted lines, the average gait cycle of the session with full black line, and 95% confidence intervals with black dotted lines.

APPENDIX TABLE 16. BETWEEN DAY VARIABILITY OF KNEE FLEXION EXTENSION DURING GAIT recorded in a laboratory simultaneously with inertial sensors and an optical motion capture system, and in a non-laboratory based environment with the inertial sensors only, during two separate sessions – Participant 8.

Between day variability of human gait	*Experimental results*		
Participant 8	Vicon	Indoor	Outdoor
Number of observations (N)	5	19	20
Difference between range of motion (ΔROM)	4.6°	4.2°	0.3°
Root mean squared error (RMS)	2.4°	3°	2.3°
Standard error (σ)	1.9°	2.2°	1.9°
Coefficient of variation (CV)	2.9%	3.8%	3.1%
Coefficient of Multiple correlations (CMC)	0.996	0.992	0.996
Pearson product-moment correlation coefficient (r)	0.996	0.990	0.995

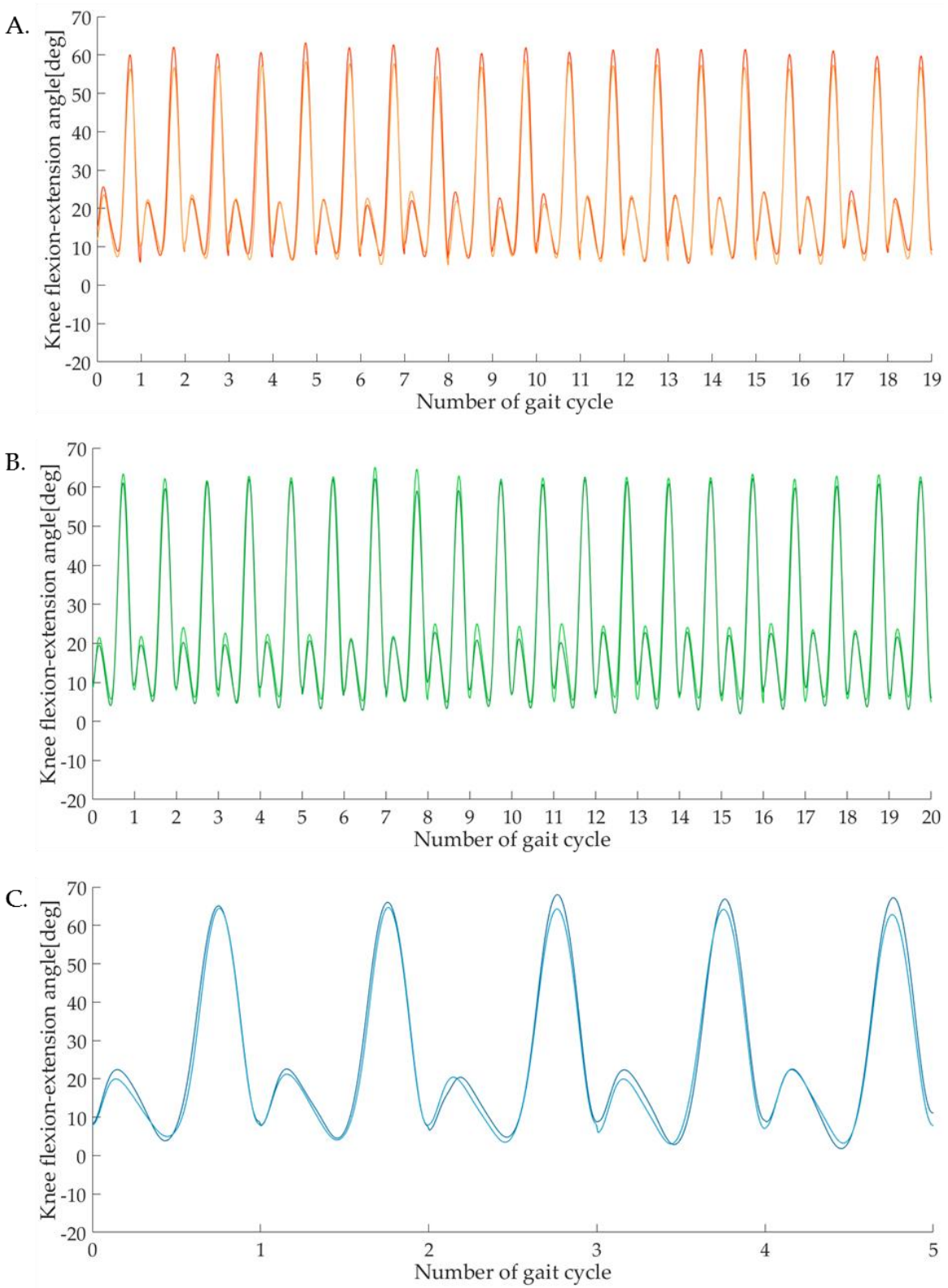

APPENDIX FIG 16. BETWEEN DAY VARIABILITY OF KNEE FLEXION EXTENSION DURING GAIT PERFORMED BY PARTICIPANT 8

A. recorded with the sensors during the first (red) and second (orange) laboratory session; B. recorded with the sensors during the first (dark green) and second (light green) outdoor session; C. recorded with the Vicon during the first (blue) and second (light blue) laboratory session outdoor.

Participant 9

APPENDIX TABLE 17. WITHIN DAY VARIABILITY OF KNEE FLEXION EXTENSION DURING GAIT recorded in a laboratory simultaneously with inertial sensors and an optical motion capture system, and in a non-laboratory based environment with the inertial sensors only, during two separate sessions – Participant 9.

Within day variability of human gait	*Experimental results*					
Participant 9	Vicon Session 1	Indoor Session 1	Outdoor Session 1	Vicon Session 2	Indoor Session 2	Outdoor Session 2
Number of observations (N)	5	19	20	6	20	20
Range of motion (ROM)	59.9°	50.2°	61.8°	62.4°	47.3°	51.2°
Root mean squared error (RMS)	1.6°	1.7°	2°	1.5°	1.8°	1.9°
Standard error (σ)	1.7°	1.7°	2.2°	1.6°	2°	2.1°
Coefficient of multiple correlations (CMC)	NaN	0.911	0.735	NaN	0.866	0.887

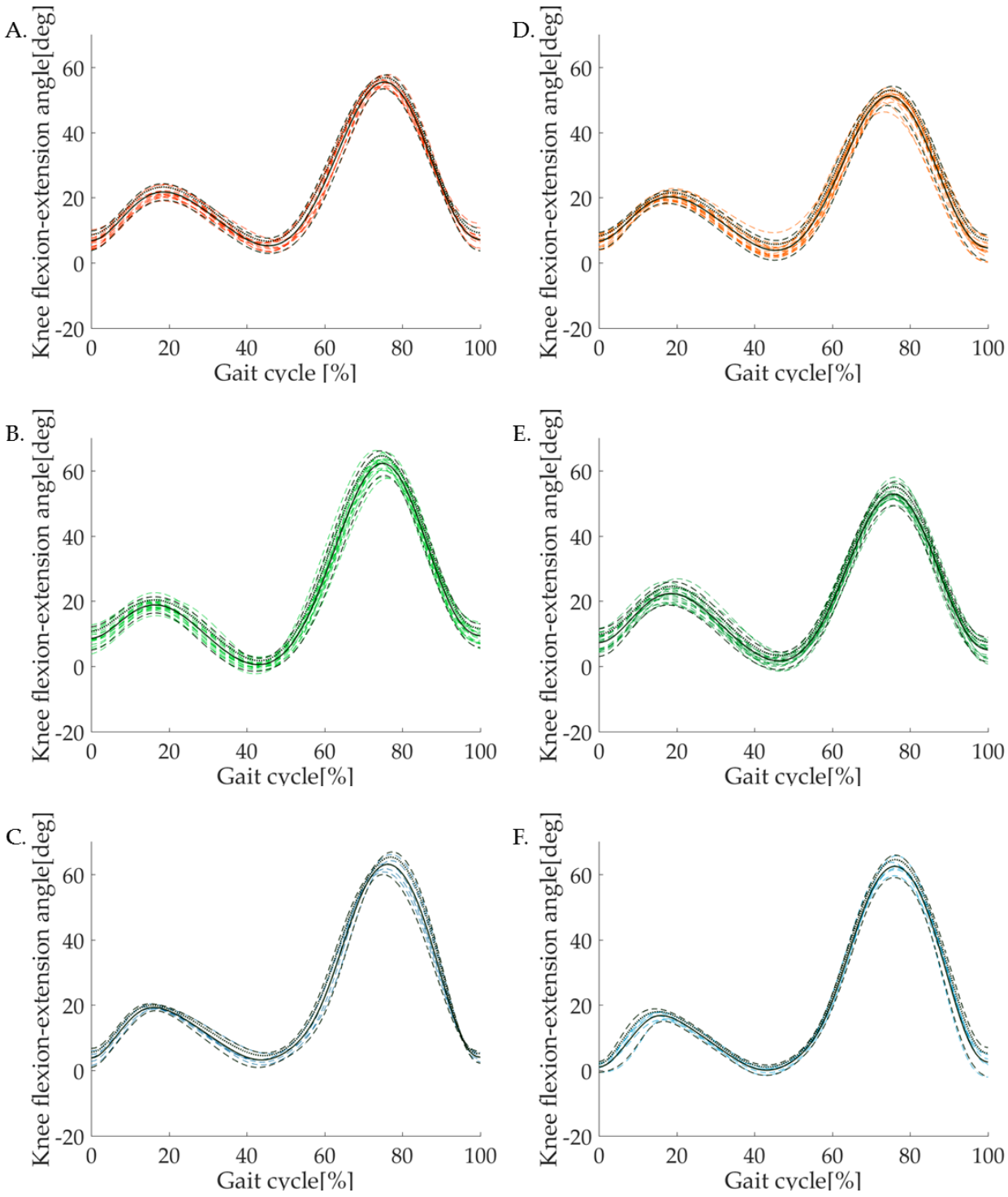

APPENDIX FIG 17. WITHIN DAY VARIABILITY OF KNEE FLEXION EXTENSION DURING GAIT PERFORMED BY PARTICIPANT 9

A. recorded with the sensors in the first laboratory session; B. recorded with the Vicon in the first laboratory session; C. recorded with the sensors in the first outdoor session; D. recorded with the sensors in the second laboratory session; E. recorded with the Vicon in the second laboratory session; F. recorded with the sensors in the second outdoor session. Where individual gait cycles are marked with coloured dotted lines, the average gait cycle of the session with full black line, and 95% confidence intervals with black dotted lines.

APPENDIX TABLE 18. BETWEEN DAY VARIABILITY OF KNEE FLEXION EXTENSION DURING GAIT recorded in a laboratory simultaneously with inertial sensors and an optical motion capture system, and in a non-laboratory based environment with the inertial sensors only, during two separate sessions – Participant 9.

Between day variability of human gait	*Experimental results*		
Participant 9	Vicon	Indoor	Outdoor
Number of observations (N)	5	19	20
Difference between range of motion (ΔROM)	2.5°	1°	9.1°
Root mean squared error (RMS)	3.3°	3.4°	6.2°
Standard error (σ)	2.8°	2.8°	5°
Coefficient of variation (CV)	4.4%	5.2%	7.2%
Coefficient of Multiple correlations (CMC)	0.993	0.988	0.968
Pearson product-moment correlation coefficient (r)	0.993	0.986	0.964

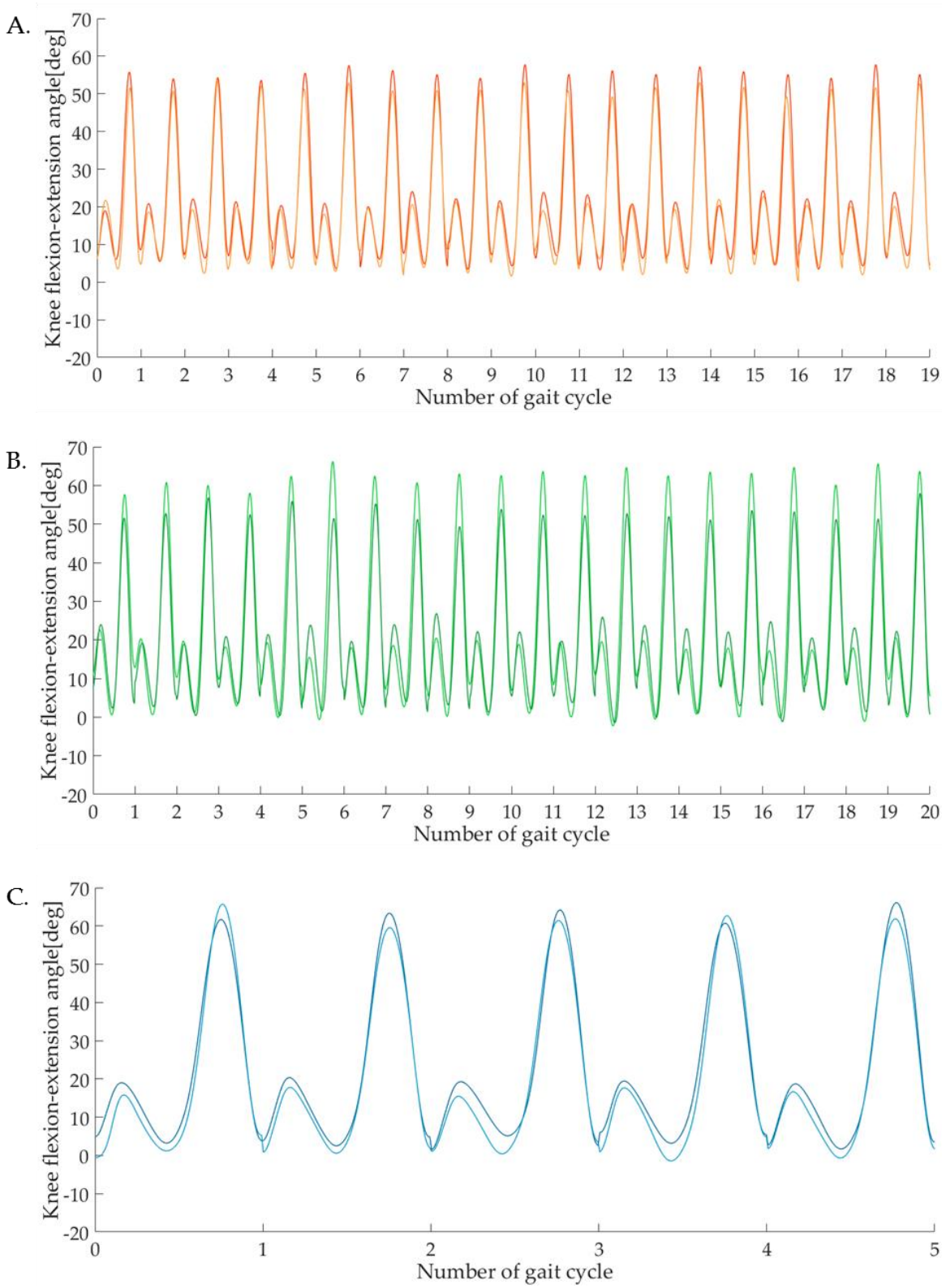

APPENDIX FIG 18. BETWEEN DAY VARIABILITY OF KNEE FLEXION EXTENSION DURING GAIT PERFORMED BY PARTICIPANT 9

A. recorded with the sensors during the first (red) and second (orange) laboratory session; B. recorded with the sensors during the first (dark green) and second (light green) outdoor session; C. recorded with the Vicon during the first (blue) and second (light blue) laboratory session outdoor.

Participant 10

APPENDIX TABLE 19. WITHIN DAY VARIABILITY OF KNEE FLEXION EXTENSION DURING GAIT recorded in a laboratory simultaneously with inertial sensors and an optical motion capture system, and in a non-laboratory based environment with the inertial sensors only, during two separate sessions – Participant 1.

Within day variability of human gait **Participant 10**	*Experimental results*		
	Vicon Session 1	Indoor Session 1	Outdoor Session 1
Number of observations (N)	7	20	20
Range of motion (ROM)	67.2°	54.7°	55.1°
Root mean squared error (RMS)	2.2°	1.5°	1.4°
Standard error (σ)	2.5°	1.6°	1.5°
Coefficient of multiple correlations (CMC)	NaN	0.936	0.933

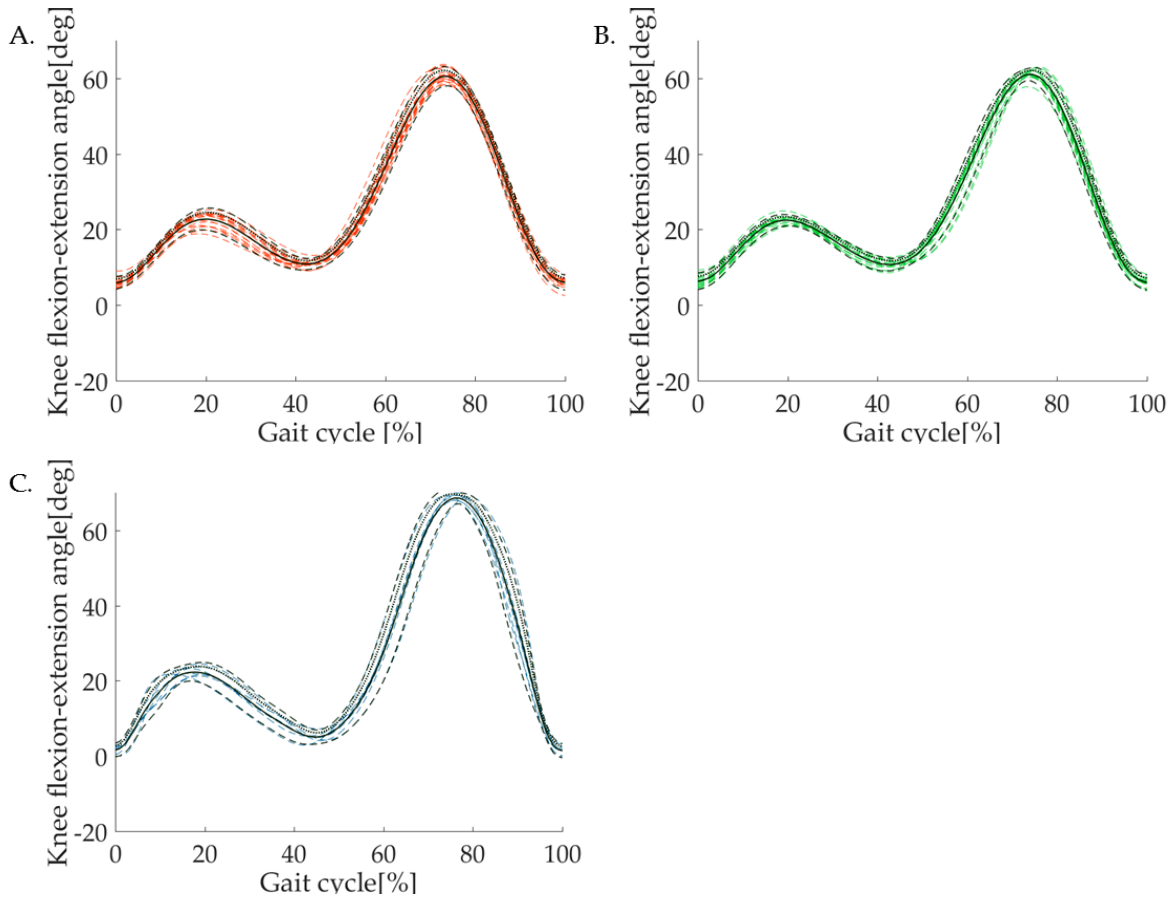

APPENDIX FIG 19. WITHIN DAY VARIABILITY OF KNEE FLEXION EXTENSION DURING GAIT PERFORMED BY PARTICIPANT 10

A. recorded with the sensors in the laboratory; B. recorded with the Vicon in laboratory; C. recorded with the sensors outdoor. Where individual gait cycles are marked with coloured dotted lines, the average gait cycle of the session with full black line, and 95% confidence intervals with black dotted lines.

Appendix 2

Laboratory based study for human knee flexion-extension during gait

Participant 1

APPENDIX TABLE 20. CORRELATION AND VARIABILITY OF KNEE FLEXION EXTENSION RECORDED WITH THE XSENS AND THE VICON SYSTEMS DURING GAIT – PARTICIPANT 1.

Between system variability of gait trials	*Experimental results*	
Participant 1	Session 1	Session 2
Number of observations (N)	5	11
Difference between range of motion (ΔROM)	2.9°	0.2°
Root mean squared error (RMS)	2.9°	3.1°
Standard error (σ)	2.5°	2.5°
Coefficient of variation (CV)	3.8%	3.3%
Coefficient of multiple correlations (CMC)	0.994	0.994
Pearson product-moment correlation coefficient (r)	0.990	0.989

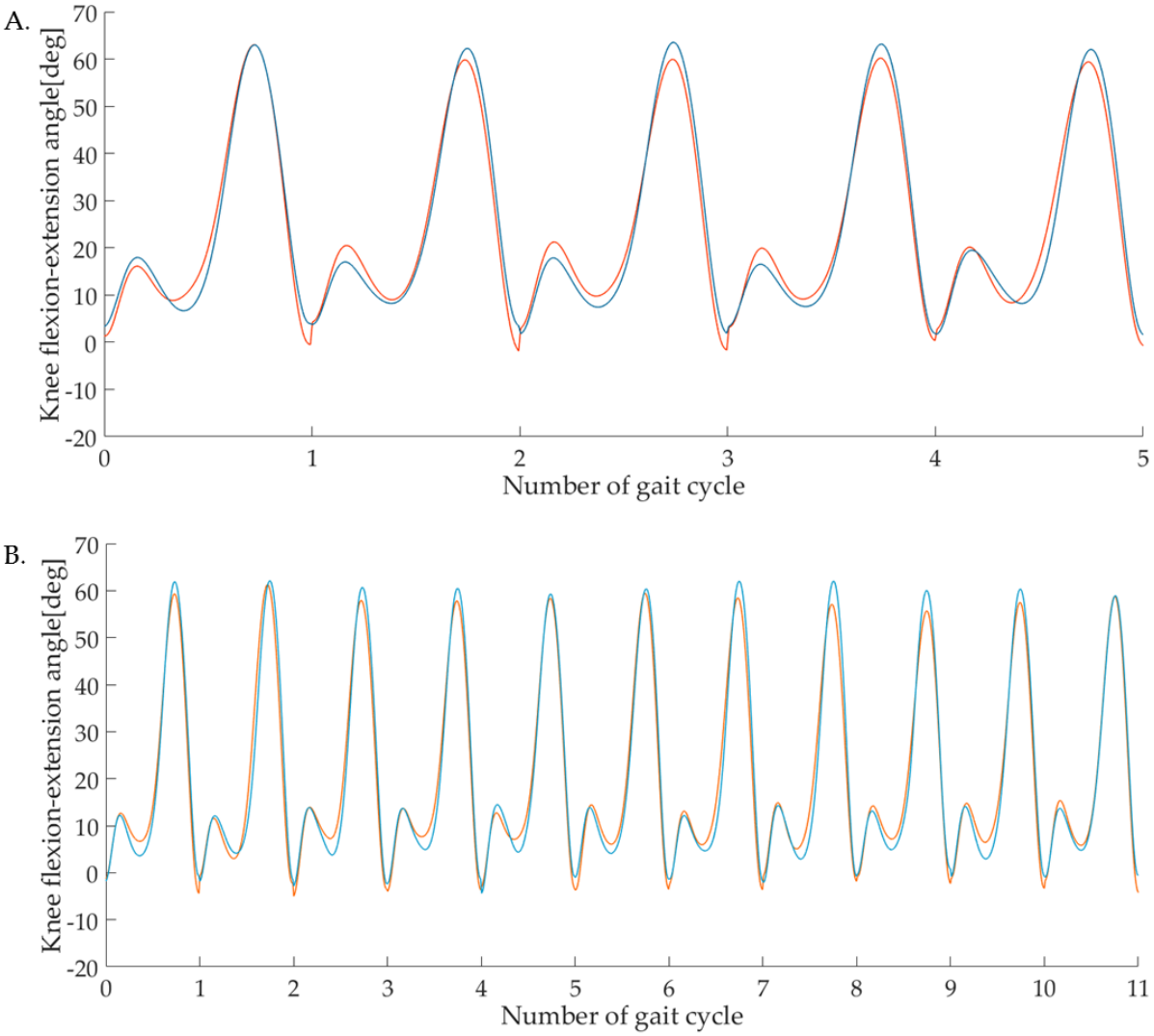

APPENDIX FIG 20. CORRELATION OF KNEE FLEXION EXTENSION RECORDED SYNCHRONOSLY WITH TWO MOTION CAPTURE SYSTEMS DURING GAIT PERFORMED BY PARTICIPANT 1

A. Data from first session, where sensor data is represented in red and Vicon data in blue; B. Data from the second session, where sensor data is represented in orange and Vicon data in light blue.

Participant 2

APPENDIX TABLE 21. CORRELATION AND VARIABILITY OF KNEE FLEXION EXTENSION RECORDED WITH THE XSENS AND THE VICON SYSTEMS DURING GAIT – PARTICIPANT 2.

Between system variability of gait trials	*Experimental results*	
Participant 2	Session 1	Session 2
Number of observations (N)	7	7
Difference between range of motion (ΔROM)	2°	0.7°
Root mean squared error (RMS)	4.2°	4.3°
Standard error (σ)	3.6°	3.5°
Coefficient of variation (CV)	6.1%	5.9%
Coefficient of multiple correlations (CMC)	0.985	0.985
Pearson product-moment correlation coefficient (r)	0.980	0.986

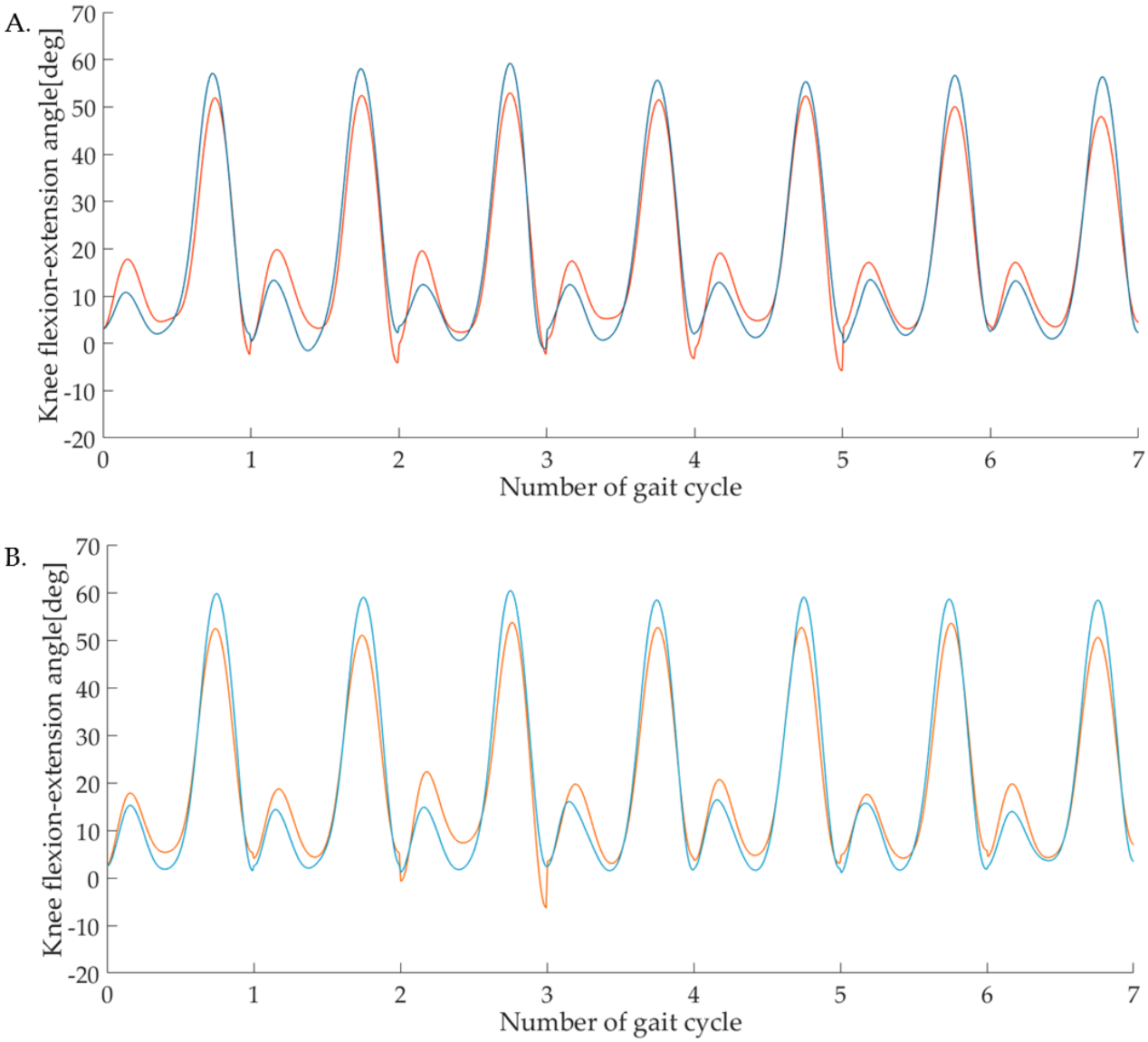

APPENDIX FIG 21. CORRELATION OF KNEE FLEXION EXTENSION RECORDED SYNCHRONOSLY BY TWO SYSTEMS DURING GAIT PERFORMED BY PARTICIPANT 2

A. Data from first session, where sensor data is represented in red and Vicon data in blue; B. Data from the second session, where sensor data is represented in orange and Vicon data in light blue.

Participant 3

APPENDIX TABLE 22. CORRELATION AND VARIABILITY OF KNEE FLEXION EXTENSION RECORDED WITH THE XSENS AND THE VICON SYSTEMS DURING GAIT – PARTICIPANT 3.

Between system variability of gait trials	*Experimental results*	
Participant 3	Session 1	Session 2
Number of observations (N)	8	10
Difference between range of motion (ΔROM)	1°	0.2
Root mean squared error (RMS)	3.2°	5.9°
Standard error (σ)	2.7°	5.1°
Coefficient of variation (CV)	4.2%	7.7%
Coefficient of multiple correlations (CMC)	0.992	0.966
Pearson product-moment correlation coefficient (r)	0.987	0.958

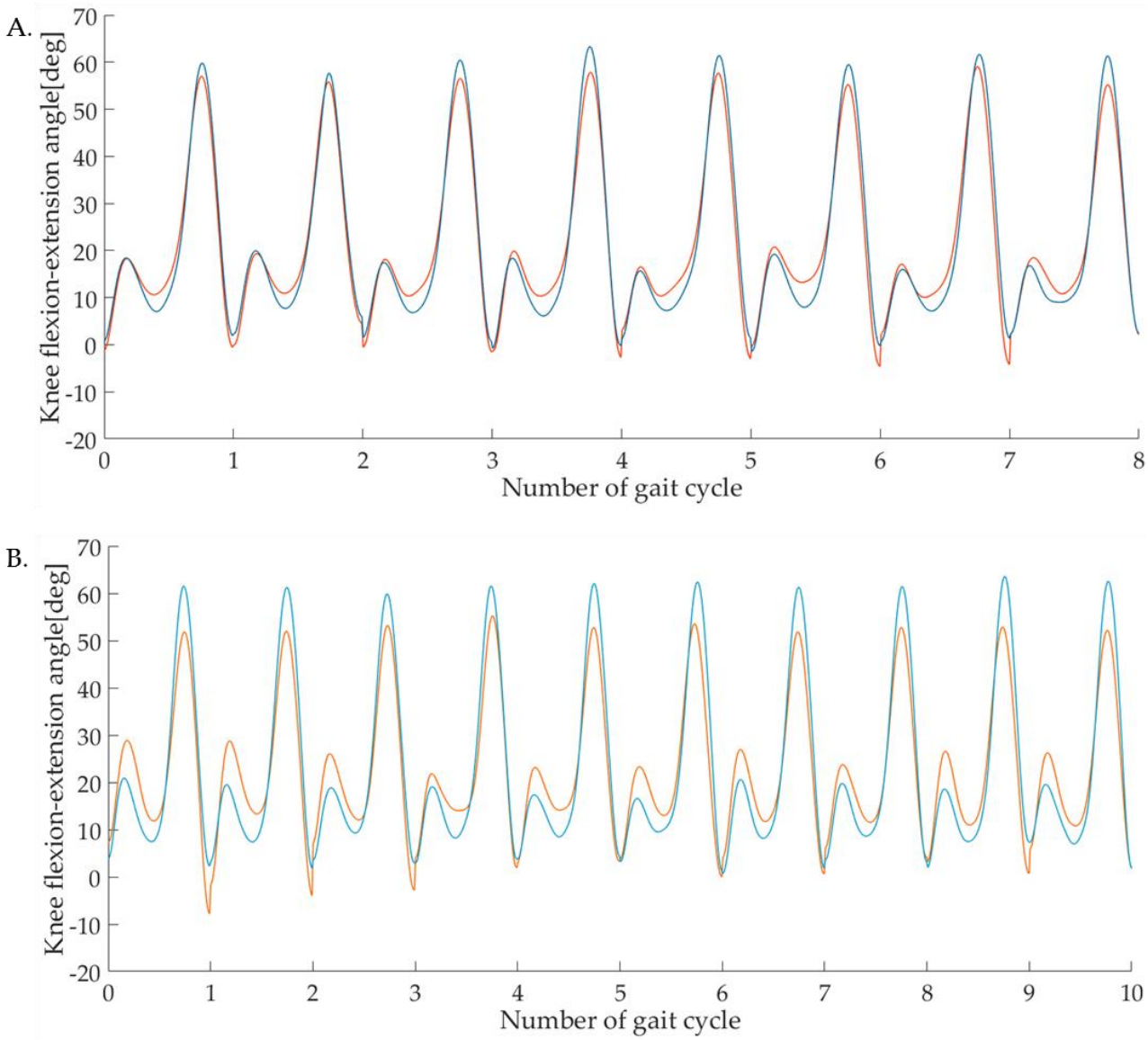

APPENDIX FIG 22. CORRELATION OF KNEE FLEXION EXTENSION RECORDED SYNCHRONOSLY BY TWO SYSTEMS DURING GAIT PERFORMED BY PARTICIPANT 3

A. Data from first session, where sensor data is represented in red and Vicon data in blue; B. Data from the second session, where sensor data is represented in orange and Vicon data in light blue.

Participant 4

APPENDIX TABLE 23. CORRELATION AND VARIABILITY OF KNEE FLEXION EXTENSION RECORDED WITH THE XSENS AND THE VICON SYSTEMS DURING GAIT – PARTICIPANT 4.

Between system variability of gait trials	*Experimental results*	
Participant 4	Session 1	Session 2
Number of observations (N)	9	4
Difference between range of motion (ΔROM)	5.5°	2.3°
Root mean squared error (RMS)	4.5°	4.9°
Standard error (σ)	3.6°	3.9°
Coefficient of variation (CV)	5.9%	5.9%
Coefficient of multiple correlations (CMC)	0.986	0.982
Pearson product-moment correlation coefficient (r)	0.972	0.971

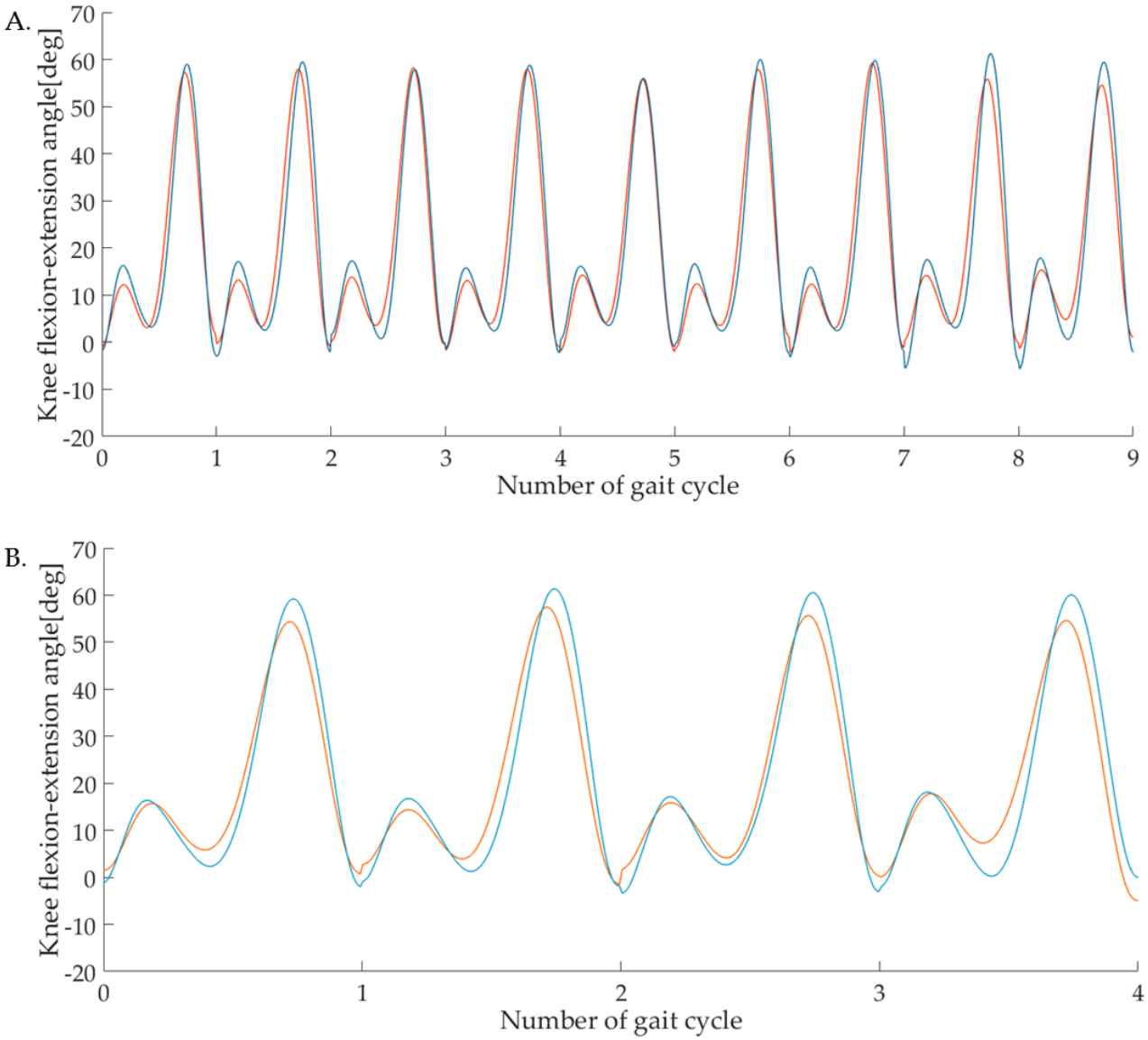

APPENDIX FIG 23. CORRELATION OF KNEE FLEXION EXTENSION RECORDED SYNCHRONOSLY BY TWO SYSTEMS DURING GAIT PERFORMED BY PARTICIPANT 4

A. Data from first session, where sensor data is represented in red and Vicon data in blue; B. Data from the second session, where sensor data is represented in orange and Vicon data in light blue.

Participant 5

APPENDIX TABLE 24. CORRELATION AND VARIABILITY OF KNEE FLEXION EXTENSION RECORDED WITH THE XSENS AND THE VICON SYSTEMS DURING GAIT – PARTICIPANT 5.

Between system variability of gait trials	*Experimental results*	
Participant 5	Session 1	Session 2
Number of observations (N)	10	8
Difference between range of motion (ΔROM)	6.8°	10.9°
Root mean squared error (RMS)	3.2°	5°
Standard error (σ)	2.7°	4.2°
Coefficient of variation (CV)	4.2%	6.4%
Coefficient of multiple correlations (CMC)	0.994	0.985
Pearson product-moment correlation coefficient (r)	0.995	0.989

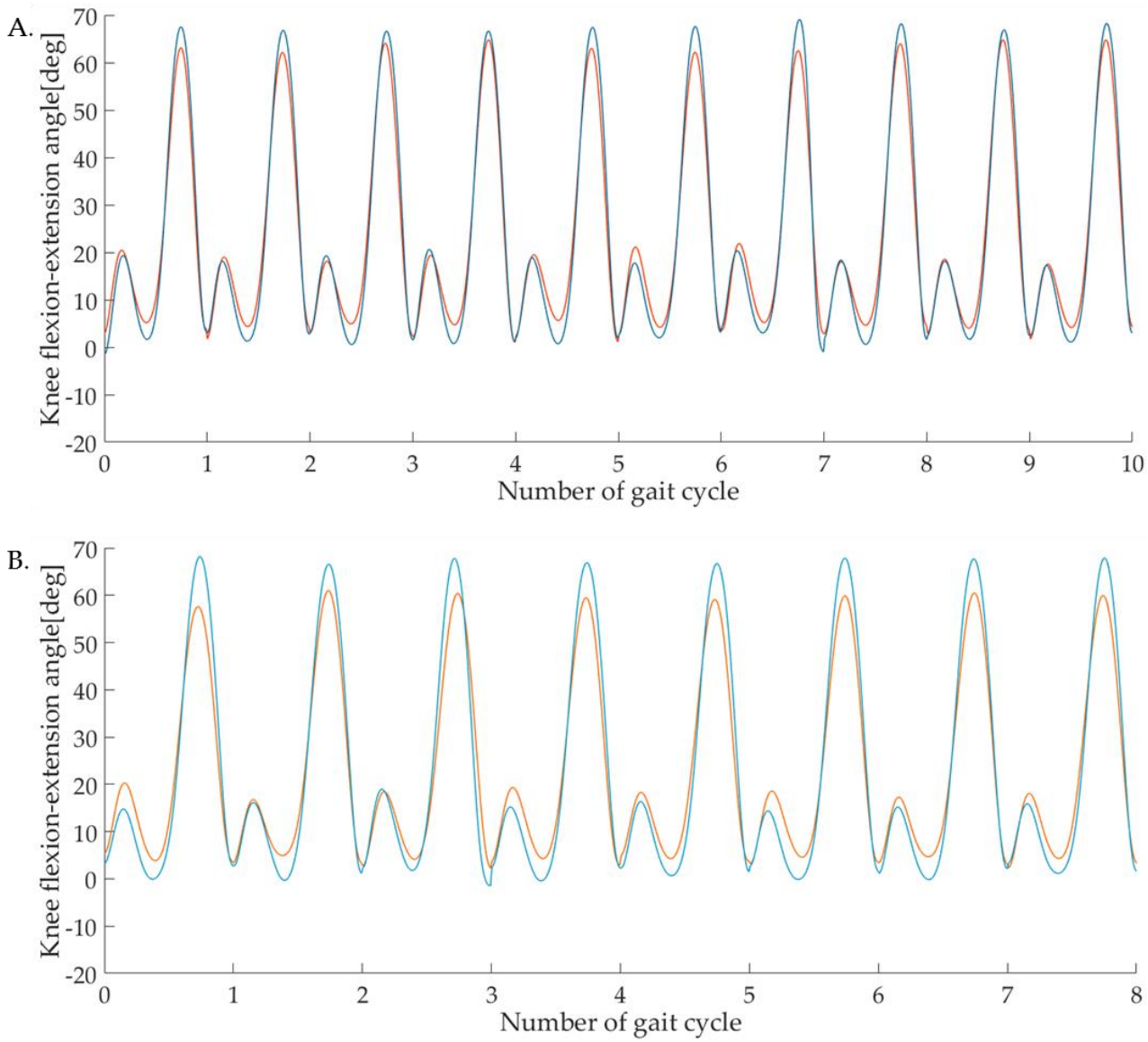

APPENDIX FIG 24. CORRELATION OF KNEE FLEXION EXTENSION RECORDED SYNCHRONOSLY BY TWO SYSTEMS DURING GAIT PERFORMED BY PARTICIPANT 5

A. Data from first session, where sensor data is represented in red and Vicon data in blue; B. Data from the second session, where sensor data is represented in orange and Vicon data in light blue.

Participant 6

APPENDIX TABLE 25. CORRELATION AND VARIABILITY OF KNEE FLEXION EXTENSION RECORDED WITH THE XSENS AND THE VICON SYSTEMS DURING GAIT – PARTICIPANT 6.

	Session 1	**Session 2**
Number of observations (N)	10	7
Difference between range of motion (ΔROM)	3.4°	7.4°
Root mean squared error (RMS)	5.7°	5.7°
Standard error (σ)	4.7°	4.7°
Coefficient of variation (CV)	7.4%	5.9%
Coefficient of multiple correlations (CMC)	0.977	0.981
Pearson product-moment correlation coefficient (r)	0.972	0.980

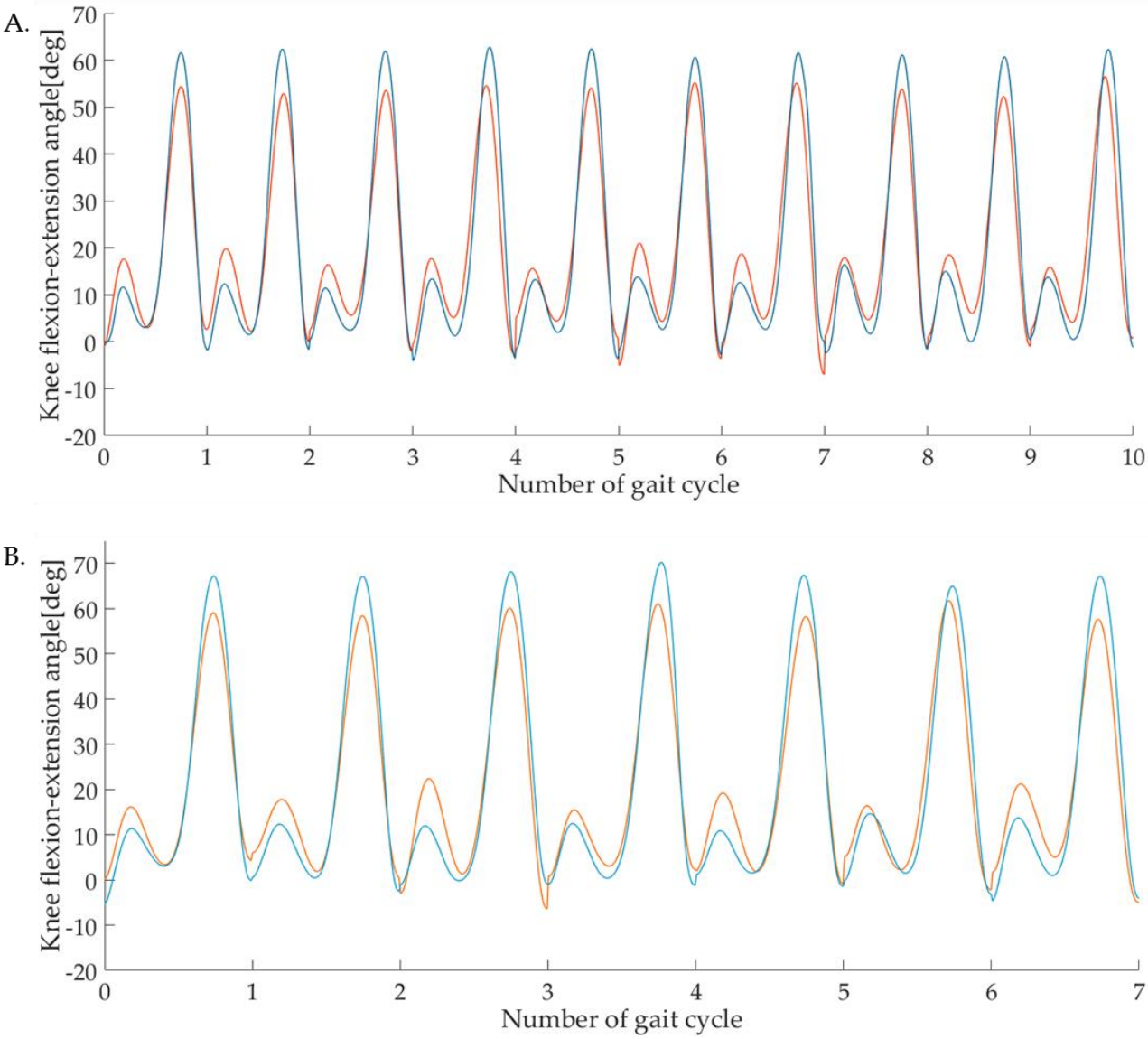

APPENDIX FIG 25. CORRELATION OF KNEE FLEXION EXTENSION RECORDED SYNCHRONOSLY BY TWO SYSTEMS DURING GAIT PERFORMED BY PARTICIPANT 6

A. Data from first session, where sensor data is represented in red and Vicon data in blue; B. Data from the second session, where sensor data is represented in orange and Vicon data in light blue.

Participant 7

APPENDIX TABLE 26. CORRELATION AND VARIABILITY OF KNEE FLEXION EXTENSION RECORDED WITH THE XSENS AND THE VICON SYSTEMS DURING GAIT – PARTICIPANT 7.

Between system variability of gait trials	*Experimental results*	
Participant 7	Session 1	Session 2
Number of observations (N)	10	7
Difference between range of motion (ΔROM)	2.3°	7.7°
Root mean squared error (RMS)	3.5°	4.1°
Standard error (σ)	2.6°	3.5°
Coefficient of variation (CV)	4%	4.5%
Coefficient of multiple correlations (CMC)	0.991	0.988
Pearson product-moment correlation coefficient (r)	0.982	0.990

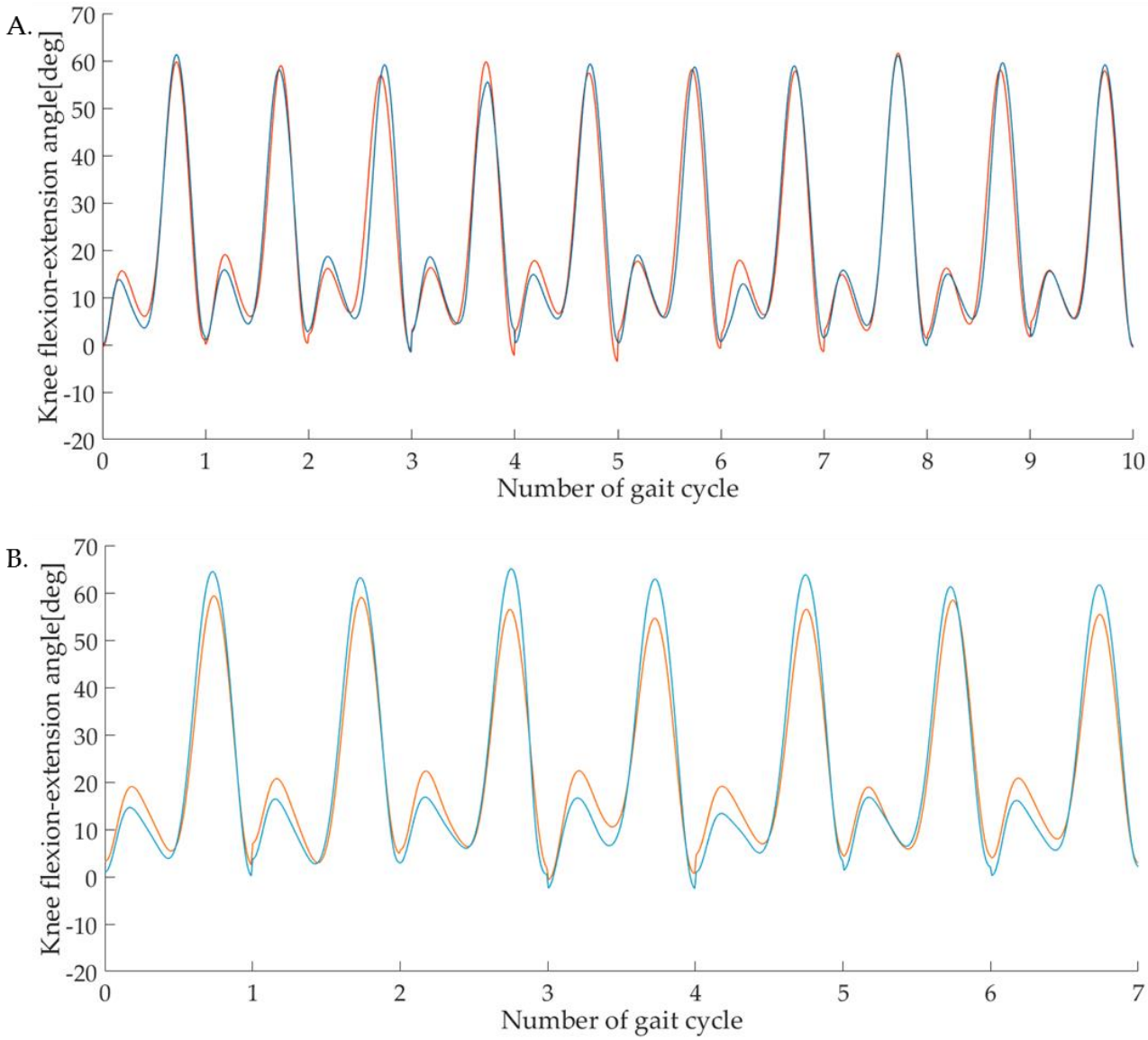

APPENDIX FIG 26. CORRELATION OF KNEE FLEXION EXTENSION RECORDED SYNCHRONOSLY BY TWO SYSTEMS DURING GAIT PERFORMED BY PARTICIPANT 7

A. Data from first session, where sensor data is represented in red and Vicon data in blue; B. Data from the second session, where sensor data is represented in orange and Vicon data in light blue.

Participant 8

APPENDIX TABLE 27. CORRELATION AND VARIABILITY OF KNEE FLEXION EXTENSION RECORDED WITH THE XSENS AND THE VICON SYSTEMS DURING GAIT – PARTICIPANT 8.

Between system variability of gait trials	*Experimental results*	
Participant 8	Session 1	Session 2
Number of observations (N)	8	5
Difference between range of motion (ΔROM)	9.8°	8.4°
Root mean squared error (RMS)	3.5°	3.7°
Standard error (σ)	2.9°	3.2°
Coefficient of variation (CV)	5.1%	5.3%
Coefficient of multiple correlations (CMC)	0.991	0.989
Pearson product-moment correlation coefficient (r)	0.993	0.995

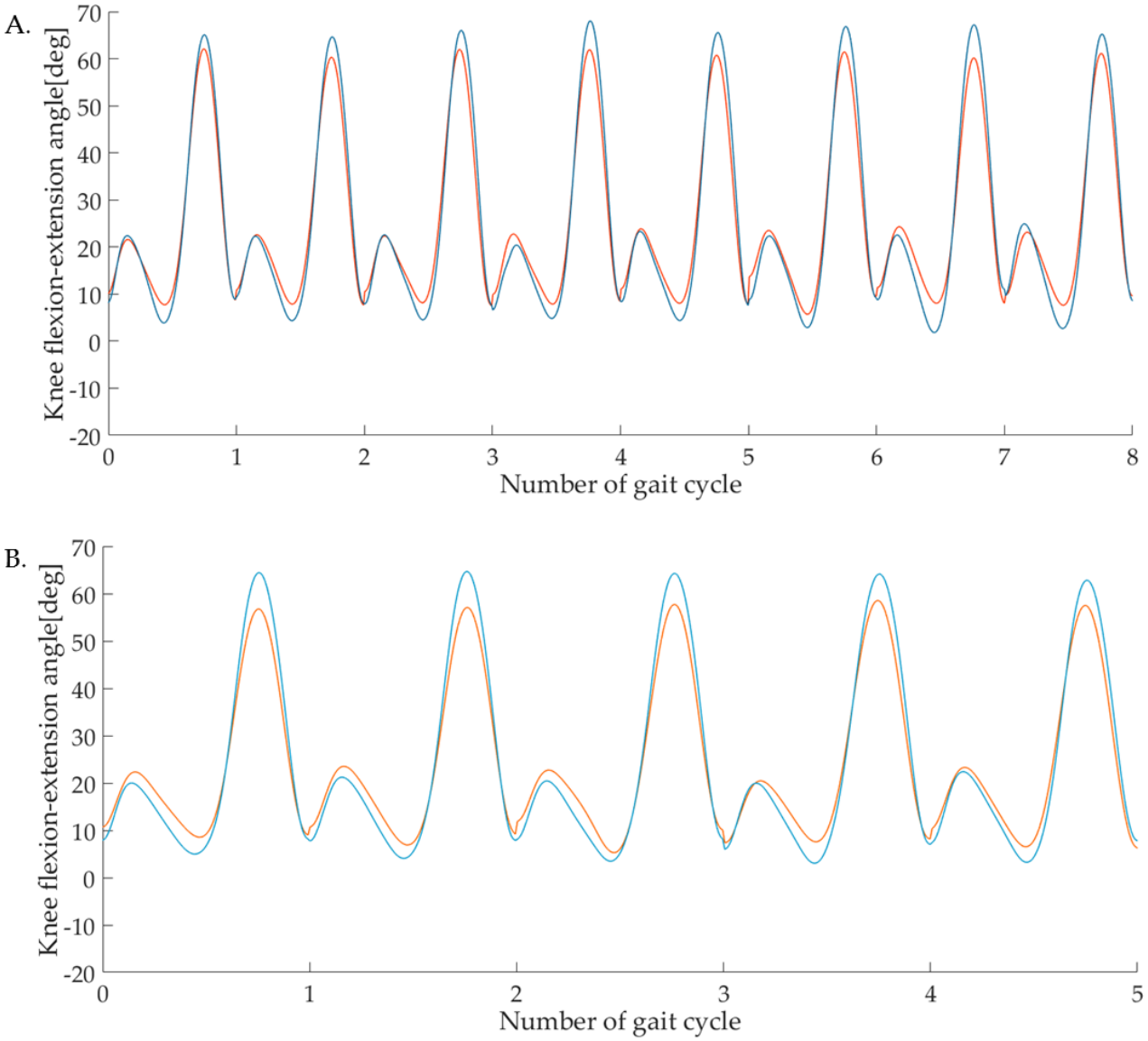

APPENDIX FIG 27. CORRELATION OF KNEE FLEXION EXTENSION RECORDED SYNCHRONOSLY BY TWO SYSTEMS DURING GAIT PERFORMED BY PARTICIPANT 8

A. Data from first session, where sensor data is represented in red and Vicon data in blue; B. Data from the second session, where sensor data is represented in orange and Vicon data in light blue.

Participant 9

APPENDIX TABLE 28. CORRELATION AND VARIABILITY OF KNEE FLEXION EXTENSION RECORDED WITH THE XSENS AND THE VICON SYSTEMS DURING GAIT – PARTICIPANT 9.

Between system variability of gait trials	*Experimental results*	
Participant 9	Session 1	Session 2
Number of observations (N)	5	6
Difference between range of motion (ΔROM)	10.9°	16.3°
Root mean squared error (RMS)	4°	6.1°
Standard error (σ)	3.3°	5°
Coefficient of variation (CV)	6.2%	7.3%
Coefficient of multiple correlations (CMC)	0.987	0.970
Pearson product-moment correlation coefficient (r)	0.992	0.983

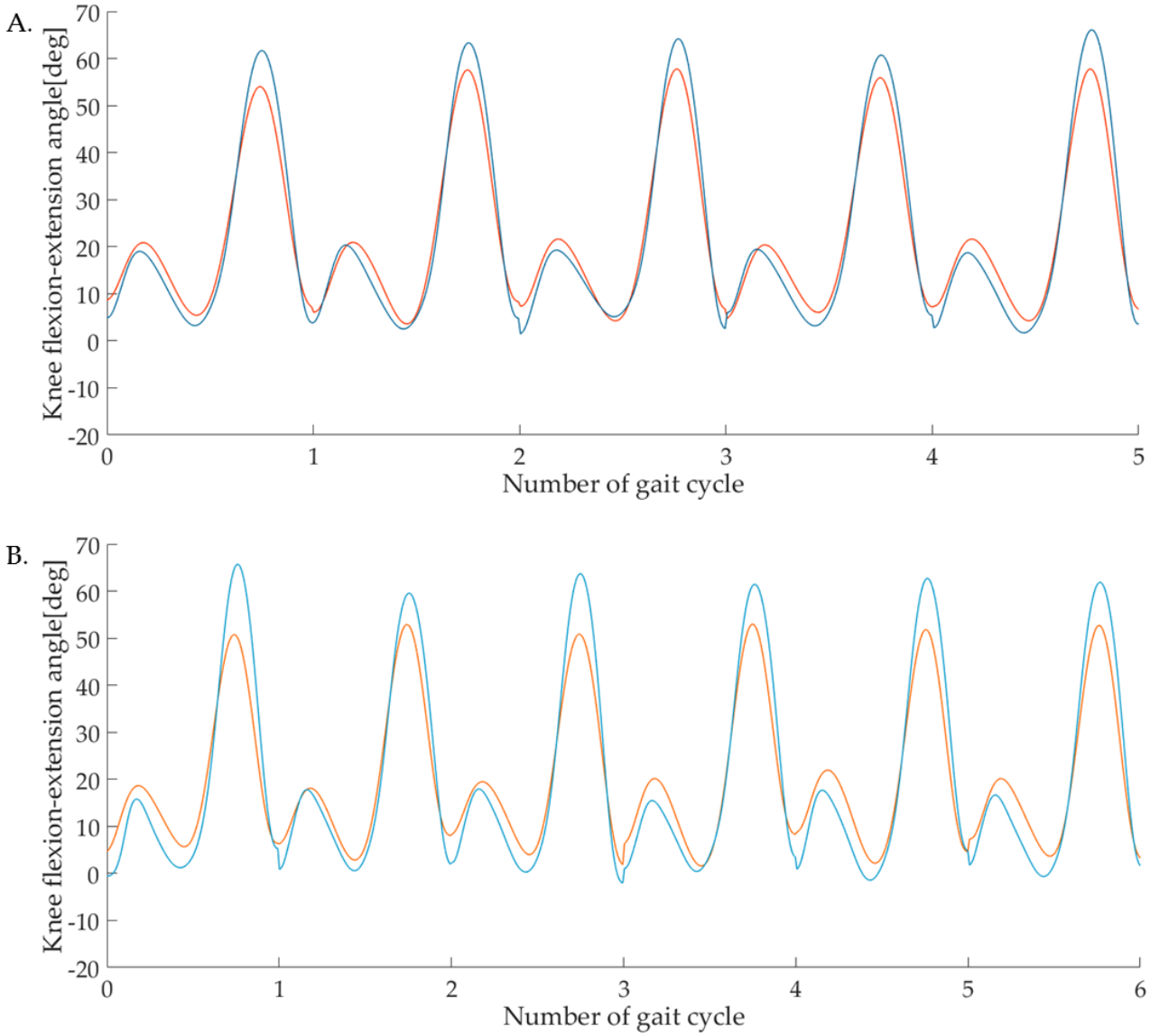

APPENDIX FIG 28. CORRELATION OF KNEE FLEXION EXTENSION RECORDED SYNCHRONOSLY BY TWO SYSTEMS DURING GAIT PERFORMED BY PARTICIPANT 9

A. Data from first session, where sensor data is represented in red and Vicon data in blue; B. Data from the second session, where sensor data is represented in orange and Vicon data in light blue.

Participant 10

APPENDIX TABLE 29. CORRELATION AND VARIABILITY OF KNEE FLEXION EXTENSION RECORDED WITH THE XSENS AND THE VICON SYSTEMS DURING GAIT – PARTICIPANT 10.

Between system variability of gait trials	*Experimental results*
Participant 10	Session 1
Number of observations (N)	7
Difference between range of motion (ΔROM)	10.9°
Root mean squared error (RMS)	6.1°
Standard error (σ)	7.9°
Coefficient of variation (CV)	10.3%
Coefficient of multiple correlations (CMC)	0.957
Pearson product-moment correlation coefficient (r)	0.936

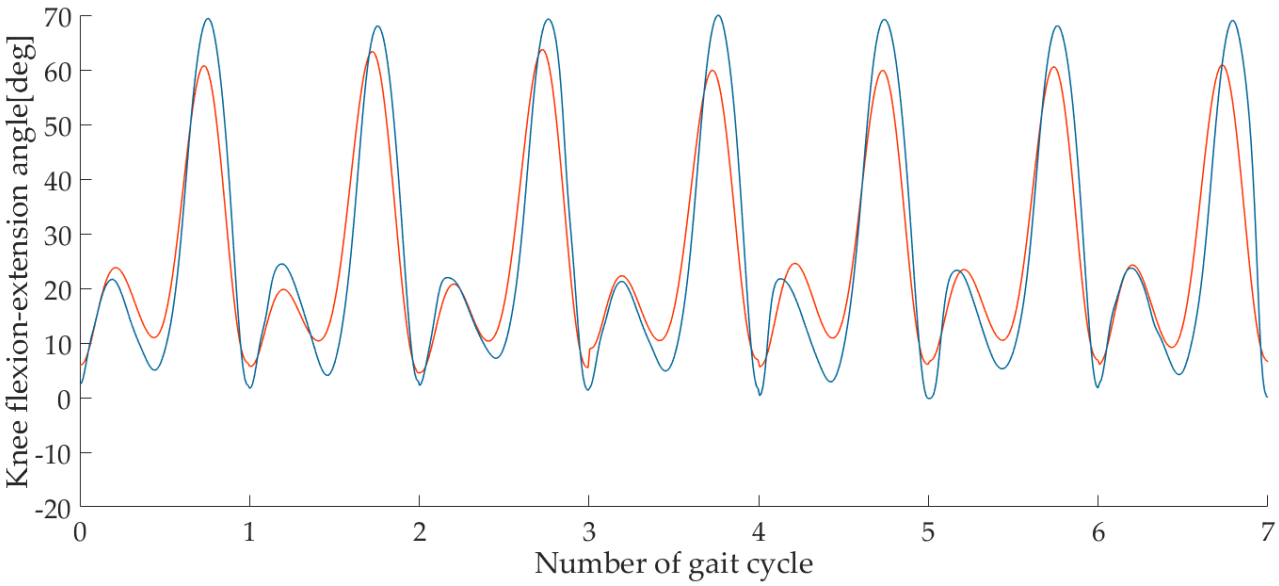

APPENDIX FIG 29. CORRELATION OF KNEE FLEXION EXTENSION RECORDED SYNCHRONOSLY BY TWO SYSTEMS DURING GAIT PERFORMED BY PARTICIPANT 10
Where sensor data is represented in red and Vicon data in blue.

Appendix 3

Non - laboratory based study for human knee flexion-extension during gait

Participant 1

APPENDIX TABLE 30. CORRELATION AND VARIABILITY BETWEEN KNEE FLEXION EXTENSION RECORDED DURING GAIT IN A LABORATORY AND A NON-LABORATORY BASED ENVIRONEMT – PARTICIPANT 1.

Between venue variability of human gait	*Experimental results*	
Participant 1	Session 1	Session 2
Number of observations (N)	20	20
Difference between range of motion (ΔROM)	7.9°	5.4°
Root mean squared error (RMS)	4.5°	3.2°
Standard error (σ)	3.6°	2.6°
Coefficient of variation (CV)	5.5%	3.5%
Coefficient of multiple correlations (CMC)	0.988	0.994
Pearson product-moment correlation coefficient (r)	0.990	0.991

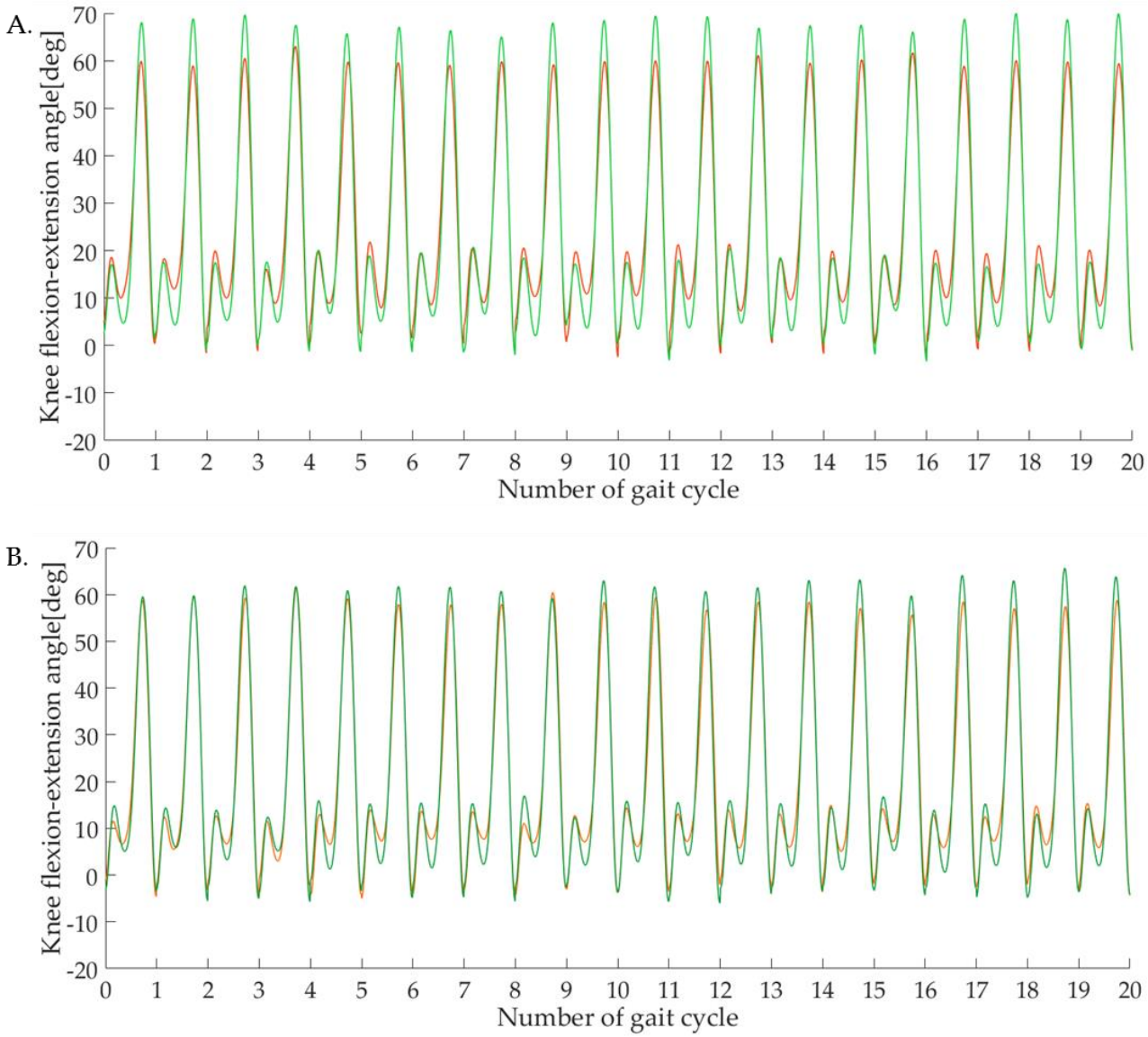

APPENDIX FIG 30. CORRELATION OF KNEE FLEXION EXTENSION RECORDED IN A LABORATORY AND A NON-LABORATORY BASED ENVIRONMENT - PARTICIPANT 1

A. Data from first session, where data recorded in the laboratory is represented in red and outdoor data in dark green; B. Data from the second session, where data recorded in the laboratory is represented in orange and outdoor data in green.

Participant 2

APPENDIX TABLE 31. CORRELATION AND VARIABILITY BETWEEN KNEE FLEXION EXTENSION RECORDED DURING GAIT IN A LABORATORY AND A NON-LABORATORY BASED ENVIRONEMT – PARTICIPANT 2.

Between venue variability of human gait	*Experimental results*	
Participant 2	Session 1	Session 2
Number of observations (N)	17	11
Difference between range of motion (ΔROM)	5.8°	0.1°
Root mean squared error (RMS)	3.3°	3.7°
Standard error (σ)	2.8°	3°
Coefficient of variation (CV)	4.3%	5.3%
Coefficient of multiple correlations (CMC)	0.990	0.988
Pearson product-moment correlation coefficient (r)	0.983	0.988

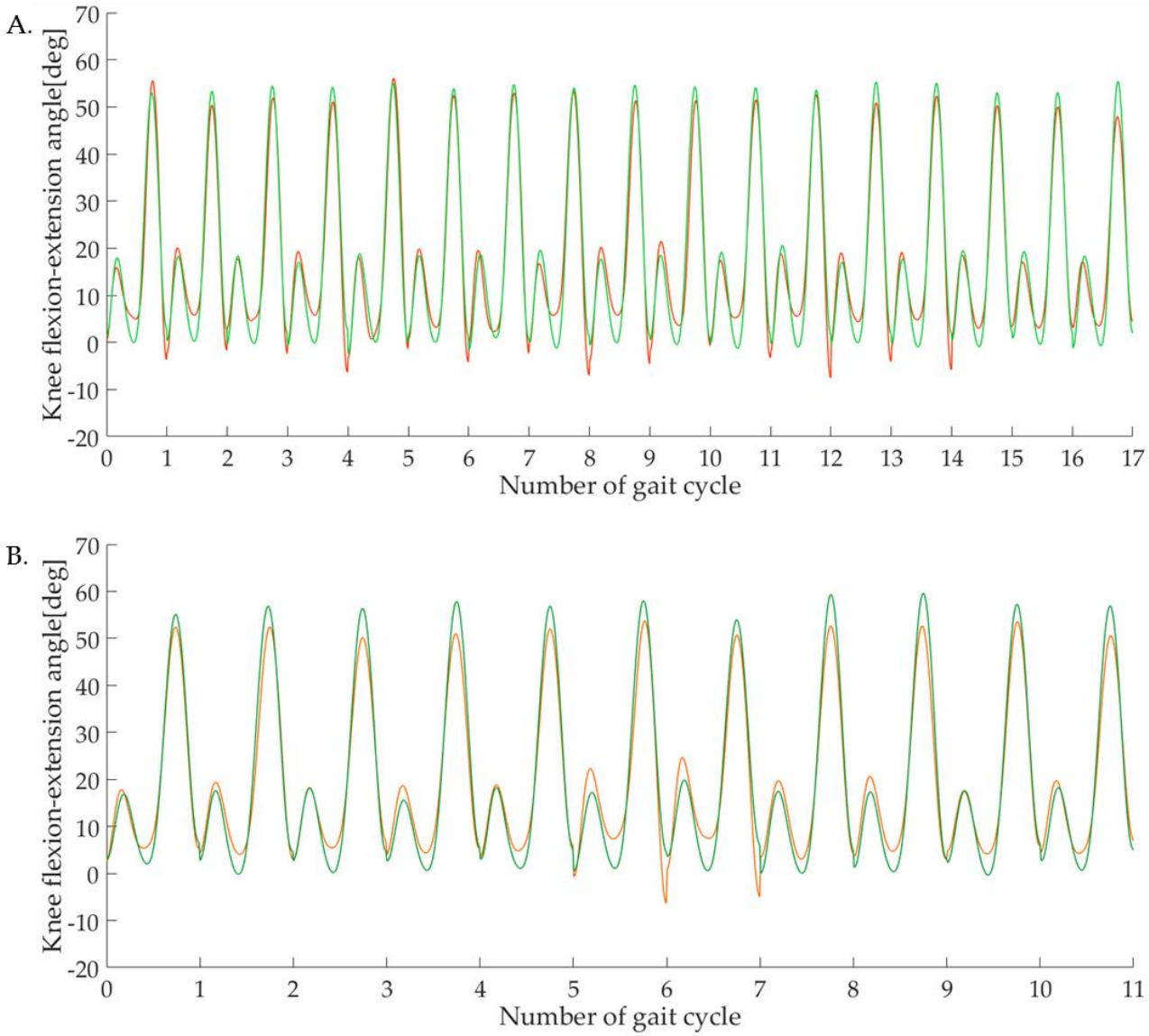

APPENDIX FIG 31. CORRELATION OF KNEE FLEXION EXTENSION RECORDED IN A LABORATORY AND A NON-LABORATORY BASED ENVIRONMENT - PARTICIPANT 2

A. Data from first session, where data recorded in the laboratory is represented in red and outdoor data in dark green; B. Data from the second session, where data recorded in the laboratory is represented in orange and outdoor data in green.

Participant 3

APPENDIX TABLE 32. CORRELATION AND VARIABILITY BETWEEN KNEE FLEXION EXTENSION RECORDED DURING GAIT IN A LABORATORY AND A NON-LABORATORY BASED ENVIRONEMT – PARTICIPANT 3.

Between venue variability of human gait	*Experimental results*	
Participant 3	Session 1	Session 2
Number of observations (N)	19	18
Difference between range of motion (ΔROM)	0.6°	1.6°
Root mean squared error (RMS)	4°	3.6°
Standard error (σ)	3.3°	2.9°
Coefficient of variation (CV)	5%	4.4%
Coefficient of multiple correlations (CMC)	0.986	0.987
Pearson product-moment correlation coefficient (r)	0.976	0.985

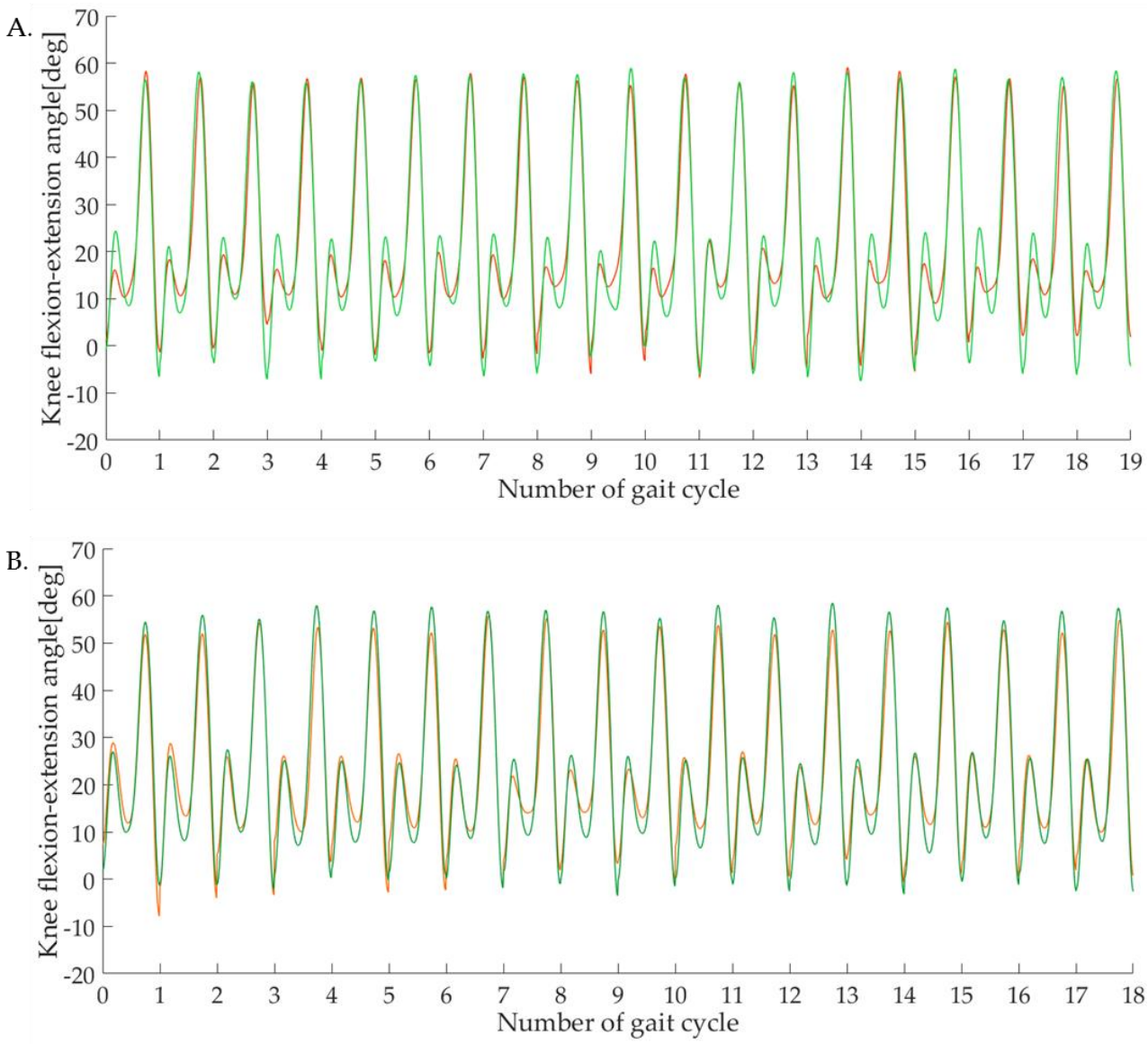

APPENDIX FIG 32. CORRELATION OF KNEE FLEXION EXTENSION RECORDED IN A LABORATORY AND A NON-LABORATORY BASED ENVIRONMENT - PARTICIPANT 3

A. Data from first session, where data recorded in the laboratory is represented in red and outdoor data in dark green; B. Data from the second session, where data recorded in the laboratory is represented in orange and outdoor data in green.

Participant 4

APPENDIX TABLE 33. CORRELATION AND VARIABILITY BETWEEN KNEE FLEXION EXTENSION RECORDED DURING GAIT IN A LABORATORY AND A NON-LABORATORY BASED ENVIRONEMT – PARTICIPANT 4.

Between venue variability of human gait	*Experimental results*	
Participant 4	Session 1	Session 2
Number of observations (N)	20	20
Difference between range of motion (ΔROM)	4°	3.3°
Root mean squared error (RMS)	1.8°	2.8°
Standard error (σ)	1.5°	2.1°
Coefficient of variation (CV)	2.3%	3.2%
Coefficient of Multiple correlations (CMC)	0.998	0.994
Pearson product-moment correlation coefficient (r)	0.996	0.989

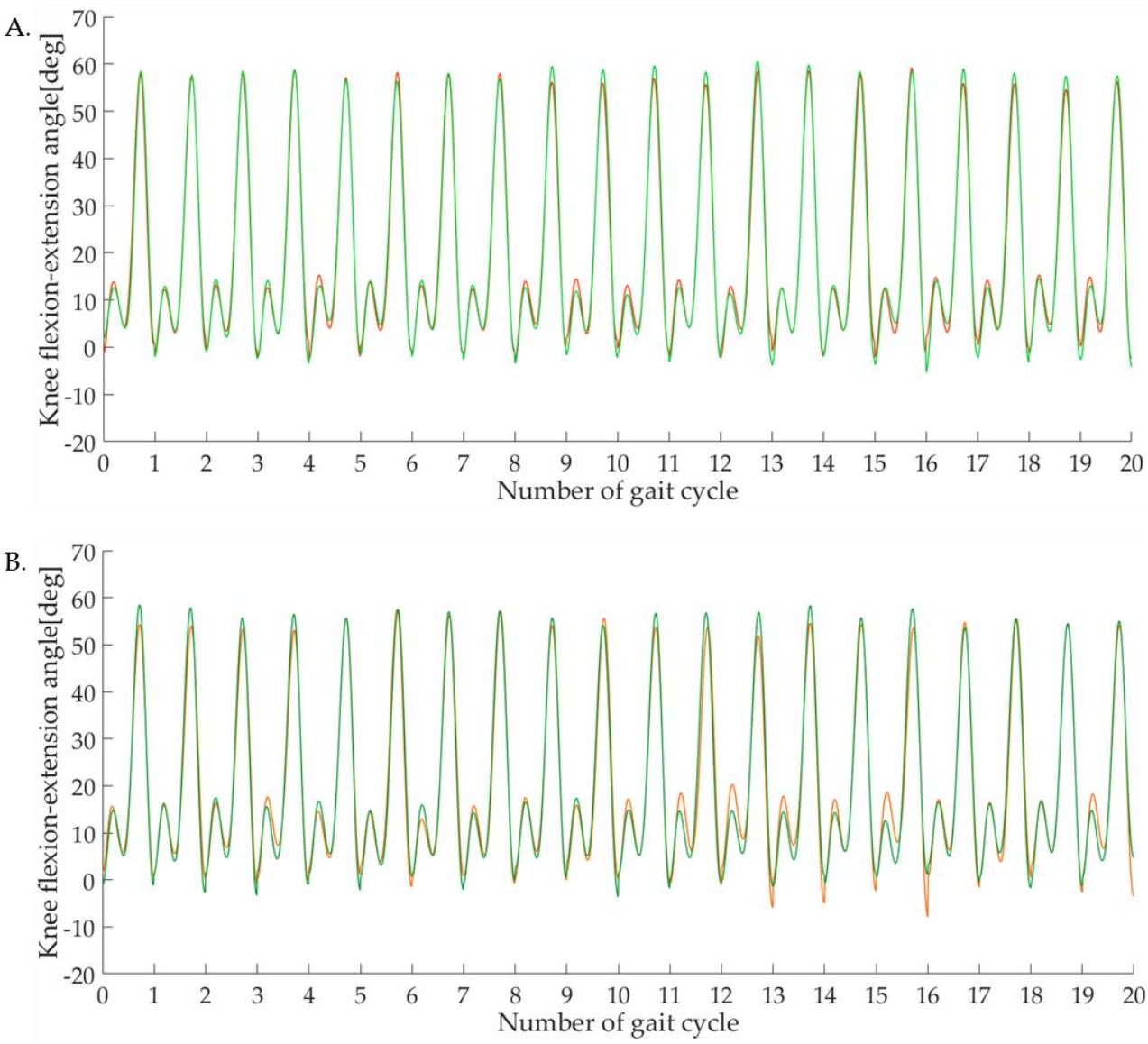

APPENDIX FIG 33. CORRELATION OF KNEE FLEXION EXTENSION RECORDED IN A LABORATORY AND A NON-LABORATORY BASED ENVIRONMENT - PARTICIPANT 4

A. Data from first session, where data recorded in the laboratory is represented in red and outdoor data in dark green; B. Data from the second session, where data recorded in the laboratory is represented in orange and outdoor data in green.

Participant 5

APPENDIX TABLE 34. CORRELATION AND VARIABILITY BETWEEN KNEE FLEXION EXTENSION RECORDED DURING GAIT IN A LABORATORY AND A NON-LABORATORY BASED ENVIRONEMT – PARTICIPANT 5.

Between venue variability of human gait	*Experimental results*	
Participant 5	Session 1	Session 2
Number of observations (N)	20	20
Difference between range of motion (ΔROM)	0.3°	2.5°
Root mean squared error (RMS)	2.4°	2.2°
Standard error (σ)	1.8°	1.8°
Coefficient of variation (CV)	2.8%	2.8%
Coefficient of multiple correlations (CMC)	0.997	0.997
Pearson product-moment correlation coefficient (r)	0.993	0.994

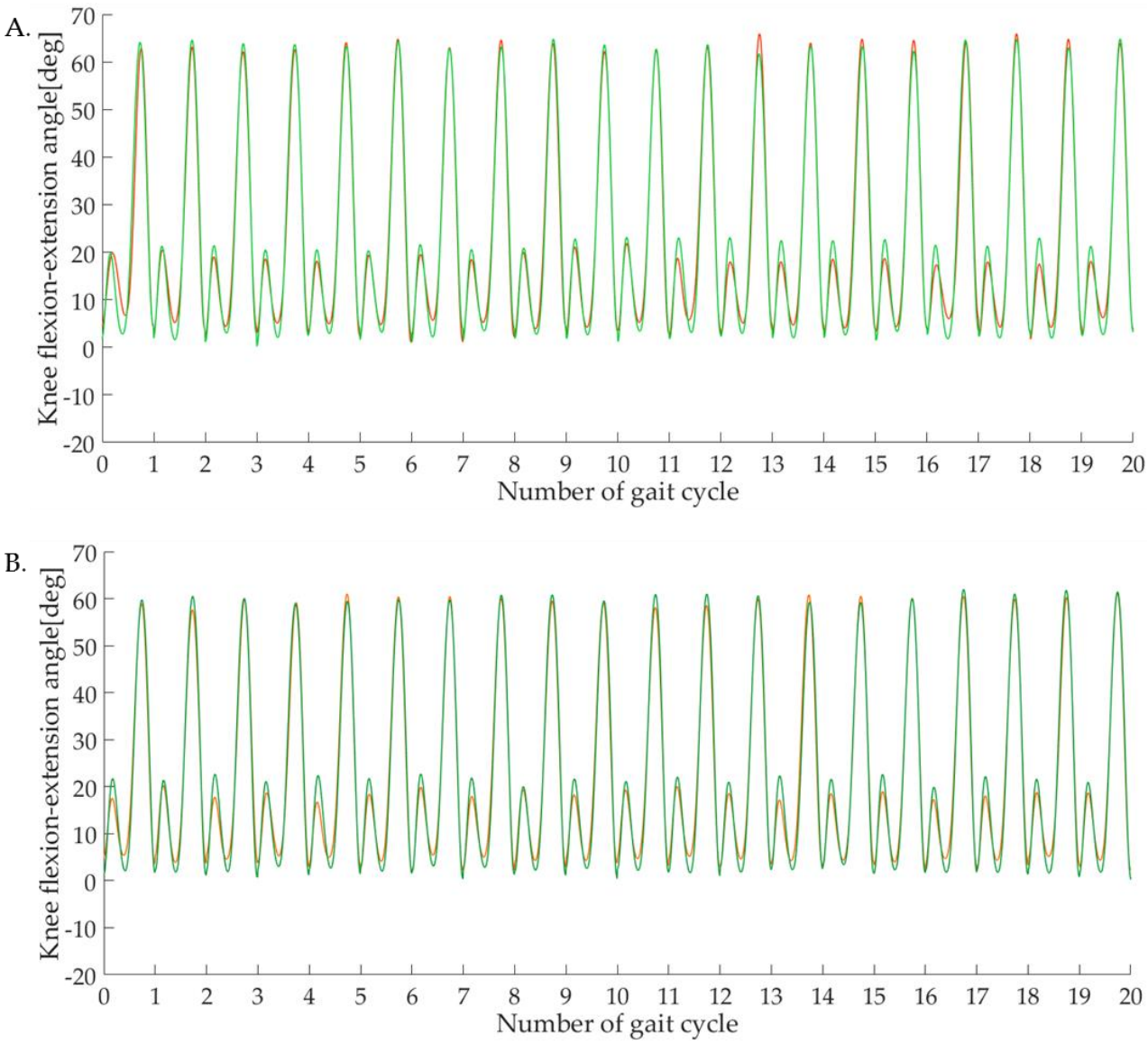

APPENDIX FIG 34. CORRELATION OF KNEE FLEXION EXTENSION RECORDED IN A LABORATORY AND A NON-LABORATORY BASED ENVIRONMENT - PARTICIPANT 5

A. Data from first session, where data recorded in the laboratory is represented in red and outdoor data in dark green; B. Data from the second session, where data recorded in the laboratory is represented in orange and outdoor data in green.

Participant 6

APPENDIX TABLE 35. CORRELATION AND VARIABILITY BETWEEN KNEE FLEXION EXTENSION RECORDED DURING GAIT IN A LABORATORY AND A NON-LABORATORY BASED ENVIRONEMT – PARTICIPANT 6.

Between venue variability of human gait	*Experimental results*	
Participant 6	Session 1	Session 2
Number of observations (N)	13	8
Difference between range of motion (ΔROM)	14.3°	6.3°
Root mean squared error (RMS)	5°	5.9°
Standard error (σ)	3.8°	4.6°
Coefficient of variation (CV)	5.9%	5.9%
Coefficient of multiple correlations (CMC)	0.981	0.978
Pearson product-moment correlation coefficient (r)	0.971	0.966

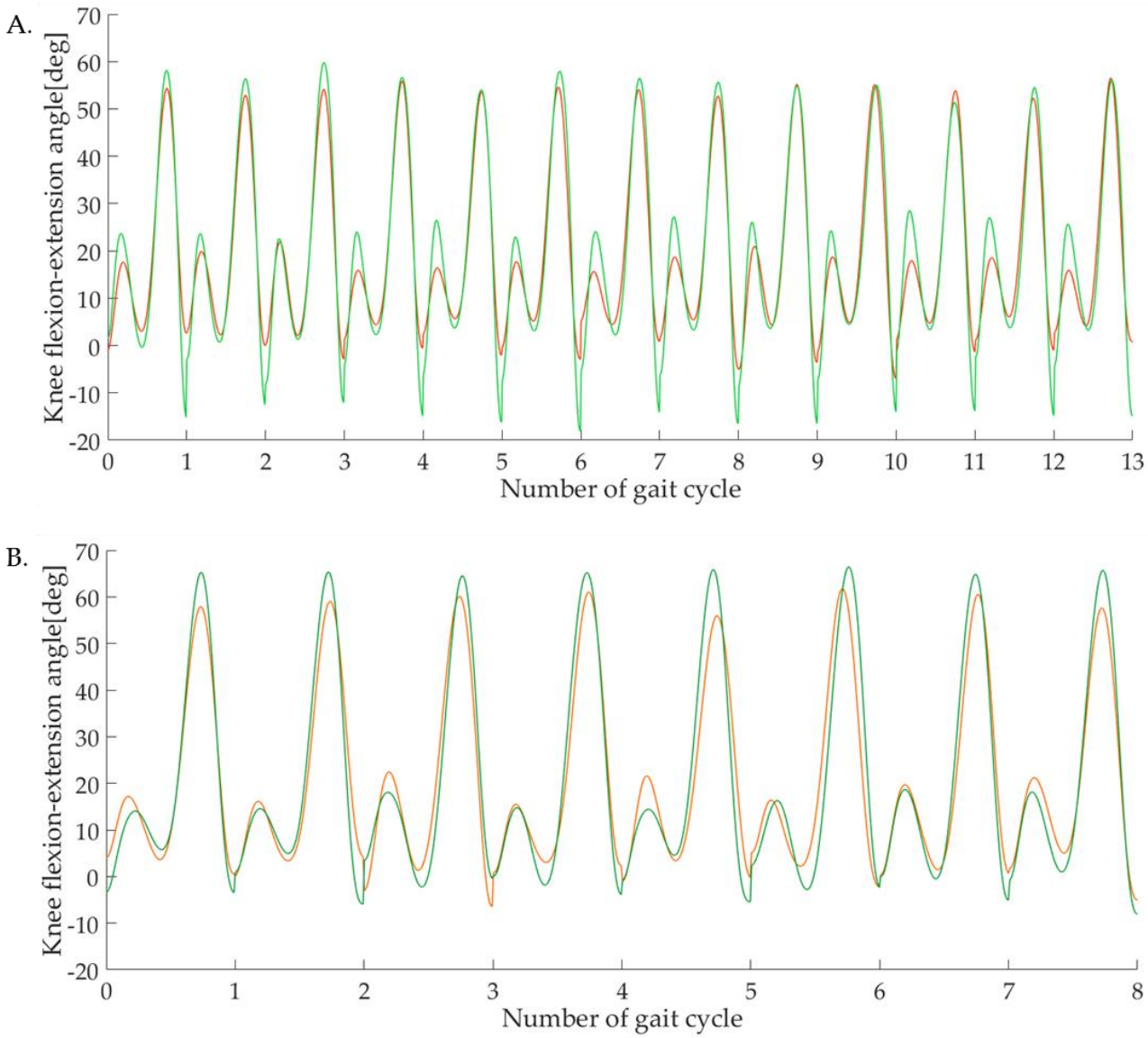

APPENDIX FIG 35. CORRELATION OF KNEE FLEXION EXTENSION RECORDED IN A LABORATORY AND A NON-LABORATORY BASED ENVIRONMENT - PARTICIPANT 6

A. Data from first session, where data recorded in the laboratory is represented in red and outdoor data in dark green; B. Data from the second session, where data recorded in the laboratory is represented in orange and outdoor data in green.

Participant 7

APPENDIX TABLE 36. CORRELATION AND VARIABILITY BETWEEN KNEE FLEXION EXTENSION RECORDED DURING GAIT IN A LABORATORY AND A NON-LABORATORY BASED ENVIRONEMT – PARTICIPANT 7.

Between venue variability of human gait	*Experimental results*	
Participant 7	Session 1	Session 2
Number of observations (N)	15	15
Difference between range of motion (ΔROM)	13.8°	13.9°
Root mean squared error (RMS)	5.4°	6.1°
Standard error (σ)	4.4°	5.1°
Coefficient of variation (CV)	6.7%	6.5%
Coefficient of multiple correlations (CMC)	0.983	0.974
Pearson product-moment correlation coefficient (r)	0.987	0.983

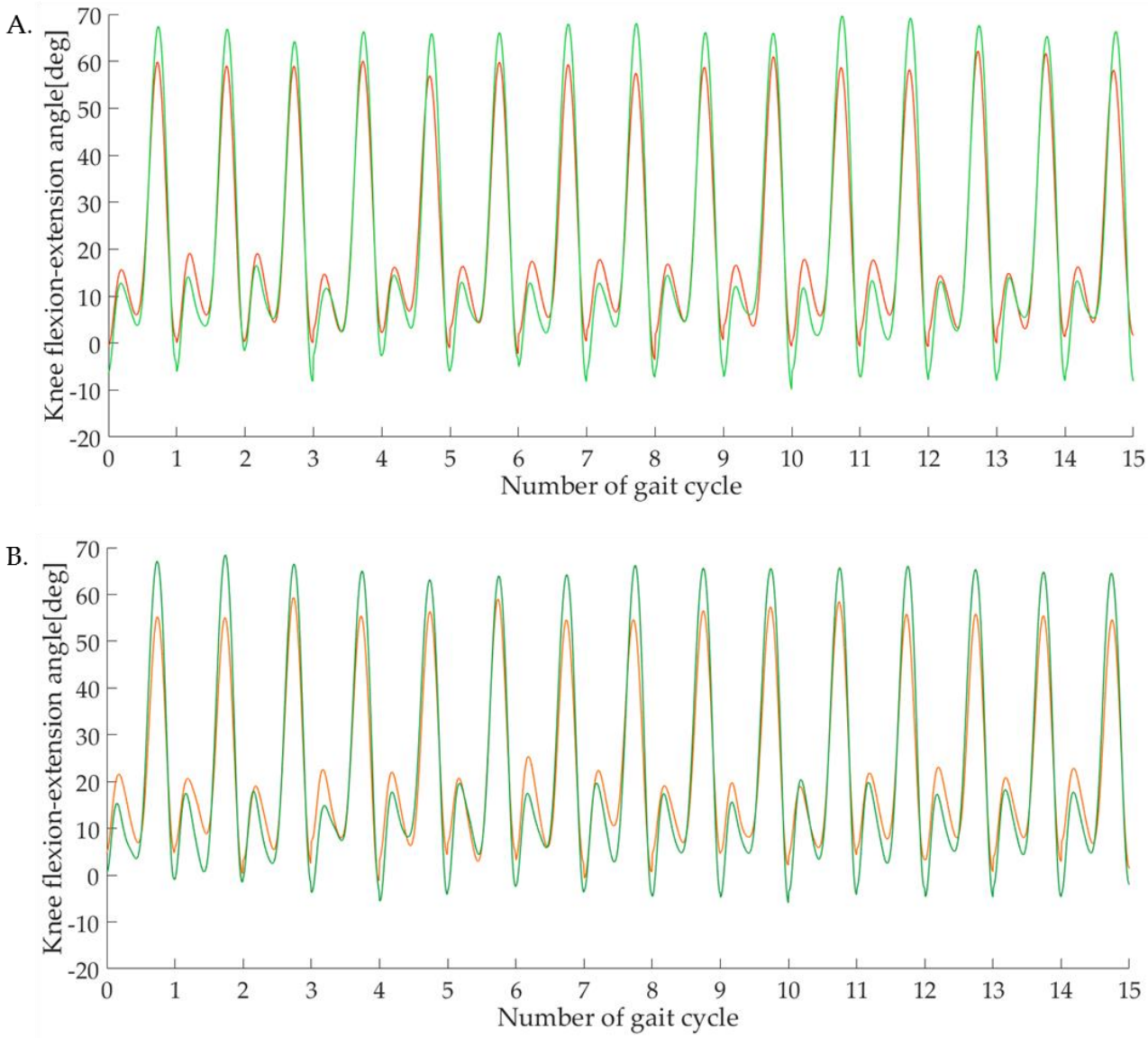

APPENDIX FIG 36. CORRELATION OF KNEE FLEXION EXTENSION RECORDED IN A LABORATORY AND A NON-LABORATORY BASED ENVIRONMENT - PARTICIPANT 1

A. Data from first session, where data recorded in the laboratory is represented in red and outdoor data in dark green; B. Data from the second session, where data recorded in the laboratory is represented in orange and outdoor data in green.

Participant 8

APPENDIX TABLE 37. CORRELATION AND VARIABILITY BETWEEN KNEE FLEXION EXTENSION RECORDED DURING GAIT IN A LABORATORY AND A NON-LABORATORY BASED ENVIRONEMT – PARTICIPANT 8.

Between venue variability of human gait	*Experimental results*	
Participant 8	Session 1	Session 2
Number of observations (N)	19	19
Difference between range of motion (ΔROM)	2.9°	6.9°
Root mean squared error (RMS)	2.8°	3.4°
Standard error (σ)	2.2°	2.8°
Coefficient of variation (CV)	3.9%	4.6%
Coefficient of Multiple correlations (CMC)	0.994	0.990
Pearson product-moment correlation coefficient (r)	0.990	0.988

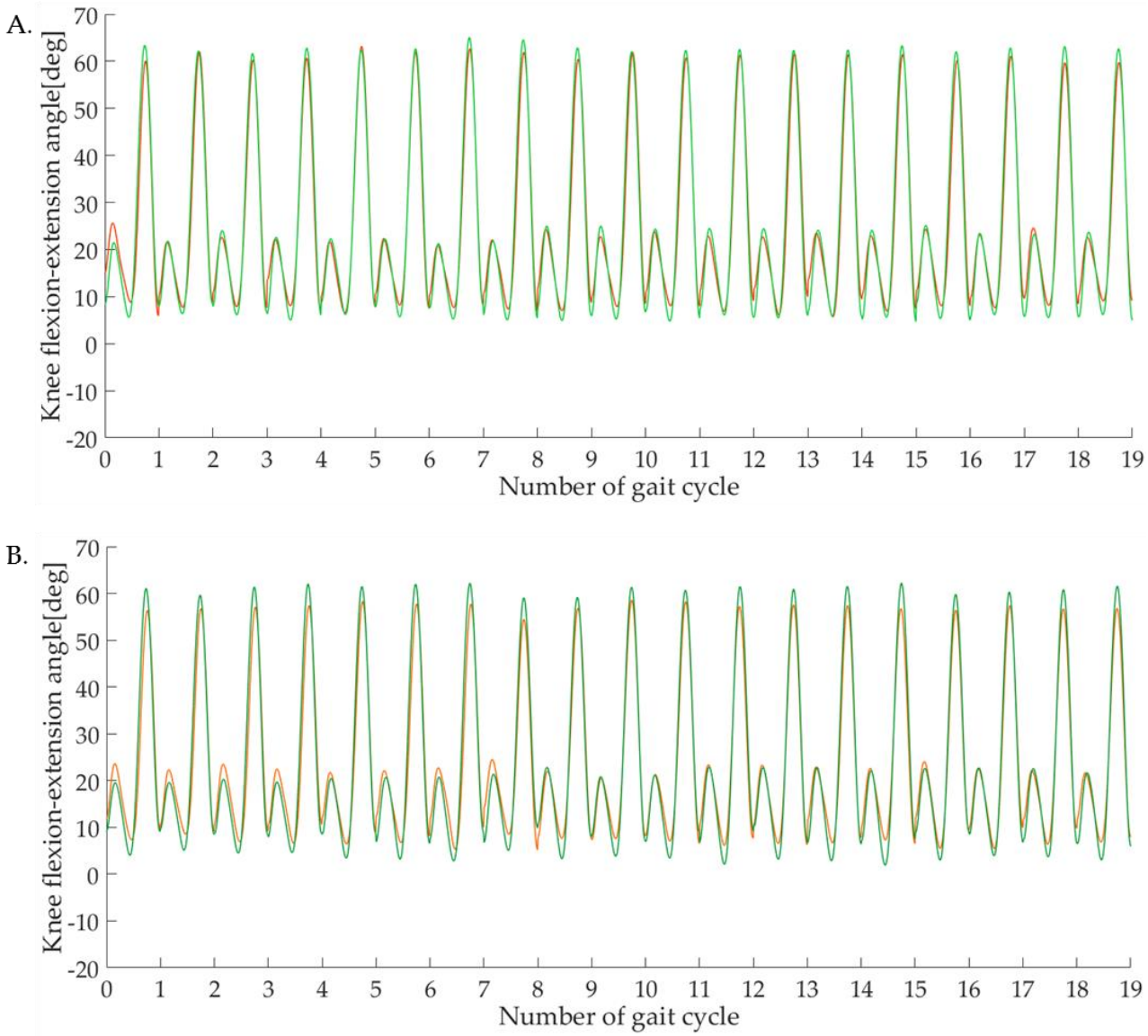

APPENDIX FIG 37. CORRELATION OF KNEE FLEXION EXTENSION RECORDED IN A LABORATORY AND A NON-LABORATORY BASED ENVIRONMENT - PARTICIPANT 8

A. Data from first session, where data recorded in the laboratory is represented in red and outdoor data in dark green; B. Data from the second session, where data recorded in the laboratory is represented in orange and outdoor data in green.

Participant 9

APPENDIX TABLE 38. CORRELATION AND VARIABILITY BETWEEN KNEE FLEXION EXTENSION RECORDED DURING GAIT IN A LABORATORY AND A NON-LABORATORY BASED ENVIRONEMT – PARTICIPANT 9.

Between venue variability of human gait	*Experimental results*	
Participant 9	Session 1	Session 2
Number of observations (N)	19	20
Difference between range of motion (ΔROM)	14°	5.9°
Root mean squared error (RMS)	5.1°	3.3°
Standard error (σ)	4.3°	2.5°
Coefficient of variation (CV)	7.8%	3.7%
Coefficient of multiple correlations (CMC)	0.979	0.988
Pearson product-moment correlation coefficient (r)	0.976	0.977

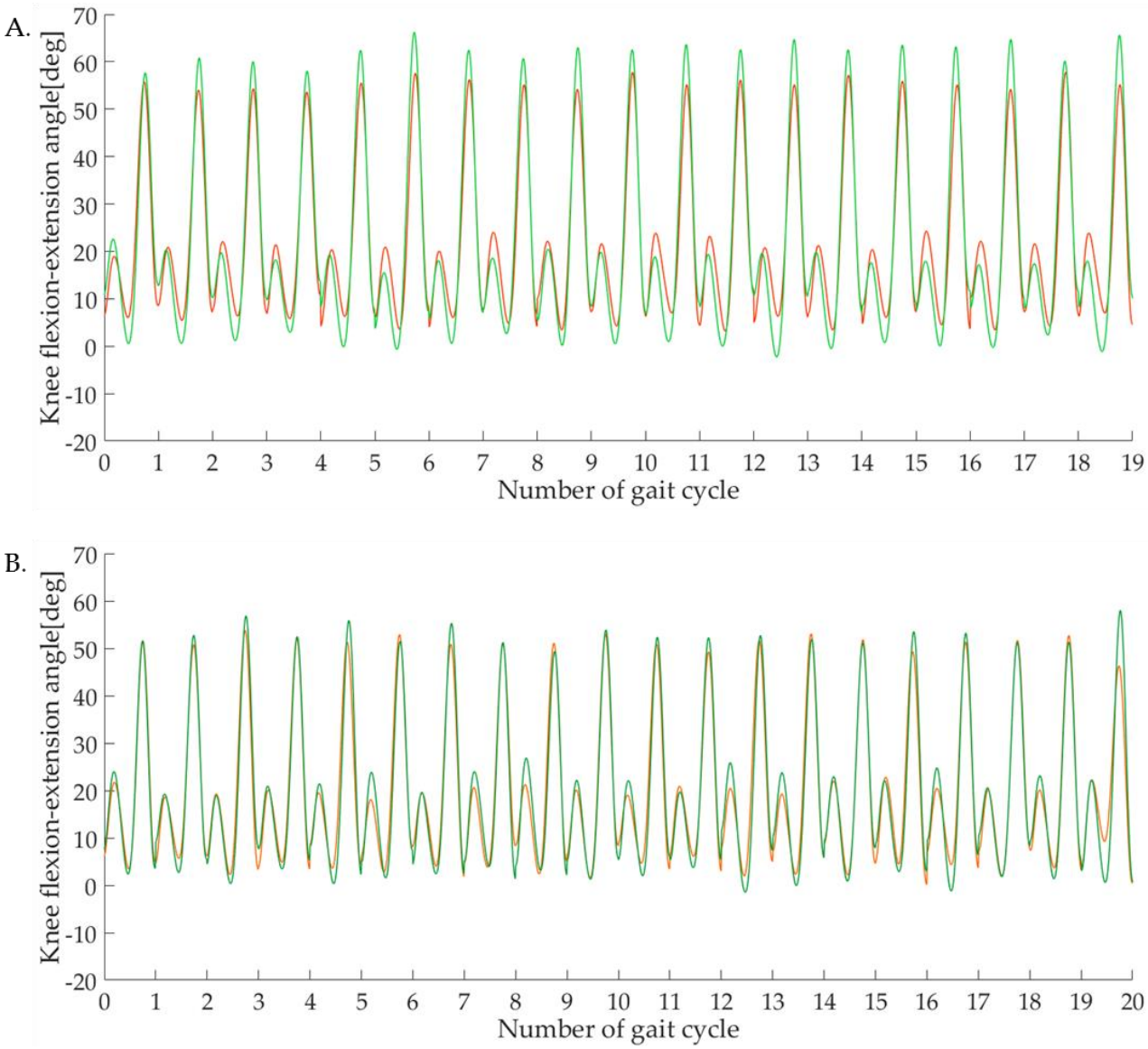

APPENDIX FIG 38. CORRELATION OF KNEE FLEXION EXTENSION RECORDED IN A LABORATORY AND A NON-LABORATORY BASED ENVIRONMENT - PARTICIPANT 9

A. Data from first session, where data recorded in the laboratory is represented in red and outdoor data in dark green; B. Data from the second session, where data recorded in the laboratory is represented in orange and outdoor data in green.

Participant 10

APPENDIX TABLE 39. CORRELATION AND VARIABILITY OF KNEE FLEXION EXTENSION RECORDED DURING GAIT IN A LABORATORY AND A NON-LABORATORY BASED ENVIRONEMT – PARTICIPANT 10.

Between venue variability of human gait	*Experimental results*
Participant 10	Session 1
Number of observations (N)	20
Difference between range of motion (ΔROM)	1.8°
Root mean squared error (RMS)	2.3°
Standard error (σ)	1.7°
Coefficient of variation (CV)	2.7%
Coefficient of multiple correlations (CMC)	0.996
Pearson product-moment correlation coefficient (r)	0.991

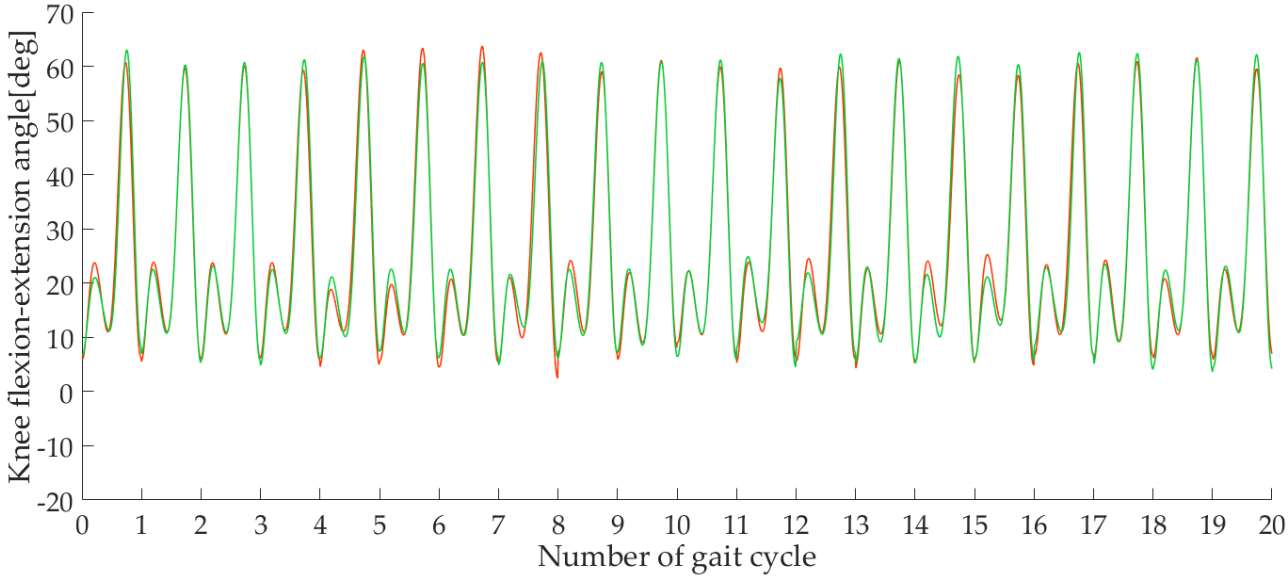

APPENDIX FIG 39. CORRELATION OF KNEE FLEXION EXTENSION RECORDED IN A LABORATORY AND A NON-LABORATORY BASED ENVIRONMENT - PARTICIPANT 10
Where data recorded in the laboratory is represented in red and outdoor data in dark green.

Appendix 4

Standardized correction vector for one cycle of rotation about Y axis of sensor local coordinate system

Percentage of gait cycle [%]	*Correction factor*	*Percentage of gait cycle [%]*	*Correction factor*	*Percentage of gait cycle [%]*	*Correction factor*
0	-0.3961	37	-1.6523	74	7.0911
1	-0.4012	38	-1.6593	75	7.4223
2	-0.2975	39	-1.6657	76	7.7257
3	-0.1357	40	-1.6695	77	8.0013
4	0.0271	41	-1.6688	78	8.2475
5	0.1641	42	-1.6620	79	8.4605
6	0.2618	43	-1.6482	80	8.6350
7	0.3152	44	-1.6277	81	8.7630
8	0.3295	45	-1.6015	82	8.8343
9	0.3145	46	-1.5716	83	8.8368
10	0.2781	47	-1.5408	84	8.7579
11	0.2216	48	-1.5120	85	8.5865
12	0.1402	49	-1.4874	86	8.3156
13	0.0301	50	-1.4681	87	7.9450
14	-0.1079	51	-1.4529	88	7.4801
15	-0.2676	52	-1.4380	89	6.9284
16	-0.4394	53	-1.4166	90	6.3018
17	-0.6133	54	-1.3793	91	5.6156
18	-0.7806	55	-1.3143	92	4.8918
19	-0.9354	56	-1.2087	93	4.1601
20	-1.0742	57	-1.0494	94	3.4529
21	-1.1954	58	-0.8249	95	2.8068
22	-1.2987	59	-0.5274	96	2.2563
23	-1.3846	60	-0.1536	97	1.8210
24	-1.4541	61	0.2941	98	1.5126
25	-1.5087	62	0.8073	99	1.3557
26	-1.5502	63	1.3728	100	1.3528
27	-1.5806	64	1.9740		
28	-1.6020	65	2.5927		
29	-1.6167	66	3.2112		
30	-1.6267	67	3.8150		
31	-1.6337	68	4.3929		
32	-1.6381	69	4.9371		
33	-1.6401	70	5.4430		
34	-1.6408	71	5.9095		
35	-1.6426	72	6.3377		
36	-1.6464	73	6.7305		

UNIVERSITY OF Southampton

Appendix 5

Participant Information Sheet

Accuracy and reliability of measuring muscle activity and hip movement in 3D in young males

Study Title:

Validation and reliability of 3D motion analysis and muscle electrical activity during hip screening and gait in young male adults

Lead Researcher: David Wilson Ethics number: 14083

Collaborator: Lavinia-Alexandra Otescu

Please read this information carefully before deciding to take part in this research. If you are happy to participate you will be asked to sign a consent form.

What is the research about?

Taking part in sports such as football has health benefits but there is also an increased injury risk including hip and groin injury, known as femoroacetabular impingement (FAI), which is a change in the bony structure of the hip. FAI may lead to osteoarthritis (OA), which is pain and stiffness in the joints. The changes in footballers' hips may be due to the way they move (their movement patterns). There is some evidence that specific exercises can improve abnormal movement patterns and muscle activity, which could reduce the risk of developing injury, FAI and OA.

A hip screening tool has been designed to detect players whose movement pattern may lead to hip and groin injury, which is linked to FAI. Changes in movement patterns (kinematics), can be accurately obtaining using equipment that measures movement in three dimensions (called 3-D motion analysis). Electromyography (EMG) can be used to measure the electrical activity of muscle. To detect if a true change in movement pattern or muscle activity has occurred, it is important to know how much these measurements vary from day to day, without any treatment or exercise.

Movement patterns may be different in the laboratory compared to on the field, so wireless sensors can be used to analyse movement outdoors. However, it is unknown how accurate and practical it is to use these sensors.

The present study will determine if the methods for measuring movement are accurate and reliable enough to use in studies. This work will then lead to a better understanding how movement can be changed to reduce injury risk and improve the long term health of hip joints.

Why have I been chosen?

We are interested in the movement patterns of young males who are unlikely to have developed any structural hip abnormalities, to compare to the young footballers who will be analysed in a later study.

If you have any of the following you will not be able to take part in the study: any lower limb pain; diagnosed with lower limb disorder; any muscle or bone problems; lower limb or spinal fractures or allergic to tape/plasters. If you are not between the ages of 18 to 29 years old you will not be able to take part.

What will happen to me if I take part?

The testing will take place in the biomechanics laboratory in building 45 of the Faculty of Health Sciences at the University of Southampton. The second part of the session will take place in the Highfield Botanical Garden. The date and time at which the testing will take place will be agreed between you and the researchers. The researchers will explain what you will be asked to do and you will have the opportunity to ask any questions before testing begins. If you agree to take part in the study we will ask you to sign the consent form.

You will be asked to wear shorts for testing in the laboratory and loose fitting clothing for the testing outdoors, which will not restrict your movement in any way. The testing will begin with measuring your height, weight and your ankle and knee widths. To prepare the skin for the small pads to measure muscle activity the areas will be shaved and cleaned with an alcohol swab to reduce the skin resistance.

Reflective markers and small pads to measure muscle activity will be attached to the skin on your thorax and legs using double sided tape.

Matchbox sized wireless sensors will be attached to your lower back, thighs and lower legs with the tape. You will then be asked to carry out movements of your legs in standing, sitting and lying. You will be asked to perform movements such as squatting and lying on your side then lifting the uppermost leg towards the ceiling that form a 'Hip screening tool', which has been designed to identify footballers that may have problems or may develop problems with their hip joints. Your movement will be recorded using the markers, remote sensors and video cameras. Another PhD student (Nadine Botha) will be present to rate your movement during the hip screening assessment alongside David Wilson. You will also walk up and down the laboratory while recordings are made.

At the end of the laboratory session, the reflective markers and electrodes will be removed, leaving only the remote sensors attached, for testing by another PhD student (Lavinia Otescu). You will be asked to walk to the outdoor venue (a few minutes walk) together with the researchers for the second part of the session. You will repeat a few selected movements, which you will have already performed in the laboratory and you will be asked to walk up and down a footpath 3 times. The entire time including both sessions should take less than 90 minutes.

A second set of sessions will be carried out at least two days later, so we can see how similar the results are.

Are there any benefits in my taking part?

There are no direct benefits to taking part in this study. The information gained from this study will help further study on measuring movement patterns and how these may be changed to decrease injury risk.

Are there any risks involved?

There are minimal risks to taking part in this study. The sensors, markers and electrodes will not cause any pain or discomfort. Removal of the markers may cause

momentary discomfort similar to removing a small plaster. The tasks you will perform only require a low level of physical effort.

Some people may have a skin irritation in response to the sticky tape used attached the markers and sensors to the skin. If you have a known skin allergy or sensitivity to sticky tape, we ask you not to take part in the study.

Will my participation be confidential?

Yes, all data collected will be kept confidential in compliance with the Data Protection Act and University of Southampton data protection policy. To keep data confidential all written data will be stored in a locked filing cabinet and all electronic data will be stored on password protected computers that only the researchers have access. Your data will be anonymised by assigning a unique ID number to your data. No one, other than the researchers, will be able to link your name with the unique ID number. Data that will be published in journal articles, conferences or meetings will not report any names or unique ID numbers to maintain the anonymity of the data. All data will be kept for 10 years.

Video footage will be transferred from an encrypted memory card and stored on a password protected University of Southampton Research Drive. Participants will be asked for consent for their videos to be used in the future to enable different assessors in the team to compare how they rate performance of the tests. This is known as inter-rater reliability. Written consent would be obtained from participants whose video footage may be used to demonstrate test movements in future studies.

What happens if I change my mind?

Participation in the study is entirely voluntary and you may withdraw at any point during the study, without giving a reason for doing so and without affecting your rights.

What happens if something goes wrong?

In the unlikely event that you wish to make a complaint, or express any concerns, you should contact: Diana Galpin (Head of Intellectual Property, Contracts and Policy) Address: Building 37, University of Southampton, University Road, Southampton, SO17 1BJ. Email: d.galpin@soton.ac.uk Telephone: 023 8059 8673

Where can I get more information?

If you require any further information or have any questions regarding taking part in this study please contact David Wilson on the details below

David Wilson – PhD Student

Senior Physiotherapist

Faculty of Health Sciences, Building 45, University of Southampton

Highfield Campus, Southampton, SO17 1BJ, Tel 02380 594332

Email: dw1y13@soton.ac.uk

Thank you for considering participating and for taking time to read this sheet.

UNIVERSITY OF Southampton

Appendix 6

Participant consent form

CONSENT FORM (v2)

Study title: Validation of a novel motion capture protocol and intra rater reliability of 3-D motion analysis, and muscle electrical activity during a hip screening assessment and gait in young male adults

Researcher name: David Wilson

Lavinia-Alexandra Otescu

Ethics reference: 14083

Please initial the box(es) if you agree with the statement(s):

I have read and understood the information sheet (insert date /version no. of participant information sheet) and have had the opportunity to ask questions about the study.	☐
I agree to take part in this research project and agree for my data to be used for the purpose of this study.	☐
I understand my participation is voluntary and I may withdraw at any time without my legal rights being affected.	☐
I am happy to be contacted regarding other unspecified research projects. I therefore consent to the University retaining my personal details on a database, kept separately from the research data detailed above. The 'validity' of my consent is conditional upon the University complying with the Data Protection Act and I understand that I can request my details be removed from this database at any time.	☐

Data Protection

I understand that information collected about me during my participation in this study will be stored on a password protected computer and that this information will only be used for the purpose of this study. All files containing any personal data will be made anonymous.

Name of participant (print name)……

Signature of participant…….

Date……

Appendix 7

Research Risk Assessment Form

IMPORTANT If you have any queries please contact the Faculty Health and Safety officer, Peter Fisk at P.Fisk@soton.ac.uk

Please read the following before completing this form

i. If this is a student project this risk assessment needs to be completed by the student (applicant) and supervisor (reviewer).

ii. If this is a staff project this risk assessment needs to be completed by the Principal Investigator (applicant) and reviewed by the head of the actual research programme/area/unit relevant to the proposal.

iii. If this is a staff project and the risk assessment is completed by a Research Assistant/Fellow, then it needs to be checked by the Principal Investigator and reviewed by the head of the actual research programme/area/unit relevant to the proposal. If the Principal Investigator is head of the actual research programme/area/unit relevant to the proposal, then the Director of Research needs to be the reviewer.

iv. If the Principal Investigator completes the risk assessment and the applicant is the head of the actual research programme/area/unit relevant to the proposal, then it needs to be reviewed by the Director of Research (reviewer).

v. If you are an international student undertaking your research fieldwork entirely within your own country this risk assessment needs to be completed by you (applicant) and supervisor (reviewer)

Once complete, the risk assessment form should be uploaded via the University Ethics system ERGO at www.ergo.soton.ac.uk

Applicant Name:	David Wilson Lavinia-Alexandra Otescu				
Project Title:	Validation of a novel motion capture protocol and intra rater reliability of 3-D motion analysis and muscle electrical activity during a hip screening assessment and gait in young male adults				
Type of project: (Please tick or insert X)	Staff		Student	x	
Supervisor's Name: *(if relevant – see point i above)*	Prof Maria Stokes Dr. Alexander Forrester Dr Martin Warner Prof. Markus Heller				
Principal Investigator's Name: *(if relevant- see point iii above)*	David Wilson				
Who will this risk assessment/research involve: *(please provide a brief description of your proposed sample and/or research site)*	Male University of Southampton undergraduate students aged 18-29 years old.				
Where appropriate list the individuals doing the work	David Wilson Lavinia-Alexandra Otescu				

Does the work/research involve lone working: *(for example working outside of office hours in your office or a lab-based environment) or conducting interviews with subject in their own homes in which case please complete Forms RA2, RA3 and RA4 as necessary with this assessment.*	Yes		No	x	

Health & Safety Risk Assessment

Work task / activity	A multienvironment, cross-sectional, reliability study consisting of repeated measures taken within and between sessions investigating the validity, accuracy, applicability and repeatability of the two proposed motion capture protocols and muscle activity screeining.				
Assessor(s)	David Wilson Lavinia-Alexandra Otescu	Responsible Manager	Dr Martin Warner	Date	27.03.2015
Faculty	Faculty of Health Sciences	Academic Unit/Team		Location	B45/2038 Highfield Campus Highfield Campus Outdoor
Brief description of task / activity	Inside the biomechanics laboratory movement will be recorded with the Vicon Motion capture system, and with the Xsens MTw sensors and the Awinda station. The participants will perform movements to the front, side and backwards in standing. A static trial will be recorded followed by repeated cycles of flexion-extension of the hip and knee, side step (to simulate abduction-adduction of the hip), closed kinematic chain (heel touches the floor) internal-external rotation of the hip and gait. The hip screening will involve assessing movements in standing on one leg and bending the knee, and involve trunk rotation. Lifting the knee to the chest in standing and sitting and in side lying lifting leg towards ceiling. The protocol that used in the lab will be applied outdoors as well, with the exception of the hip screening protocol.				

Additional notes (e.g, references, persons at risk, risk factors, etc.) [optional]	

Declaration by responsible manager: I confirm that this is a suitable & sufficient risk assessment for the above work activity / task.					
Signed		Print Name	Dr Martin Warner	Date	
Declaration by users: I confirm that I have read this risk assessment, will implement the controls outlined herein, and will report to the responsible manager any incidents that occur or any shortcomings I find in this assessment.					
Signed		Print name	David Wilson	Date	
Signed		Print name	Lavinia-Alexandra Otescu	Date	

(1) Identify all hazards and reasonably foreseeable worst-case consequences. A 'hazard' is anything with the potential to cause an adverse consequence, such as an injury or illness.

Reasonably foreseeable worst-case consequence: 'Worst case' means it is not necessarily the most likely consequence that should be considered, but, 'reasonably foreseeable worst case' means that far-fetched, improbable hazards and consequences need not be considered.

(2) Estimate inherent risk for each hazard. 'Inherent' risk is that without any controls applied.

Risk: Is likelihood of hazard event and reasonably foreseeable worst-case consequence combined.

In estimating risk, consider factors that could exacerbate risk, such as reasonably foreseeable emergencies, lone work, inexperience, new & expectant mothers, waste disposal, potential effects on others such as contractors or visitors, etc. A separate 'row' for a particular hazard / consequence may be needed to account for these.

Estimate risk using the matrix on the next page, and place an X in the appropriate box.

'High' risks must be reduced before activity / task can commence or continue. 'Medium' risks must be reduced as much and as soon as is reasonably practicable.

(3) Devise controls for each hazard. A 'control' is a measure taken to reduce risk.

Controls: As a general principle, the 'hierarchy' of control that is to be applied (from most to least preferable) is: avoid the risk; substitute something less hazardous that gives same or similar outcomes; 'engineering' controls (ie, equipment and articles that mitigate or contain a hazard); safe system of work (ie, a prescribed work method); and personal protective equipment ('PPE', eg, gloves, helmet, boots, etc). So, PPE is a last resort.

Other controls that should be considered: training and supervision, planning for possible emergencies, health surveillance, validation and maintenance of any engineering controls, and correct specification of any PPE.

'Low' risks, by definition, do not require controls.

(4) Estimate residual risk for each hazard. 'Residual' risk is that with controls applied.

Residual risk is estimated as above, and the objective is for all risks to be low so far as is reasonably practicable.

(5) The responsible manager, principal investigator, project leader, etc must sign the Declaration on the front page.

- Health & safety risk assessments must be 'suitable and sufficient',ie, cover all relevant issues and include enough detail.

- It is activities / tasks should be risk assessed, and not, as such, substances(but rather use of substances), or equipment (but rather use of equipment),
or locations (but rather activities therein), or people (but rather what they do).
- This template is for 'general' health & safety risk assessment, suitable for most hazards,but certain hazards require additional regulatory and technical detail (eg, ionising radiations,biological agents, genetic modification, noise, hazardous chemicals, etc).
- Health & safety risk assessments can be generic, provided they remain 'suitable and sufficient'.
- Health & safety risk assessments need to be reviewed periodically (at least every two years or sooner if inherent risk is high), and also after incidents, after significant changes to the activity / task, if staff raise any concerns, if there is a relevant change to the law or to other relevant standards, or if there is anything to suggest the assessment is not suitable or sufficient.
- You may remove pages 4 and 5 from the final assessment.
- A reassessment date is required on page 9

Health & safety risk estimation matrix

High risk – requires controls to reduce risk before activity / task can commence (or continue).

Medium risk – requires controls to reduce risk as much and as soon as is reasonably practicable.

Low risk – all risk should be reduced to this tolerable level, so far as is reasonably practicable.

Reasonably foreseeable worst case consequence Likelihood [3] of hazard event	Minor superficial injury; or slight and temporary health effect	Moderate significant injury or illness [1]; or temporary minor disability x	Major serious injury or illness [2]; or significant or permanent disability	Critical fatal injury or illness; or substantial and permanent disability	Catastrophic fatal injury or illness for multiple persons x
Likely high probability, 1 in 10 chance or higher, once in two	medium risk	high risk	high risk	high risk	high risk

weeks or longer for activities on a daily basis					
Possible significant probability, 1 in 100 chance or higher, once in six months or longer for activities on a daily basis	low risk	medium risk	high risk	high risk	high risk
Unlikely low probability, 1 in 1,000 chance or higher, once in four years or longer for activities on a daily basis	low risk	low risk	medium risk	high risk	high risk
Rare very low probability, 1 in 10,000 chance or higher,	low risk	low risk	low risk	medium risk	high risk

once in a decade or longer for activities on a daily basis					
Almost never extremely low probability, less than 1 in 100,000 chance, once in a century or longer for activities on a daily basis	low risk	low risk	low risk	low risk	medium risk

[1] 'Significant injury' could include, for example, laceration, burn, concussion, serious sprain, minor fracture, etc.
'Significant illness' could include, for example, dermatitis, minor work-related musculoskeletal conditions, partial hearing loss, etc.

[2] 'Serious injury' could include fracture or dislocation (other than digits), amputation, loss of sight, penetration or burn to eye, electric shock, asphyxia, or any injury leading to unconsciousness or requiring resuscitation or admittance to hospital for more than twenty-four hours. 'Serious illness' could include, for example, requiring medical treatment after chemical, biological or radiological exposure,
severe debilitating musculoskeletal conditions, severe dermatitis, asthma, etc.

[3] For likelihoods in between the listed values, use the higher likelihood to estimate risk. These probability definitions are only a guide.

Hazards and reasonably foreseeable worst case consequences	Inherent risk (no controls) From matrix (mark with X)		Controls (measures to reduce risk)	Residual risk (with controls) From matrix (mark with X)	
Injury	High		The risk of injury will be minimised by a warm-up session and by taking breaks between tests, when participants are tired. The tests will only include physical tasks, which can be carried out effortlessly by the participants.	High	
	Medium			Medium	
	Low	x		Low	x
Allergic reaction to tape	High		Participants, which show any signs of allergic reaction to the double-sided tape, used to attach the markers and sensors during the testing, will be excluded from the study. A tape removal spray will be used to remove the kinesiology tape with ease and without any pain or irritation of the skin	High	
	Medium			Medium	
	Low	x		Low	x
Psychological and	High		The privacy of the participants will be respected during preparation for data collection. The test will be stopped as soon as the participant feels any type of physical or psycological discomfort. The application	High	

Hazards and reasonably foreseeable worst case consequences	Inherent risk (no controls) From matrix (mark with X)		Controls (measures to reduce risk)	Residual risk (with controls) From matrix (mark with X)	
physical discomfort	Medium	x	of markers and sensors will be carried out quickly and carefully. Any type of physical contact will be kept to a minimum. Two researchers will be present at all times during the study.	Medium	

To be completed by the Reviewer					
Can the risks be further reduced?			Further precautions/additional controls required	Date to be completed	
YES		NO			

Reviewer name	Reviewer Signature	Date

Part 3: To be completed by the Applicant (if required)		
3a. Please outline how you have addressed the reviewer's comments: *Please resubmit your study protocol along with this form to the original reviewer*		
Applicant name	Applicant signature	Date

Part 4: To be completed by the Reviewer (if required)						
4a. Are the precautions now satisfactory?	Yes		No			
Reviewer name	Reviewer Signature				Date	
Date reassessment required						